Annual Report of the Marshall Space Flight Center

Research and Technology 1988

The Expansion of Man's Knowledge in the Universe.

Research and Technology 1988

Annual Report of the
Marshall Space Flight Center

NASA TM – 100343

National Aeronautics and
Space Administration

George C. Marshall Space Flight Center
Marshall Space Flight Center, Alabama 35812

ORIGINAL PAGE
COLOR PHOTOGRAPH

The Marshall Space Flight Center's perennial strength has been based on the extensive research and technology development activities that take place here. Our projects have always been underpinned by our in-house engineering strength and our basic space research activities.

In conjunction with our continuing emphasis on the Shuttle Program, and as we begin to look toward the challenges of man's move outward into the solar system, we turn once again to our own research and technology base. Here we find the new ideas, the basic research, and the proof of concept studies required to meet the exciting challenges of the final decade of the 20th century.

This report chronicles the work now in progress at the Marshall Center and attests to our strength and readiness to accept the science and technological challenges that lie ahead for the United States space program.

James R. Thompson, Jr.

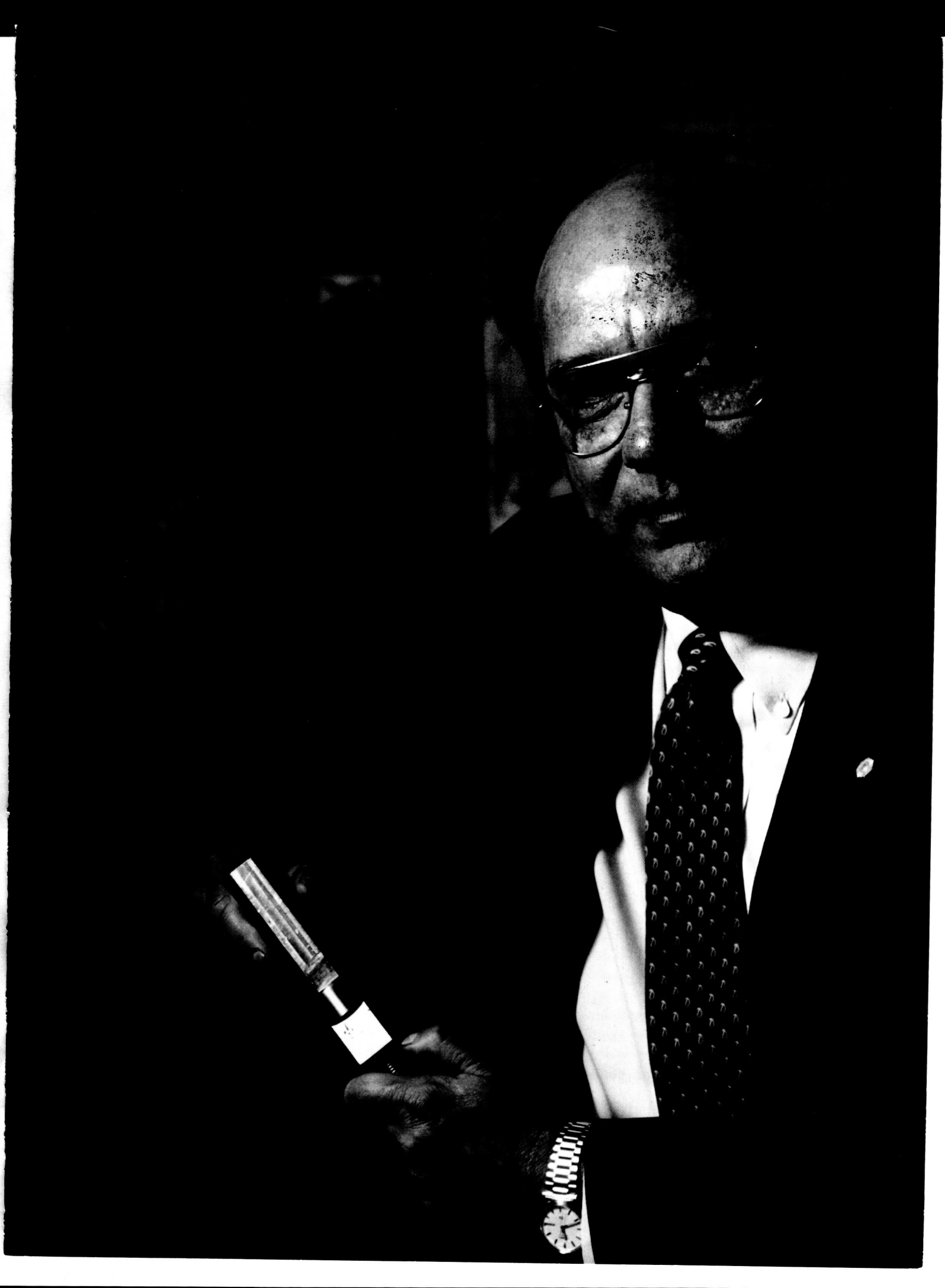

Acknowledgments

The point of contact and coordinator at MSFC for this report is P. Y. Potter [ER01/(205) 544-5723]. She was assisted by an editorial committee consisting of E. A. Tandberg-Hanssen, S. F. Morea, C. R. Chappell, W. C. Snoddy, and T. W. Moorehead. Detailed editorial support and production assistance was provided by MSI, a division of the Bionetics Corporation. The work at MSFC is a cooperative effort, but because of space restrictions it is impossible to list all those involved in the projects described in this report.

To assist the reader, the MSFC contact, office code, telephone number, and sponsoring agency are included at the end of each article. An alphabetical index of all contacts is presented at the end of this report.

Table of Contents

Advanced Studies

Research Programs

Materials and Processes

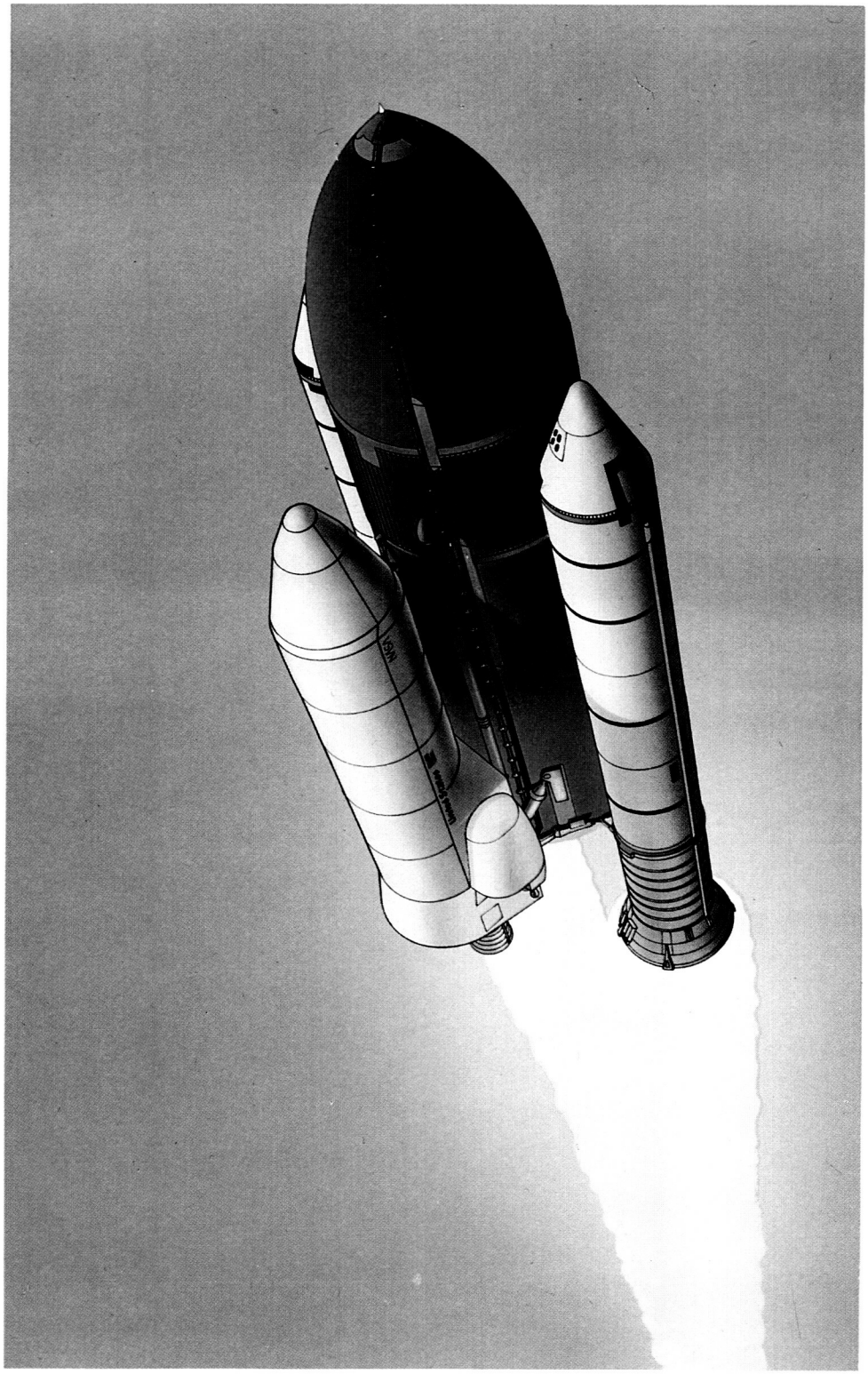

Advanced Studies

From its beginning, NASA has looked toward new frontiers to advance and new horizons to reach. Forecasts of long-range plans and goals, as well as detailed definition studies of future systems, are continual elements of the Agency's research and development evolution. Today's advanced studies of future space flight systems and payloads are critical ingredients for the foundation on which tomorrow's exciting challenges in space exploration will be met.

Safe and reliable space transportation systems are the key elements to future initiatives in space exploration. MSFC has long been preeminent in providing much of the nation's civil space transportation capability. To meet future needs, MSFC's advanced studies include new generation launch vehicles, advanced propulsion systems, high-energy upper stages, planetary and lunar transportation systems, and a wide variety of orbital systems.

A major national goal is to preserve the nation's preeminence in critical aspects of space science. Among the many space science and applications systems under investigation are large astronomical observatories that would succeed or complement the Great Observatories, Earth and microgravity science instruments and facilities, geostationary platforms, and a variety of Space Station Freedom payloads.

Transportation Systems

Shuttle Cargo Vehicle

The Shuttle Cargo Vehicle (Shuttle-C) proposed for first launch in 1994 will be used for missions that require a heavy lift capability greater than the Space Shuttle.

The Shuttle-C vehicle (Fig. 1) can satisfy a variety of missions (Fig. 2), offering an opportunity to reduce the workload of the Space Transportation System (STS) and reduce the use of the STS to missions requiring manned activities. The competitive price of the Shuttle-C compared with other currently-available launch vehicles will help meet foreign competition, while providing synergistic cost benefits for the STS and increasing the availability of equipment spares. With an appropriate upper stage, such as Centaur, Shuttle-C can place an 18,000 to 20,000 lb payload in geosynchronous orbit. More ambitious planetary missions; i.e., shorter trip times, larger payloads, etc., will be possible with the greater lift capability.

Shuttle-derived launch vehicle studies conducted by NASA over the last 12 to 13 years indicate that Shuttle-C is economically feasible for near-term mission needs.

Analysis and evaluation by NASA and various contractors during Phase I of the Shuttle-C Systems

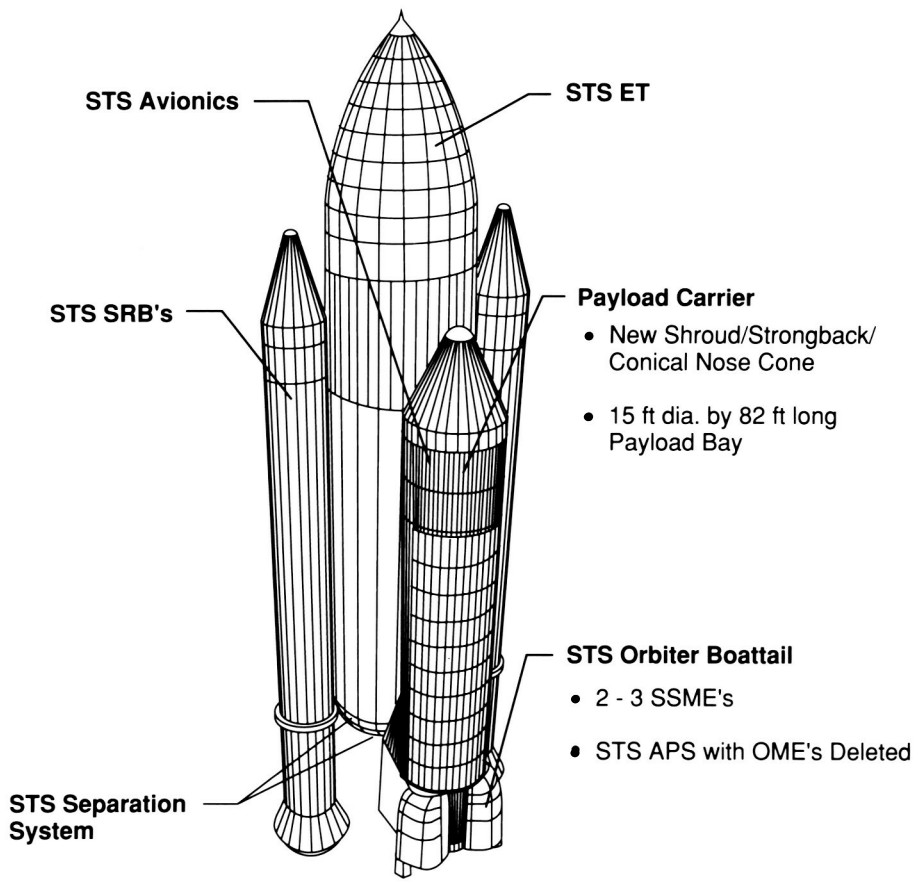

Figure 1. The Shuttle-C Vehicle

Definition studies managed by the Marshall Space Flight Center have reduced the number of Shuttle-C concepts. As a reference for trades analyses, the configuration has been defined as an STS-type vehicle consisting of two standard 4-segment solid rocket boosters, a standard expendable external tank, a minimally modified orbiter boattail, standard Space Shuttle Main Engines, and a new payload carrier. This configuration has been selected because of early availability; a reduced design, development, testing, and evaluation cycle; synergism with STS; efficient utilization of STS infrastructure; and low development risk. Phase II of the Shuttle-C Systems Definition studies, currently underway, is directed at refinement of the Shuttle-C reference configuration.

J. Walker/PF24
(205) 544-3963
Sponsor: Office of Space Flight

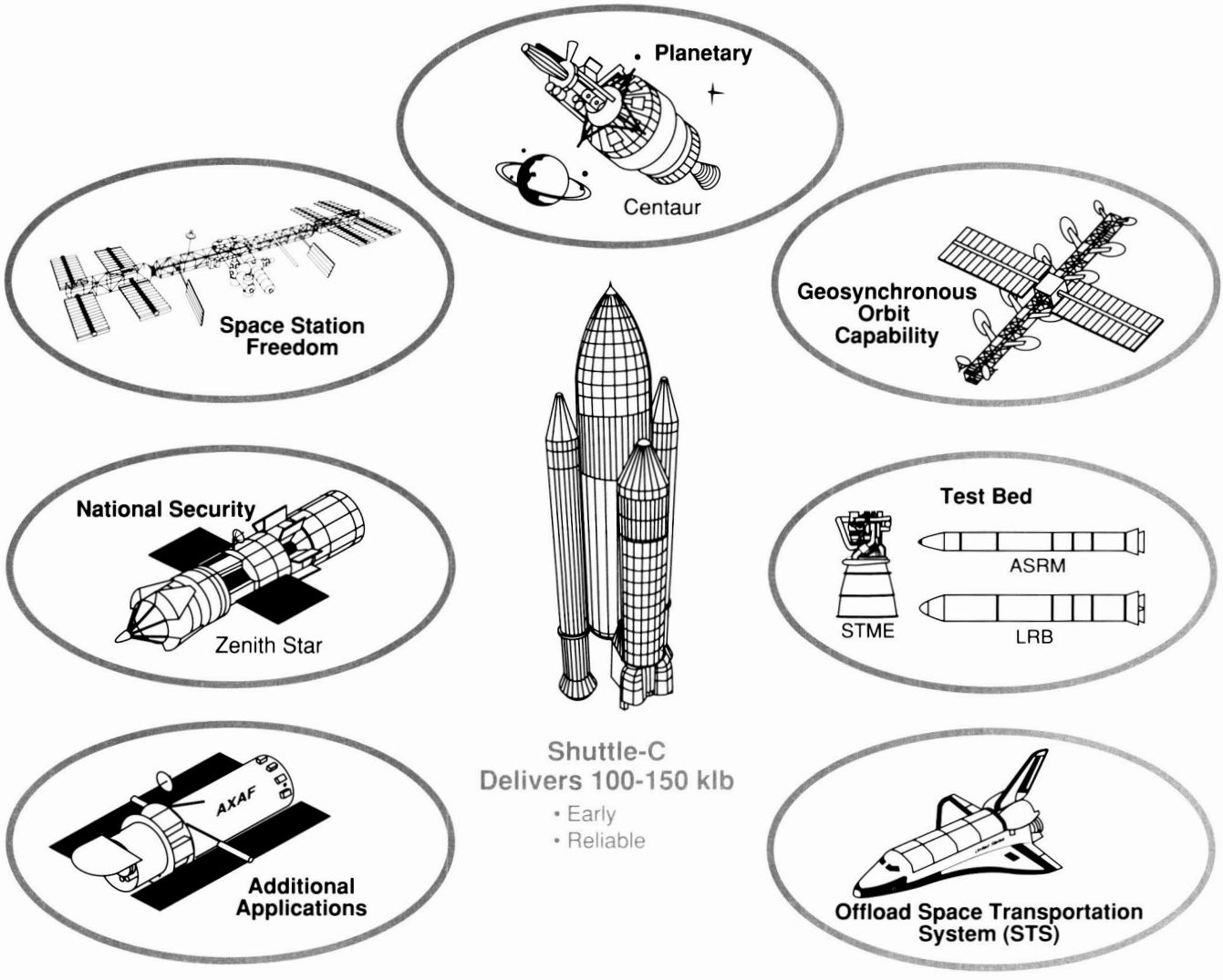

Figure 2. Shuttle-C Applications

ORIGINAL PAGE
COLOR PHOTOGRAPH

Liquid Rocket Boosters for the Space Transportation System

The concept of Liquid Rocket Boosters (LRBs) as a replacement for the current Solid Rocket Boosters (SRBs) has been studied in some detail this year. The intent has been to define both pump fed and pressure fed concepts which would enhance both the performance, and the flight safety of the Shuttle vehicle.

The selected configuration for the pump fed LRB (Fig. 3) is approximately 15 ft in diameter and 165 ft long. The propellants are LOX and RP-1. Four engines of approximately 700,000 lb each are used on each of the two boosters. The pressure fed booster also uses LOX and RP-1 propellants, and four thrust chambers on each booster.

Some of the more significant benefits of the LRB versus the current SRB include: engine out capability provides abort to orbit capability from lift-off and higher overall system reliability; all propulsion systems can be verified prior to vehicle launch release; and the LRB is delivered to the Vehicle Assembly Building (VAB) and erected on the Mobile Launch Platform. Propellants are, of course, not loaded until the vehicle is at the launch pad, thereby eliminating what is now a major hazard in the VAB, i.e., handling loaded Solid Rocket Motor (SRM) segments. Booster stacking, which now is the controlling factor in Shuttle launch rate, is significantly reduced.

J. E. Hughes/PF23
(205) 544-6544
Sponsor: Office of Space Flight

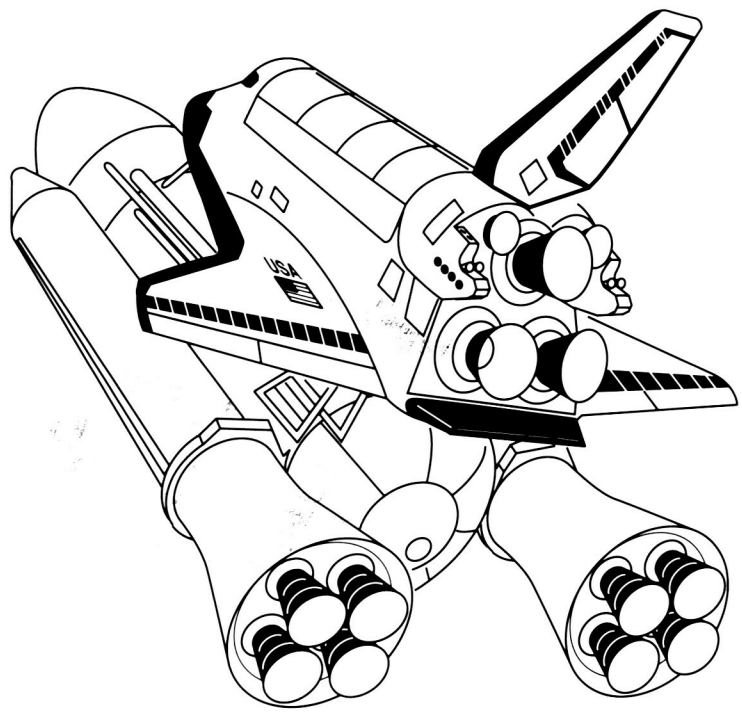

Figure 3. The Pump-Fed Liquid Rocket Booster

Shuttle Evolution/ Shuttle II

Based on currently projected flight rates for the Space Shuttle, major refurbishment or replacement will most likely be required by the year 2000. The Shuttle's basic technology level will be approximately 30 years old by then. In view of this situation, the Langley Research Center (LaRC) has been studying an all-new advanced second-generation Space Shuttle, or Shuttle II, that would be built based on technologies projected for a vehicle initial flight in about 2005 or later. However, a number of issues/ questions have surfaced since the Challenger accident (relating to reliability, safety, maintainability, performance, wear out, etc., on the current Shuttle system) that indicate the need to look at an interim vehicle, or "Block II" Shuttle that would come online prior to the 2000 time period. It is envisioned that this Block II Shuttle would incorporate appropriate technology advancements and improvements while providing a step, or evolutionary path, to the more advanced Shuttle II vehicle (Fig. 4).

An intercenter working group, consisting of representatives from Johnson Space Center (JSC), LaRC, Kennedy Space Center, and MSFC, has recently identified about 800 to 900 potential Space Transportation System improvement items, of which a large majority fall into the category of near term/ product improvements applicable to Orbiter Vehicle 105 or 106. Effort is underway to assess the proposed improvements and reduce the total list to less than 50 items for more detailed evaluation. Emphasis will be placed on selecting those items which offer the highest benefits relative to the following criteria: safety, reliability, maintainability, lower recurring costs, operational flexibility, resiliency, performance, growth potential, etc. The candidate improvements range from: automation and application of expert systems, electromechanical actuators, canards/tip

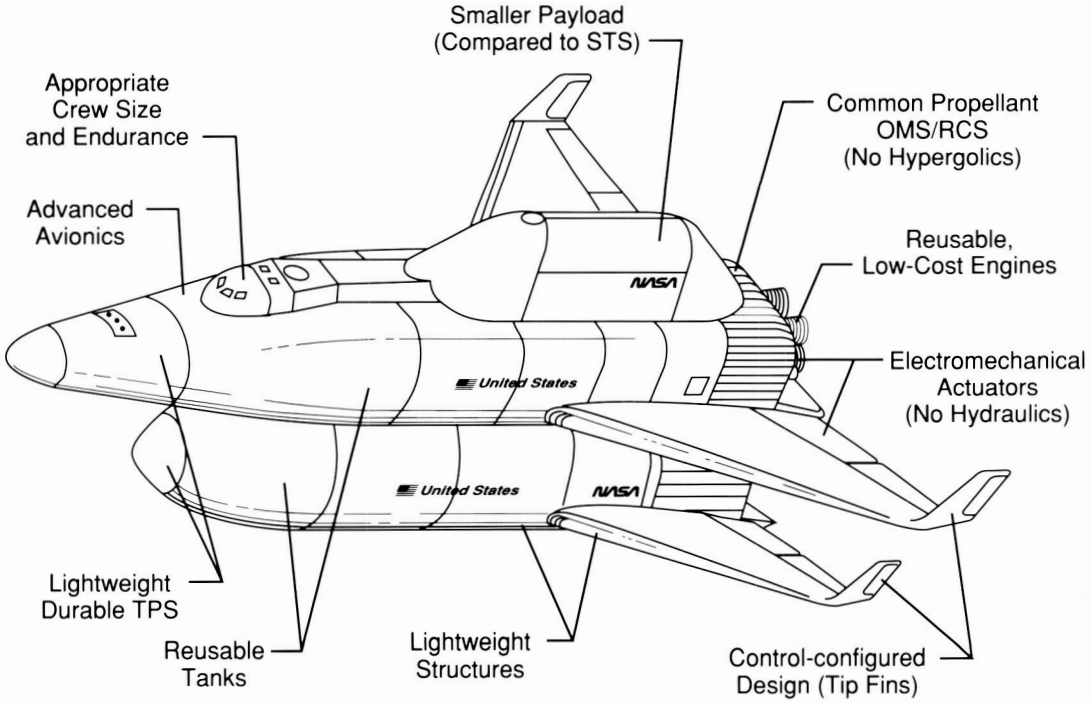

Figure 4. Shuttle II Representative Concept

fins, new liquid main engines, etc., to an all new liquid rocket flyback booster which would later serve as the booster for the more advanced Shuttle II vehicle.

The Shuttle II's primary goal is to provide routine, low cost access to and from space. It must meet changing mission needs, the changing transportation architecture, and take advantage of new technology opportunities for the post-2000 time frame. Typical Shuttle II missions include personnel transport for Space Station Freedom, man-critical missions, rescue, and manned exploration, as well as delivery of small payloads, return of commercial products to Earth, and servicing space platforms. Various concepts are under study, including single stage-to-orbit, two-stage fully reusable, and partially reusable vehicles having recoverable propulsion and avionics.

The Shuttle evolution/Shuttle II span of vehicle options encompasses the following technology areas: propulsion; structures; the thermal protection system; guidance, navigation, and control; power; communications; automation/artificial intelligence; aerodynamics/aerothermodynamics; flight performance; and operations.

Talay, Theodore A.: Shuttle II/Space Shuttle Evolution Joint Status Review. Space Systems Division, LaRC, May 25, 1988.

Teixeira, C.: Shuttle Evolution, Office of Space Flight Management Council Review. Advanced Programs Office, JSC, February 19, 1988.

B. W. Shelton/PD24
(205) 544-0513
Sponsor: Office of Space Flight

Advanced Launch System

An Advanced Launch System (ALS) (Fig. 5) is being defined as a joint United States Air Force/NASA initiative to provide more affordable, responsive, and reliable access to space. The program was established by Presidential order, responding to a Congressional act mandating joint effort by the two principal launch agencies. The ALS program has three objectives: to develop mature technologies to support ALS deployment in the 1990's, to transfer technology to existing systems, and to identify a family of future launch vehicles to satisfy assured access to space requirements.

The program goal is to place payloads in low earth orbit for $300 per pound by the year 2005. Current system requirements are keyed to Strategic Defense Initiative objectives:

Initial Launch Capability (ILC)	1996
Initial Operational Capability (IOC)	1998
Launch Rates	
Nominal Model	20 to 30/Yr
Expanded Model	30 to 40/Yr
Payload Capability	
Nominal Model	50,000 kg (110,000 lb) at 28.5°
Expanded Model	73,000 kg (160,000 lb) at 90°
Shroud Size	
Nominal Model	10 m (33 ft) Dia.
Expanded Model	12 m x 38 m (40 x 125 ft)

A management plan has been established by the Joint Project Office to define the areas of prime and support responsibilities between USAF and NASA. Those areas are:

Program Management	Joint Project Office
Systems Engineering	USAF with NASA support
Vehicle	USAF with NASA support
Liquid Engine System	NASA with USAF support
Solid Motors	NASA with USAF support
Flyback Booster	To be defined
Payload Module	USAF with NASA support
Logistics	USAF with NASA support
Focused Technology	NASA with USAF support

Assessments of the required technologies have been made and prioritized as follows:

LH_2/LO_2 Core Vehicle
Efficient Production/Operations
Improved Solid Rocket Motors
Reuseability
Other Subsystems/Activities

A Focused Technology program has been established to develop the necessary advanced technology to support current ALS concepts and to ensure their availability prior to mid-1992. Development of the necessary technology has been assigned per the above areas of responsibility with the budget allocations shown in Table 1.

In addition to the technology funding, propulsion facilities budgets have been established as shown in Table 2.

Phase I (definition) contracts were awarded to seven prime system contractors in July 1987: Boeing, General Dynamics, Hughes, Martin Marietta, McDonnell Douglas, Rockwell, and United Technologies. The resulting proposals have been delivered to a Source Evaluation Board that is currently in session. The principal design concepts are focusing on an evolving approach; i.e., LH_2/LO_2 core vehicles with either solid or liquid boosters with varying degrees of reuseability, including potential flyback concepts (Fig. 5). Current plans include selection of a minimum of two contractors to continue into the Phase II design phase.

The enabling legislation establishing the ALS program required formal review via the Department of Defense acquisition board system with NASA senior management participation. Release of the technology funding or Phase II contracting was reviewed in September 1988.

L. O. Wear/PF23
(205) 544-3215
Sponsors: Office of Space Flight, NASA Headquarters
Advanced Launch Systems Joint Program Office

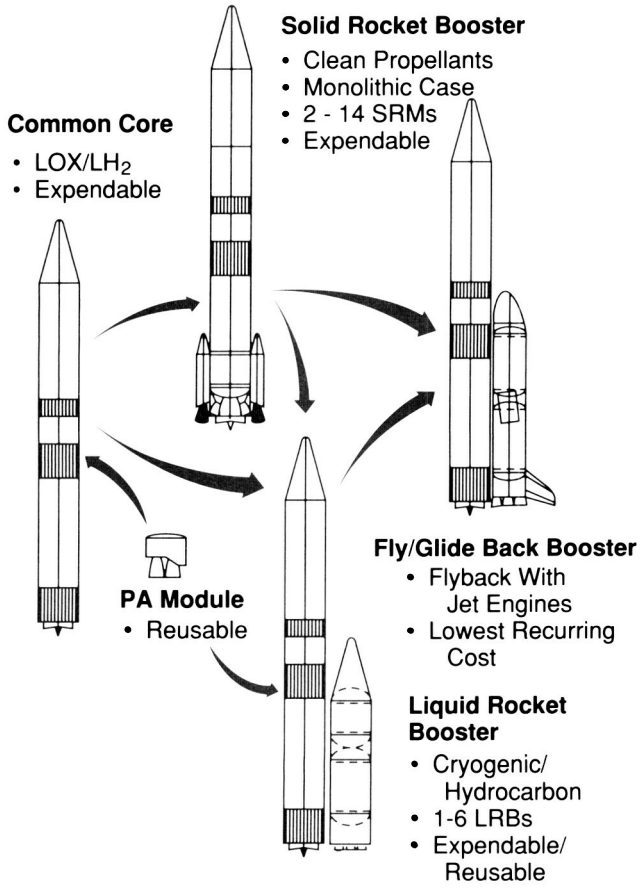

Figure 5. The Advanced Launch System Vehicle

Table 1. Technology Budget Allocation

Propulsion ($M)	94	96	134	105	76
Avionics/Software	27	9	10	7	8
Structures/Materials	26	29	35	34	26
Aero/Thermo	4	4	5	5	2
Ground & Flight Operations/Manufacture	24	17	25	22	15

Table 2. Propulsion Facilities Budgets

MSFC ($M)	4	6	3	2	0
Stennis Space Center					
Special Test Equipment	10	10	0	0	1
Construction of Facility	5	10	5	0	0
USAF	5	8	12	5	1

Space Transportation Main Engine

The Space Transportation Main Engine (STME) is designed to provide earth-to-orbit propulsion for the next generation of launch vehicles. Original STME Phase A and the Phase A extension studies have been refocused to provide engine system data required by the Advanced Launch System (ALS) vehicle contractors for the core vehicle, and booster vehicle. Parametric cost and performance data are included for both expendable and reusable configurations. To support the engine definition activities a baseline gas generator cycle engine configuration was selected. Performance of this engine falls within the spread currently being evaluated by the ALS vehicle contractors. When the vehicle requirements are decided, adjustments will be made to reconfigure the STME as required, including alternate engine cycles if warranted. The engine system development and production test facilities and the ALS core vehicle cluster test facility will be located at the Stennis Space Center. This high performance liquid rocket engine system will use liquid hydrogen fuel and liquid oxygen. The STME will be designed as a robust, simple, and inexpensive expendable rocket engine. Low cost design philosophy will be maintained throughout the design, development, testing, and evaluation of the system to ensure that the cost goals are achieved. This includes incorporation of low cost manufacturing processes developed in the focused technology program as well as design features that promote a robust, simple system. The STME utilizes a gas generator to provide turbine gases. The STME primary performance characteristics are:

Thrust	580 kgf (vacuum)
Specific Impulse	447 sec (vacuum)
Chamber Pressure	2,250 psi
Area Ratio	75:1
Engine Weight	6,500 to 7,500 lbs

J. C. Monk/HA31
(205) 544-7110
Sponsors: NASA/Office of Space Flight
Strategic Defense Initiative Organization
USAF/Space Division

Space Transportation Booster Engine

The Space Transportation Booster Engine (STBE) will provide main boost propulsion for the nation's next generation of launch vehicles. The original STBE Phase A and Phase A extension studies have been refocused to provide engine system data required by the Advanced Launch Service (ALS) vehicle contractors. Parametric cost and performance information are included for both expendable and reusable configurations. To support engine definition activities, a baseline gas generator cycle engine configuration was selected. This engine falls within the performance spread currently being evaluated by contractors for the ALS booster. When the vehicle requirements are decided, adjustments will be made to reconfigure the STBE as required. The engine system development and production test facilities and the ALS booster vehicle cluster test facility will be located at the Stennis Space Center. The current baseline version of this high-performance liquid rocket engine system will use liquid oxygen and the hydrocarbon fuel methane, which was selected in tradeoffs with RP-1 and propane. The STBE will be designed for low cost, high reliability and long-life operation with very low maintenance. Low cost design philosophy will be maintained to ensure the cost goals are achieved. This includes incorporation of low cost manufacturing processes developed in the focused technology program. In addition, vehicle safety, economics, and the high cost of some of the payloads will dictate the need for engine-out capability. The STBE will include the capability to throttle-up 20 percent above its normal operation point to provide engine-out from liftoff. The STBE utilizes a gas generator to provide turbine gases. The engine thrust chamber will be cooled with liquid methane, which is subsequently burned in the main combustion chamber. The current baseline STBE primary performance characteristics are:

Thrust	750 kgf (Sea Level)
Specific Impulse	325 sec (Sea Level)
Chamber Pressure	3,150 psi
Area Ratio	48:1
Engine Weight	6,500 to 7,500 lb

J. C. Monk/HA31
(205) 544-7110
Sponsors: NASA/Office of Space Flight
Strategic Defense Initiative Organization
USAF/Space Division

Booster Propulsion/ Vehicle Impact Study

The use of different propellants in the boost phase of launch vehicles has an impact on the size of both the booster stage and the overall launch vehicle. Generally, the dry weight of a launch vehicle is an indicator of the ultimate development cost of the vehicle. An analysis of the impact on the booster stage dry weight gives an indication of the probable trends in overall development cost resulting from the use of various boost phase propellant candidates. This study, conducted in parallel efforts at the Boeing Aerospace Company and the Martin Marietta Corporation, examined the use of booster engines using three different hydrocarbon fuels: RP-1, propane and methane with liquid oxygen as the oxidizer. The impact of using both fuel cooled engines and hydrogen cooled engines was examined. Two vehicle types were evaluated. For Boeing a partially reusable, two-stage vehicle with a 68-Mg (150-klb) payload capability to a 220-nmi, circular, 28.5° orbit; and a single-stage vehicle that is fully reusable with a 4.5-Mg (10-klb) payload to a 100-nmi, circular, 90° orbit were examined. For Martin Marietta a fully reusable, two-stage vehicle with a 29.5-Mg (65-klb) payload to a 56-nmi by 151-nmi by 28° orbit and a

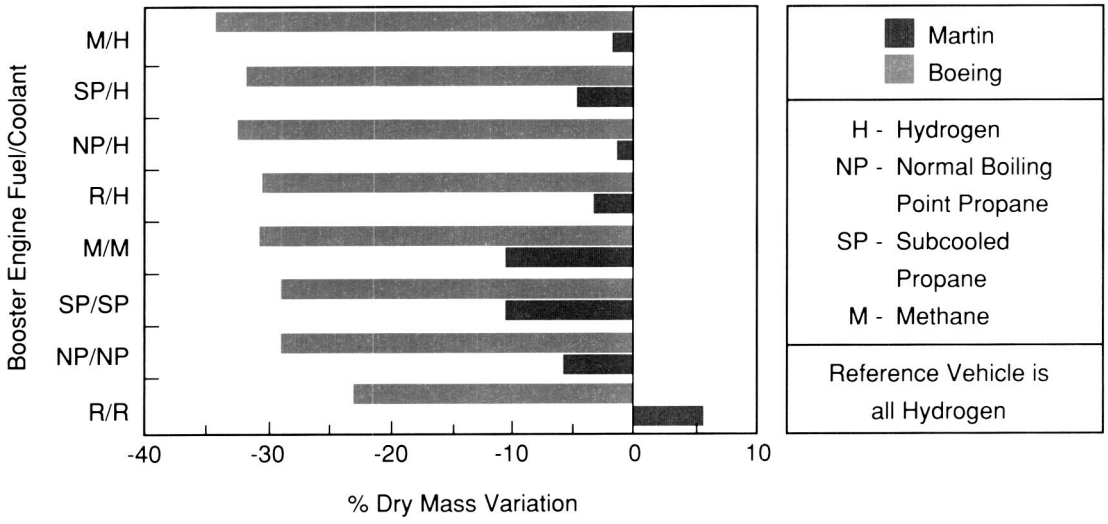

Figure 6. Two-Stage Vehicle Dry Mass Variation

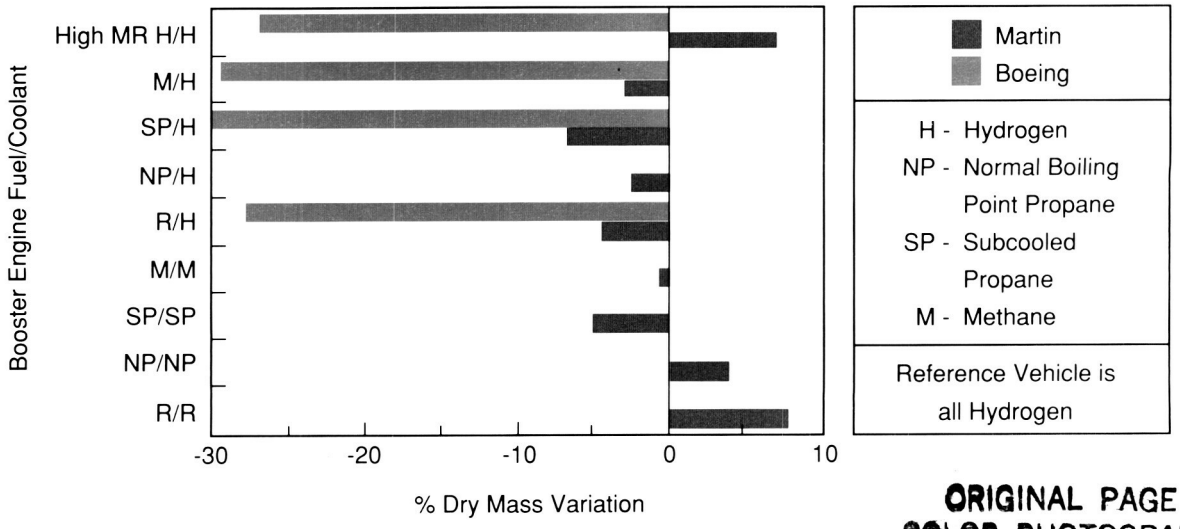

Figure 7. Single-Stage Vehicle Dry Mass Variation

ORIGINAL PAGE
COLOR PHOTOGRAPH

fully reusable, single-stage vehicle with a 13.6-Mg (30-klb) payload to a 93 nmi by 186 nmi by 28° orbit were examined.

Vehicle dry weights were determined for each engine fuel/coolant combination and compared to an all hydrogen mixture ratio of 6.0 version of the vehicle. Figure 6 shows the two-stage vehicle total dry weight comparisons. The comparison shows a basic difference in results between the two companies conducting the studies due primarily to the basic vehicle assumptions each contractor chose to use. One of the basic vehicle differences was that the Martin Marietta booster stage was a "twin-boom" design. The Boeing data shows that using hydrogen cooling for the hydrocarbon fueled booster engines results in a 32 percent decrease in vehicle dry mass while the Martin Marietta data shows only a 2.7 percent decrease. For the fuel cooled engine cases both studies indicated that methane and propane fuels give the lowest vehicle dry mass.

Figure 7 shows the single-stage vehicle total dry weight comparisons. Again the difference in results between the two companies due to vehicle assumptions is apparent. This comparison shows that the single stage vehicle using a hydrogen cooled engine burning LOX/propane would have the lowest weight compared to an all hydrogen vehicle. Also shown is a high mixture ratio hydrogen case in which the boost phase engines are operated with hydrogen at a mixture ratio of approximately 10.0. For this case the Boeing analysis showed a significant weight reduction while the Martin Marietta analysis indicated a weight increase when compared to the reference mixture ratio of 6.0 case.

F. W. Braam/EP52
(205) 544-7055
Sponsor: Office of Aeronautics and Space Technology

Advanced Recovery Systems

Many studies of advanced launch vehicles, including new designs, Space Shuttle derivatives, and more recently, the joint Air Force/NASA Advanced Launch System effort, have shown the potential economic and operational advantages of recovering main engines and other high-cost equipment for reuse. By incorporating the main propulsion and avionics into a single package, generally referred to as the Propulsion/Avionics (P/A) Module, the launch vehicle's most expensive and complex components are combined into a relatively compact package for expeditious recovery, refurbishment, and reuse. This approach allows rapid reuse of the components while maximizing payload placement capability. In concert with future launch vehicle efforts, the development of a precision recovery system for soft touchdown of the P/A Module at the launch site is necessary. The Advanced Recovery System, with a target capacity of over 27,000 kg (60,000 lb), represents a significant advance in the weight carrying capability of deployable ram-air gliding parachutes. The greatest weight the system has demonstrated to date was about 2,300 kg (5,000 lb).

As shown in Figure 8, the P/A Module is being considered in two basic configurations. The high lift-to-drag ratio (L/D) configuration has the advantages of using wheels for a conventional aircraft-type landing, while affording increased landing opportunities when returning to the launch site from orbit. The ballistic, low L/D, configuration is relatively less complex, lighter in weight, and costs less. Weights range from about 25,500 kg (56,000 lb) for a low L/D configuration to almost 30,000 kg (66,000 lb) for a high L/D module. These properties, along with a more detailed definition of each configuration and an assessment of use of the module for cargo return, were the primary activities addressed this year in P/A Module studies. Use of the general shape of the ballistic module for cargo return is feasible, but a Shuttle-sized, 4.57 m (15 ft) diameter object cannot be fitted into the flat shape of the high L/D module.

To provide precision return capability of the ballistic P/A Module (and potentially other applications such as Space Station Freedom crew return), studies have been made of various systems ranging from ballistic parachutes to advanced gliding deployable wings for land recovery. Benefits of a land touchdown as opposed to ocean splashdown include elimination of salt water corrosion, simpler recovery logistics, avoidance of cross-country transportation of large objects (if recovered at the launch site), simpler refurbishment operations, and a potentially smaller inventory of modules because of faster ground processing operations.

Phase I of the Advanced Recovery System for the Advanced Launch Vehicles program examined a broad range of candidate recovery concepts and ultimately defined a system using a 985 m^2 (10,600 ft^2) ram-air gliding parachute (also known generically as the parafoil) for soft-landing the module at a prepared area near the launch site. Phase II extends the effort to include a scaled demonstration of this concept. This program, which is currently underway, will include wind tunnel tests in the 24.4 m x 36.6 m (80 ft x 120 ft) test section at the National Full-Scale Aerodynamic Complex at Ames Research Center. Two similar model parafoil systems, including 3.05 m x 9.15 m (10 ft x 30 ft) and 6.10 m x 18.30 m (20 ft x 60 ft) canopies, will be used to establish scaling effects. Data collected will include basic aerodynamic parameters, control forces, and deflections. Wind tunnel tests are scheduled to begin in August 1988.

The next portion of the program will include a series of 11 aircraft drop tests with weights ranging from 4,500 kg to 9,000 kg (10,000 to 20,000 lb.) The parafoil and weights to be used are about one-third full-scale so the tests will represent the wing loadings of a full-scale module. Man-in-the-loop controls for steering and flare to landing will be incorporated into the later stages of the program. Reliable, controlled

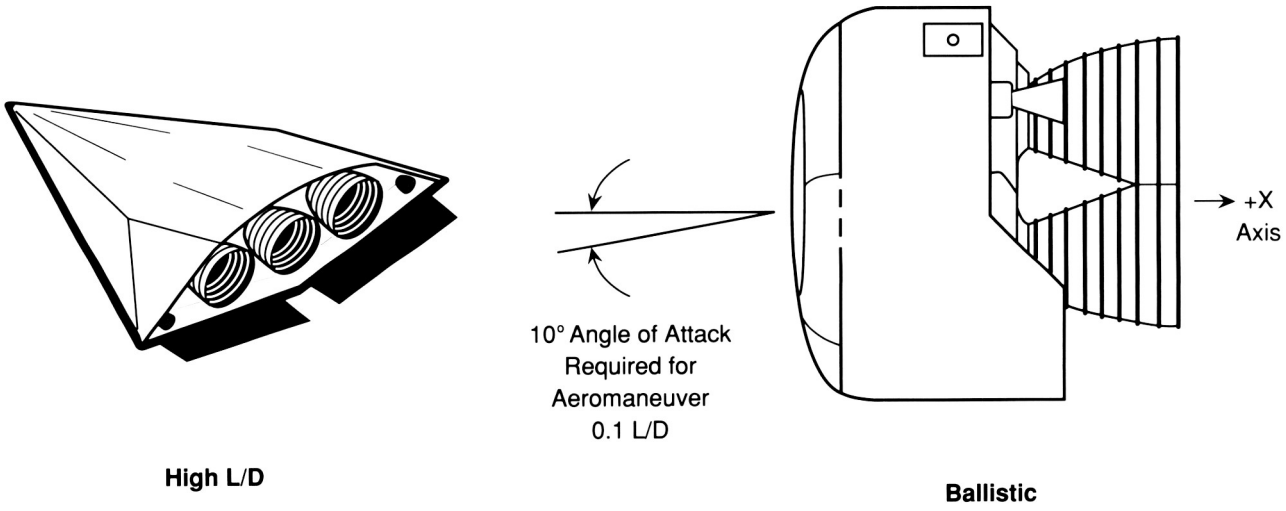

Figure 8. Propulsion/Avionics Module Configurations

deployment of any parachute is critical for successful recovery. The deployment method to be used in this program is unique in that the cells are folded much like an accordion and allowed to open in a controlled manner to minimize opening shock loads. Three stages of controlled opening will be incorporated (Fig. 9). The basic objectives of the drop test program are to demonstrate reliable deployment of the parafoil; demonstrate stability, direction control, and flare to a soft landing; and establish a data base to be used for further parafoil research and provide the basis for development of autonomous control systems. Drop tests will begin at Edwards Air Force Base in California in late summer or early fall 1988 and continue for about one year.

G. W. Johnson/PT01
(205) 544-0636
Sponsors: Office of Space Flight, NASA Headquarters
United States Air Force

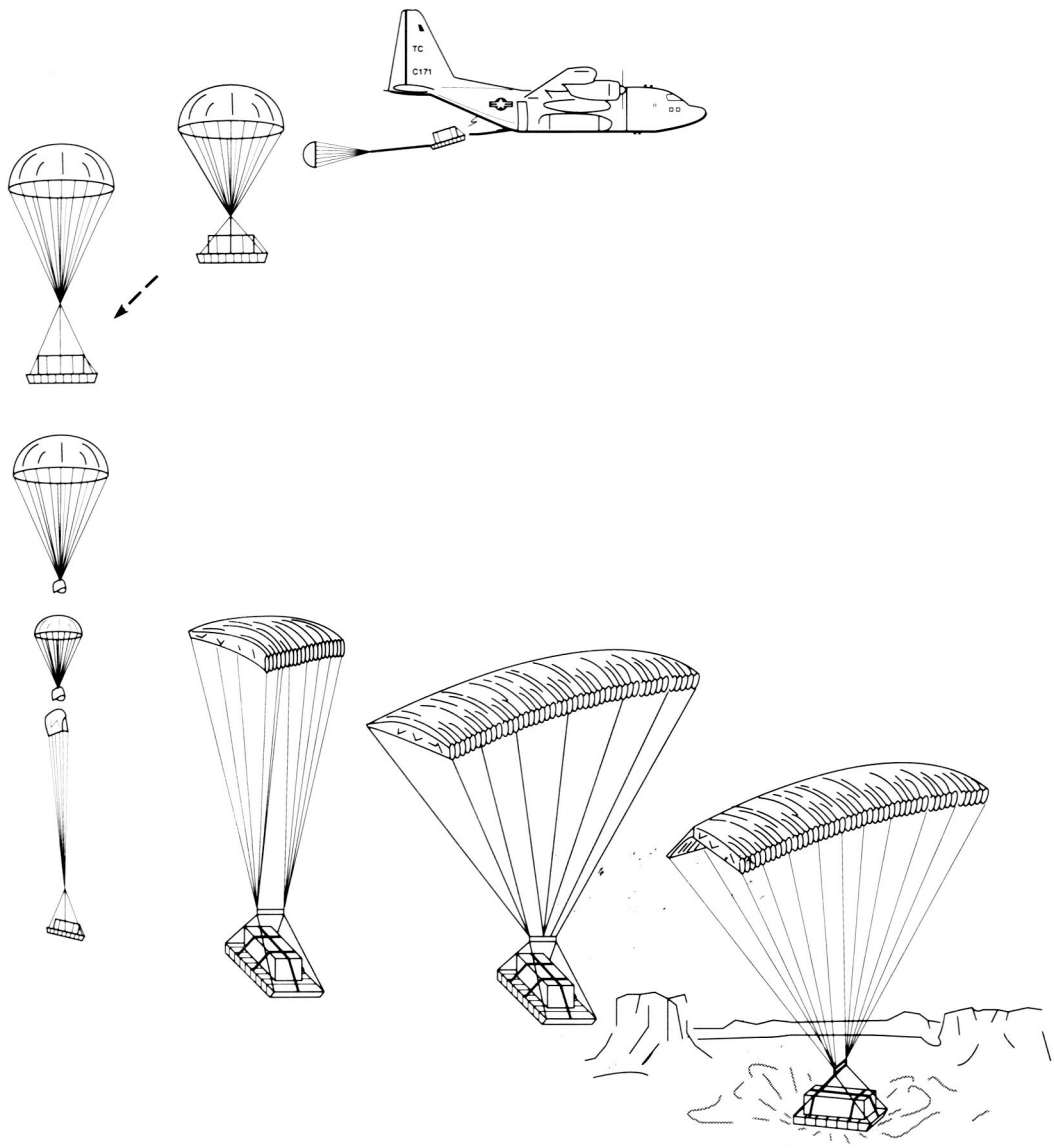

Figure 9. Advanced Recovery System Airdrop Testing

Manrated Orbital Maneuvering Vehicle

The expansion of human presence in space is a major thrust of NASA's current programs. One way to increase the envelope of space accessible to man is to provide a system for short duration and local excursions around the Space Shuttle, Space Station Freedom, and other assets in Earth orbit. Such a system could be constructed from a manrated Orbital Maneuvering Vehicle (OMV), and a manned capsule.

This study analyzes hardware, operations, and software requirements the OMV design must satisfy to qualify as manrated. A major part of the study is the identification of present manrating criteria which apply to the vehicle. The study includes definition and comparison of design and programmatic options for implementing manrating criteria. The study presumes a manned capsule can be attached to the front face of the OMV by standardized mechanisms. Personnel inside the capsule would control the combined OMV and capsule during maneuvers in the proximity of other spacecraft. The manned capsule will be treated as a typical OMV kit to the maximum extent possible. Any major technical concerns with this concept will be identified and analyzed in the study.

The study consists of three tasks: consolidation and update of manrating criteria; analyses of manrating criteria applicable to the OMV, and identification of the impact of those criteria on vehicle systems and operations; and identification of design and programmatic options for implementing manrating requirements.

S. B. Hall/PD24
(205) 544-0517
Sponsor: Office of Space Flight

Lunar and Planetary Transportation

In February 1988, the President announced a comprehensive space policy intended to assure United States leadership in space. One of the three main goals of this policy was the establishment of a long range goal to expand human presence and activity beyond Earth orbit into the solar system. Dr. Sally Ride's report, "Leadership and America's Future in Space," set forth goals for the establishment of manned bases on the Moon and Mars during the 21st Century. These initiatives will require new and advanced vehicle concepts and propulsion systems.

During FY88 MSFC has continued studies in transportation vehicle design and propulsion systems to support both lunar and Mars missions. One emphasis of these studies has been to assess mission scenarios and develop the transportation element requirements and concepts, including spacecraft and landers, to support the missions. Figure 10 shows a preliminary concept for a Mars Transfer Vehicle, required to support a Mars mission in the 2000-2010 time frame. Figure 11 is the Mars Cargo Vehicle that provides ascent and descent modules for the split type missions being studied. Additional study in this area includes identification and evaluation of feasible transportation concepts for the mission scenarios along with trade and sensitivity analyses.

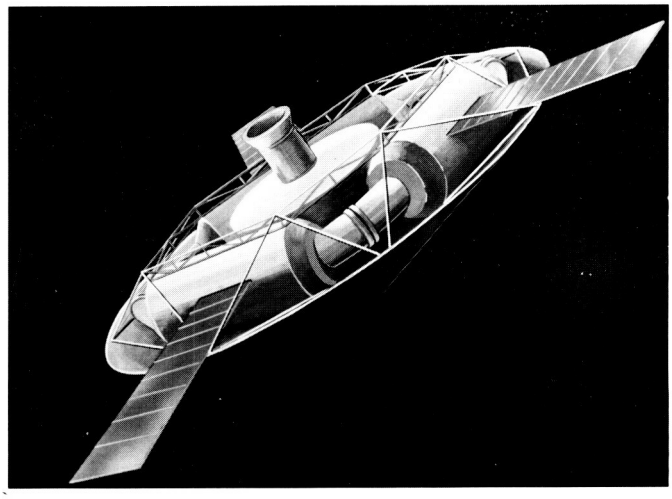

Figure 10. Mars Piloted Transfer Vehicle

Investigations in the propulsion area include analysis of current propulsion systems and their applications to mission scenarios. Propulsion systems investigated have included both high thrust, chemical systems as well as low thrust nuclear-electric and nuclear-thermal vehicle concepts that are being considered for a Mars mission. Trade studies are being conducted based on current predictions of propulsion advancements over the next two decades to determine the impact of these advancements on mission scenarios.

C. F. Huffaker/PT31
(205) 544-0633
Sponsor: Office of Exploration

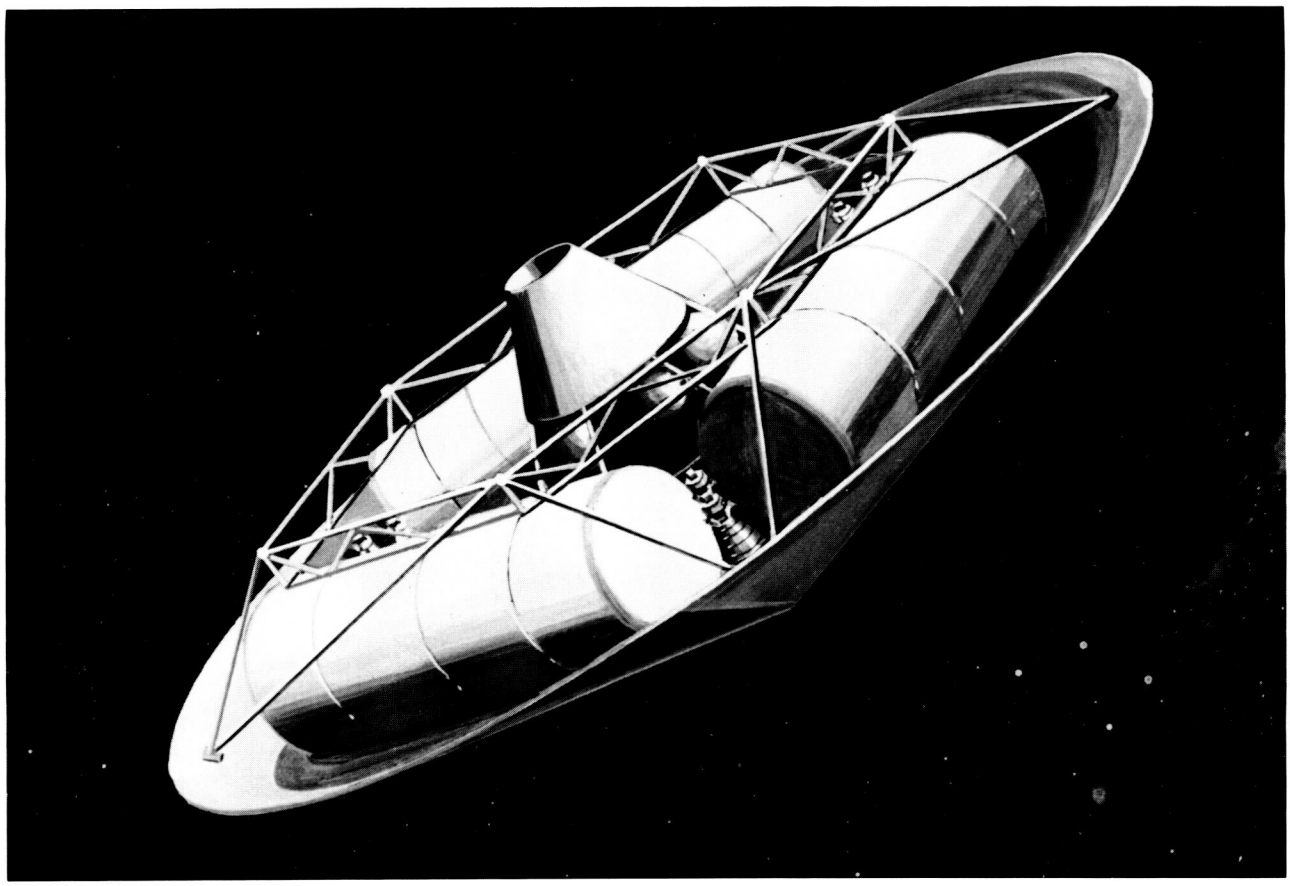

Figure 11. Mars Cargo Vehicle

Space Systems

Materials Processing in Space

The dramatic advances in science and technology in our generation are derived in large measure from the development of new, advanced techniques of research. The capability of space flight opened up an entirely new field of advanced research techniques —microgravity research. Utilizing the microgravity environment, with its reductions in buoyancy forces, hydrostatic pressure, sedimentation, thermal convection flows, and surface contamination, entirely new techniques for manipulating materials, investigating phenomena, and exploiting basic processes are made possible, much like pressure and temperature are now used to optimize processes on Earth. The microgravity environment of space has been shown to have novel, and potentially exploitable effects on key phenomena involved in technologically important processes. Space experiments have potential in both terrestrial and space applications by improving understanding of basic phenomena involved in important industrial processes in the first instance and in the second, producing unique high value-added products in space.

In addition to microgravity, the concept of an orbiting wake shield, Space Ultra-Vacuum Research Facility (SURF), is being studied to exploit the high-vacuum and infinite pumping speed achievable in the wake of a shield moving through space at an orbital speed of 8 km/s or 17,896 mi/h. A Center for the Commercial Development of Space (CCDS) has been established to exploit the potential space applications for the SURF for thin film semiconductor epitaxial growth processes. Other applications such as metals purification in a containerless vacuum environment have also been identified. Math modeling techniques are being developed to predict the environment anticipated in the wake of the SURF shield.

A Materials Processing in Space (MPS) data base was released early in 1988. The document contains information that has been collected and developed to assess the utility of intermediate commercial carriers to pave the way to Space Station Freedom in satisfying the flight requirements of the commercial program. It contains payload descriptions as well as accommodation and system requirements on a group of 70 existing and near-term domestic and foreign MPS payloads. This data base, together with the existing data base of 30 advanced MPS payloads, is being used to perform accommodation studies and operational analyses for MPS R&D on the S.S. Freedom and other proposed accommodating systems.

Studies of advanced payloads to support scientific investigations of materials processing in space in the S. S. Freedom era are in process at MSFC. These studies include: the Space Station Furnace Facility (SSFF), Advanced Protein Crystal Growth (APCG), Modular Electromagnetic Levitator (MEL), and High-Temperature Acoustic Levitator (HAL). These experiment apparatuses for space experiments on technologically important processes are to some extent experiments themselves since they push technology development.

The SSFF will accommodate research and development on a wide range of solidification phenomena and solidification mechanics involved in electronic materials and metallurgy. The facility will be designed to process multiple samples in an automated mode, but will be man-tended for sample exchange, facility reconfiguration, and servicing.

The APCG will concentrate on growing precise, large crystals of medically significant proteins. In addition to the vapor diffusion method of crystal growth, new techniques such as liquid diffusion and containerless growth will be employed.

The MEL is a joint NASA-Department of Energy project. Current plans call for completion of the conceptual design and a technology demonstration in early 1989.

The HAL is a next generation acoustic levitation facility for processes up to 2000 °C. Breadboarding of subsystems is now in progress and flight tests on the KC-135 (low-g) aircraft are planned for late 1988.

The CCDS program was instituted by the Office of Commercial Programs to provide a focus for industrial, academic, and governmental elements to advance through an orderly transition from pure research, through development, to full commercialization of space. Sixteen CCDS's have been established. Of this total, seven are associated with MSFC and five of the seven specialize in MPS. These five centers contain 44 industrial, 16 academic, and 7 other members.

In addition, MSFC, under the auspices of the Office of Commercial Programs, NASA Headquarters, is working on 14 joint agreements with commercial users to do research and development on potential applications of MPS. Two new agreements were added this year.

J. R. Watkins/PS05
(205) 544-0645
Sponsors: Office of Commercial Programs
Office of Space Science and Applications

Gamma Ray Imaging Telescope

A potential follow-on mission to the Gamma Ray Observatory (GRO) currently under study is a Gamma Ray Imaging Telescope using the Shuttle External Tank (Fig. 12). The telescope which may be launched in the early 1990's has been under investigation at MSFC and the Smithsonian Astrophysical Observatory. It would have a collecting area of 2.5×10^5 cm^2 and provide about 10 times the resolution of the GRO. MSFC is now conducting extensive studies to solve the technical problems which have been identified during systems studies. Among these concerns are the protection of the pressurized tank from micrometeoroid penetration and the generation of secondary space debris caused by existing space debris and micrometeoroid impact with the tank insulation. Experimental studies in the MSFC light gas gun facility are currently being prepared to determine the damage to insulation and aluminum tank structure caused by hypervelocity particle impact. Another area of initial concern was the installation of an

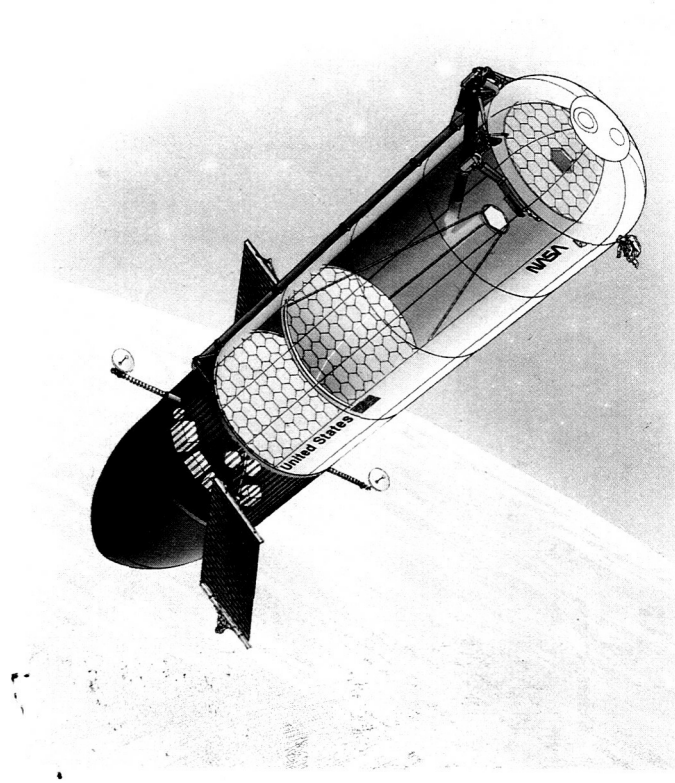

Figure 12. Gamma Ray Telescope in Shuttle External Tank

inflatable mirror through the 36 inch diameter manhole in the aft end of the tank. Testing in the MSFC Neutral Buoyancy Simulator, using a full scale mock-up of the External Tank bulkhead showed that packaging of an 8 m (27 ft) diameter inflatable mirror, and entry through the manhole is possible. Figure 13 shows the inflatable thin film mirror (simulated mirror surface) installed in the tank after entry through the manhole.

In FY88 MSFC continued the development of thin-film mirror technology, which will be required for development of this telescope.

M. E. Nein/PS02
(205) 544-0619
Sponsors: Office of Space Flight
Office of Space Science and Applications

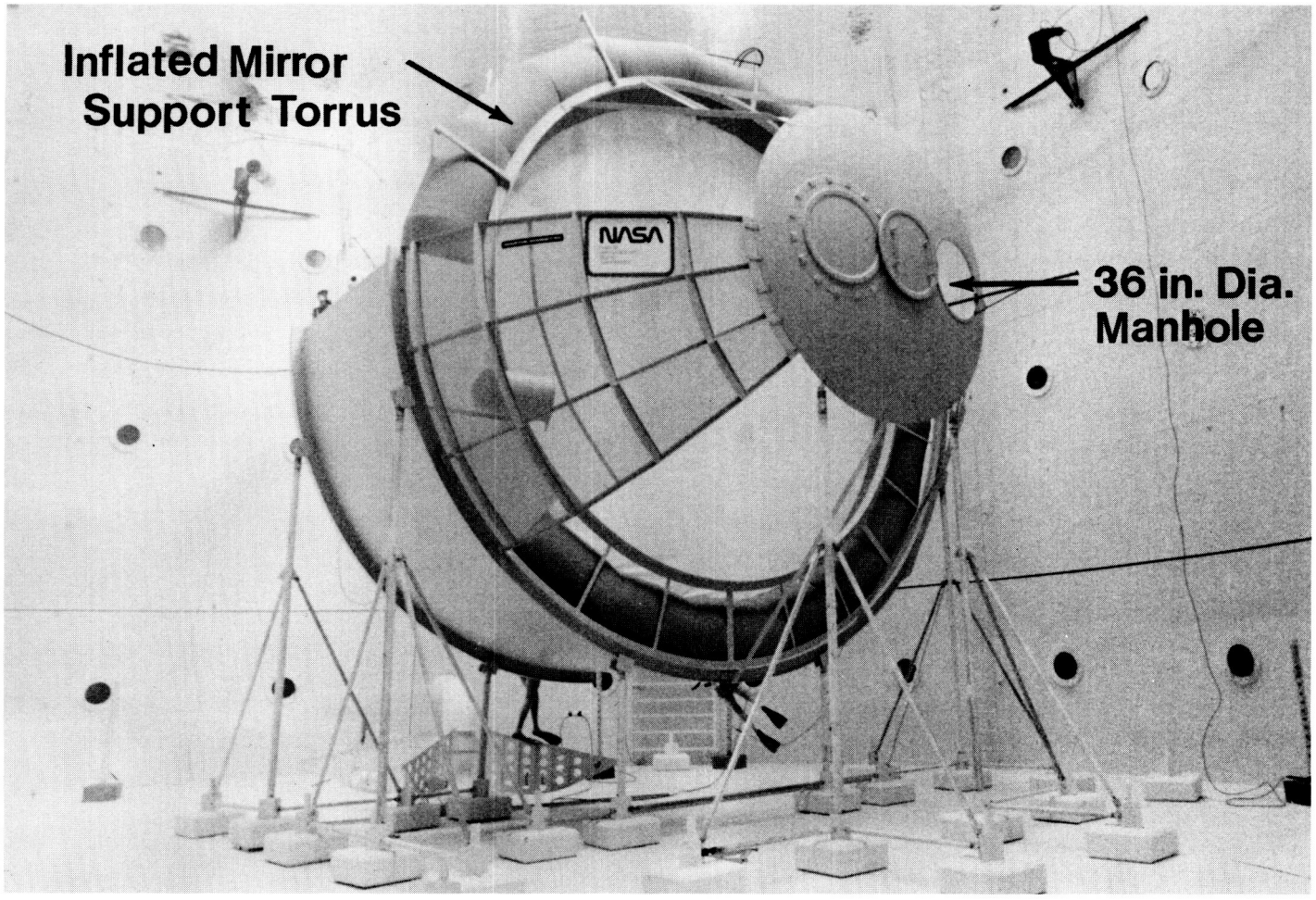

Figure 13. Inflatable Thin-Film Mirror Simulator Installed in Hydrogen Tank Mock-up

Superconducting Gravity Gradiometer

The goal of the Earth System Science Program is to obtain a scientific understanding of the entire Earth system on a global scale. Among the discipline areas supporting this goal is NASA's geodynamics program, which strives to understand the structure, composition, and dynamics of the solid Earth through the use of satellite technology. A vital requirement that is necessary to address many key geodynamics questions is precise knowledge of the Earth's global gravity field.

During the past several years the University of Maryland, under NASA sponsorship, has made progress in the development of a Superconducting Gravity Gradiometer (SGG). This instrument, planned for a satellite mission in the late 1990's, would disclose the global gravity field to a precision of 2 to 3 mgal (1 gal = 10^{-2} m sec^{-2}) with a resolution of 50 km. Besides this primary scientific objective, SGG will also present opportunities to test Newton's inverse square law of gravitation, and could offer an independent experimental test of the Lense-Thirring effect of general relativity.

The SGG utilizes many properties of superconductors to obtain improvement in the sensitivity and stability of gravity sensors. In addition to the obvious reduction of thermal noise and the high mechanical stability of the instrument, the quantization of magnetic flux can be used to obtain very stable means of signal transduction. The instrument concept is shown in Figure 14. An in-line component SGG consists of a pair of spring-mass accelerometers coupled together by a superconducting circuit. Any acceleration will cause a displacement of the proof mass which, because of the Meissner effect, will modulate the inductance of the coil at frequencies down to direct current.

The flight instrument will consist of gradiometers along three orthogonal axes integrated with a six-axis superconducting accelerometer. The accelerometer is required to precisely measure the linear and angular accelerations of the instrument platform. The gravity gradient sensitivity design goal of the SGG is 3 x 10^{-4} E $Hz^{-1/2}$ (1E = 1 Eötvös = 10^{-9} cm^{-2}).

During the past two years an interagency study team, managed by MSFC, has developed preliminary concepts of a free-flying science mission (Fig. 15) and a precursor orbital flight test of the instrument aboard the Shuttle. Progress in instrument development during the past year includes the completion of the first test of the three-axis gradiometer, an extensive analysis of the three-point laboratory suspension system, improvement in the laser tilt sensor, and the fabrication of the mechanical components of the third generation SGG instrument (Model III SGG).

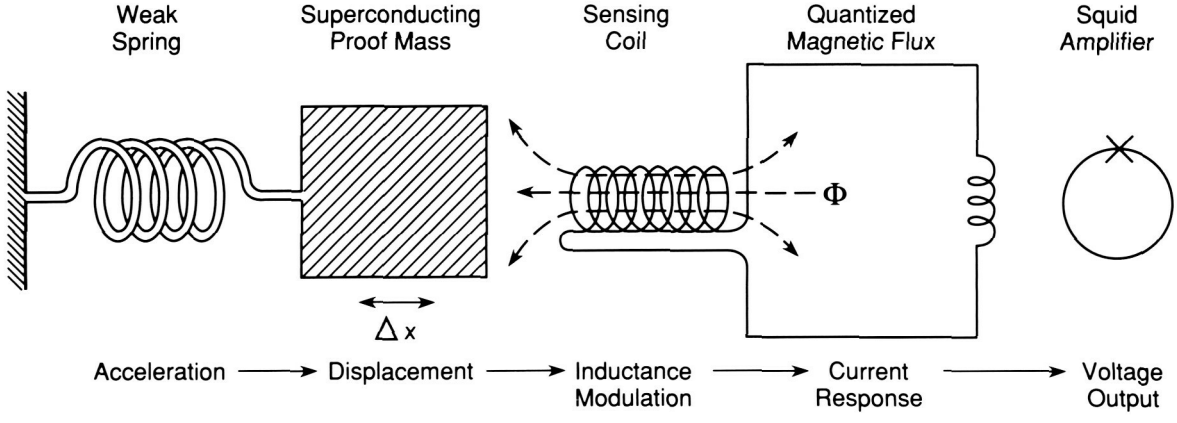

Figure 14. Superconducting Gravity Gradiometer Instrument Concept

The development of the superconducting six-axis accelerometer (sponsored by the Air Force Geophysics Laboratory) with electronic feedback and computer control is an integral part of the SGG. During the past year progress has included the fabrication, assembly, and testing of the prototype accelerometer. An improved design has also been partially fabricated.

During the next year a Phase A study of the precursor test flight of the instrument is planned. Instrument development will continue with improvements to the gradiometer platform, additional tests of the three-axis SGG, and continued work on the Model III SGG.

McNutt, M. and Flinn, E.A. (ed): Geophysical and Geodetic Requirements for Global Gravity Field Measurements 1987-2000. Report of a Gravity Workshop. Colorado Springs, Colorado, February 1987, NASA, November 1987.

Morgan, S.H. and Paik, H.J. (ed): Superconducting Gravity Gradiometer Mission. Vol. II: Study Team Technical Report. NASA TM 86592, August 1988.

S. H. Morgan, Jr./PS02
(205) 544-0614
Sponsor: Office of Space Science and Applications

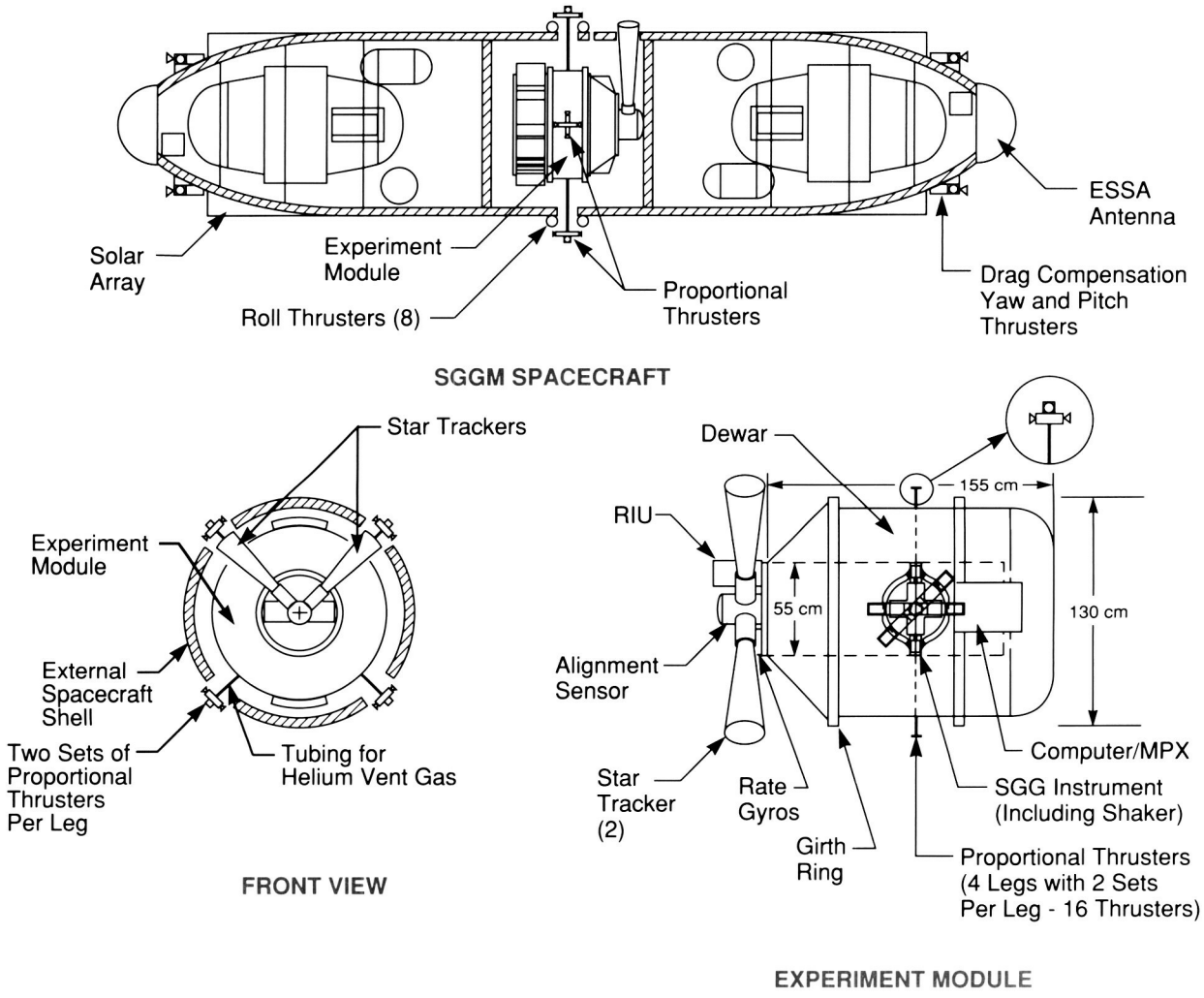

Figure 15. Free-Flying Superconducting Gravity Gradiometer

Tether Applications in Space

Tether Applications in Space (TAS) covers a variety of small experiments currently under study at MSFC. Three of these are described below. The one that has received the greatest attention during the past year is the Small Expendable Deployer System (SEDS). SEDS is a lightweight spinning-reel system designed to deploy a payload attached to a 20-km (12-mi)-long tether that is cut and discarded after use. The primary objectives are to study the dynamics of tether deployment and to validate the SEDS design concept. The deployer system weighs about 16 kg (35 lb) including the 2 kg (5 lb) electronic package and the 6-kg (13-lb) tether and is approximately 25 cm (10 in) in diameter and 36 cm (14 in) in length. The tether is made from a new high-strength, low-density polyethylene fiber called SPECTRA. The hardware development should be completed in 1989 allowing SEDS to fly on a Delta II launch vehicle in 1990 or 1991, if the decision is made to proceed with a flight experiment. Later SEDS versions may fly on the Shuttle. On the first flight, a passive end-mass weighing 14 kg (30 lb) will be deployed toward the Earth at the end of a 20-km tether. The experiment will last about two hours, ending when the full 20 km tether length is deployed and has swung to a vertical position, i.e., the tether is pointing straight toward the Earth. The tether is then cut, allowing it and the end-mass to reenter the Earth's atmosphere. The SEDS concept is shown in Figure 16.

A proposed application of SEDS is the periodic deorbiting of Space Station Freedom waste materials packaged in lightweight containers that can be folded for easy storage during Shuttle trips to the station. A study of this application concluded that a 200-kg (440-lb) SEDS-type deployer using a 100-km (62-mi) length tether can deorbit 2,000 kg (4,400 lb) of S. S. Freedom waste.

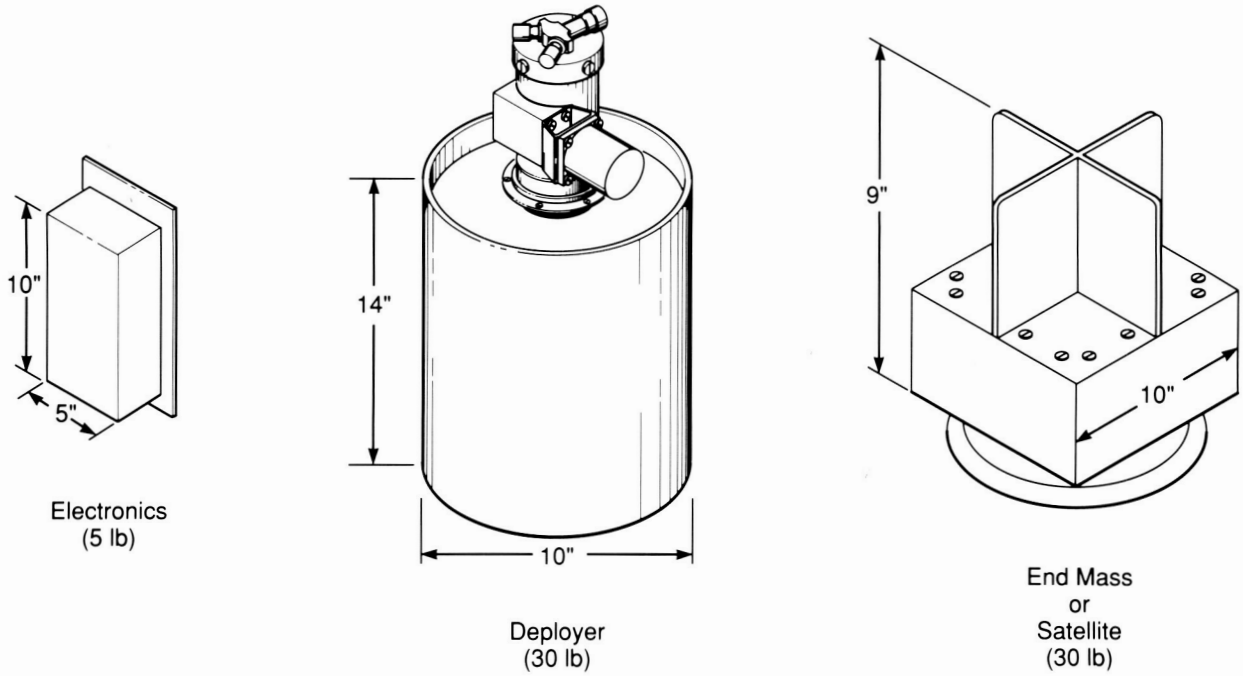

Figure 16. The Small Expendable Deployer System

A study is underway to examine the feasibility of the SEDS-type of deployment of waste materials, and other packages as well, from S. S. Freedom. To do this, MSFC is studying a Shuttle-based Tether Initiated Space Recovery System (TISRS) experiment which would use SEDS to reenter an existing reentry capsule. To date, the major conclusions are that the TISRS is feasible even though some fairly major capsule modifications have been identified as necessary. Another significant result is that the placement accuracies of the capsule using SEDS have been calculated and appear to be adequate. Current TISRS activity is focused on examining and solving the problems of integrating an instrumentation and data system, built by the Italian Space Agency, into the existing reentry capsule.

Another TAS activity is a study to define a small free-flying satellite, called the Getaway Tether Experiment (GATE), that is Shuttle launched. Its primary purpose is an examination of tether dynamics during deployment and operational periods.

Other GATE experiment goals are to measure particle impacts and the radar cross sections of tethers and to obtain some data on the ultra-low-frequency radio propagation effects of tethers. After launch, GATE will split into two smaller satellites (mother-daughter) and be connected by a 1-km (.62-mi)-long electrodynamic tether. The mission scenario for GATE is shown in Figure 17. During the 10-day experimentation period, the electrodynamic tether will alternate between periods of power generation (to recharge batteries) and thrust generation (to boost the orbit altitude).

J. K. Harrison/PS04
(205) 544-0629
Sponsor: Office of Space Flight

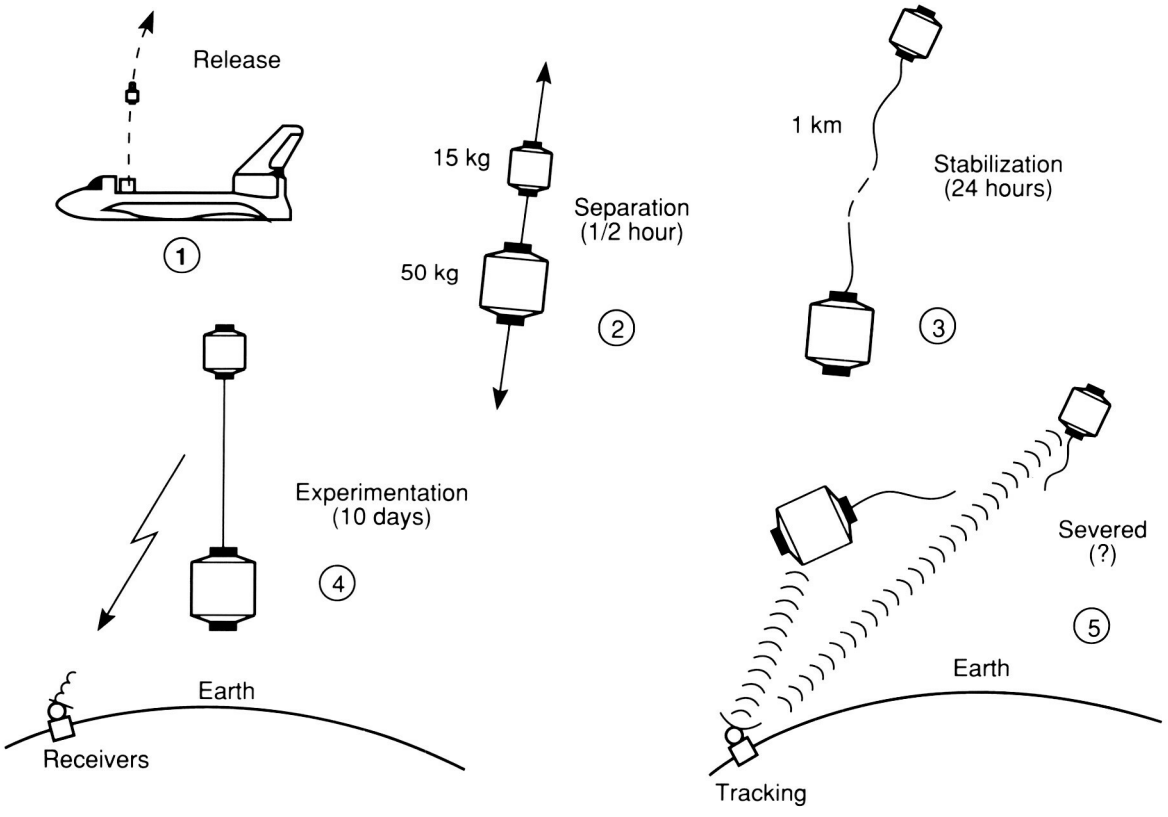

Figure 17. The Getaway Tether Experiment

Advanced Solar Observatory/ Space Station Freedom Payloads

Several scientific payloads are currently being studied which may be implemented on Space Station Freedom. The payloads take advantage of the unique resources provided by S. S. Freedom (Fig. 18), such as high power and thermal dissipation, the ability to host instruments of large mass that require large footprints, the ability to coordinate observations from multiple instruments, maintenance and servicing functions, and the ability to perform instrument modifications and upgrades while on orbit.

The objectives of the Advanced Solar Observatory (ASO) (Fig. 19), are to significantly advance the study of the Sun to determine and understand the fundamental processes which drive solar dynamic phenomena. Development continues on a comprehensive set of solar telescopes and instruments which permit simultaneous and coordinated measurements across the energy spectra ranging from gamma rays and energetic neutrons, soft x-rays, extreme-ultraviolet and ultraviolet, visible light, and low-frequency radio emissions. Space Station Freedom will host a set of high energy spectrometers, a multitelescope high resolution telescope cluster, and the low-frequency radio facility. A ground based command and data facility will be used to coordinate measurements taken from S. S. Freedom instruments with data taken from other free flying and ground based solar instruments.

A contracted study is defining the accommodation requirements for the ASO on S. S. Freedom.

W. T. Roberts/PS02
(205) 544-0621
Sponsors: Office of Space Science and Applications
Office of Space Station

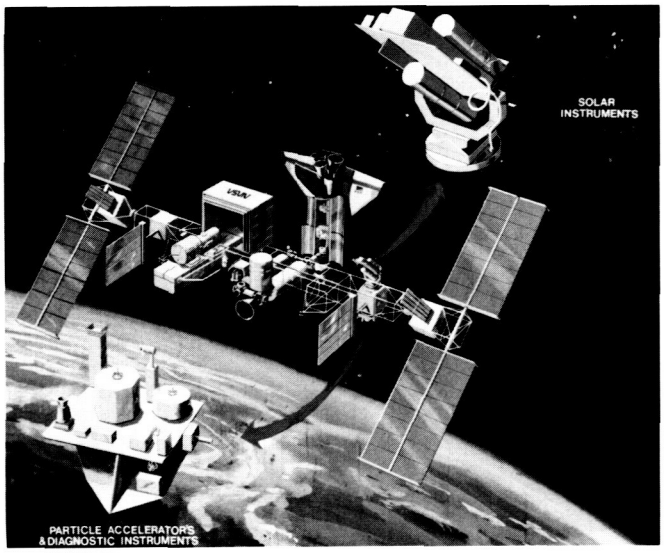

Figure 18. Advanced Solar Observatory S. S. Freedom Payloads

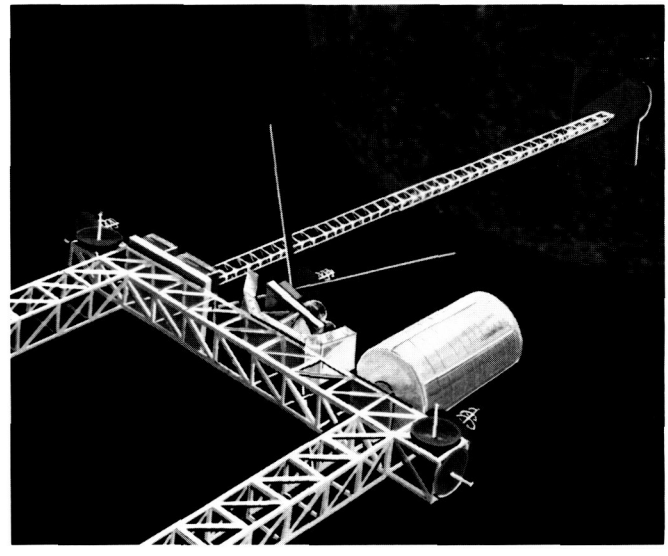

Figure 19. The Advanced Solar Observatory

Solar Terrestrial Observatory

The Solar Terrestrial Observatory (STO), a candidate Space Station Freedom payload (Fig. 20), is comprised of a combination of scientific instruments intended to perform coordinated experiments and observations of great interest in solar physics, magnetospheric/ionospheric physics, and atmospheric physics. The goal of STO is to study the energy coupling processes of the solar terrestrial system. To accomplish this goal, continuous measurement must be made of solar irradiative output in the important spectral regimes, and simultaneous measurements of atmospheric emissions and dynamics. Measurements of magnetospheric and ionospheric processes and dynamics are required to completely measure the energy propagation. In addition, active experiments will be performed to stimulate the environment to determine the energy coupling mechanisms of the Earth-space system.

Several international solar terrestrial meetings have been held to coordinate the development of the STO. A solar terrestrial summer study is currently being planned this year. The Solar Terrestrial Strategy Panel will be comprised of scientists active in the fields of solar terrestrial research.

W. T. Roberts/PS02
(205) 544-0621
Sponsors: Office of Space Science and Applications
Office of Space Station

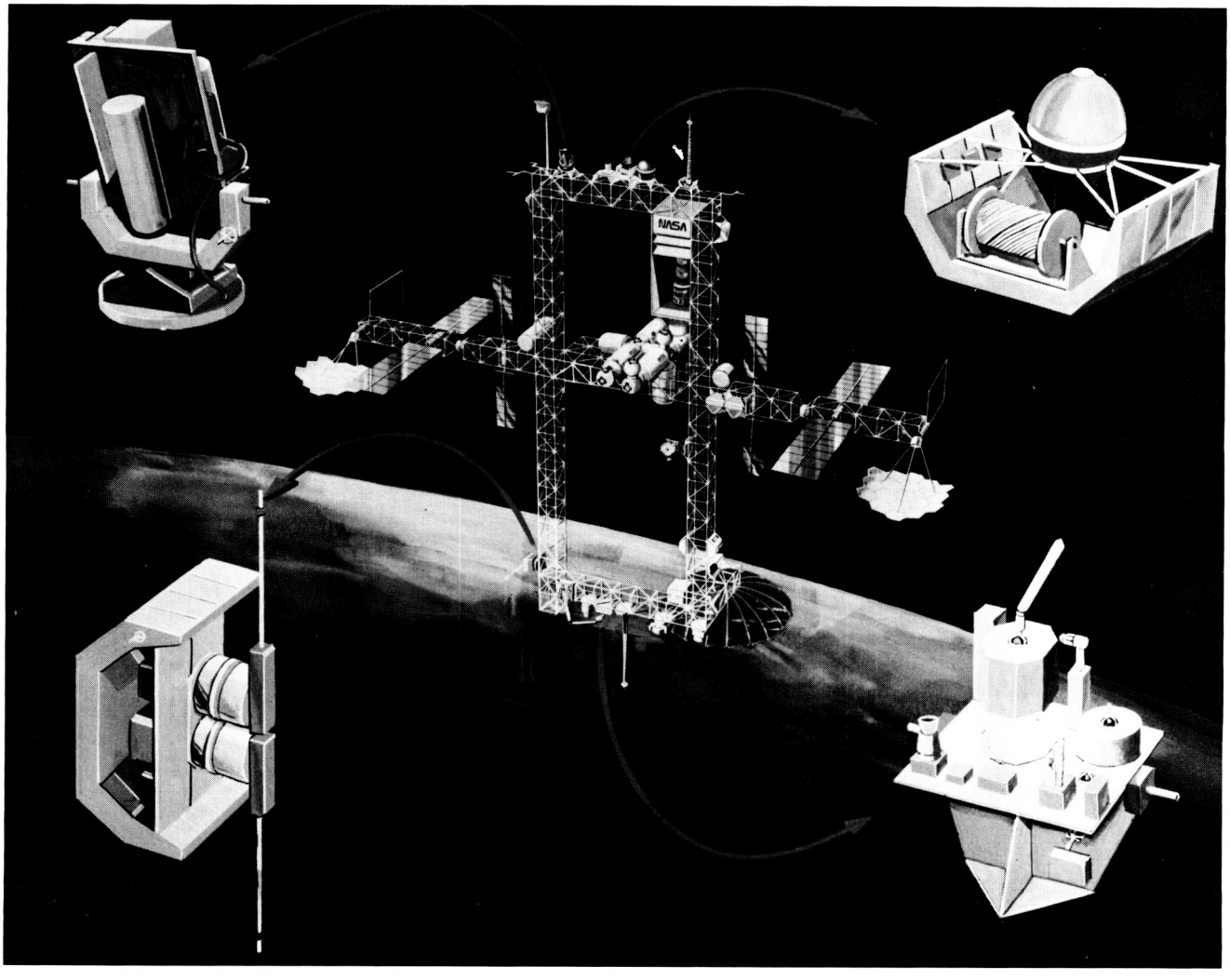

Figure 20. Solar Terrestrial Observatory Instruments on S. S. Freedom

Pinhole Occulter Facility

The Pinhole Occulter Facility (POF) is an important solar observatory. It will be flown as a Space Station Freedom attached payload using nonrefracting optical techniques to image hard x rays from the sun to study nonthermal processes at the solar surface. The large separation needed for this imaging requires the use of a 32 m (105 ft) boom. The long baseline is also used to provide external occulting for white light and ultraviolet coronal instruments. The x rays will be imaged to sub-arc-second resolution and in higher energies than previously possible. Coronal observations will be with higher spatial resolution, lower scattered background radiation, and to a lower depth in the solar corona than was possible before.

During 1988, developmental work on the science instruments and facility subsystems continued. The Gamma Ray Imaging Detector Balloon Program is being developed as a test bed of the Fourier-transform imaging experiment on the POF. In 1988, the POF will be proposed as an S. S. Freedom attached payload. The aspect sensor subsystem will be breadboarded in 1989. An accommodation study of the POF on S. S. Freedom will also be completed in 1989.

J. R. Dabbs/PS02
(205) 544-0623
Sponsor: Office of Space Science and Applications

Tropical Rainfall Measurement Mission

The Tropical Rainfall Measurement Mission (TRMM) is being proposed as a joint U.S.–Japan mission for the study of tropical rainfall systems and their impact on global weather cycles. TRMM would include the first precipitation radar ever flown in space, which would be provided by Japan. MSFC Program Development has completed a Space Station Freedom accommodations study of the TRMM payload (a radar, at least one microwave radiometer, and a visible and infrared cloud imager – Fig. 21). The study concluded that TRMM could be accommodated by S. S. Freedom. For the purposes of the study it was assumed that all of the instruments would be mounted on a Spacelab pallet, which would be pointed by a payload positioning system which would be offset by 45° to avoid a possible gimbal-lock situation while the positioning system was trying to keep the payload pointing vertically downward.

A separate activity at Goddard Space Flight Center has addressed the possibility of flying TRMM on a multimission spacecraft. Recently the TRMM payload has been reduced in scope to cut costs due to the high expense of this satellite in a low altitude (350 km) orbit. In an effort to cut their costs, Japan has recently decided to provide a single frequency radar instead of a double frequency radar for TRMM. The radar design now uses an electrical scanner. Japan has also volunteered to launch TRMM on its H-2 rocket if TRMM is flown by itself.

R. W. Spencer/ED43
(205) 544-1686
Sponsor: Office of Space Science and Applications

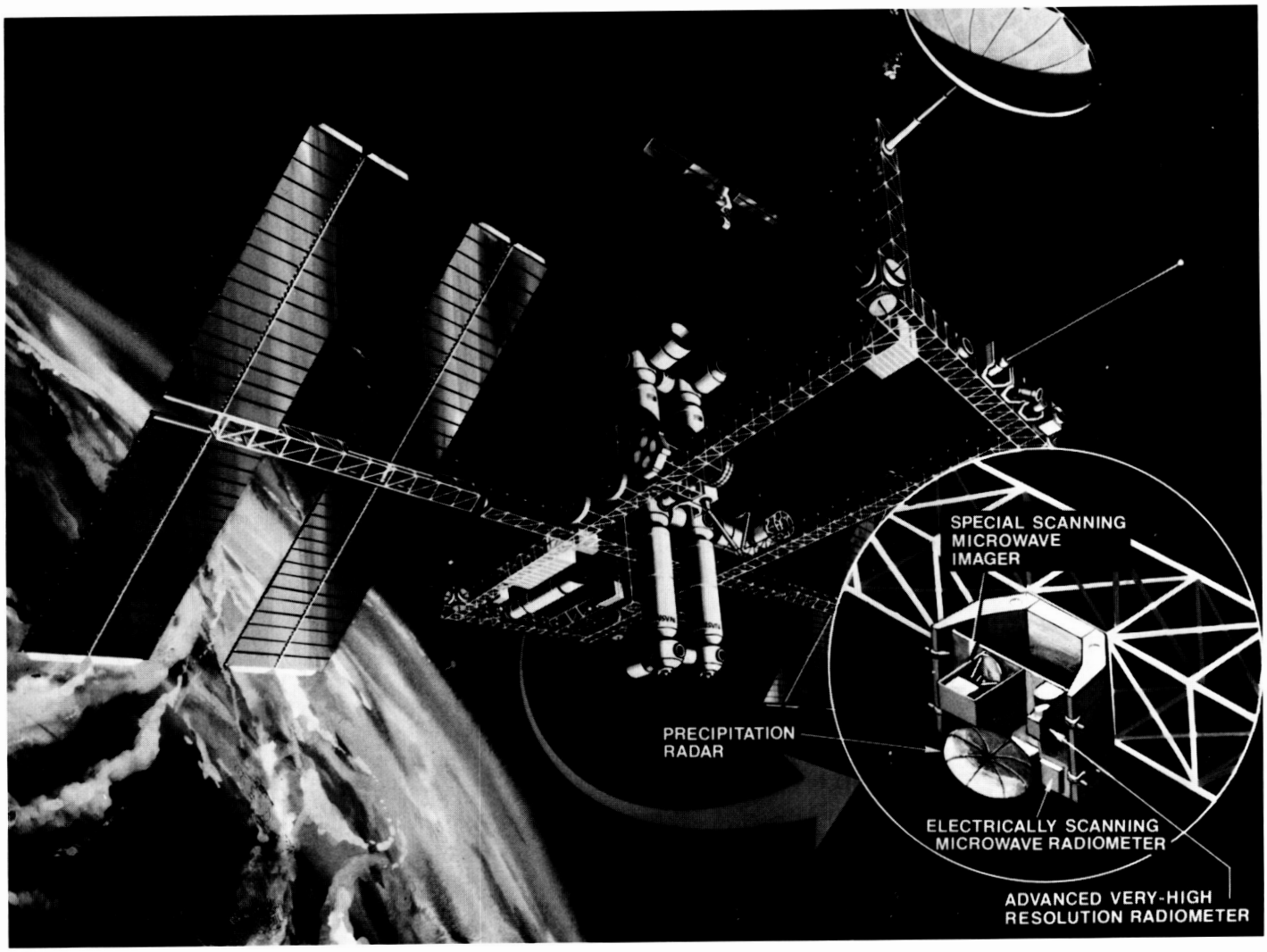

Figure 21. The Tropical Rainfall Measurement Mission on S. S. Freedom

Laser Atmospheric Wind Sounder

The Laser Atmospheric Wind Sounder (LAWS) represents a major step toward the goal of making routine global wind profile measurements from space. Its purpose is to improve our understanding of the atmospheric wind field by investigating many interdisciplinary scientific questions from a polar orbiting platform of the Earth Observing System (EOS) (Fig. 22) or from Space Station Freedom (Fig. 23). Wind profiles obtained by the LAWS system will provide research information essential for advancing the skill of numerical weather prediction, furthering our knowledge of large-scale atmospheric circulation and climate dynamics, and improving our understanding of global biogeochemical and hydrologic cycles. LAWS is a facility instrument on the EOS and is also being proposed as an S. S. Freedom attached payload.

The system technology required for space-based operation is the coherent CO_2 Doppler lidar technique. This system, operating in the eye-safe infrared wavelength (9 to 10 μm) has been used successfully in ground-based and airborne wind measurement systems. The space system currently envisioned consists of a pulsed, frequency-controlled CO_2 laser transmitter, a continuously scanning transmit-and-receive telescope, a heterodyne detector, and a signal processing system. Initial studies have shown that this instrument concept for LAWS can be accommodated on the EOS polar orbiting platform or S. S. Freedom.

A request for proposal to further define the optimum LAWS configuration was released during the second quarter of 1988. One or more contracts will be awarded for this initial effort. Option provisions in the contract will permit proceeding to the preliminary design phase. A LAWS science team will be selected in early 1989 composed of scientists active in the fields of atmospheric dynamics and laser technologies.

D. E. Fitzjarrald/ED43
(205) 544-1651
Sponsors: Office of Space Science and Applications
Office of Space Station

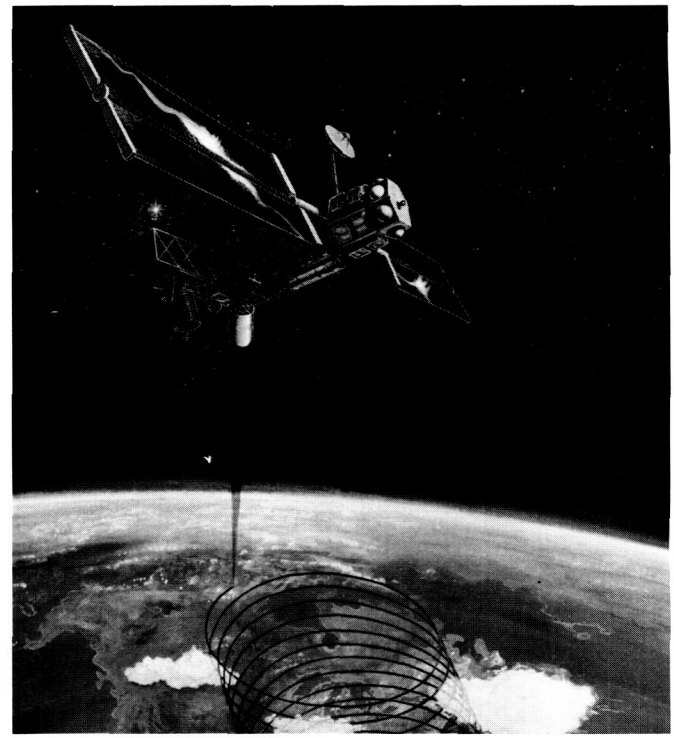

Figure 22. The Laser Atmospheric Wind Sounder Mounted on a Free-Flying Polar-Orbiting Platform

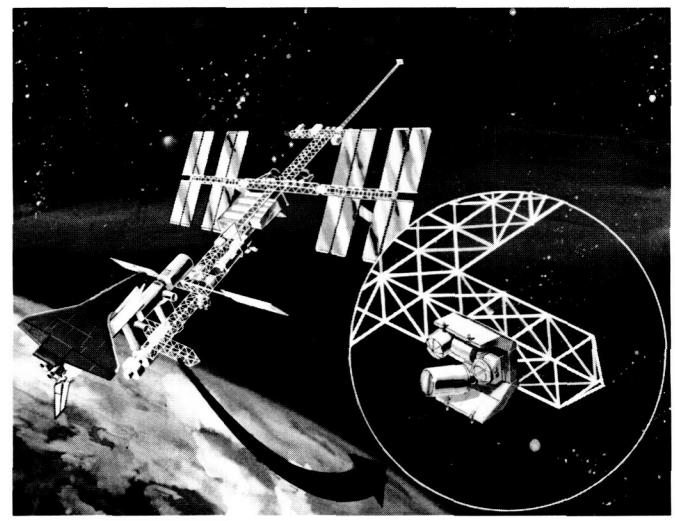

Figure 23. The Laser Atmospheric Wind Sounder Mounted on S. S. Freedom

Geostationary Lightning Mapper

A geostationary based instrument called the Lightning Mapper Sensor (LMS) is currently under development. This sensor will be capable of detecting and locating up to 90 percent of all lightning flashes that occur within its field of view. The proposed spatial coverage includes all of the continental United States, Latin and South America as far south as the Amazon Basin, the Caribbean, and parts of the Pacific and Atlantic oceans.

The LMS uses an innovative optical design that has been optimized for the unique signal from lightning. Lightning is accompanied by the sudden release of electrical energy which is converted into rapid heating in the vicinity of the channel, the generation of a shock wave, and electromagnetic radiation ranging from extremely low-frequency radio waves to x rays. One of the strongest radiation regions is at visible wavelengths, which account for almost 1 percent of the total energy released: 100 to 1,000 MW of light. These optical emissions result from the dissociation, excitation, and subsequent recombination of atmospheric constituents which are primarily affected by electron bombardment and the sudden heating of the lightning channel. The heating is so intense that emissions occur primarily at discrete atomic lines, with some continuum at shorter wavelengths. The strongest emission lines are produced by neutral oxygen and neutral nitrogen and occur in the near-infrared from 7774 Å to 8683 Å.

With present technology, the two viable approaches for the detection and location of lightning events are either optical or radio frequency (RF) techniques. For ground-based operations, RF approaches have been preferred because optical systems suffer from obscuration, attenuation, and limited range (line of sight). Conversely, for remote sensing from space, optical techniques offer many advantages. Light is not affected by the ionosphere or magnetosphere. The relatively short wavelengths of light permit accurate direction-finding with small detectors. The large signal strength of the lightning event at optical wavelengths provides usable signals from a geostationary orbit. On the other hand, radio signals, at longer wavelengths, are strongly attenuated or refracted by the ionosphere and thus are unsatisfactory for accurate lightning direction-finding from orbit. At higher RF the lightning source strength is weaker than the cosmic ray background noise at geostationary altitudes and thus lightning detection would be extremely difficult.

A space-based sensor for the optical detection of lightning is conceptually a simple device. It is basically a staring imager that is optimized to detect and locate lightning events. The LMS images a scene in much the same manner as a television camera; however, because of the transient nature of lightning, its spectral characteristics, and the difficulty of daytime detection of lightning against the brightly lighted cloud background, actual data handling and processing differs vastly from that required by simple images. The heart of the lightning mapper consists of a very large mosaic-array, focal-plane assembly, tightly coupled to high-speed processing electronics. This signal processor performs real-time discrimination between lightning events and the background, compressing the total data rate by approximately a factor of 1,000,000. A request for proposal for the lightning mapper is being released to industry. The resulting contract will require a detailed design of the LMS and will contain a hard option, which, if exercised, will cover the final design and fabrication of the instrument. The LMS is scheduled to fly aboard the National Oceanic and Atmospheric Administration's Geosynchronous Operational Environmental Satellite-M.

H. J. Christian/ED43
(205) 544-1649
Sponsor: Office of Space Science and Applications

Control and Structures Experiment in Space

The Control and Structures Experiment in Space (CASES) will investigate critical control technology that is needed to stabilize and point large flexible structures in space. The control of a deployable 32-m boom, of a design identical to the one used in the Solar Array Flight Experiment program, will be implemented using small cold-gas thrusters for pointing. Angular momentum exchange devices will be used for active damping to suppress vibrations. Since the boom is rigidly attached to the orbiter, the orbiter/boom system may be pointed to a predetermined target for a period of at least 30 minutes. In addition, tracking and slewing of the orbiter at small angular rates will be demonstrated. A significant side effect of this control method is that the orbiter can be stabilized for significant periods of time with very low g levels.

The CASES will provide for accommodation of an astrophysics/solar hard x-ray imaging experiment. This experiment will address important issues in high energy astronomy, such as the identification and characterization of the energy source seen at the galactic center and the energy release mechanisms in solar flares. Imaging of hard x rays is accomplished by aperture plates placed at the tip of the boom. This provides both coded aperture and Fourier-transform imaging on position sensitive proportional counter arrays placed in the cargo bay at the base of the boom. The large separation between masks and detectors makes possible high spatial resolution.

J. R. Dabbs/PS02
(205) 544-0623
Sponsors: Office of Aeronautics and Space Technology
Office of Space Science and Applications

Geostationary Facilities

MSFC's geostationary facilities studies this year have been concentrated in two areas. The largest area of activity has been the study of an Earth Observing System (EOS) platform. This would be one element of the proposed new Mission to Planet Earth initiative. This proposed segment would consist of at least five geostationary platforms, spaced around the globe, with the first one placed into operation in the late 1990's. International participation is expected to include Japan and Europe, with each providing and operating a platform. Each of these EOS platforms would include perhaps a dozen sophisticated instruments, primarily for observing the Earth's atmosphere and surface. A group of scientists, including National Space Development Agency of Japan and European Space Agency scientists, have been working with NASA platform designers to identify the most functional concepts and verify overall feasibility of the EOS platform idea. Figure 24 illustrates one of the many EOS platform concepts being considered. This particular platform would weigh about 5,900 kg (13,000 lb).

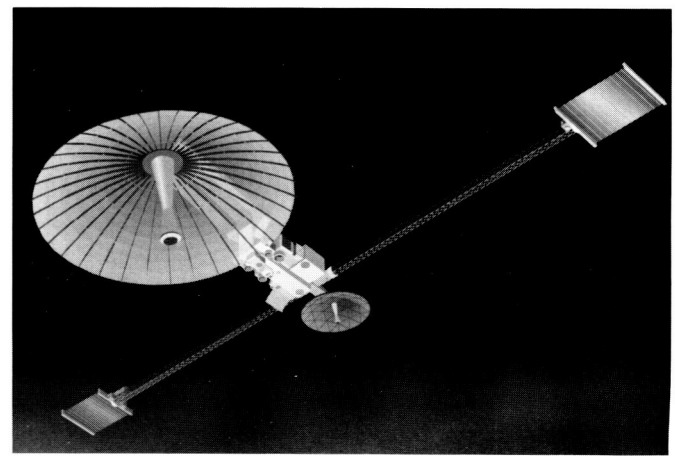

Figure 24. A Typical Geostationary Earth Observing System Platform

A major challenge of the Mission to Planet Earth initiative will be to integrate and manage the flow of data from all sources, including the planned polar EOS platforms. Since this is an international program, information will have to be disseminated to and communicated among scientists all over the world in a timely manner. These platforms may be interconnected by interplatform data links to facilitate the data flow.

MSFC's second area of concentration has been a broad assessment of geostationary facilities, manned and unmanned, which are likely to be implemented in the first half of the 21st century. This study investigated potential interrelationships and sequences/paths for the evolution of such facilities. Major facilities at geosynchronous orbit (GEO) are likely to include Earth observing platforms and large unmanned astrophysical facilities as well as communication platforms. Commercial communications platforms will probably become an absolute necessity, due to the crowding of the high-demand regions of the GEO equatorial arc. These platforms will benefit from the large-antenna experiences of earlier Earth-observing platforms.

The projected proliferation of large expensive facilities in space will motivate the establishment of a servicing infrastructure. This will be especially true for GEO facilities due to their high investment value and their increasing complexity. Growth of GEO facilities will undoubtedly be favorably impacted by concurrent international planetary and lunar exploration activities. Contributing factors will be the existence of low-Earth orbit assembly and testing facilities, the reduced cost of space transportation, availability of more mature space transportation vehicle technologies, and the by then widespread availability of humans in space.

R. H. Durrett/PS04
(205) 544-0628
Sponsor: Office of Space Science and Applications

Cryogenic Storage Facility

Advanced NASA mission planning, such as the Space Transfer Vehicle (STV), Lunar initiatives, and the Manned Mars Mission will require enhanced space support facilities. Long-term, orbital storage of cryogens in a microgravity environment will be vital to such advanced missions.

Propellant depot conceptual studies concluded that a 90,000 kg (200,000 lb) liquid hydrogen/liquid oxygen facility would be capable of supporting a space based STV. Additionally, growth options to support a Lunar initiative, requiring approximately 227,000 kg (500,000 lb), appear feasible. However, the Manned Mars Mission places severe requirements on a depot facility, upwards of 454,000 kg (1 million lb), and may best be supported by alternative means.

The propellant depot tankset design (Fig. 25) contains several advanced cryogenic storage and management devices, such as a thermodynamically coupled tankset utilizing vapor cooled shields, thick multilayer insulation, a screen channel liquid acquisition device, and possibly an active refrigeration system. The depot tankset, 45,400-kg (100,000-lb) capacity, is configured for a dry launch in the Shuttle Orbiter bay and designed to be returned to Earth for refurbishment by way of a Shuttle mission. The depot design is also compatible with expendable launch vehicle (ELV) concepts.

Design trades indicate that a Space Station Freedom based depot would require a no-vent active thermal control system, due to station safety/contamination concerns. A coorbiting platform depot facility could be an all-passive system, reducing depot risk and complexity. ELV resupply tanker trades have resulted in Earth-to-orbit propellant tanker capacities of 45,400 to 54,480 kg (100,000 to 120,000 lb) to support facility operations. The tanker designs are compatible with Shuttle-C and advanced launch system concepts for Earth to orbit delivery.

Technology and advanced development programs are underway to support advanced cryogenic systems needs. The requirements have been identified and prioritized. Combinations of ground testing (components and systems) have been initiated. Space flight testing options are being evaluated by NASA in order to develop a realistic test program.

Further planned study activities include: enhancing depot sensitivity analysis with respect to advanced mission models and the development of a systems-level thermodynamic code to support depot designs. The code, Cryogenic On-Orbit Liquid Analytical Tool (COOLANT), will model a depot tankset configuration and yield boiloff estimates, tank heat leaks, and transfer operation predictions. COOLANT (planned availability – first quarter 1989) will be utilized in concept design efforts as a quick turnaround depot performance analysis tool.

N. S. Brown/PD22
(205) 544-0505
Sponsor: Office of Space Flight

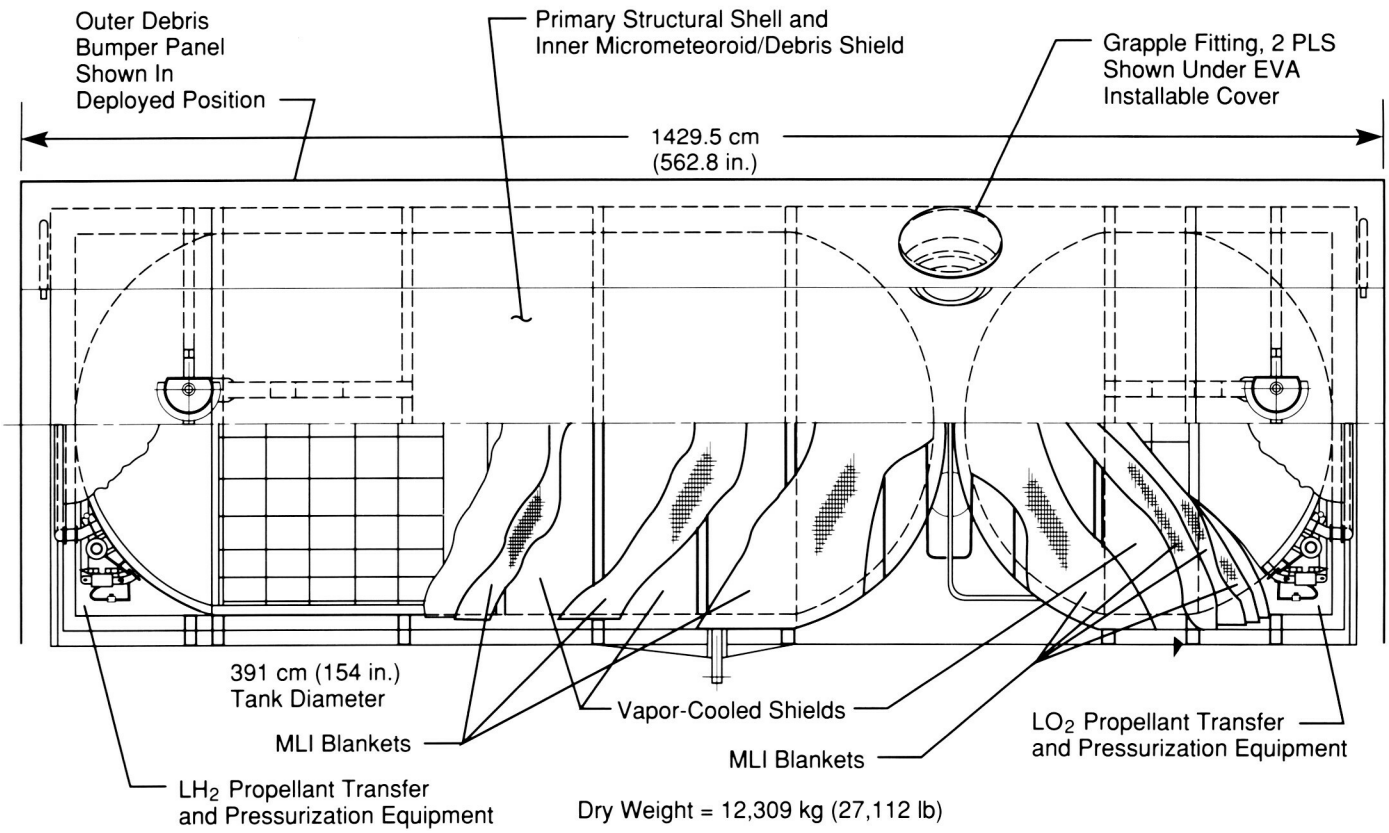

Figure 25. All-Passive, 45,400 kg (100,000 lb) Propellant Depot

Satellite Servicer System

During 1988, a concentrated effort has been initiated to define a Satellite Servicer System (SSS). This system draws on many years of analytical studies and robotic simulation activities conducted at MSFC in the area of automated maintenance of free flying spacecraft at the module level. These studies have clearly shown that spacecraft programs may derive considerable economic benefits by combining modular maintenance and expendable resupply. Further, real-time demonstrations conducted at MSFC have shown that the technology exists to build an automated system. Such a system could find application as a kit on the Orbital Maneuvering Vehicle (OMV), operating out of the Shuttle or from Space Station Freedom.

It is expected that the system will be jointly funded and developed by NASA and the Department of Defense (DOD). Current project phasing calls for an Orbiter in-bay demonstration of the system by mid-1993 and a free-flight demonstration on the OMV by mid-1994 shortly after the OMV becomes available.

The DOD elements require a fully autonomous system which would automatically rendezvous and dock. Subsequent to docking, the system would perform automated maintenance characterized by module exchange plus expendables resupply.

System concepts which may mature into the final design range from the MSFC Integrated Orbital Servicing System (Fig. 26) to the Space Station defined Flight Telerobotic Servicer (Fig. 27). NASA Headquarters plans to establish system requirements by October 1988 to support the preliminary design initiation in early 1989.

Center roles have not yet been finalized; however, it is expected that MSFC, JSC and GSFC will be involved. Since the system must be integrated as a kit on the OMV to support a servicing mission and subsequently removed to allow the OMV to perform other types of missions, a significant OMV integration role must be performed by MSFC. Further, the MSFC robotic demonstration laboratory and servicer system concepts should make a large contribution to the project.

J. R. Turner/PS01
(205) 544-0617
Sponsor: Office of Space Flight

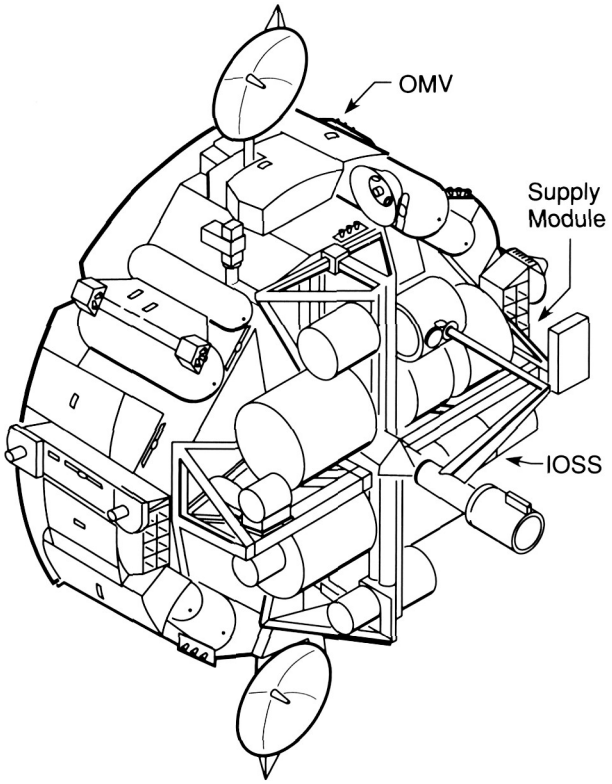

Figure 26. The Integrated Orbital Servicing System

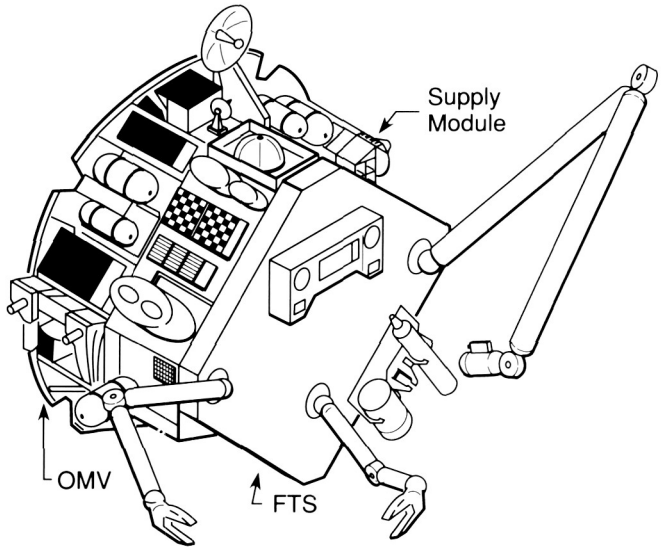

Figure 27. The Flight Telerobotic Servicer

Tumbling Satellite Recovery

The Orbital Maneuvering Vehicle (OMV) is currently being designed to retrieve free flying spacecraft in a stable control mode. OMV spacecraft recovery capability can be extended to include unstable spacecraft and certain classes of orbital debris by the addition of special purpose mission kits. A Tumbling Satellite Retrieval (TSR) kit has been under study at MSFC for several years in both in-house and contracted studies.

The need for capture and retrieval or disposal of uncontrolled satellites has been recognized for some time. Use of an OMV to recover a valuable satellite that has failed prematurely, for potential repair and re-use, or to retrieve one that has completed its design life and has ceased operation, could provide significant economic and scientific benefits. Removal and disposal of "junk" satellites, spent upper stages/motor casings, and other space debris to preserve operational integrity in space, is also of concern.

The TSR ongoing contracted study is being conducted in two phases. The first phase, which is scheduled to be completed in August 1988, will define the system concept. In the second phase, the ground test articles will be fabricated and physical system demonstrations will be conducted in contractor and MSFC facilities. The general concept is pictured in Figure 28; however, there are many variants and areas of investigation, study, and simulation which must be performed leading to the final concept.

Table 3 reflects several approaches to resolving system requirements including analytical analysis, ground simulation, and flight experiments.

The product of these studies and demonstration activities will be the development of a TSR kit requirement document to support the development of a TSR flight system when program funds become available.

J. R. Turner/PS01
(205) 544-0617
Sponsor: Office of Space Flight

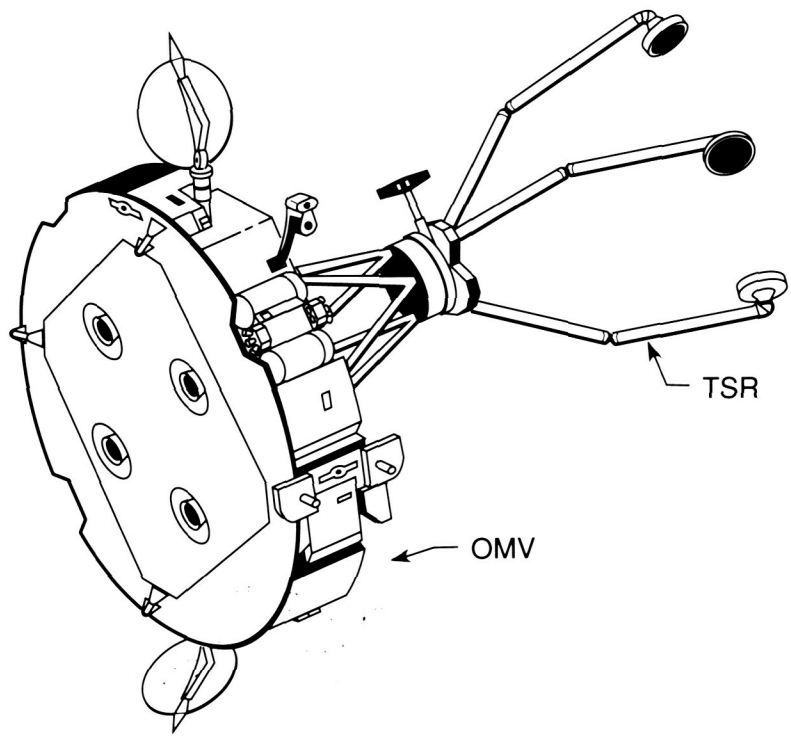

Figure 28. Tumbling Satellite Retrieval Kit

Table 3. Tumbling Satellite Retrieval Flight System Issues

Issues	Resolution Approaches		
	Analysis	Ground Simulation	Flight Experiment
Debris characteristics (physical and dynamic)	√		
SAT characteristics (physical and dynamic)	√		
• Capture interface and mechanism design	√	√	
• Capture technique	√	√	√
• Capture object transport technique	√	√	√
• Spin/despin interface design	√	√	
• Extension arm(s) design	√	√	
• OMV thrust vector and control authority	√	√	
• OMV protection approach	√	√	
• Retrieved capture subject handoff approach	√	√	√
• Time delay operations	√	√	√
• Autonomous versus tele-op control mix	√	√	
• Control system design and integration	√	√	
• Viewing and lighting requirements	√	√	√
• Number/variety of kits	√		
• Kit modularity level	√		
• Reconfiguration capability during flight	√	√	
• Hazards handling and avoidance	√	√	
Abort capabilities and methods	√		
• Deorbit techniques and systems	√	√	√

Microgravity Apparatus Development

The MSFC ground-based microgravity program is an active and integral part of the overall microgravity research program providing a test bed for the development of apparatuses that will evolve into flight facilities for the space microgravity program. Lessons learned through industrial outreach and development initiatives indicate that investigators need to have early and easy access to low-g in order to develop concepts and plans for more ambitious experiments on the Shuttle and Space Station Freedom. Use of low-g ground-based facilities to implement precursory experiments fills this need and often leads to more ambitious investigations or applications. As part of the ground-based program, the KC-135 aircraft furnace development provides realistic flight hardware design requirements and serves as a test bed for flight furnace development. During the Shuttle down-time the ground-based program has been strongly emphasized and the hardware inventory increased as follows: a Transparent Polymer Furnace was delivered to MSFC in March 1988; a Rapid Melt/Rapid Quench Furnace was delivered in July 1988; a Hi-Temperature Containerless Aircraft Furnace flies regularly and an up-grade is planned; and a commercial Zirconia Furnace is under evaluation.

MSFC is also developing flight microgravity apparatus for the Shuttle and the S. S. Freedom under the sponsorship of the Office of Space Science and Applications, Microgravity Science and Applications Division. Modular reconfigurability is emphasized in the design of each apparatus. Through utilization of different furnace modules or configurations of modular furnace elements, a variety of diverse experiments can be conducted, samples can be

Table 4. Microgravity Apparatus Currently Under Development

Features	Sample Size	Operating Temperature Hot Zone	Special Features	Quench Capability	Transfer Rate	Furnace or Sample Translation
Apparatus						
AADSF	2 cm X 25 cm	200-1,600 °C	Variable Gradient Peltier Pulsing	No	0.5 – 50.0 mm/h	Sample
CGF	2 cm X 20 cm	200 – 1,600 °C	Variable Gradient Peltier Pulsing Multiple Sample	No	0.24 – 50 mm/h	Furnace
MASA	2 cm X 18 cm	200 - 1,600 °C	Multiple Sample Cap.	100 °C/s	0.06 – 1,200 mm/h	Furnace
ALF	0.2 – 0.6 cm	20 – 1,750 °C	3-Axis Control & Stabilization & Multiple Sample Capability	0 – 20 °C/s	N/A	N/A

1. Advanced Automated Directional Solidification Furnace (AADSF)
2. Crystal Growth Furnace (CGF)
3. Metals and Alloys Solidification Apparatus (MASA)
4. Acoustic Levitation Furnace (ALF)

installed and removed, and repairs can be made during orbital operations. The technology involved in the development of these apparatuses pushes the state-of-the-art in many areas, such as high temperature heater technology, very precise temperature control, insulating materials, sample ampoule materials, and containerless processing. Table 4 lists the flight furnaces currently under development along with some key features and capabilities.

R. Ise/JA51
(205) 544-1962
Sponsors: Office of Space Science and Applications
Office of Commercial Programs

Advanced X-Ray Astrophysics Facility

The Advanced X-Ray Astrophysics Facility (AXAF) (Fig. 29) program reached the status of agency approval as a candidate new start in the FY89 budget submittal to Congress. Supporting information requested by Congress to demonstrate AXAF technology readiness has been provided to ensure continued support for FY89 initiation of the development program.

The technology required for AXAF continued to mature during 1988. One of the critical technology areas is the x-ray optical system. The principal effort in support of this technology is represented by the Technology Mirror Assembly (TMA) program. Polishing was completed and preparations for coating, assembly, alignment, and x-ray testing are under-

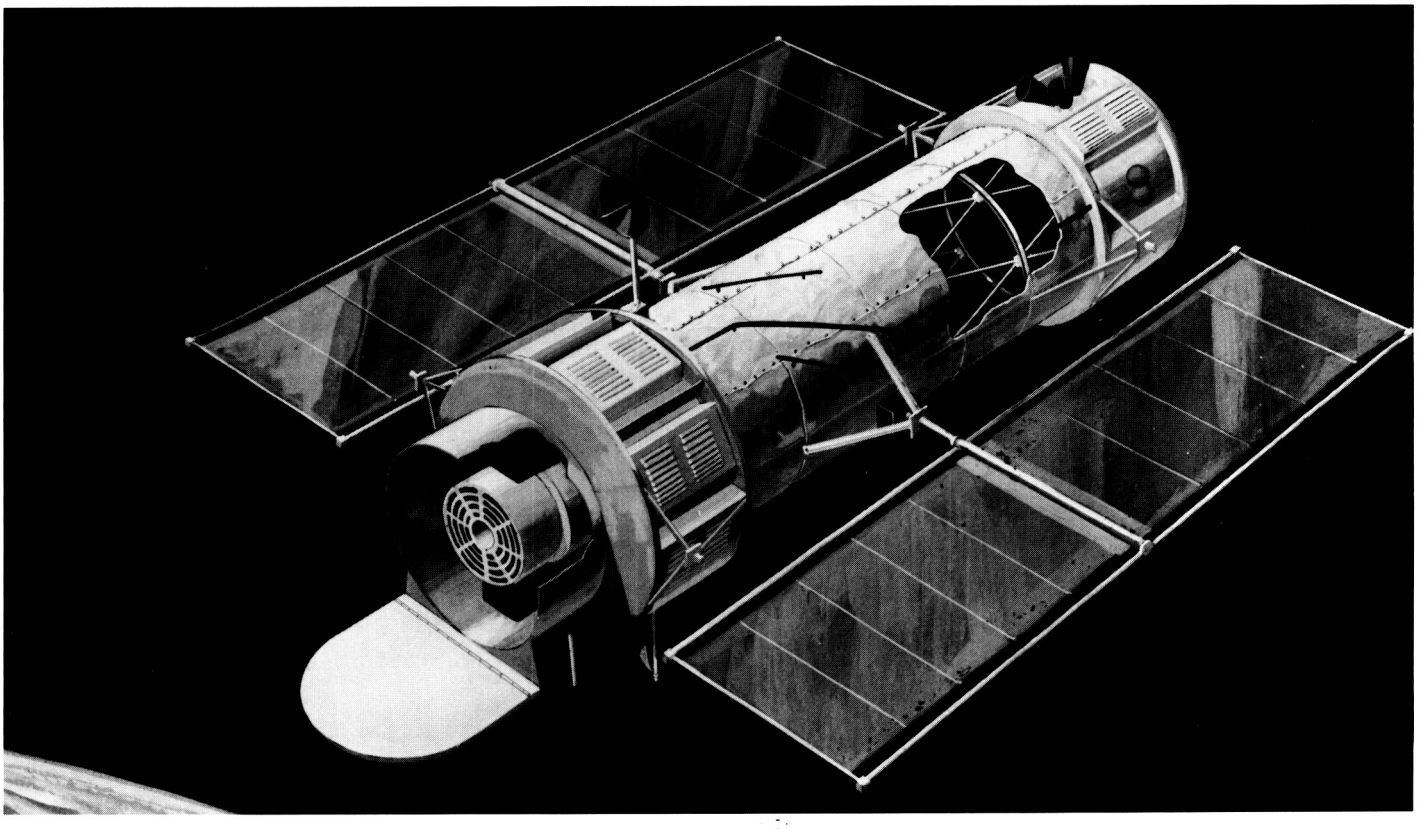

Figure 29. The Advanced X-Ray Astrophysics Facility

way. It is anticipated that the tests will verify that a 0.5 arc-sec angular resolution mirror system with encircled energy performance exceeding Level I program requirements is achievable.

The chief technology accomplishment in the science instrument areas in 1988 was the successful demonstration of a charge coupled device (CCD) chip approaching the flight instrument requirements for the Advanced CCD Imaging Spectrometer (ACIS). This chip, being developed by Lincoln Laboratories, Cambridge, MA, shows for the first time an acceptable level of quantum efficiency, charge transfer efficiency, and noise. The physical properties of the chip, such as pixel size, physical chip dimensions, and location of leads (permitting three sides to be abuttable) also meet ACIS requirements. Some further improvements in response at both the high and low x-ray energies are now being investigated by Lincoln Laboratories. The availability of this device represents a significant accomplishment in the efforts to bring the ACIS instrument to a responsive technology readiness level before initiation of flight development.

Based on the results of analytical studies, the effects of contamination on the AXAF mirrors are receiving increased attention. Specifically, particulate contamination is now considered to have a potentially significant effect on mirror performance. To verify this conclusion, coated glass samples are being fabricated to be placed near the TMA as it proceeds through assembly and alignment at Perkin-Elmer, shipment to MSFC, and x-ray testing (scheduled for late 1988 to early 1989). It is planned that particulate contamination deposited on these samples during this period will be representative of that on the TMA itself. The samples will be removed and optically measured periodically to determine the rate of accumulation. X-ray testing of the samples will then provide a correlation of the level of contamination with the x-ray performance. This effort will be extremely important in the establishment of a contamination control policy for the AXAF program.

C. C. Dailey/TA71
(205) 544-0571
Sponsor: Office of Space Science and Applications

Gravity Probe-B

The purpose of Gravity Probe-B (GP-B) is to conduct a new and unique test of Einstein's general theory of relativity by measuring extremely small changes in the spin axis of ultra precision gyroscopes in Earth orbit. The experiment is being developed for NASA by Stanford University. It will measure two predicted relativistic effects: geodetic precession due to the orbital motion of the gyroscope through the curved space-time surrounding the Earth, and frame-dragging or "gravitomagnetic" precession due to rotation of the Earth itself.

The experiment hardware consists of four electrostatically supported, cryogenic gyroscopes that measure the two effects to a precision of less than 1-milli-arc-sec per year. The gyros are aligned with an internal star tracker telescope which provides a highly precise absolute reference. The entire experiment is contained within a superfluid liquid-helium dewar that provides a very stable low temperature and allows the use of superconductivity in the gyro readout and magnetic shielding systems. The spacecraft (Fig. 30) will be launched into a 650 km polar orbit where data will be taken for a period in excess of one year.

Early technology development concentrated on demonstrating and advancing the state-of-the-art of individual subsystems. The present effort is to assemble a complete experiment system for a ground demonstration test scheduled for late FY89.

Milestones scheduled and accomplished during FY88 were: completion of single-flight configuration gyro performance testing at cryogenic temperatures; completion of the Superconducting Quantum Interference Device readout test under simulated gyro conditions to milli-arc-sec resolution; completion of quartz block fabrication for the Ground Test Unit (GTU); and completion of dewar fabrication for the GTU.

Major milestones scheduled for FY89 include: assembly and fit check of the GTU quartz block assembly; integration of the experiment probe assembly for the GTU; checkout and test of the GTU dewar; and assembly of the GTU and start of integrated system testing.

R. Ise/JA51
(205) 544-1962
Sponsor: Office of Space Science and Applications

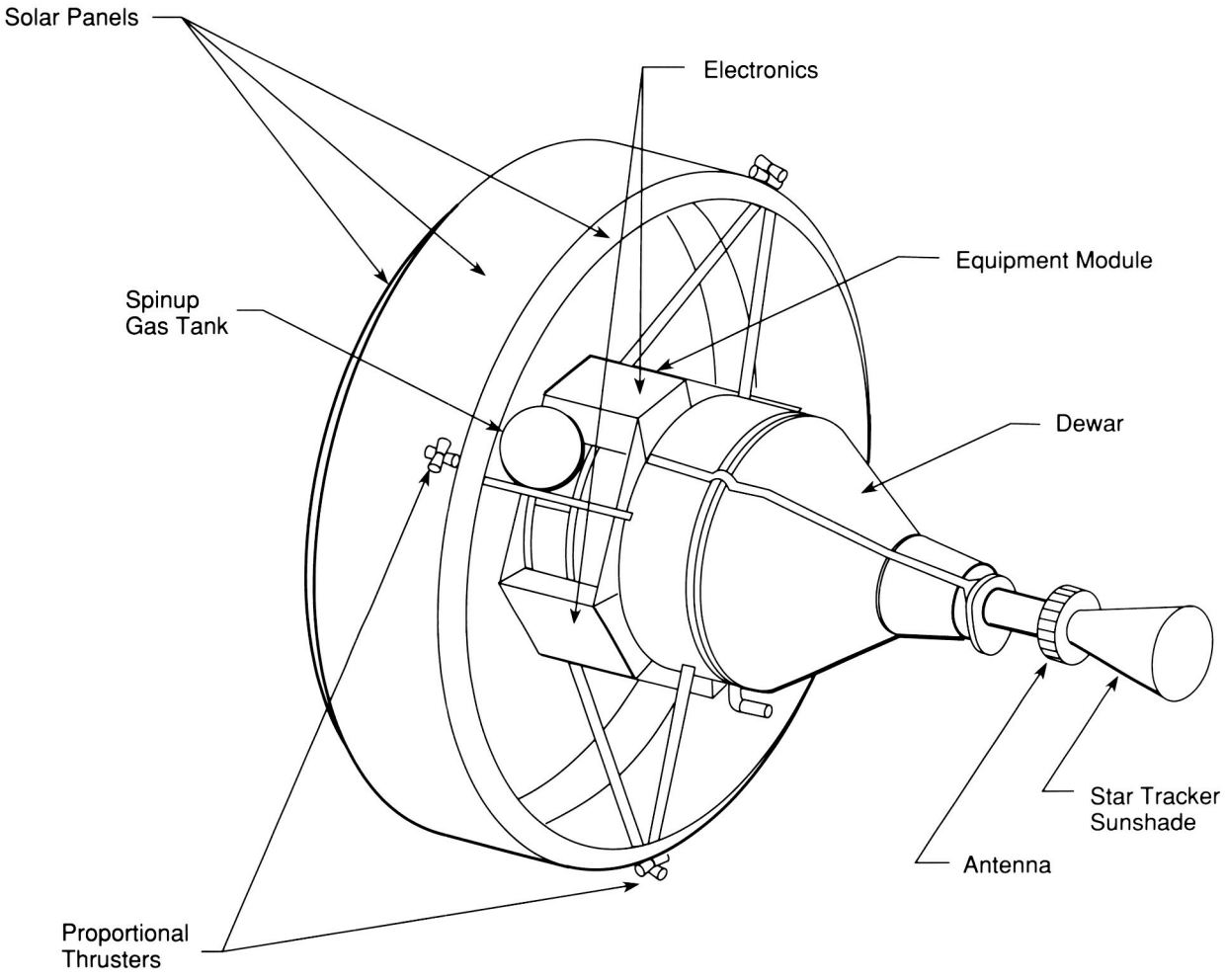

Figure 30. Gravity Probe-B Spacecraft

Data Systems

Low Gravity Fluids and Materials Processing Data Base

A data base documenting fluids and materials processing experiments performed in space has been created at the Structures and Dynamics Laboratory. This compilation, which identifies research efforts performed during sounding rocket, Apollo, Apollo-Soyuz, Skylab, Space Shuttle, Soyuz, and Salyut missions, reflects scientific contributions and technology from more than 25 countries. Research avenues included in the documentation extend from basic fluid flow examinations to complex materials science initiatives. Examples of included research are presented in Table 5.

Although more than 600 experiments have been completed in the space environment, fluid response related to low gravity accelerations is still not well understood. Thus, creation of the data base was motivated by the need to highlight basic flow processes which govern most low gravity fluids experiments. It is expected that by categorizing research efforts by similar flow physics, dependence of fluid response to low gravity acceleration can be more efficiently determined by flexible computational and experimental models.

In addition to highlighting important flow processes, the data base will provide engineering and science communities with information concerning past space efforts. Although it is imperative that proposals for new space research build on lessons learned in the past, many researchers are unaware of the number of low gravity experiments which have been completed in their subject area. To aid in the search for experiments of interest, the data base categorizes experiments by major and minor subject titles. A detailed thesaurus listing these titles is being prepared.

There are two versions of the data base available. Version 1 documents all low gravity fluids and materials processing research efforts except those which have been performed in a Soviet spacecraft. It includes approximately 50 experiments from the Apollo and Skylab programs, encompasses approximately 215 sounding rocket experiments from the

Table 5. Examples of Types of Research Included in the Data Base

Fluid Experiments	Materials Science Experiments
Drop/Bubble Dynamics	Crystallization Methods
Floating Zone Technology	Solidification Methods
Liquid-Liquid Diffusion	Soldering/Welding Techniques
Nucleate Pool Boiling	Material Coating
Heat Pipe Development	Metallic Foaming
Fluid Transfer	Glass Formation
Critical Point Examinations	Containerless Processing
Flow Containment Physics	Electrophoresis Separation

Principal Investigator(s): Hart, J. E.
From: University of Colorado, Boulder, CO

Co-Investigator(s): (1) Toomre, J., (2) Gilman, P.
1) University of Colorado, Boulder, CO
2) National Center for Atmospheric Research, Boulder, CO
3) Fichtl, G., 4) Fowlis, W., 5) Leslie, F.
3, 4, 5) NASA Marshall Space Flight Center, Huntsville, AL

Mission: STS 51-B, Spacelab 3
Date: Apr 1985
Payload Type: Spacelab, Rack #11

Processing Facility: GFFC
Builder: Aerojet, Azusa, CA

Experiment: Geophysical Fluid Flow Cell (GFFC)

The interaction of rotation and convection similar to that which occurs in the atmosphere of rotating Earth was examined on Spacelab 3. A central gravitational field which varied from parallel at the poles to perpendicular at the equator, was made possible in reduced gravity by applying an alternating high voltage across the inner and outer boundaries of a hemispherical shell filled with dielectric silicone oil. Radial and latitudinal temperature gradients imposed on the rotating shell generated thermally driven circulations. When rotation is the dominating parameter, north-south oriented columnar convection is observed. "As the differential heating is increased these rolls interact with the mid-latitude waves, ultimately being destroyed by turbulent, horizontally-isotropic convection that moves down from the pole. When a large equator to pole temperature difference is imposed on the boundaries, spiral waves develop on top of a strong meridional circulation" (Reference 1). Experimental results are compared to numerical simulations.

Key Words
Fluids*, Thermal Circulations, Rotating Fluids, Convection, Rotating Atmospheres

Materials
Silicone Oil

Experiment Applications
Simulation of planetary atmospheres is achieved by producing rotating, spherical convective flows.

Publications
1) Hart, J. E., Glatzmaier, G. A., Toomre, J.: Space-Laboratory and Numerical Simulations of Thermal Convection in a Rotating Hemispherical Shell with Radial Gravity. Journal of Fluid Mechanics, Vol. 173, 1986, p. 519-544. (Post Flight Results)

2) Hart, J. E., and Toomre, J.: Geophysical Fluid Dynamics with Dielectric Polarization Forces, Rep. 2, NASA Contract NAS-8-31958, 1977, 66 pp.

3) Hart, J. E., Toomre, J., Deane, A. E., Hurlbert, N. E., Glatzmaier, G. A., Fichtl, G. H., Leslie, F., Fowlis, W. W., and Gilman, P. A.: Laboratory Experiments on Planetary and Stellar Convection Performed on Spacelab 3. Science, Vol. 234, October 1986.

4) Leslie, F. W.: Geophysical Fluid Flow Experiment. In Research and Technology 1987, Annual Report of the Marshall Space Flight Center, NASA, pp. 62-63 (Short Description)

Contacts
Dr. John E. Hart
Department of Astrophysical, Planetary and Atmospheric Sciences
University of Colorado, Boulder, CO 80309

Figure 31. A Typical Experiment Within the Fluids and Materials Processing Data Base

United States (SPAR), Federal Republic of Germany (TEXUS), Japan (TT500-A), and Sweden (MASER) programs, and documents some 225 research initiatives performed in the mid-deck, laboratory environment, and payload bay of the Space Shuttle.

A typical experiment within Version 1 is represented in Figure 31.

General information concerning principal and co-investigators, mission, launch date, etc. is available for all experiments. Short descriptions outlining payload configuration, research directions, and available results are being prepared. Key words identifying experiments which involve similar flow processes aid the searching process. A listing of materials used as the experiment medium allows a quick look at all space efforts concerning the substance of interest. Publications offering additional information related to the equipment, ground-based research or flight results are also presented.

Principal investigators are being asked to review information for accuracy and to make additions where appropriate. Because experimental results are often published a year or more after the flight of a payload, new information is included in the data base as it becomes available. A published release of Version 1 discussing experiments performed prior to February 1986 is targeted for early 1989.

Version 2 represents a partial listing of experiments performed under the Soviet Space Program. Approximately 130 research efforts completed during sounding rocket, Soyuz, Salyut, and MIR missions have been identified. Version 2 is outlined in the same format as that of Version 1, but information is often incomplete, as publications describing the payloads and results have proved difficult to obtain.

Currently, the compilation is maintained on a commercially available data base software package. It is manipulated on a personal computer which supports approximately 1.5 megabytes of random access memory. In this application, the menu driven system is easy to use, and searching and sorting capabilities are, for the most part, extremely efficient. At present Version 1 or Version 2 (but not both), can be loaded on a two-sided, high-density floppy disk for easy use and transport. Data base distribution to users outside MSFC is being examined. The current software, coupled with the data base information on a floppy disk allows any personal computer user to access the information quickly and easily, yet requires an update of the floppy periodically. Networking allows network users access to all information including the most current, while possibly restricting data transfer speed, searching capabilities, and ease of use. Relative merits of these two approaches to data base release are being examined.

C. A. Morroni/ED42
(205) 544-1695
Sponsor: Office of Space Science and Applications

Improved Two-Dimensional Kinetics Computer Program

The main Joint Army, Navy, NASA, and Air Force reference program for rocket thrust chamber performance calculation is the Two-Dimensional Kinetics (TDK) code. During its development over the last 25 years, the program has been advanced continuously to satisfy needs arising with the design and optimization of numerous rocket engines. Many options have been included, and coupling with other programs is available so that many problems can be solved in a very convenient way. The current effort is conducted by Software and Engineering Associates of Carson City, Nevada.

The most recent program improvements are first, the supersonic flow field calculation was extended to include shock waves to the nozzle exit plane. Solutions from this analytical capability can be directly compared with nonintrusive diagnostic measurements in the nozzle exit plane, providing an excellent method of program verification. Figure 32 shows constant Mach number contours calculated for the entire supersonic flow field of the Space Shuttle Main Engine (SSME). The location of the induced shock-wave emanating from the throat region is clearly detectable. In Figure 33, the radial pressure distribution in the SSME nozzle exit plane, calculated with and without the shock option, demonstrates the discrete pressure jump. The static pressure, species mass fraction, velocity, and Mach number profiles also exhibit similar transitions caused by the shock.

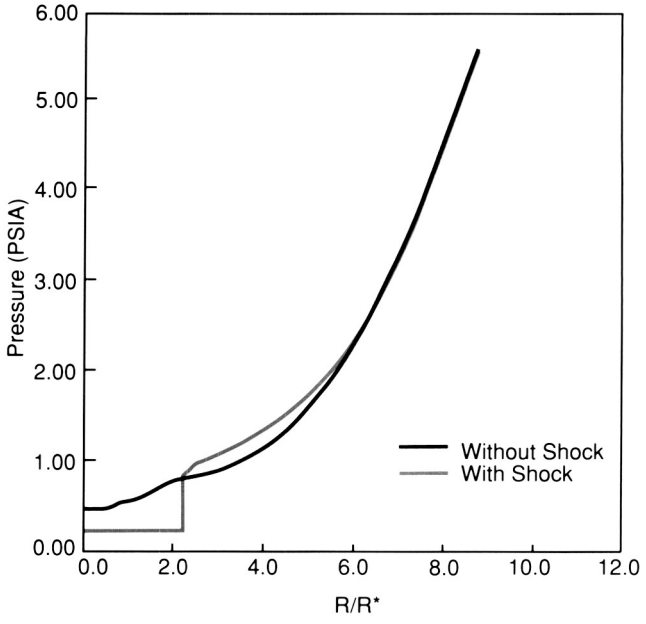

Figure 33. Exit Plane Properties

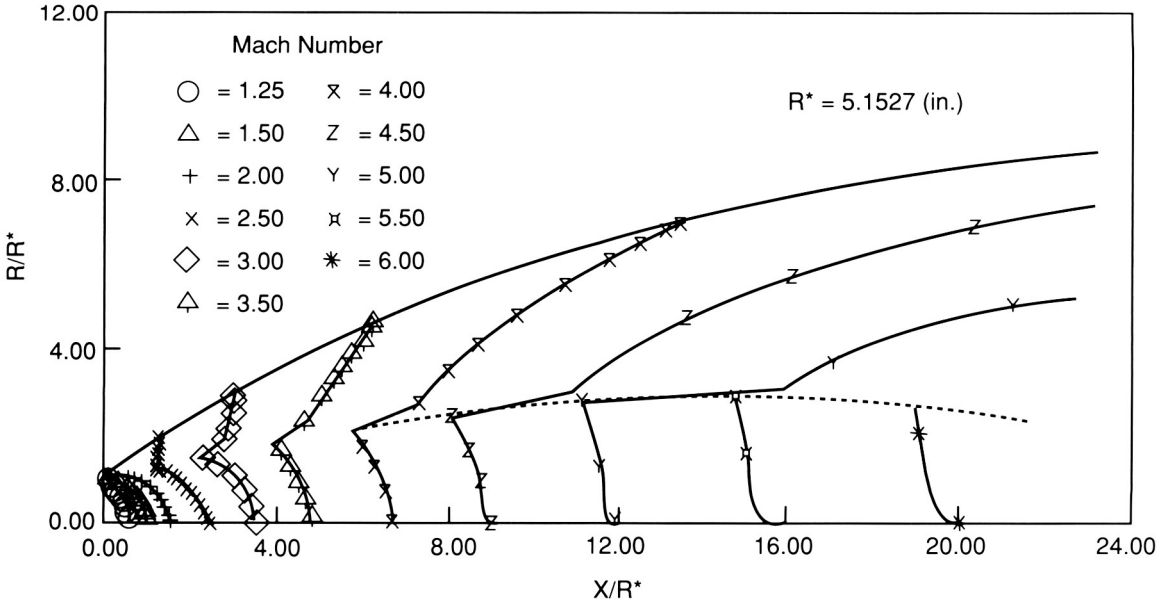

Figure 32. SSME Mach Number Contours

Second, new boundary layer features are available now to treat wall roughness, flow-relaminarization, heat-flux adjustment to match measured data, automatic boundary layer start using one-dimensional equilibrium edge conditions upstream of the TDK start, and a second boundary layer calculation after the wall-contour has been adjusted by a displacement thickness accounting for viscous effects.

Third, the Rao method nozzle-contour optimization program has been advanced with a variable specific heat ratio gamma option, and direct use of the predicted contour, employing a slope change selection process of points to meet the limited array sizes in the TDK program.

Fourth, a preprocessor interactive program was developed to prepare input data files for the operation of the TDK program which is coupled with the Boundary Layer Module (BLM). This approach has been selected to educate a person not familiar with the TDK code to set-up and execute a problem quickly. There are three different levels of prompting from which the engineer may select, depending on the progress and knowledge attained. To avoid mistakes the program internally checks on limits and signs. Arrays of data such as wall contour geometry, slope continuity, and temperature profiles are plotted to locate any erroneous situation.

The TDK/BLM, Rao and preprocessor programs, plus a Mass Addition Boundary Layer module are available in their present states to the propulsion community. The programs in card image format and the associated documentation can be obtained from Mr. Tom Reedy, Chemical Propulsion Information Agency, John Hopkins University, Laurel, MD 20707. Responses from program users will be considered in the final versions.

K. W. Gross/EP55
(205) 544-2262
Sponsor: Office of Aeronautics and Space Technology

Environmental Data Base Management

In the spring/summer of FY86, NASA conducted the Satellite Precipitation And Cloud Experiment (SPACE) to contribute to the understanding of precipitation processes associated with mesoscale and small convective meteorological systems. An understanding of these physical processes is essential to evaluate and improve existing remote sensors, and develop new ones for space-based applications. SPACE ran concurrently with the Microburst and Severe Thunderstorm (MIST) experiment, sponsored by the National Science Foundation, and the Federal Aviation Administration (FAA) – Lincoln Laboratory Operational Weather Study (FLOWS), sponsored by the FAA. SPACE, MIST, and FLOWS experiments comprise a joint multiagency atmospheric science study called the Cooperative Huntsville Meteorological Experiment (COHMEX). COHMEX provided a complex, voluminous, high spatial and temporal resolution data base from conventional and developmental sensors.

The Global Backscatter Experiment (GLOBE) was initiated last year to determine the typical values and the spatial/temporal variability of aerosol backscatter at carbon dioxide wavelengths in global clean-background air masses and subglobal backscatter variability including diffuse high backscatter targets (dust plumes, subvisible cirrus, and volcanic plumes). Data from GLOBE include global ground-based and aircraft-flown laser radars, chemical/optical property measurements, and conventional meteorological surface and satellite observations. This information is crucial to the simulation and design studies for

the Doppler Laser Atmospheric Wind Sounder (LAWS), a component of NASA's Earth Observing System. Measurements from initial GLOBE field experiments are being compiled and analyzed to provide a comprehensive backscatter data base for use in LAWS Phase A/B studies.

Work has continued during FY88 to assimilate COHMEX and GLOBE data and develop a data base management system to archive, manipulate, and retrieve these data files. ORACLE, a powerful commercial relational data base manager, was chosen as the driver of the system. ORACLE attributes include data base access and manipulation through a high level structured query language that can interface and be embedded into program statements, networking computers together (from PC/ATs to mainframes), menu and form capability for user interface, and full security with multilevel entry. Through the use of a menu driven log-on system, researchers will be able to catalog, display, and transfer data to local computers. Remote researchers will have access to data bases through computer networking. Data archival methods such as optical disks and Masstor cartridges are presently being evaluated. Both COHMEX and GLOBE data bases provide prototype large data sets to study the efficient data acquisition and management for NASA's Earth Observing System planned for the mid-1990's.

J. E. Arnold/ED43
(205) 544-1646
Sponsor: Office of Space Station and Applications

Four-Dimensional Man-Computer Interactive Data Access System Technology

The Man-computer Interactive Data Access System (McIDAS) has been under development at the Space Science and Engineering Center (SSEC) of the University of Wisconsin-Madison for 18 years. During this period, its software and data bases have grown extensively. It has been used for the analysis and display of two-dimensional meteorological data, e.g., satellite imagery, temperature contours, etc. Under support from MSFC during FY88, SSEC has been developing a four-dimensional (4-D) analysis and display tool. Since the Earth-atmosphere system is a volume which is evolving in time, a tool is needed that will allow the scientist to visualize various and multiple parameters from varied viewing geometries.

The eventual goals of this effort are to design and implement a 4-D data management system within McIDAS and design and develop the software and hardware necessary for interactive display of Earth systems data. This should provide tools which will render complex 4-D fields of environmental data sets on an interactive basis, allowing rapid integration of interdisciplinary Earth science data sets into one display. The system will be used for qualitative and quantitative interpretation.

Toward these goals, the following tasks have been accomplished during FY88. Great progress has been achieved in viewing data from 4-D model output. The system has been used to view data from various models used by researchers across the country. Data from the Limited Area Mesoscale Prediction System (LAMPS) model has been viewed. This has afforded the opportunity to more fully understand the true four-dimensional characteristics of multiparametric quantities. The software is generalized such that any scale of motion can be observed. Analyses have been performed on Doppler radar data. Radar data showed the growth and development of a thunderstorm which contained a weak microburst. A microburst is an intense downdraft of air which has been shown to be

responsible for several major airline crashes. Also viewed have been observations of climate changes for the globe. Software has been under development at MSFC to utilize the capabilities of this data base. Some of that software includes the ability to cut through nearly any slice of a data volume, with the ability to time-animate that cut. A great deal of effort has gone into exploring the capabilities of commercially available hardware. Computer graphics hardware currently exists which may achieve near real-time interactive graphics rendering capabilities. We have been evaluating the capabilities of the devices available from several vendors and attempting to understand their strengths, limitations, and generality. We envision using a device of this sort to actually perform the graphics rendering required. This would make the mainframe computer strictly a data base handler.

Planned activities for FY89 include improved capabilities for display, additional analysis software, and further investigation of commercially available hardware. Improved display capabilities planned include: better parameter combination, better use of color, and type of presentation. Analysis software will allow the derivation of parameters from available data, as well as classification of data using classification algorithms. This also includes generalization of coordinate systems. The commercially available hardware should allow us to replace the 1980-generation video interface system with the sophisticated video interfaces now being built.

Hibbard, W. L.: A Next Generation McIDAS Workstation. Preprints, Conf. Interactive Information and Processing Systems for Meteorology, Oceanography, and Hydrology, Anaheim, American Meteorological Society, pp. 57-61, 1988.

Meyer, P. J., and Seablom, M. S.: Application of the Four-Dimensional McIDAS to LAMPS Model Output. Preprints, Conf. Interactive Information and Processing Systems for Meteorology, Oceanography, and Hydrology, Anaheim, American Meteorological Society, pp. 33-36, 1988.

P. J. Meyer/ED43
(205) 544-1654
Sponsor: Office of Space Science and Applications

Wetnet – A New Earth Science Data Access and Display System

The access, display, and manipulation of remotely sensed Earth science data from a wide variety of sensors and platforms has always posed a challenge to the Earth scientist wishing to perform research. With the approach of the Earth Observing System (EOS) in the 1990's, the need for a generic data access, display, and manipulation capability will be critical as more sensors with high data rates and many channels are designed and flown on new Earth-orbiting satellites. Further complexity in such a data system will arise due to a growing emphasis on discerning global change in geophysical parameters on time scales of several to many years. Addressing global change on such long time scales will involve the manipulation of large quantities of data.

In response to this challenge, an EOS Data Information System prototype is being developed which utilizes data from the new Defense Meteorological Satellite Program Special Sensor Microwave/Imager (SSM/I), launched in 1987. Because current and future SSM/I's will provide several years of continuous data which contain information on precipitation, atmospheric water vapor, oceanic wind speed, sea ice, and snow cover, they are a logical choice for such a prototype activity. The capability of SSM/I's to measure several components of the global hydrologic cycle, and the desire to network scientists together with this data systems tool, have resulted in the name "Wetnet" for the project.

The system will build upon the 15 years of development that the Man-computer Interactive Data Access System (McIDAS) has undergone for the access and image display of Geostationary Operational Earth Satellite data, as well as data from radars, the National Weather Service, and other data sources. Many of the mainframe McIDAS's capabilities have been transferred to personal computers (PC's). These PC's will be provided to a team of scientists who will use them to access SSM/I data in near-real time (as well as radar, other satellite, and ground station data) over high speed modems from MSFC, manipulate the data for their own particular algorithm development applications, and share their algorithms and results electronically with the other science team members. It is hoped that such a tool will ease the data processing burden from scientists, allowing increased useful information extraction from the raw data.

R. W. Spencer/ED43
(205) 544-1686
Sponsor: Office of Space Science and Applications

Image Processing and Computer Graphics

The Integrated Computer-Aided Design (CAD)/ Image Processing System is a dedicated computer graphics system based on the VAX-11/785 superminicomputer. An International Imaging Systems image processing system and an Intergraph CAD workstation, along with image translation software, provide a powerful graphical analysis capability. Both remotely sensed imagery and digitized photographs can be viewed, enhanced, manipulated, and overlaid with a two-dimensional or three-dimensional (3D) graphics design file. The digital image can also be warped to match control points in the design file. Also the results of 3-D hidden surface rendering of a design model can be transported to the image processing station for further enhancement and frame loop animation.

The system is used for image analysis and data visualization tasks associated with sensor development and atmospheric phenomena studies, and also supports mission projects in phases from conceptual design to flight analysis. The integration of image processing and CAD has resulted in a more generalized approach to the solution of a wide variety of research and development problems.

J. V. Parker/ED43
(205) 544-1526
Sponsor: Office of Space Flight

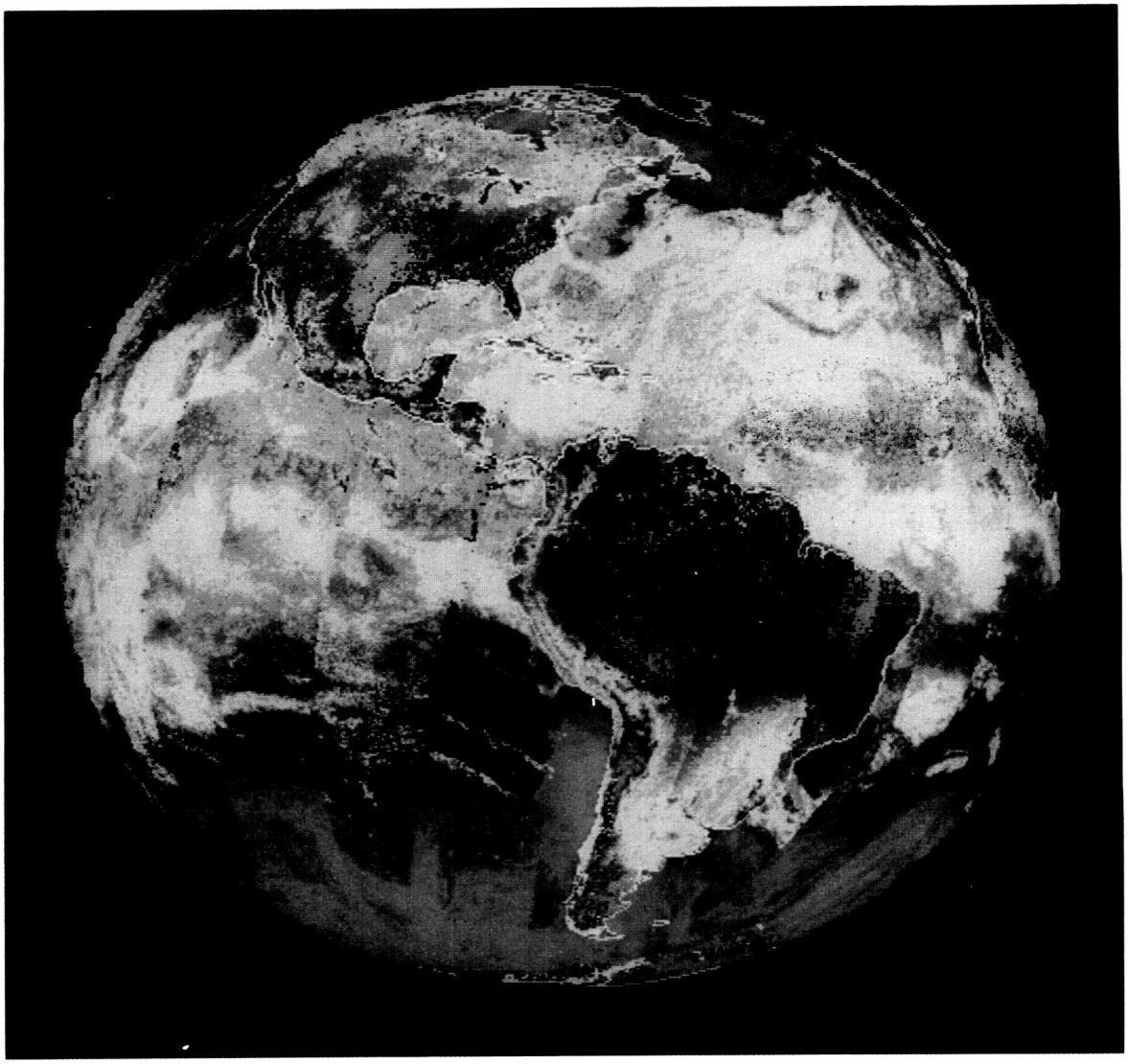

Research Programs

MSFC has developed considerable expertise in a number of scientific areas, specifically Low-Gravity Science; Astrophysics; Solar, Magnetosphere, and Atomic Physics; and Atmospheric and Earth Science. MSFC scientists and engineers working in these areas are involved both in basic research and in scientific support of the center's many projects in Earth and space sciences. This research involves instrument development, data analysis, and theoretical studies.

New experiments are being designed for flights on free-flying satellites and the Space Shuttle, and planning is underway for new programs intended for the Space Station Freedom.

Microgravity Science

In preparation for using flight experiments to study the influence of weightlessness on basic physical processes, a number of ground-based microgravity research programs are continuing at a high level of activity. MSFC scientists and engineers are heavily involved in research using the MSFC Drop Tube/ Drop Tower and the NASA KC-135 aircraft. More than 25 principal investigators had contracts selected as a result of peer review in MSFC microgravity-managed ground-based disciplines.

Our scientists and engineers are preparing state-of-the-art experiments for a number of flight programs aimed at the U. S. Microgravity Laboratory, the International Microgravity Laboratory, the Materials Science Laboratory, Space Station Freedom, and other shuttle flight opportunities. Such experiments will clarify how the absence of, for example, gravity-driven convection can beneficially influence solidification and crystallization processes.

Alloy Directional Solidification Experiments

The effects of low gravity on the solidification processes of alloy systems were studied by directional solidification (in a Bridgman-type furnace) aboard a NASA KC-135 aircraft flying parabolic arcs, generating alternate periods of low and high gravity. Sample quench subsequent to directional solidification gives information on solid/liquid interface morphology and composition in low gravity. Peltier pulsing provides solid/liquid interface demarcation and absolute growth rate. An apparatus has been developed to provide video observation of sample macrostructure through transparent crucibles during low-gravity directional solidification.

Under Technical Exchange Agreements additional NASA/industry collaborative, low-gravity experiments have been flown on KC-135 aircraft. The studies include: iron-carbon type alloys, with John Deere and Co.; metal matrix composites, with Abex; semiconducting alloys, with Rockwell International; and superalloys, with Pratt and Whitney. These efforts are complemented by NASA-sponsored academic research in aircraft low-gravity alloy solidification including: immiscible metal matrix ceramic composites, with the Massachusetts Institute of Technology; eutectic metal matrix ceramic composites, with The University of Alabama (UA); ternary immiscible alloys, with The University of Alabama in Birmingham; superalloys, with Cleveland State University (also participating are MSFC's Materials and Processes Laboratory and the Lewis Research Center); and high transition temperature superconducting oxides and metal matrix composites, with The University of Alabama in Huntsville and UA. Six papers are currently in press in Metallurgical Transactions covering this research.

A Space Shuttle furnace system, the Metals and Alloys Solidification Apparatus, is being developed by NASA for the United States Materials Laboratory for Spacelab flights. The initial temperature capability is 1,600 °C. The Bridgman-Stockbarger directional solidification furnace will provide solid/liquid interface quenching and will allow sample exchange on orbit.

Curreri, P. A. and Stefanescu, D. M.: Low-Gravity Effects During Solidification. Metals Handbook: Casting, Vol. 15, American Society for Metals, 1988.

P. A. Curreri/ES74
(205) 544-7763
Sponsors: Office of Space Science and Applications
Office of Commercial Programs

High Temperature Superconductors

Research on high temperature superconducting materials is being carried out at MSFC in collaboration with Professor M. K. Wu and The University of Alabama in Huntsville and also with other groups.

Research has been concentrating on the 1-2-3 ceramic superconductors which have superconducting transition temperatures around 90 K. By adding silver oxide to $YBa_2Cu_3O_x$ prior to heat treatment in oxygen, enhanced properties have been produced in granular samples. A major enhancement is observed in the magnitude of magnetic flux pinning, which provides positive magnetization properties. Attractive forces are produced in the gradient field of permanent magnets, which enables samples to be picked up and supported beneath a magnet (Fig. 34). The stronger pinning forces provide greater stability for applications such as levitating objects, or use in

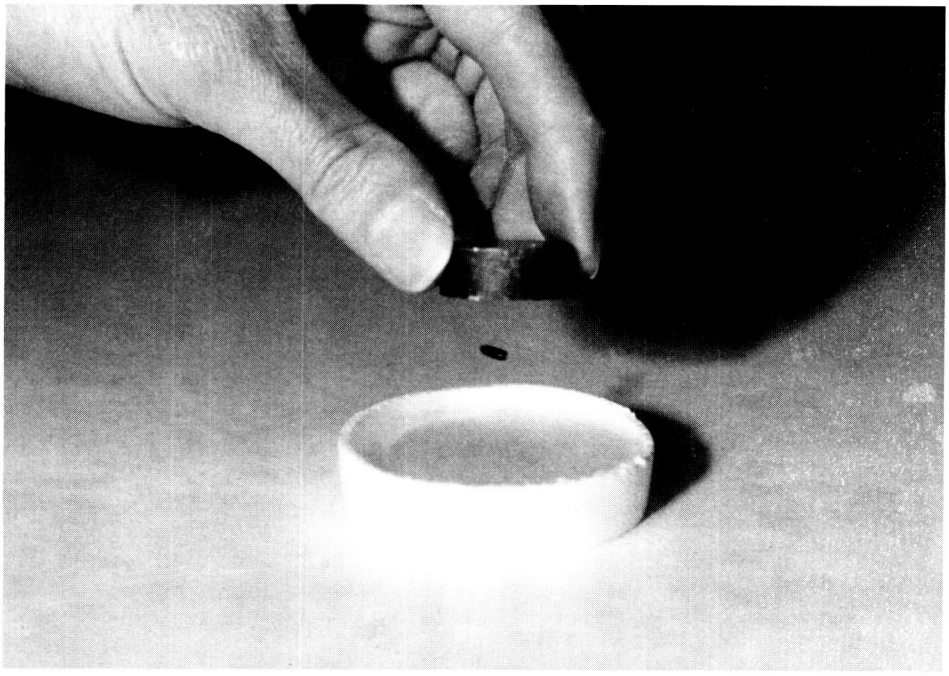

Figure 34. Superconducting Silver Oxide Doped $YBa_2Cu_3O_x$ Suspended Beneath a Magnet

bearings, etc. In addition, due to the presence of the silver, the material resistance at room temperature is lowered, wires can be easily soldered to the materials, the critical current density is increased, the material is less brittle, and the magnetic properties and critical fields are enhanced, compared to pure $YBa_2Cu_3O_x$ granular materials.

Similar properties have been demonstrated in other compounds where different rare-earth elements have been substituted for yttrium, and attempts are being made to produce thin films of these materials. It is anticipated that stronger pinning forces will modify the response of granular films to electromagnetic radiation.

The model used to describe the effects observed assumes that multiple Superconducting Quantum Interference Devices, or SQUID loops, are involved, and that these loops provide the flux pinning and chaotic switching that occurs when flux moves from one pinning configuration to another.

Peters, P. N., Sisk, R. C., Urban, E. W., Huang, C. Y., and Wu, M. K.: Observation of Enhanced Properties in Samples of Silver Oxide Doped $YBa_2Cu_3O_x$. Appl. Phys. Lett., Vol. 52, No. 24, pp. 2066-2067, 1988.

P. N. Peters/ES63
(205) 544-7728
Sponsors: Center Director's Discretionary Fund
U. S. Army Strategic Defense Command

Solution Crystal Growth of Organic and Polymeric Materials

Polymeric materials consisting of parallel chains which serve as a delocalized π-electron system are one of the most promising of the substances that possess nonlinear optical properties. Examples of these materials are the polydiacetylenes. These materials not only have very large nonlinear optical susceptibilities but also very short response time.

The need for pure, defect-free single crystals of such materials makes the method and conditions for growing large single crystals a determinant factor in technological applications. The growth of such crystals under Earth-gravity conditions invariably involves convection. The reduction of such buoyancy-driven convections would require a low-gravity growth environment.

A ground-based study to explore the role of gravity in the processing of such materials is in progress. The model diacetylene TCDU ($RC{\equiv}C\text{-}C{\equiv}CR$, $R = -(CH_2)_4OCONHC_6H_5$) was studied, using the evaporation technique from ethanol-ethyl acetate solutions. The results of these trials were encouraging as crystals 15 by 10 by 2 mm were grown. X-ray diffraction has shown them to be of excellent quality. They polymerize under gamma-ray irradiation to an extent of 30 percent, while keeping their single crystal character.

Preliminary work has also been started on a new and promising nonlinear optical material, L-arginine phosphate. Crystal growth from aqueous solution has produced large crystals of 6 mm by 6 mm. They have extremely good quality and are optically transparent.

M. Vlasse/ES74
(205) 544-7781
Sponsor: Office of Space Science and Applications

Model Immiscible Systems

Differential scanning calorimetry and partial molal volume data combine to suggest the nature of preferred succinonitrile-water aggregates at temperatures ranging from the monotectic to critical in succinonitrile-rich homogeneous solutions. These structures are arguable in terms of trans and gauche rotational conformers of succinonitrile and "mixture-model" zero-bonded water. The gauche-conformer is about 360 cal $mole^{-1}$ more stable than trans and tends to dominate at lower temperatures. A sizable percentage of succinonitrile-water interacts by hydrogen bonding of zero-bonded water at higher temperature (>35 °C). Succinonitrile-rich aggregates dominant at high temperatures may be incapable of hydrogen bonding with hydrophilic surfaces. The gauche rotamer interacts electrostatically with the water oxygen as well as by hydrogen bonding with water hydrogens. The only interaction likely between water and the trans rotamer, with its zero dipole moment, is hydrogen bonding. As temperatures lower toward the monotectic temperature, a decreasing trans/gauche ratio and decreasing zero-bonded water content accompanies an increase in water aggregates hydrogen bonded to succinonitrile-water aggregates. High temperature equilibrium clusters lead to steeper compositional gradients between the bulk and the Gibbs surface excess on hydrophilic surfaces while low temperature equilibration leads to more diffuse compositional gradients near the surface. This yields a cleaner separation of the water-rich adsorbed layer and less monotectic reaction undercooling in the bulk when equilibrated at a high temperature than at a low temperature. This is true particularly in small volume samples where surface-to-volume ratios are high. Regardless of sample size, the ingot morphology must depend, to some extent, on equilibration temperature prior to a fast quench in all solutions where preferred structures vary with temperatures (most solutions). The feasibilities of suggested models (publications in progress) are under study using ab initio self-consistent field techniques. A succinonitrile-benzene Fourier transform infrared spectroscopic study shows an immediate preference (~1 degree below the consolute temperature) for benzene at a zinc selenide surface. As demonstrated in an earlier report, benzene preferentially wets zinc selenide in a succinonitrile-benzene two-phase mixture. Efforts here are to determine the maximum temperature, with respect to a given consolute temperature, at which the spectroscopic preference is observable. Further, interests include noting the times required for the development of intensity shifts as temperatures change incrementally.

Frazier, D. O. and Facemire, B. R.: Non-Ideality Near the Monotectic Composition of a Miscibility-Gap Type System: Succinonitrile-Water. Metall. Trans., submitted, 1988.

D. O. Frazier/ES75
(205) 544-7825
Sponsors: Office of Space Science and Applications
Office of Commercial Programs

Undercooling Studies in Metals and Alloys

To improve present metals and alloys or to produce new alloys through space processing, it is necessary to understand the effect space processing has on their structure and properties. Niobium-based peritectics were originally selected for study for two main reasons. First, these alloys are important because they have superconducting phases, in particular the A15 phase at or near 75 atomic percent niobium in each system. Second, work on these alloys will add a new dimension to materials processing in space because of their refractory and thus high melting nature. Presently, only lower temperature metals and alloys are studied in space and low-gravity processing.

The method selected for studying undercooling in alloys has been the low-gravity containerless environment of the MSFC 105-m Drop Tube. This environment allows samples to cool in an environment conducive to undercooling. Undercooling is the cooling of materials below their normal solidification temperature without solidification or crystallization (i.e., the material remains in the liquid state). After undercooling the alloy will solidify very rapidly. This could result in the formation of nonequilibrium phases in both composition and structure. The result of undercooling is being studied in selected niobium-based peritectic systems through low-gravity containerless processing.

In FY88, analysis was completed on undercooled NbGe, NbSi, and NbPt alloy samples. Results in the NbPt samples of 16 to 18 atomic percent Pt showed that undercooling results in single phase, single crystal samples of the A15 phase. In contrast, cast materials of the same composition contained two-phase morphology with alpha-Nb and A15 in agreement with the equilibrium phase diagram. All undercooled NbPt samples nucleated with the primary phase of A15 which is Nb_3Pt, indicating a nucleating agent for this phase. At present the exact nucleating agent is not known.

In the NbSi system, undercooled samples reached an unreported coupled zone. Samples resulted from two-phase growth of alpha-Nb and tetragonal Nb_3Si. These results contrast to splat-quenched samples which indicated alpha-Nb and Nb_5Si_3. These results indicate a basic difference between deep undercooling and splat-quenching techniques. In addition to the above metallurgical results, an analysis of the solidification velocities was completed by studying the recorded recalescence peaks of the undercooled samples. A model was applied to these peaks which resulted in a solidification velocity. These velocities were compared to current dendritic-solidification velocity theories and agreed very well. Current efforts are to extend this technique to faster solidification velocities.

A parallel effort involves the design and calibration of a special two-color pyrometer for use in the drop tube. This device is expected to give an actual temperature of the falling sample at one point in the facility. In this way the undercooling estimations can be checked by experiment.

In addition to Nb-based peritectic studies, a wide variety of pure metals have been undercooled and studied metallographically. Results were correlated with current nucleation theory and published.

Robinson, M. B. and Bayuzick, R. J.: Undercooling Studies of Niobium-Platinum and Niobium-Silicon Binary Alloys. Second International Symposium on Experimental Methods for Microgravity Materials Research, 117th TMS-AIME Annual Meeting, Phoenix, Arizona, January 25-29, 1988.

Robinson, M. B., Hofmeister, W. H., and Bayuzick, R. J.: Undercooling Studies on Nb-Pt and Nb-Si Alloys Using the 105-Meter Drop Tube. 27th Plenary Meeting of COSPAR, Espoo, Finland, July 18-29, 1988.

Bertero, G. A., Hofmeister, W. H., Bayuzick, R. J., and Robinson, M. B.: Splat-Quenching of Undercooled Nb-Based Alloys of Near-Eutectic Composition. ASM International Materials Congress, Chicago, Illinois, September 26-30, 1988.

M. B. Robinson/ES74
(205) 544-7774
Sponsor: Office of Space Science and Applications

Solution Crystal Growth — Ground and Flight Experiments

Research is continuing on the growth of crystals from solution. This effort includes both ground-based laboratory studies and flight experiments. Holograms taken of triglycine sulfate crystals growing in the Fluids Experiment System (FES) during the 1985 Spacelab 3 mission are being analyzed. This study consists of reconstructing holograms to obtain interferograms, digitizing the resulting images, determining the concentration profiles surrounding the crystals, and comparing these values to a mathematical model of the growth process. Design modifications to the FES cells are being developed to facilitate study of new materials and growth techniques. The next step in the low-gravity solution crystal growth research program will require nucleation of crystals instead of insertion of seed crystals as was done on Spacelab 3. A prototype cell now being designed will be used in ground-based studies to develop features needed in the new FES cell. Supporting basic research on nucleation from solution has begun in the laboratory.

Ground-based research areas include studies of crystal properties as a function of growth conditions using a reciprocating rotary crystallizer and the development and use of optical techniques for the study of growth processes and crystal properties. A unique technique of shadowgraph imaging has been developed and is being used for precise determination of the equilibrium temperatures of growing crystals in known solution concentrations.

A second generation solubility measuring system of this kind has been built (Fig. 35) and is being used to generate solubility curves for aluminum potassium sulfate and other materials being considered for flight experiments. A laser-scattering technique used in conjunction with a microscope, a detector and a computer system, collectively termed a laser scattering ultramicroscope, has been developed. An enhanced ultramicroscope system (Fig. 36) with greatly improved sensitivity and data handling capabilities has been built and tested. It will be used to produce three-dimensional maps of the distribution of scattering centers, such as voids and inclusions, within a crystal. The density and distribution of inclusions can strongly affect the optical and electrical

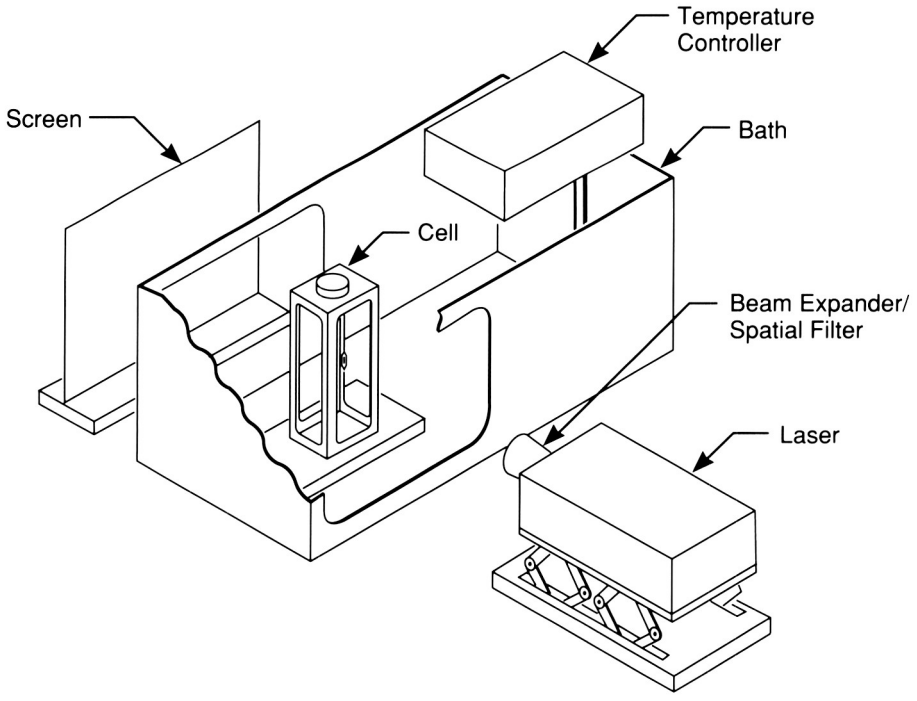

Figure 35. Solubility Measurement System

quality of crystals. Therefore the laser-scattering technique will be useful in characterization of crystals grown in planned flight experiments.

Ground-based research focused on the growth of nonlinear optical and electro-optical materials has identified l-arginine phosphate as a candidate material for a space flight experiment. It is of interest because its nonlinear optical properties exceed those of materials currently in use in industry and because it can be grown from low temperature aqueous solution. The physical properties of crystals and growth solutions are being investigated to determine the possible effects of a low-gravity environment on growth of this material.

Two new techniques for nucleation and growth of crystals from solution have been developed. One technique uses a rotating growth chamber in which small crystallites are maintained suspended in solution. The other technique uses a forced convection cell in which the flow of solution pumped through a nozzle holds a larger crystal suspended where it cannot contact the cell walls. These techniques have been used to nucleate and grow materials such as Rochelle salt and triglycine sulfate. After further development they will be used to grow protein crystals.

Lal, R. B., Aggarwal, M. D., Batra, A. K., Kroes, R. L., Wilcox, W. R., Trolinger, J. R., and Cirino, P.: Growth of Triglycine Sulfate Crystals Aboard Spacelab 3. Spacelab 3 Mission Science Review, NASA Conference Publication 2429, 1987.

Reiss, D. A., Kroes, R. L., and Anderson, E. E.: Growth Kinetics of the (001) Face of TGS Below the Ferroelectric Transition Temperature. J. Crystal Growth, Vol. 84, no. 1, pp. 7-10, 1987.

Kroes, R. L., Reiss, D. A., and Anderson, E. E.: Analysis of the Growth of Ferroelectric Single Crystals of TGS. J. Crystal Growth, submitted, 1988.

R. L. Kroes/ES76
(205) 544-7770
Sponsor: Office of Space Science and Applications

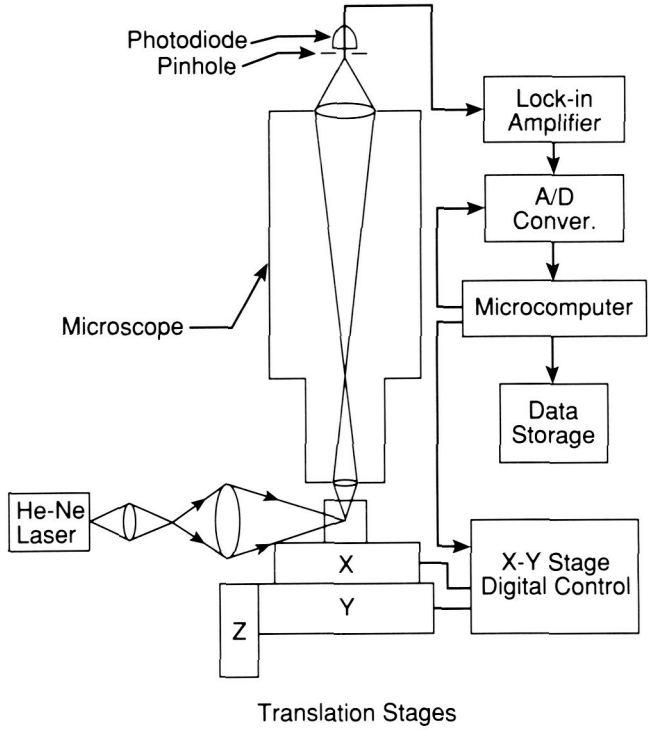

Figure 36. Laser-Scattering Microscope

Electrophoresis

Prior theories involving electroosmosis, electrokinetics, and other effects have proven inadequate to explain the observed sample spreading and performance degradation in continuous flow electrophoresis. Electrohydrodynamic flows are suggested as the main cause, and these findings should contribute to efforts to improve the performance of electrophoresis in the laboratory and in space.

It has been shown theoretically that an electric field (ac or dc), parallel to a circular filament of conducting fluid surrounded by fluid of a different conductivity, produces an electrohydrodynamic flow that distorts the filament into an ellipse or ribbon (Fig. 37). The major axis of the ellipse is either parallel to or normal to the field, depending on the conductivity and dielectric constant of the filament fluid relative to those of the surrounding fluid. For equal dielectric constants, the major axis is parallel to the field if the filament conductivity is greater than that of the surrounding fluid (Fig. 37c) and normal to the field otherwise (Fig. 37b). The flow and distortion rate is proportional to the square of the applied field.

It has been further shown theoretically that the flow associated with an elliptic cross section maintains the elliptic shape while it continues the distortion, provided the deviation from a circular cross section is small. As the ellipse stretches, small deviations from an elliptic cross section appear. Using an energy argument based on the assumption of an elliptic cross section, the circular filament continues to flatten indefinitely, forming a ribbon, either parallel to the field or normal to it. The nature of the analysis, the physics of the flow, and the related experiments appear to confirm this behavior.

In laboratory experiments, an aqueous electrolyte (barbital buffer) and a sample of the same material were used with polystyrene latex added for visibility in a free flow electrophoresis apparatus. The flow rate and configuration were typical of commercial instruments and the McDonnell Douglas Continuous Flow Electrophoresis System. Electrokinetic and electrophoretic effects, and electroosmosis were eliminated by using an ac field. Distinctive ribbons were formed, in both directions, at small fields of order 50 V/cm or less. All observations were consistent with the theories described above.

Rhodes, P. H. and Snyder, R. S.: Electrohydrodynamic Distortion of Sample Streams in Continuous Flow Electrophoresis. Journal Colloid and Interface Science, in press, 1988.

R. S. Snyder/ES76
(205) 544-7805
Sponsor: Office of Space Science and Applications

a. No Stream Distortion

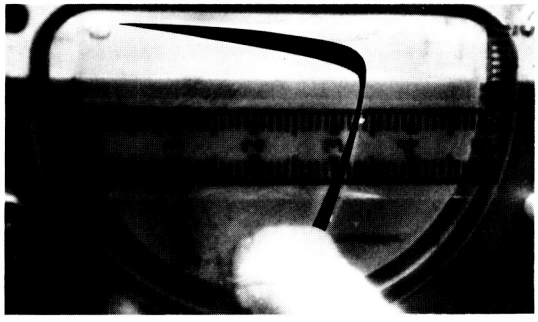

b. Vertical Ribbon Formation when Field is Applied to Low Conductivity Sample Stream

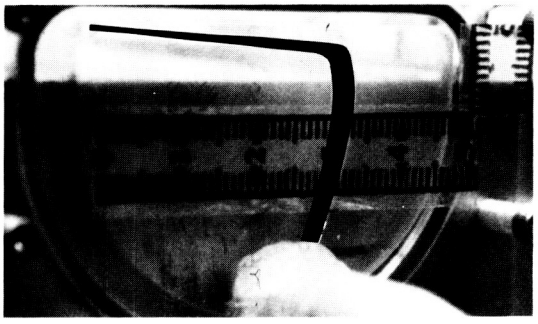

c. Horizontal Ribbon Formation when Field is Applied to High Conductivity Sample Stream

Figure 37. End-on View of Polystyrene Latex Sample Stream at Zero Voltage in Thick Electrophoresis Chamber

Protein Crystal Growth

Protein crystallography is currently the most powerful method for the determination of the three-dimensional structure of proteins and other macromolecules. This method usually requires crystals which are relatively large (0.5 to 1.0 mm) in size and possess a reasonably high degree of internal order. Consequently, protein crystal growth has become the subject of an increasing number of fundamental studies, including several ongoing microgravity experiments. The knowledge of the three-dimensional structure of macromolecules is of fundamental importance to the field of molecular biology, and is presently receiving considerable attention from the biotechnology industry based on its promising potential for application in rational drug design and protein engineering.

A diffraction facility has been recently constructed for evaluating results from both ground-based and future flight experiments manifested on STS-26, STS-29, and others. In addition to the routine evaluation of the diffraction properties of protein crystals, this facility is utilized to determine the three-dimensional structures of several challenging problems in molecular biology. One structural problem of particular interest in this laboratory is that of human serum albumin (HSA).

The serum albumin proteins are among the most highly studied and applied in biochemistry. More than 25,000 literary citations involving the biochemistry and/or applications of serum albumins have been published since 1969. The mammalian serum albumin proteins are known to be the product of three tandem gene duplications, possess high helical content (50 percent) and high cysteine content (17 disulfides), and have approximate molecular weights in the range of 65,000 daltons. Although the principal function of serum albumin remains disputed, it contributes significantly to colloidal osmotic blood pressure and to many transport and regulatory processes. A number of studies have focused on the multifunctional binding properties of serum albumin. This protein binds a wide variety of substrates, ranging from metals such as calcium and copper, to fatty acids, hormones, and a broad spectrum of therapeutic drugs. The majority of these binding studies have involved human serum albumin and have shown that the distribution, free con-

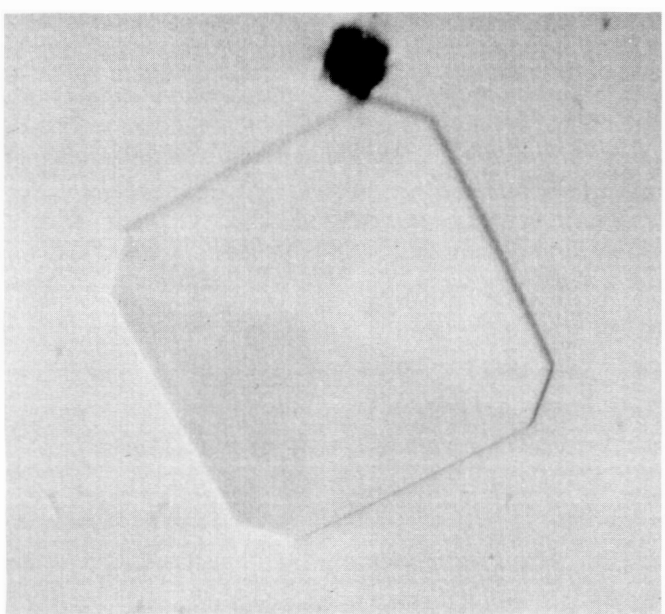

Figure 38. Tetragonal $P4_12$ Crystal of Human Serum Albumin

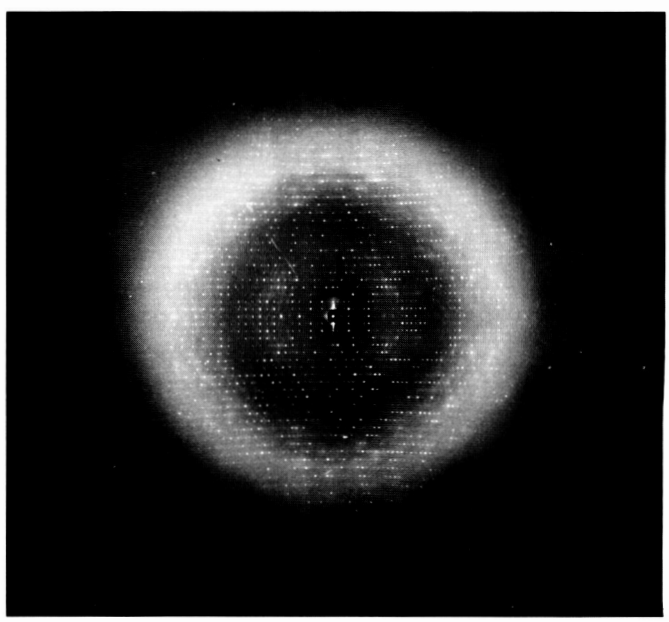

Figure 39. X-Ray Oscillation Photograph of Human Serum Albumin Crystal Taken at Brookhaven Synchrotron Light Source

centration, and metabolism of various pharmaceuticals can be significantly altered as a function of their binding constant to HSA.

A detailed knowledge of the three-dimensional structure of serum albumin is imperative to fully understand the binding modes as well as many of the physical properties of this multifaceted protein. In addition, since many therapeutic agents are rendered less effective or entirely ineffective by virtue of their interaction with HSA, it is apparent that the complete knowledge of the three-dimensional structure of HSA will find extensive and unlimited application in pharmaceutical research. Increasing the in-vivo efficacy of pharmaceuticals based on the knowledge of their interaction with HSA will create the second step in rational drug design. Although the structure of human serum albumin has been the goal of ongoing crystallographic investigations for many years and several crystal forms have been obtained, the crystal structure remains unknown presumably due to difficulties with crystal size, quality, and/or reproducibility.

Because of the importance of the protein, its availability, and the problems associated with the documented crystal forms, human serum albumin is one of several proteins for which the effect of microgravity on protein crystallization is being studied. As part of MSFC's ground-based research in protein crystal growth, a new crystal form of HSA has been obtained and its structure determination initiated. The crystals grow reproducibly as large tetragonal plates (Fig. 38) in the space group $P42_12$ and are of sufficient quality to determine the three-dimensional structure (Fig. 39).

D. C. Carter/ES76
(205) 544-5492
Sponsor: Office of Space Science and Applications

Phase Partitioning

There is need in many areas of biomedical research and technology for separation processes by which discrete subpopulations of cells can be isolated from more complicated mixtures. Ideally such processes should be safe, cost-effective, easily scaled-up, and capable of isolating viable, normally functioning cells. The separation method termed phase partitioning meets the above criteria and is understandably enjoying widespread interest and application as a biomedical and biotechnical separation technique. Phase partitioning involves suspending particles in a biphasic liquid system made by adding two polymers to a buffered, aqueous, isotonic solution. The mixed phases readily demix (isothermally) with cells differentially partitioning between either liquid phase and/or the phase interface.

The microgravity environment of space offers a unique opportunity to study particle partition under conditions of true equilibrium, free of effects caused by cell sedimentation or rapid (i.e., turbulent) convective phase demixing. Microgravity provides an opportunity to carry out cell partitions unobtainable on Earth.

Space-based research presently centers around a Phase Partition Experiment (PPE) scheduled to fly in 1988 on STS-26. The PPE on STS-26 (Fig. 40) is a simple hand-held experiment designed to yield experimental factors (e.g., chamber wall material/coatings, phase volume ratio, interfacial tension) to affect the demixing rate of select phase systems known to be useful for the separation of cells on Earth. In addition, the experiments are designed to shed light on the ability of chamber wall material/coatings to control the final disposition of the demixed phases. The experiment consists of shaking a PPE unit containing 18 different chambers, each containing a mixing ball and unique phase system. (In each chamber one of the phases has been dyed with an inert dark blue dye.) The PPE unit is then photographed as the phases demix, with time-sequence data being spontaneously imprinted on each negative. The resulting

photographs are densitometrically analyzed to provide kinetic information concerning phase demixing. The results of the STS-26 PPE should allow design of a meaningful microgravity cell partition experiment.

Walter, H., Brooks, D. E., and Fisher, D.: Partitioning in Aqueous Two-Phase Polymer Systems. Academic Press, Orlando, 1985.

Karr, L. J., Van Alstine, J. M., Snyder, R. S., Shafer, S. G., and Harris, J. M.: Cell Partition by Immunoaffinity Phase Partitioning with PEG-Modified Protein A. J. Chromatog., Vol. 442, pp. 219-227, 1988.

Bamberger, S., Van Alstine, J. M., Harris, J. M., et al.: Demixing of Aqueous Polymer Two-Phase Systems in Low Gravity. Sep. Sci. and Technol., Vol. 23, pp. 17-38, 1987.

R. S. Snyder/ES76
(205) 544-7805
Sponsors: Office of Space Science and Applications

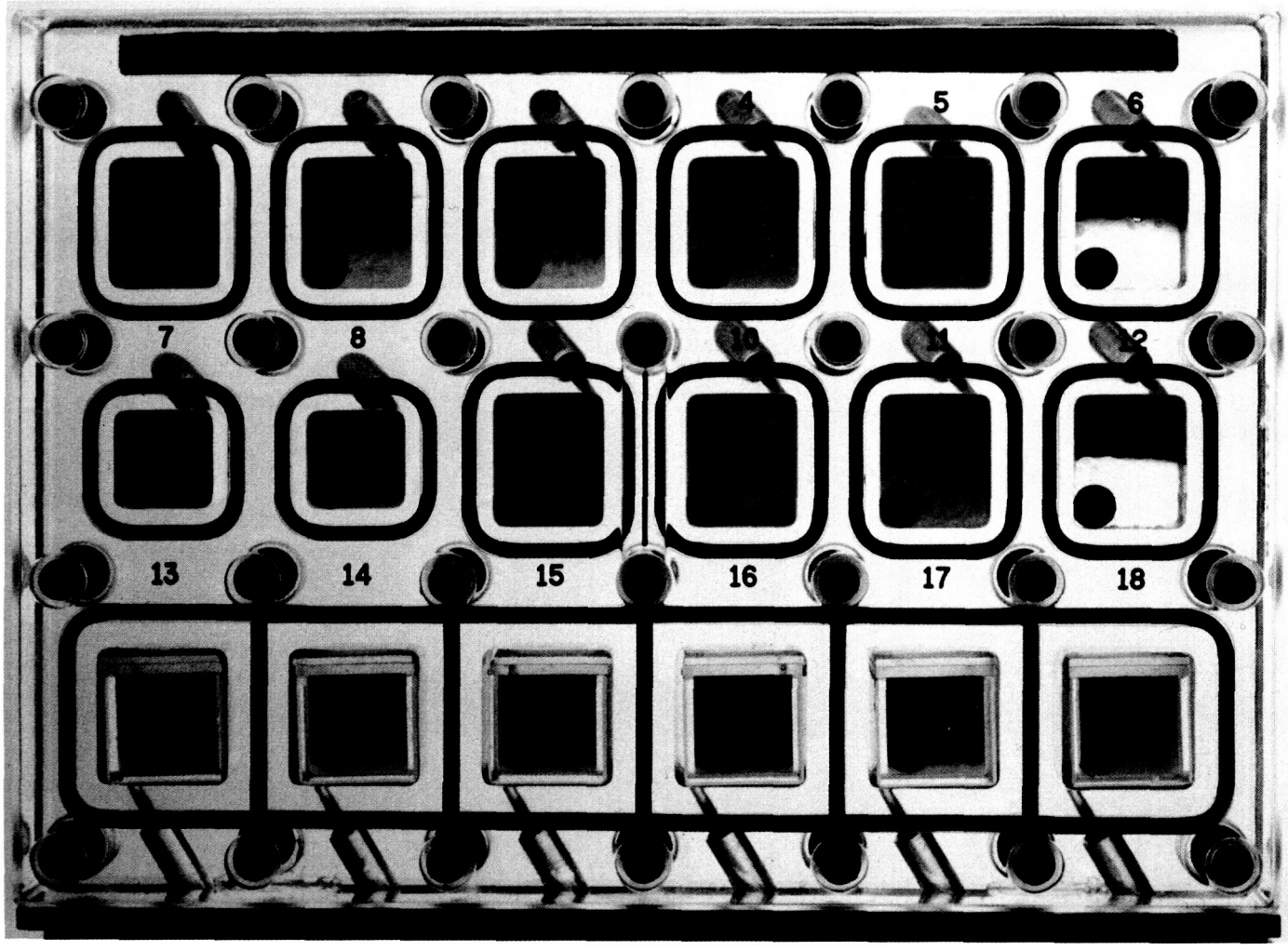

Figure 40. Phase Partition Experiment (PPE) Module for STS-26

ORIGINAL PAGE
COLOR PHOTOGRAPH

Astronomy and Astrophysics

Astronomy and astrophysics have played an important role in the space program since its beginning. MSFC has had key science and engineering involvement in astronomy and astrophysics experiments, payloads, and missions including Skylab, the High Energy Astronomy Observatory, Spacelab, the Hubble Space Telescope, the Astro mission, the Gamma Ray Observatory, and, more recently, the Advanced X-Ray Astrophysics Facility (AXAF). The Space Science Laboratory is engaged in experimental and theoretical research in x-ray astronomy, gamma ray astronomy, astrophysics, infrared astronomy, and cosmic rays. New detector systems, instruments, and experiments for future space flight missions are under development. Balloon-borne experiments and ground-based astronomical observations are being conducted, and, in connection with the AXAF program, an increasing role in astrophysics at MSFC can be foreseen.

Infrared Astronomy and Cometary Research

This year, infrared (IR) astronomy at MSFC has focused on two research areas: the extensive observation of comets and star-forming regions with the previously developed MSFC mid-IR camera and the development of two new IR detector systems. The mid-IR camera, which has been fully operational for 2 years, was developed for astronomical observations at 8 to 30 μm. The key component is a spatial array of 20 gallium-doped germanium bolometers, which are extremely sensitive in the high thermal background environment of ground-based observations. Because of its relatively large spatial coverage, the camera permits many types of observations that are not possible with smaller field-of-view, single-channel IR photometers.

The unique capabilitiesof this camera were demonstrated when it was used to obtain the first ground-based thermal-IR image ever made of a comet, Giacobini-Zinner, followed by images of Comet Halley and Comet Wilson (March 1987). This year, the first detection was made in the thermal IR of Comet Tempel 2 which is being studied widely by astronomers. These observations were made at the NASA IR Telescope Facility on Mauna Kea. The IR radiation from comets is emitted by dust grains which have been expelled from the comet nucleus and heated by sunlight. Detailed analysis of the IR images has provided insight into the rate at which particulates leave the nucleus, the types of particles, and their temporal behavior. Because nearby comets rapidly change their appearance, the MSFC IR camera is uniquely suited to obtain an image in a short enough time period for the results to be meaningful.

In addition to its application in cometary research, the MSFC IR camera has studied IR radiation from galaxies detected by the Infrared Astronomical Sat-

ellite. The camera permits detailed maps to be made of these galaxies, which often are strong IR sources. The IR radiation is produced when dust is heated by newborn stars, and currently provides the only means to determine how rapidly stars are forming. The efficiency of the IR camera is demonstrated by the capability to map more than ten galaxies in an observing night, whereas with previous IR instruments a whole night was needed to map just one galaxy.

In parallel with the observational program using the mid-IR camera, which has moderate spatial resolution (about 4 arc-sec), is the development of a new bolometer array which will have very high spatial resolution (about 0.4 arc-sec). This system, which will be cooled to 0.3 K, will be used to study the 8- to 30-μm emission from extremely distant or very compact sources such as ultraluminous galaxies and quasars. The array design is nearing completion and some procurement has begun. In addition, construction has begun on a unique camera for use in the near-IR, at 1 to 5 μm. The near-IR camera will contain an integrated array with 4,000 pixels and will be used for a broad range of projects including the search for newly forming galaxies.

Campins, H., Telesco, C. M., Decher, R., and Ramsey, B. D.: Thermal Infrared Imaging of Comet P/Halley. Astron. and Astrophys., Vol. 187, p. 601, 1987.

Decher, R., Telesco, C. M., Golisch, W. F., and Campins, H.: Comet P/Temple 2. IAU Circular 4580, 1988.

Telesco, C. M., Wolstencroft, R. D., and Done, C.: The Enhancement of Infrared Emission in Interacting Galaxies. Astrophys. J., Vol. 329, p. 174, 1988.

C. M. Telesco/ES63
(205) 544-7723
Sponsor: Office of Space Science and Applications

Experimental X-Ray Astronomy

The x-ray astronomy laboratory has concerned itself primarily with the development of advanced detectors to explore the energy range of 5 to 100 keV. This regime is above that accessible to conventional reflecting x-ray telescopes, such as the type flown on the Einstein High Energy Astronomy Observatory-2 and the European X-Ray Astronomy Satellite, and thus remains ripe for exploration.

The basic requirements for detectors in this energy range are well satisfied by xenon-filled multiwire proportional counters (MWPC) which combine large collecting areas with reasonable energy and spatial resolution. While the standard MWPC has been in use for a long time, several techniques have been developed that dramatically improve the performance of the device. The first of these is multistep operation, wherein the detector is divided into two regions, one devoted to measuring the energy of the incoming x-ray photon and the other devoted to position sensing. In this way the detector can be simultaneously optimized for both parameters, a condition which is impossible to achieve in a standard MWPC. The second technique is that of fluorescent gating, which makes use of the fact that above the K shell in xenon (35 keV), true x-ray interactions predominantly induce fluorescence in the detector gas. By detecting this fluorescence and accepting only those events that produce it, the pervasive cosmic ray background, against which all sources must be measured, is effectively discriminated against.

These two techniques have been combined in a flight detector which is currently under construction. It will form the heart of a coded mask telescope that will give 7 arc-min angular resolution, 6 percent energy resolution (at 60 keV) and have a useful collecting area of about 600 cm^2. The instrument will operate over the energy range of 20 to 100 keV and

will be flown on a high-altitude balloon in conjunction with a telescope developed by the Harvard-Smithsonian Center for Astrophysics. The first flight of the joint payload is scheduled for March 1989.

In addition to building a flight instrument, work continues on further improving the detector performance and toward this end several promising areas are currently being explored. Typical of these is the role played by the quench gas which is added to the xenon to stabilize the detector. A judicious choice here can lead to increased ionization, through a process called the Penning effect, which in turn lowers the operating voltage and improves the energy resolution. Tests are currently being carried out on many candidate binary and tertiary mixtures.

As a complement to the pure x-ray work the group is collaborating on a joint x-ray/infrared project to develop a near infrared camera based on an InSb 58 by 62 array. This instrument will be used for detailed study, in the 2 to 5 μm region, of celestial sources discovered at x-ray wavelengths. The array and its associated drive electronics have been delivered and the in-house development of the dewar/optics and the data handling electronics is midway toward completion. The system should be operational in late 1988 or early 1989.

Ramsey, B. D. and Weisskopf, M. C.: The Performance of a Multistep Proportional Counter for Use in X-Ray Astronomy. IEEE Trans. on Nucl. Sci., Vol. NS-34, p. 672, 1987.

Ramsey, B. D., Weisskopf, M. C., and Elsner, R. F.: A Fluorescent Gated Proportional Counter for X-Ray Astronomy. Proceedings of the Second International Symposium on Optical and Electro-Optical Applied Science, SPIE, Vol. 597, p. 213, 1986.

Ramsey, B. D. and Agrawal, P. C.: Quench Gases for Xenon and Krypton Filled Proportional Counters. Nucl. Instr. and Meth. in Phys. Res., in press, 1988.

M. C. Weisskopf/ES65
(205) 544-7740
Sponsors: Office of Space Science and Applications
Center Director's Discretionary Fund

Observational and Theoretical X-Ray Astronomy

During the past year, research in x-ray astronomy focused on three topics: quasi-periodic oscillations (QPOs) from galactic bulge x-ray sources, models for the x-ray and gamma ray emissions from the recent supernova (SN1987A) in the Large Magellanic Cloud, and studies of active galactic nuclei.

The study of QPOs is of great interest because of their potential use as a probe of the physical properties and processes taking place in galactic bulge binary x-ray sources. During the past year, various aspects of shot-noise models for QPOs have been explored and related to physical models for these sources. Calculations were completed this year of the cross-correlation functions and cross-spectra expected under conditions in which the x-ray source is encased in a hot electron scattering cloud. These results allow observers to compare their results to physically meaning formulae rather than to empirical formulae with no physical basis. The first discussion and calculations of the application of third moment analysis to QPO x-ray sources were also completed and published this year. European X-Ray Astronomy Satellite timing data have been obtained for three bright QPO sources for the purpose of measuring their third moments and providing further physical constraints on physical models for these sources. Studies continue of the physical properties and effects of the electron scattering cloud thought to encase the QPO sources. This work entails the Monte Carlo simulation and analytical calculation of the scattering process leading to predictions for the expected relative delays between photons of different energies as well as for the emergent spectrum. The calculated cross-correlation functions and cross-spectra, mentioned previously, provide the mathematical tools necessary for linking observational results with this theoretical work.

The supernova SN1987A discovered in February 1987, in the Large Magellanic Cloud, has generated great excitement among astronomers because of the opportunity to study one of the most violent events in

the universe at relatively close range. Theoretical calculations carried out in the X-Ray Astronomy Branch during the past year show that significant mixing has already taken place in the supernova ejecta. This mixing is required in order to account for the early appearance of x rays and gamma rays from the supernova. In addition, these calculations provide predictions for the evolution of the x-ray and gamma ray light curves and spectra over the course of the coming months and years. The effects of mixing on the gamma ray lines expected from the supernova are especially important as these lines provide an important probe into the composition and distribution of matter in the supernova ejecta.

The most luminous discrete x-ray sources in the Universe are quasars and clusters of galaxies. In contrast with the thermal bremsstrahlung emission from the intracluster plasma of the galaxy cluster sources, the physical processes occurring in quasars and other active galactic nuclei (AGNs), such as blazars (highly polarized quasars), radio galaxies, and Seyfert 1 galaxies, are not well understood. It is, however, generally believed that AGNs are powered by accretion onto a supermassive black hole, which frequently leads to the formation of a relativistic jet which emits nonthermally by way of the synchrotron and Compton-scattering mechanisms. This year a research program was initiated into x-ray emission from AGNs and its relationship to radiation observed in other spectral domains. In collaboration with the National Radio Astronomy Observatory, Virginia Polytechnic Institute, and the University of Puerto Rico, it has been shown that the radio emission from the blazar AO 0235+164 is well explained in terms of synchrotron emission from an adiabatic, relativistic jet, and that the absence of strong Compton-scattered x rays required an apparent velocity of the jet exceeding 25 times the speed of light, a value supported by very long baseline radio observations. In collaboration with the Lawrence Livermore National Laboratory, a numerical code is being developed to determine self-consistently the structure and emergent spectra of thermal accretion disks, which may account for some of the ultraviolet emission from AGNs. When completed, this code will also be applicable to other thermal accretion disks, such as those in the x-ray binaries and cataclysmic variables.

Elsner, R. F., Shibazaki, N., and Weisskopf, M. C.: Moment Constraints on Physical Models for Quasi-Periodic Oscillations from Galactic X-Ray Sources. Ap. J., Vol. 327, p. 742, 1988.

Ebisuzaki, T. and Shibazaki, N.: The Effects of Mixing of the Ejecta in the Hard X-Ray Emissions from SN1987A. Ap. J. Lett., Vol. 327, p. L5, 1988.

O'Dell, S. L., Dennison, B., Broderick, J. J., Altschuler, D. R., Condon, J. J., Payne, H. E., Mitchell, K. J., Aller, H. D., Aller, M. F., and Hodge, P. E.: Radio Variability of the Blazar AO 0235+164. Ap. J., Vol. 326, p. 668, 1988.

M. C. Weisskopf/ES65
(205) 544-7740
Sponsor: Office of Space Science and Applications

Directional Model for Geomagnetically Trapped Protons in Low-Earth Orbit

The highly anisotropic nature of the radiation in low-Earth orbit has previously been ignored for spacecraft shielding calculations because standard environmental models describe the omnidirectional flux only, because the varying attitude of the spacecraft in the environment is assumed to average out the effect, and because of the added complexity of the calculation. Space Station Freedom is planned for a 28.5° inclination circular orbit with an altitude in the range from 300 to 500 km. It will be stabilized and oriented so that one end of the habitation modules points along the velocity vector. For this orbit the galactic cosmic rays and the geomagnetically trapped Van Allen protons contribute most of the internal ionizing flux. Both sources are strongly modulated by the Earth's magnetic field. Here we consider only the trapped protons. Almost all the proton flux will be encountered in the region called the South Atlantic Anomaly produced because the Earth's magnetic field, though approximately dipolar, is not centered on the Earth. The protons follow helical paths about magnetic field lines as shown in Figure 41. As the field intensity increases, both the diameter and the pitch of the helix decrease until the pitch becomes zero. From there the helix reverses direction and protons travel up the field line. In the station's orbit almost all the protons observed are near their mirror points. Thus the flux is anisotropic with most of the flux arriving from a narrow band perpendicular to the local geomagnetic field direction. Atmospheric interactions also affect the proton angular distribution. Protons that are observed traveling eastward are following guiding centers above the observation point and protons traveling westward are following guiding centers below the observation point. The gyroradius for energetic protons in the anomaly is on the same order as the atmospheric density scale height. Thus westward traveling protons encounter a significantly denser atmosphere and are more likely to suffer atmospheric interactions and be lost. The resulting energy-dependent anisotropy is called the east-west effect. Although the anisotropy was previously documented, Henley first noted its greater importance for S. S. Freedom.

At MSFC a directional model of the trapped protons has been developed that can be used directly in the

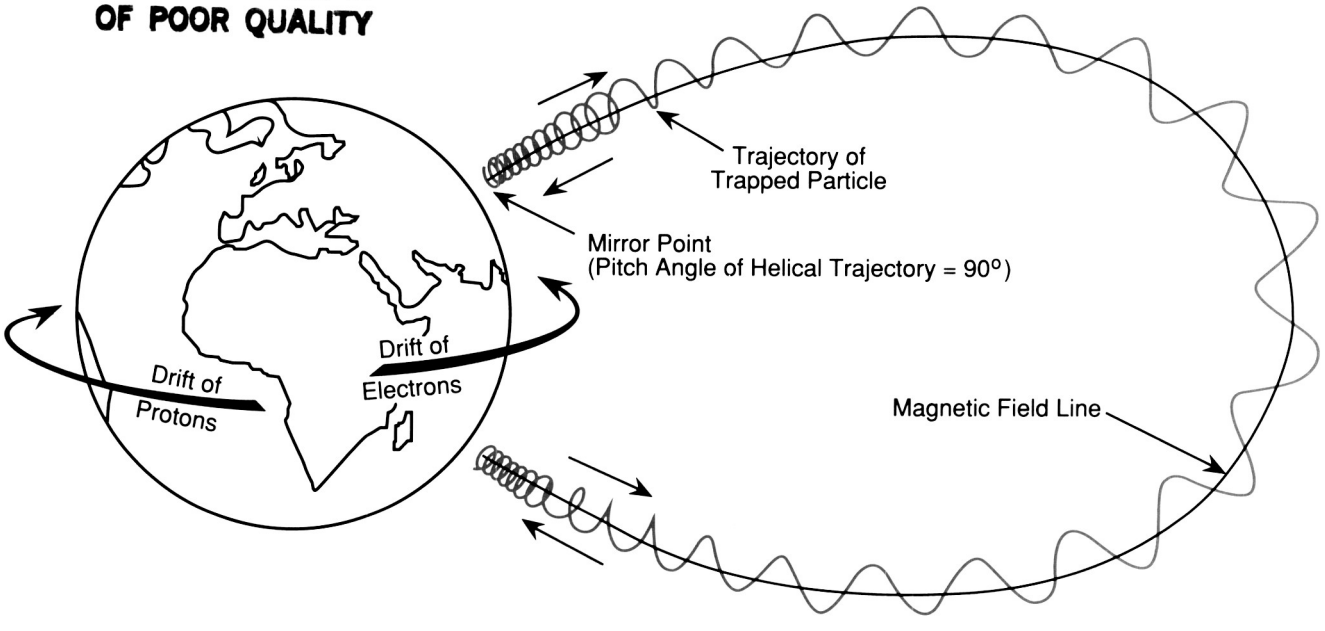

Figure 41. Path of Charged Particles in the Geomagnetic Field

calculation of particle flux and dose within spacecraft with complex shielding. The current omnidirectional proton environment model is the "Vette" model which is used with associated magnetic field models. The spacecraft orbit is used to generate magnetic field coordinates, and the Vette model yields the omnidirectional proton flux as a function of energy along the spacecraft trajectory. In this work a proton angular distribution, which depends on the atmospheric density gradient and local magnetic field direction, is calculated to replace the omnidirectional flux. This flux model can then be used directly to calculate the dose at internal points in a complex spacecraft with a sector mass shielding model. Figure 42 illustrates the directional effect of the protons on radiation dose calculated with the directional proton model and a simple example geometry. Here the shielding is a sheet of aluminum 1.8 cm thick. Behind the "detector" point is very thick shielding (greater than 25 cm). Results are shown with the shield oriented normal to the four geographic directions as well as to the vertical. The radiation dose differs by a factor of up to 3 depending on attitude. Directional effects on radiation dose have been noted as early as the Gemini missions. On Skylab and the Space Shuttle, which were not continuously stabilized with respect to trajectory or magnetic field, internal dose variations of factors of 2 have been observed primarily due to differences in shielding distributions. For S. S. Freedom the internal dose variations may be more extreme. The directional proton model will allow more accurate flux and dose calculations to be made as S. S. Freedom structure and equipment is designed.

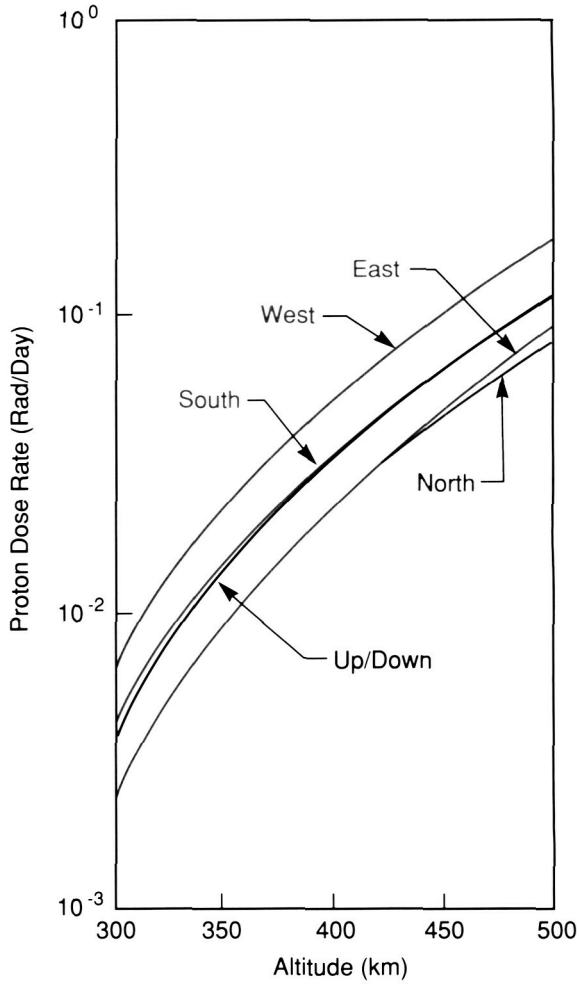

Figure 42. Average Proton Dose Rates for 28.5° Orbit

Heckman, H. H. and Nakano, G. H.: J. Geophys. Res., Vol. 74, p. 3575, 1969.

Henley, M. W.: J. Spacecraft and Rockets, Vol. 23, p. 108, 1986.

Watts, J. W., Parnell, T. A., and Heckman, H. H.: Approximate Angular Distribution and Spectra for Geomagnetically Trapped Protons in Low-Earth Orbit. Conference on the High Energy Radiation Background in Space, November 3, 1987; NASA TM, in press, 1988.

J. W. Watts/ES62
(205) 544-7696
Sponsor: Office of Space Station

Nuclear Interactions at Very High Energy

In 1986 and 1987 the European Center for Nuclear Research (CERN) accelerated oxygen and sulfur nuclei to 200 GeV per mass number (6.4 x 10^{12} eV total energy for sulfur.) This is ~50 times the energy available from other contemporary heavy ion beams. MSFC, in cooperation with The University of Alabama in Huntsville, Columbia University, Osaka University, and the University of Tokyo, performed 2 of 12 approved experiments with the beams. One of these, designated EMU05, used a novel arrangement of nuclear track emulsions in a magnetic field. This visual apparatus was somewhat similar to bubble or streamer chambers. The high spatial resolution of the emulsions (1 μm) allowed a very compact arrangement, and much smaller magnet, compared to streamer or bubble chambers, and also a variety of target nuclei (lead, silver, carbon, oxygen) to be used in the same exposure. The distributions of produced particles (mesons) were studied according to multiplicity (number), production angles, and transverse momenta.

A major objective was to study in detail the collision characteristics that affect the energy calibration of most cosmic ray composition experiments at very high energy. At energies above 10^{14} eV all cosmic ray experiments depend on nuclear interactions in the energy measuring process.

Another objective was to search for evidence that compression and heating of the nuclear complex during head-on collisions with target nuclei had formed a state of matter different from the constituent protons and neutrons. Theorists have predicted that at energy densities of about six times that of the undisturbed nucleus, the protons and neutrons might "melt" into a plasma of their constituents (quarks and gluons). This change should be signaled by unusual characteristics (varieties, momenta, angles) in produced particles.

The emulsion chambers comprised 200 μm thick target layers of lead and emulsion; and separated downstream thin (50 μm) emulsion tracking layers. The small emulsion chambers of approximately 10 cm^3 were transported into a standard beam magnet (1.8 Tesla) each accelerator cycle (12 sec) to expose the chamber to 10^3 sulfur nuclei/cm^3. Approximately 10^4 interactions of oxygen and sulfur nuclei in the targets were accumulated. The high spatial resolution of the emulsions has allowed the full range of produced particle (meson) numbers to be determined. The number of produced charged mesons ($\pi^{\pm}$, $K^{\pm}$, etc.) ranged up to 500, which saturated other experiments. Figure 43 gives the EMU05 observed multiplicity distribution in comparison with a recently calculated theoretical distribution. EMU05 also measured the transverse momentum distribution of produced charged mesons for individual events. Figure 44 shows data on a typical event which gives 400 MeV/c for the average of the mesons' transverse momenta.

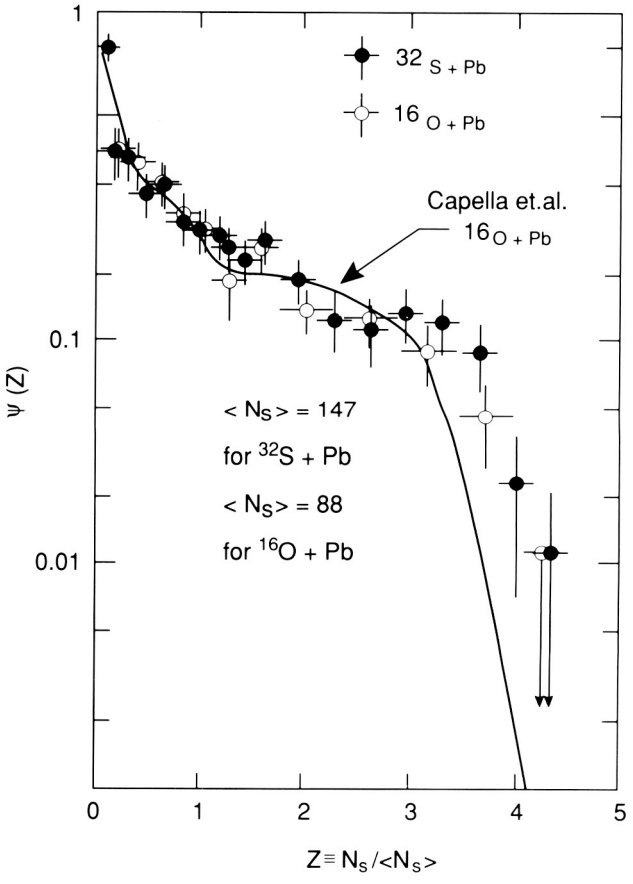

Figure 43. Frequency Distribution of the Number of Charged Mesons Plus Protons Produced in the Interactions of Oxygen and Sulfur on Lead Target Nuclei

Taken together the data so far analyzed from EMU05 indicate that collisions of the heavy nuclei can be interpreted with models which are based on a superposition of proton-like collisions. No tangible evidence for formation of a new state of nuclear matter is evident at this stage in the analysis, and the inferred energy density produced in the collision complex is below the predicted threshold for such production (according to most calculations). The data are being applied to calibrate energy measuring techniques used in cosmic ray experiments which are in progress at MSFC.

T. A. Parnell/ES62
(205) 544-7690
Sponsors: Office of Space Science and Applications
Center Director's Discretionary Fund

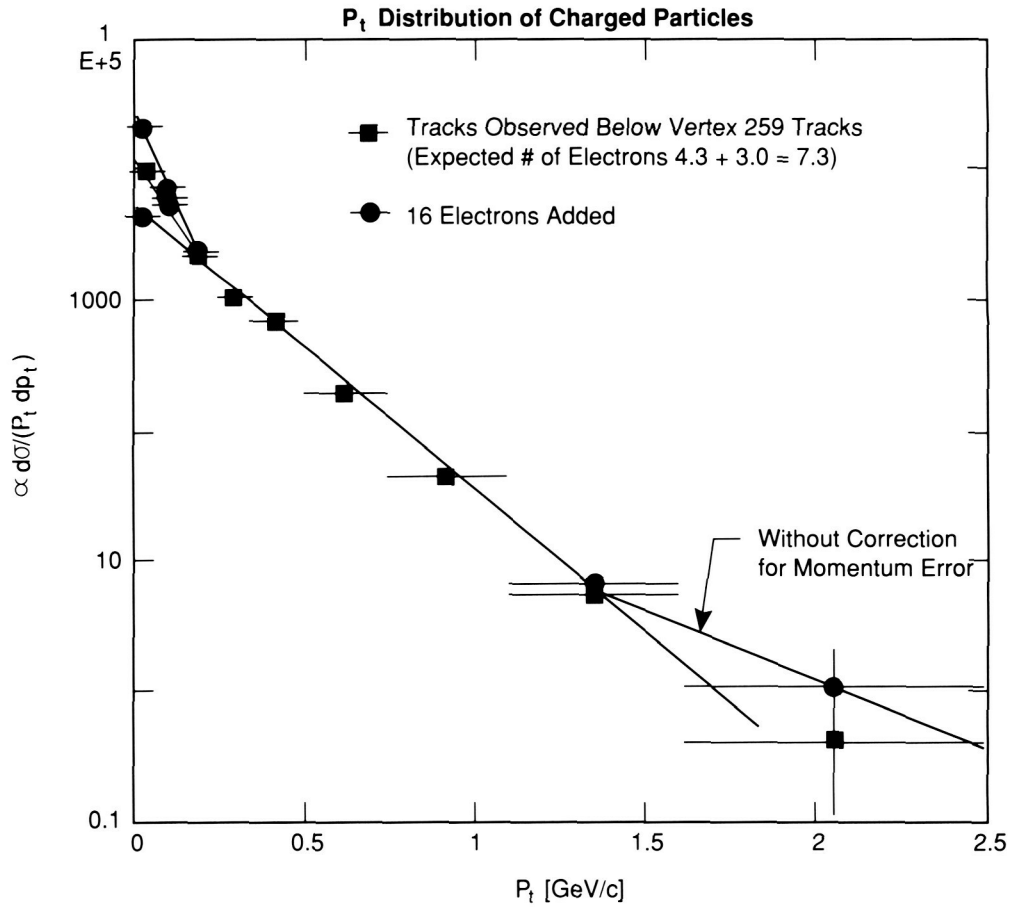

Figure 44. The Differential Transverse Momentum Distribution of Mesons Produced by Interaction of Oxygen Nuclei at 200 GeV/amu with Lead Nuclei

Balloon-Borne Observations of Supernova SN1987A

Supernovae are among the most important phenomena in astrophysics: they are the major site of nucleosynthesis, the formation of the elements. They provide enriched, new material into the interstellar medium, and they are a source of energetic particles and compact objects such as neutron stars and black holes. Furthermore, they contribute a significant fraction of the total luminosity of galaxies and the Universe.

Astronomers worldwide were elated when the nearest and brightest supernova in almost 400 years appeared on February 23, 1987, in the Large Magellanic Cloud (Fig. 45), a neighboring galaxy. The relatively nearby SN1987A (160,000 light years) provided an unprecendented opportunity to study this important phenomenon over all spectral regions. (The previous nearby supernova, in our own galaxy, was observed several years before the invention of the telescope.) The detection of neutrinos from this event was a major triumph for theoretical astrophysics. Nuclear gamma rays from newly-formed, radioactive isotopes had also been expected and their observation is a key to our understanding of nucleosyntheses.

The gamma ray astronomy research team at MSFC, in collaboration with the Lockheed Palo Alto Research Laboratory, was one of seven groups selected by NASA to perform balloon-borne observations of SN1987A from Alice Springs, Australia. Three successful balloon flight experiments were conducted in 1987 and 1988. Among the accomplishments of these experiments were the first high resolution detection of gamma rays from SN1987A and the most accurate measurements of the hard x-ray continuum radiation from SN1987A.

A balloon flight gondola was developed in the Space Science Laboratory of MSFC to carry the Lockheed detector, and on the later flights, two collimated scintillation detectors were also flown. These detectors were similar to those developed at MSFC for the Burst and Transient Source Experiment which will be aboard the Gamma-Ray Observatory. All gondola systems, including the pointing system, aspect, power, and detector interfaces, were developed at MSFC. Experience and components from previous MSFC balloon flights aided the development.

The first balloon flight observation took place on May 29, 1987, just 3 months after the discovery of the supernova. The Lockheed germanium detector flown on this flight was the first high resolution gamma ray detector to attempt an observation of

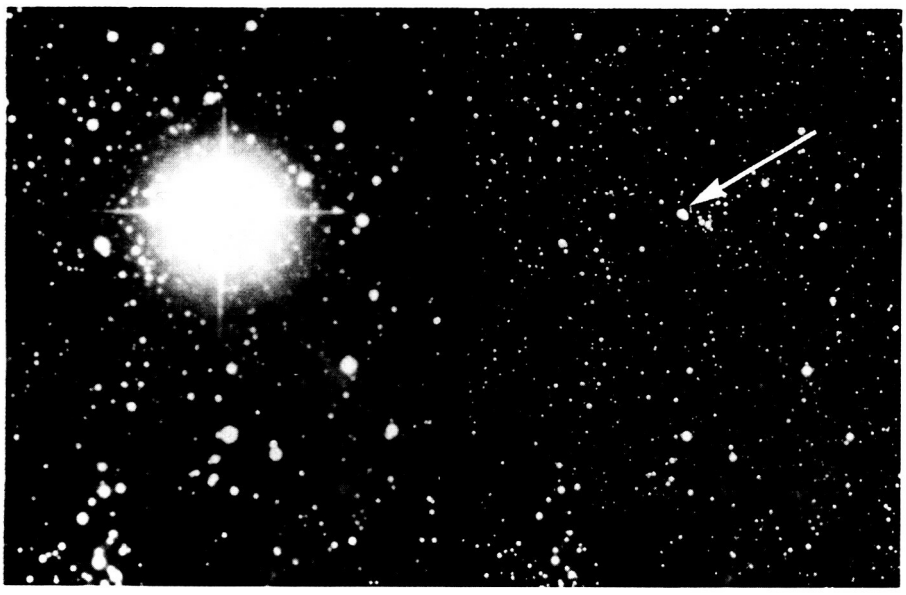

Figure 45. SN1987A In The Large Magellanic Cloud. The Arrow in the Right Half of the Figure Shows the Pre-Supernova Star

ORIGINAL PAGE
COLOR PHOTOGRAPH

SN1987A. The lack of detectable gamma rays on this flight indicated that the outer, expanding regions of the exploding star were still too thick to allow the transmission of radiation from the radioactive material inside.

By August of 1987, instruments aboard Japanese and Soviet spacecraft discovered x rays from the supernova, presumably from the inner regions of the supernova remnant. The next MSFC/Lockheed balloon flight occurred on October 29, 1987. This flight resulted in the first high resolution detection of gamma rays from SN1987A. Gamma rays at 847 keV were seen from the supernova. This gamma ray line results from the decay of radioactive Co^{56}, which, in turn, comes from the decay of Ni^{56}, the most abundant radioactive isotope expected to be produced during the supernova explosion. This isotope has a half-life of 80 days and decays into stable Fe^{56}.

The last two balloon flights also carried the MSFC-developed scintillation detectors. These detectors have provided the most accurate hard x-ray measurements of SN1987A that have been made to date. The spectrum of hard x rays agrees with that expected from higher energy gamma rays in the supernova being scattered and degraded in energy. The last flight, on April 8, 1988, produced follow-up observations over a broad energy range after the outer shells of the supernova had expanded considerably. Gamma rays and hard x rays were again seen but at a reduced intensity.

Data from SN1987A in all spectral regions will continue to be studied over the next years and decades, to give us the most comprehensive picture ever of the supernova process.

G. J. Fishman/ES62
(205) 544-7691
Sponsors: Office of Space Science and Applications
Center Director's Discretionary Fund

Composition of Galactic Cosmic Rays at High Energy

Galactic cosmic rays (GCRs) consist of the nuclei of elements in the energy range from 10^7 to $\geq 10^{20}$ eV, and have a composition (below ~10^{14} eV) considerably enriched in heavy elements compared to the average solar system abundance. The GCRs flux contains the most energetic particles in nature, accelerated by efficient cosmic processes which, to a large extent, are not yet understood. The GCRs bring to Earth the only sample of galactic material accessible. Thus, the site(s) of the GCRs origin, and differentiation in chemical composition due to acceleration processes, and propagation through intragalactic space are of interest. Since GCRs are charged particles and they encounter the magnetic field of the galaxy (and locally stronger ones around many objects, e.g., supernova remnants), they arrive at the Earth isotropically. Thus the observables that allow the origin(s), acceleration mechanism(s), and propagation parameters to be inferred are the chemical and isotopic composition over a large energy range of each element or nuclide. Of particular interest in this context is the chemical composition around 10^{15} eV, where the energy spectrum and intensity of cosmic rays depart from the smooth power law ($I = CE^{-2.5\pm0.2}$) observed at lower energies, first rising slightly and then falling rapidly. This is thought to be due to the end of galactic confinement of the GCRs by magnetic fields, the threshold of observing an extragalactic flux, and possibly a change in chemical composition or perhaps an admixture of elements from discrete sources. The region from 10^{15} to 10^{16} eV known as the "knee of the spectrum" has previously been measured by the large air shower (LAS) technique in which large arrays of detectors on the ground observe showers of particles caused by the primary nucleus interacting in the atmosphere. The LAS technique, which can be employed only above 10^{13} eV, measures the charge and energy of the primary indirectly. Various air shower experiments agree on the all-particle spectrum, but are inconsistent on the composition, finding that it is dominated by either protons or heavy nuclei.

Because of the rapid decrease of particle intensity with energy, experiments above 10^{13} eV require large exposure factors (M^2 – days) and consequently very few experiments have tried to measure the cosmic rays directly at higher energies. One of the few is the Japanese-American Cooperative Emulsion Experiments (JACEE). This collaboration includes scientists from MSFC, three U.S. universities, and five Japanese universities. Flying large (0.8 m^2 by 0.25 m) stacks of nuclear track emulsions and other passive detectors on balloons, the JACEE collaboration has accumulated about 12 M^2 – days of exposure at altitudes near 40 km. At 40 km the instruments are above 99.6 percent of the atmosphere and the cosmic rays penetrate the residual atmosphere with only a few percent interactions.

The instrument, known as an emulsion chamber, consists of about 150 layers of nuclear track emulsion (photographic material), acrylic plastic, etchable plastic nuclear track detectors, lead plates, and x-ray films. The cosmic ray nuclei undergo nuclear interactions in the chamber material, producing showers of particles that produce visible dark spots on the x-ray film (above ~10^{12} eV). The shower can then be traced upward in the emulsions until the nuclear interaction and the primary particle is found. The primary charge (atomic number of the nucleus) is then identified in both the emulsion and the etchable plastic track detector. Since the emulsion chamber technique depends on nuclear interactions and showers of particles, it bears some similarity to the large air shower technique. However, in the chamber

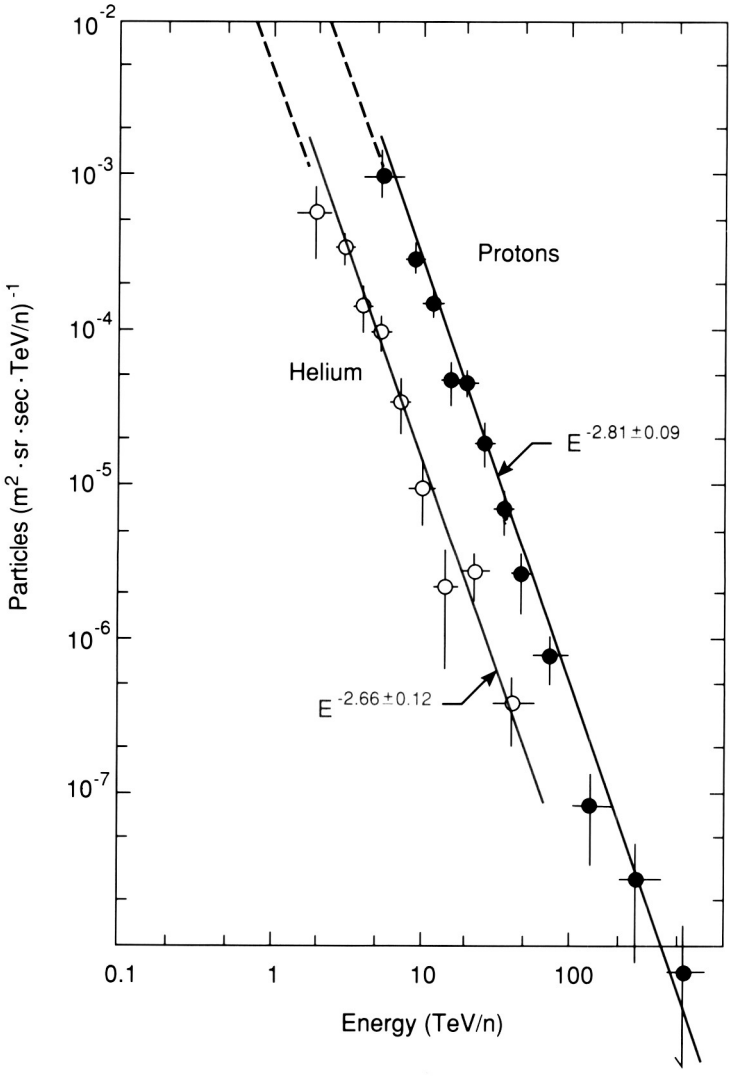

Figure 46. The Differential Spectra of Protons and Helium

the longitudinal development of the shower, the nuclear interaction, and the primary particle are all directly observable.

Using the emulsion chamber technique, personnel at MSFC, along with colleagues at the University of Alabama in Huntsville, and other JACEE colleagues, have made the most definitive measurement yet of cosmic ray composition above 10^{13} eV. Figure 46 shows the differential energy spectrum of cosmic ray protons up to ~10^{15} eV and helium to ~10^{14} eV. These spectra are not appreciably different from those measured at much lower energies by other balloon flight experiments, but the proton spectrum is significantly flatter than that measured by a previous experiment on the Russian PROTON spacecraft. In Figure 47 is the "all-particle" spectrum from the JACEE experiment which is the combined energy spectrum of all the elements in units of total energy per particle. In this data there is evidence of a small increase in the abundance of heavy elements with increasing energy above 10^{14} eV. Further balloon-borne experiments are planned to extend the energy range of these observations to cover the entire region of the "knee."

Burnett, T. H., et al.: Phys. Rev. Lett., Vol. 51 , p. 1010, 1983.

Burnett, T. H., et al.: Nuclear Instr. and Methods in Physical Research, Vol. A251, p. 583, 1986

Grigorov, N. L., et al.: In 12th ICRC Conf. Papers, Hobart, Tasmania, Vol. 5, p. 1746; ibid., p. 1752; ibid., p. 1760, 1971.

J. H. Derrickson/ES62
(205) 544-7698
Sponsor: Office of Space Science and Applications

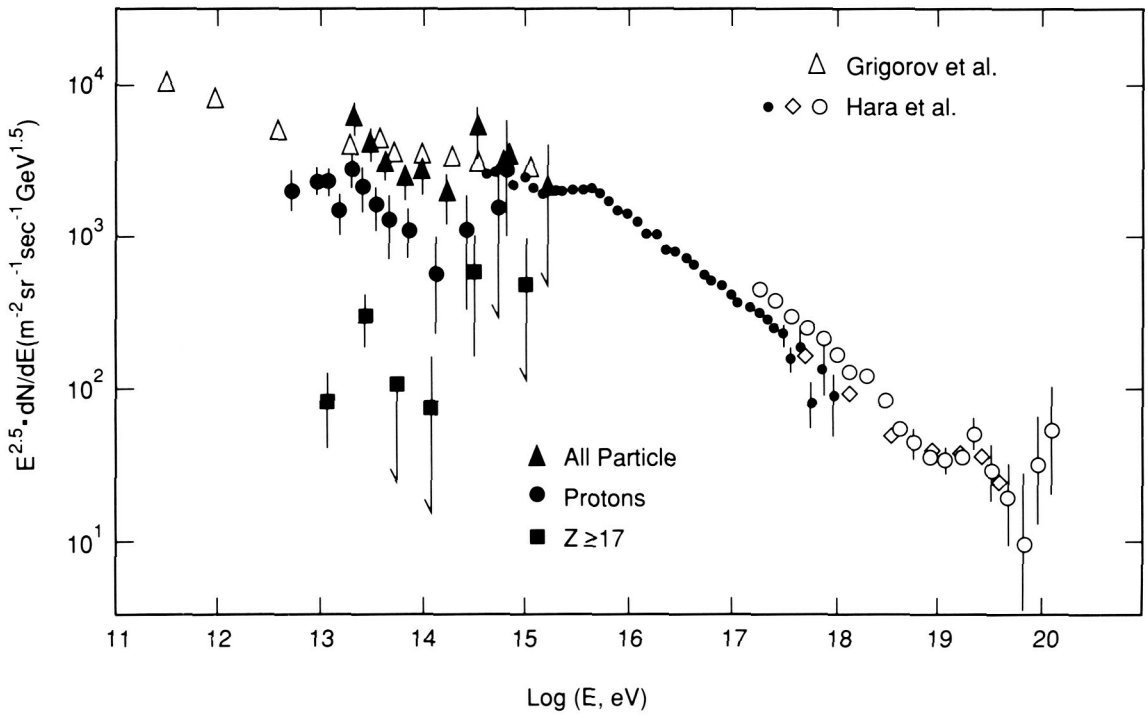

Figure 47. The All-Particle Energy Spectrum, the Proton Spectrum, and the Heavy Component (Z ≥ 17) from JACEE

Solar Physics

The Sun is the nearest star and as such is the source of energy which governs the environment of both the Earth and the space surrounding the Earth. To understand how the Sun influences terrestrial systems and controls the space environment, through which man will soon travel to explore the solar system, knowledge of the processes that occur in the Sun's outer atmosphere and lead to the generation of the high-energy particles and radiation that pervade interplanetary space is needed.

These phenomena are intimately connected to the Sun's magnetic field which is thought to be generated by a dynamo action arising from the interaction between convective and rotational motions at the base of the convection zone deep within the Sun. As the magnetic field emerges into the solar atmosphere it heats and concentrates atmospheric material into a wide range of structures. The instability of the structures gives rise to flares and coronal mass ejections whose products propagate through space to Earth and, together with the solar wind, create the environment of space.

The properties of the solar magnetic field form the basis of the research at MSFC. Through direct observation of the vector field, a capability developed at MSFC and still quite unique, we are attempting to understand how the energy stored in the magnetic field, by the convective motions of the Sun's atmosphere, is released and what the products of this release are. A new technology, normal incidence multilayer optics, has been pioneered for imaging the million degree plasma that forms the solar corona. This technology will allow us to observe how the influence of the magnetic field extends into the outer solar atmosphere, and coupled with new theoretical and analytical approaches, to understand how the magnetic field is transported through the solar system to the distant boundaries with interstellar space.

Solar Magnetic Fields

The interaction of magnetic fields and plasmas is a common process throughout the Universe and is the controlling force in the dynamic, high-energy phenomena observed on the Sun. Flares, mass ejections, and eruptive filaments are but a few examples of the energetic processes generated by solar magnetic activity. The origin, evolution, and development of the Sun's magnetic field to produce this activity are central themes in today's solar research and the focus of extensive work in observational studies.

MSFC has a unique instrument for observing the Sun's magnetic field, the MSFC Solar Vector Magnetograph. This instrument measures all three components of the magnetic vector on the Sun's surface, not just the single component that is measured with most other magnetographs in the United States and throughout the world. The additional information derived from observations of the complete vector field has made significant contributions to an understanding of the magnetic Sun. Because of this unique research, MSFC is recognized worldwide as a leader in the study of solar magnetic fields.

One area of research at MSFC that has had substantial import in the solar physics community has been the study of the nonpotential characteristics of the magnetic fields in active regions on the Sun and their relation to solar flares. Since a flare is a sudden release of magnetic energy, with energy built up in the preflare magnetic field by deformation of the field from its minimum energy, or potential configuration, then to understand the flare phenomenon, we need to measure the nonpotentiality of the field. A direct measure of the nonpotential nature of magnetic fields is provided by observations made with the MSFC Solar Vector Magnetograph of all three components of the photospheric magnetic field. The nonpotentiality of the field can be measured by

comparing the observed field with the field that would be observed if the field was in its lowest energy (or potential) state, and this potential field can be calculated from the boundary condition dictated by one component of the observed field. The greater the differences between the other two components of the observed and computed fields, the greater the nonpotentiality of the field. Such a comparison is demonstrated in Figure 48, which shows the magnetic field in a region where one of the greatest flares of the last solar cycle erupted on April 24, 1984. The flare is shown in Figure 48a, a photograph from the Big Bear Solar Observatory. Figure 48b displays the vector magnetic field measured with the MSFC magnetograph. The contours represent one component of the field (the line-of-sight component) with solid (dashed) contours designating fields rising out of (falling into) the photosphere. The other two components of the field are displayed in magnitude and direction by the length and angular orientation of the line segments. The potential field is displayed in the same format (Fig. 48c.) This potential field was calculated using the observed line-of-sight field as the boundary condition, so that nonpotential fields will be in areas where large differences in the length and orientation of the line segments are seen in comparisons of observed and potential fields. Comparison of Figure 48b and c shows that there are indeed large differences in the angles of the line segments along portions of the neutral line, the line separating rising and falling fields that meanders from top to bottom of the field-of-view. Comparison of panels a and b in Figure 48 shows that the great flare straddled this neutral line in the area where there were the greatest angular deviations in the line segments, i.e., where the field deviated the most from a potential configuration.

From quantitative analyses such as these, evidence has been established that there exist threshold values for the degree of nonpotentiality, the strength of the field, and the extent of the area of nonpotential fields, and these thresholds must be exceeded before a major solar flare erupts. Moreover, there always seems to be a local maximum of nonpotentiality on the neutral line right at the location where a flare starts.

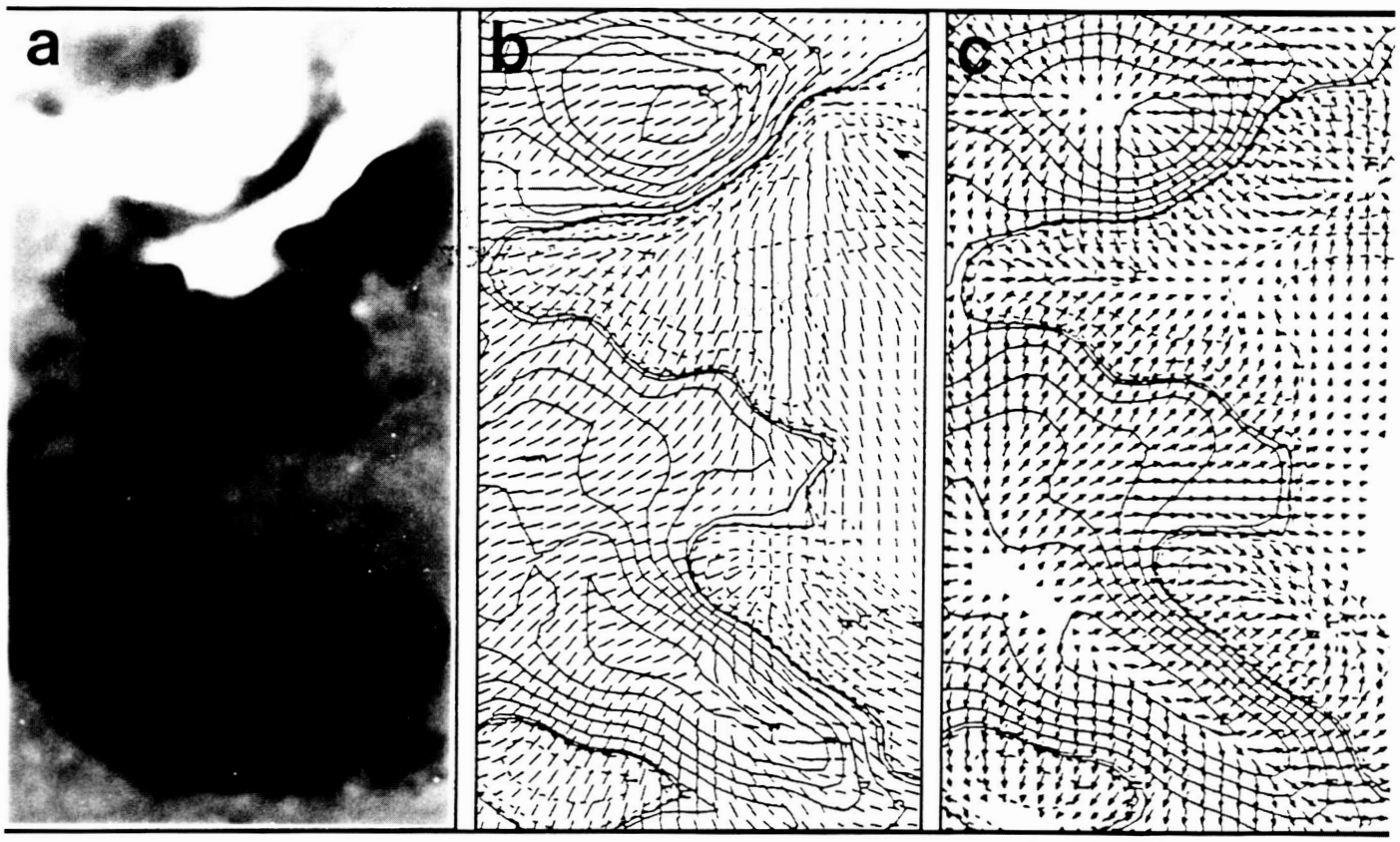

Figure 48. Nonpotential Magnetic Fields at Flare Sites

In work recently completed, techniques were improved in analyzing the magnetic field data by incorporating methods to eliminate projection effects* and to calculate the potential field for data that exhibit projection effects.† These techniques have enabled a correct analysis of the nonpotential characteristics of regions observed away from the center of the Sun so their evolution can be followed as they rotate from one edge of the Sun to the other. Initial results of a study of this evolution for the active region shown in Figure 48 indicate that significant increases in the length of the nonpotential area along the neutral line over several days could possibly herald the occurrence of major flares.

Another manifestation of solar activity is the enhanced heating seen in the chromosphere above active regions. Areas of intensified brightness produced by this heating are called solar plage; a good example is seen in Figure 49b. In Figure 49a, the active region is shown as it appears in the lowest visible layer of the Sun's atmosphere (the photosphere); the dark sunspots of this active region observed on September 23, 1980, are clearly visible. In the overlying atmosphere (the chromosphere), the plage appears mostly in the area between the three major sunspots. Of particular note is the manner in which the plage divides the inner, darkest part (umbra) of the largest sunspot. A recent study of this bifurcation phenomenon has demonstrated that this marked division of plage intensity in spot umbrae correlates strongly with the direction of the vector magnetic field there. Figure 49c shows this correlation: the direction of the field (indicated by the arrows) reverses in step with the abrupt change in emission. This correlation suggests that the heating is associated with magnetic fields that rise from the sunspot and fall into areas interior to the active region. The physical explanation is that the enhanced heat generated by magnetic reconnection of the strong fields interior to the active region is conducted along the magnetic field into the umbra. Since there is no equivalent heating source exterior to the active region (where the fields are much weaker), no heat is conducted along the magnetic field coming into the umbra from outside the region. Hence the sharp division of umbral emission in step with the change in field direction.

*Venkatakrishnan, P., Hagyard, M. J., and Hathaway, D. H.: Elimination of Projection Effects from Vector Magnetograms: The Pre-Flare Configuration of Active Region AR4474. Solar Phys., in press, 1988.

†Venkatakrishnan, P. and Gary, G. A.: Potential Field Calculations from Vector Magnetograms Obtained Away From the Center of the Solar Disk. Solar Phys., submitted, 1988.

M. J. Hagyard/ES52
(205) 544-7612
Sponsor: Office of Space Science and Applications

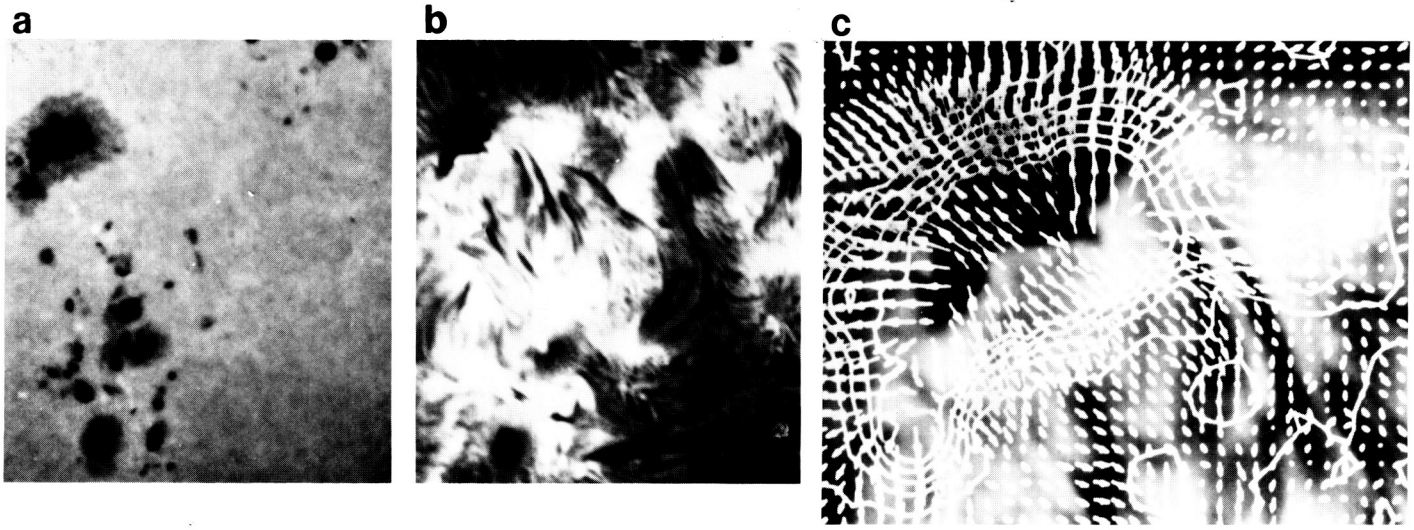

Figure 49. Correlation of Enhanced Emission in Sunspots with the Direction of the Magnetic Field

Convection Zone Dynamics

The gases at the surface of the Sun (the photosphere) are constantly in motion. Characteristics of these motions provide us with important information about the dynamics of the solar convection zone which extends from the photosphere down to a depth of about 200,000 km (120,000 mi). The motions themselves can be measured using the Doppler effect in which the wavelength of light emitted from the gas is shifted to the blue or red depending upon whether the gas is moving toward or away from the observer.

There are several different types of motion in the photosphere. One of these is an oscillatory motion in which areas of the photosphere move up and down with a period of about 5 min and velocities of about 300 m s^{-1} (700 mph). These 5-min oscillations are now known to be acoustic waves (sound waves) that are trapped inside the Sun. In addition to the 5-min oscillations there are several steady, or nearly steady, flows such as solar rotation, differential rotation, meridional circulation, and convective motions.

Each of these types of motion provides different information concerning the structure and dynamics of the convection zone. In order to study these motions, each component needs to be cleanly separated from the others so that their characteristics are not mixed. During the last year a filter was developed to separate the 5-min oscillations from the nearly steady flows.

The filter is a running average in time of observations typically taken every 60 to 75 sec. Several different types of averages were tested but one type consistently outperformed the others. This filter used a weighted average of every other data point so that the data are separated by 120 to 150 sec. Very little weight is given to points on either end of the average and most of the weight is on the three central points which are separated by 4 to 5 min. The results from one of these filters are shown in Figure 50 for artificial data that contained only the 5-min oscillations. This particular filter was 14 min long and used eight data points spaced at 2-min intervals. This simple filter removes nearly 99 percent of the signal due to the 5-min oscillations. A string of images filtered in this manner will contain only the nearly steady flows. The filtered images can then be sub-

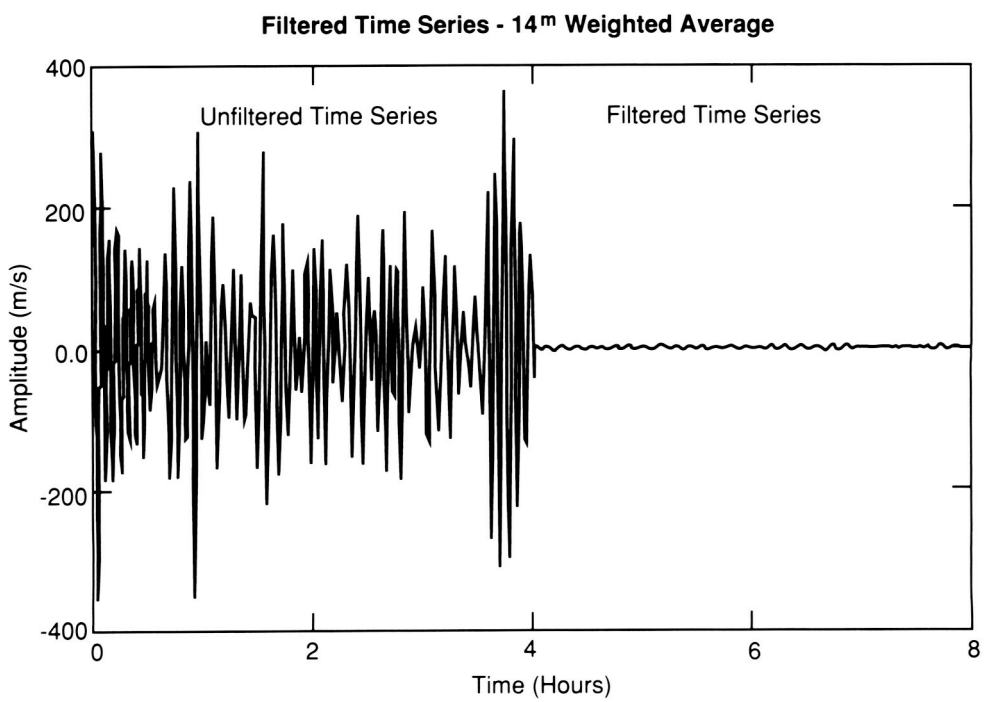

Figure 50. Effects of Filtering Artificial Solar Data Containing 5-min Oscillations

tracted from the unfiltered images to produce a string of data that contains only the 5-min oscillations.

Longer filters could be used to reduce the signal from the 5-min oscillations even further. However, the rotation of the Sun will tend to smear the flow patterns when very long filters are used. Experiments were conducted in which the filter length was varied to find the length that minimizes the errors from the combination of the 5-min oscillations and the rotational smearing of the steady flow pattern. Twenty minutes was found to be the optimum length. Shorter filters had larger errors due to the oscillations; longer filters had larger errors due to the smearing. The size of the errors for the 20-min filter is only about 0.1 percent of the signal amplitude for the nearly steady flows.

The efficiency of this filter in separating the 5-min oscillations from the nearly steady flows will enable highly accurate measurements of the different flow types. The 5-min oscillations can be used to probe the depths of the Sun in much the same manner as seismic waves are used by geologists to probe the interior of the Earth. The nearly steady flows transport magnetic fields in the photosphere and are ultimately responsible for producing the sunspot cycle, magnetic activity, and solar flares. Determining the nature of these flows will increase understanding of these processes and may lead to predictions of future solar activity.

This temporal filter will be used on data obtained with the Solar Oscillation Imager on the Solar and Heliospheric Observatory. This joint European Space Agency/NASA mission is scheduled for launch by the Space Shuttle in the mid-1990's. Ground-based data are currently available from the Jet Propulsion Laboratory's Magneto-Optical Filter in use at the Mount Wilson Observatory. Data from this instrument are currently being analyzed for scientific merit in anticipation of future data from the spacecraft instrument.

Hathaway, D. H.: Spherical Harmonic Analysis of Steady Photospheric Flows. Solar Phys., Vol. 108, pp. 1–20, 1987.

Hathaway, D. H.: Temporal Filters for Isolating Steady Photospheric Flows. Solar Phys., in press, 1988.

D. H. Hathaway/ES52
(205) 544-7610
Sponsor: Office of Space Science and Applications

Solar Flares

A solar flare is an explosive event in a strongly magnetic region of the solar atmosphere, a violent burst of plasma heating, particle acceleration, and bulk mass motion. Large solar flares are the greatest explosions in the solar system: the power of the energy burst, $\sim 10^{32}$ erg in $\sim 10^{3}$ s, or $\sim 10^{29}$ erg s^{-1}, far exceeds the steady power of the solar wind ($\sim 3 \times 10^{27}$ erg s^{-1}).

It is widely held that flares draw their energy from the free energy of the magnetic field in the volume of the flare, the free energy being that stored in the field as a result of deformation of the field from its current-free, minimum-energy, potential configuration. If this view is correct, then the magnetic energy should decrease during a flare; the field should undergo a change to a more relaxed, more nearly potential configuration. Definite before-to-after magnetic changes have been detected in only a few flares. In most of these cases, it is not clear that the observed change even represents a decrease in magnetic energy rather than an increase. In no case has it been shown that the observed before-to-after change quantitatively accounts for the flare energy. Hence, a continuing central quest of flare research is to determine the magnetic field configuration at flare sites and how the configuration changes during flares.

During the past year, new evidence was found supporting the view that the flare energy comes out of the magnetic field. Both in solar regions of strong (100 to 1,000 gauss) magnetic field (active regions) and in regions of weaker field (quiet regions), filaments of chromospheric material reside in and trace out sheared magnetic fields over magnetic inversion lines. Such filaments, and hence the sheared fields that they trace, often erupt in flares and coronal mass ejections. The basic character of the eruption appears to be expansion and untwisting of the flux tube in which the erupting filament is embedded; the filament eruption in Figure 51 is archetypal. The new evidence concerns the decrease of magnetic energy in this flux tube as the tube erupts.

The dependence of the flux tube's magnetic energy on the tube's expansion and untwisting was derived for a simple model flux tube. This model was used with estimates of the field expansion and decrease in twist in observed erupting filaments to empirically evaluate the energy decrease. The evaluation was made for three observed eruptive events: a small confined filament-eruption flare, a coronal mass ejection from the eruption of a large quiescent filament without a flare, and a large filament-eruption flare in which the filament was probably ejected in a spray and coronal mass ejection. The estimated decrease in magnetic energy was compared with the total released energy estimated from the observed magnitude of the flare in H-alpha and x rays or from the observed mechanical energy of the mass ejection. In each case, the estimated decrease in magnetic energy was of the order of the total energy released. This result suggests that both in filament-eruption flares and in coronal mass ejections from filament eruptions, the basic drive is magnetic energy shedding by the eruption of the magnetic field in and around the filament; and contained filament-eruption flares, filament-eruption flares with sprays and coronal mass ejections, and coronal mass ejections from quiescent filament eruptions are all events of the same kind.

Moore, R. L.: Observed Form and Action of the Magnetic Field in Flares. Solar Phys., Vol. 113, p. 121, 1987.

Moore, R. L.: Evidence that Magnetic Energy Shedding in Solar Filament Eruptions is the Drive in Accompanying Flares and Coronal Mass Ejections. Astrophys. J., Vol. 324, p. 1132, 1988.

R. L. Moore/ES52
(205) 544-7613
Sponsor: Office of Space Science and Applications

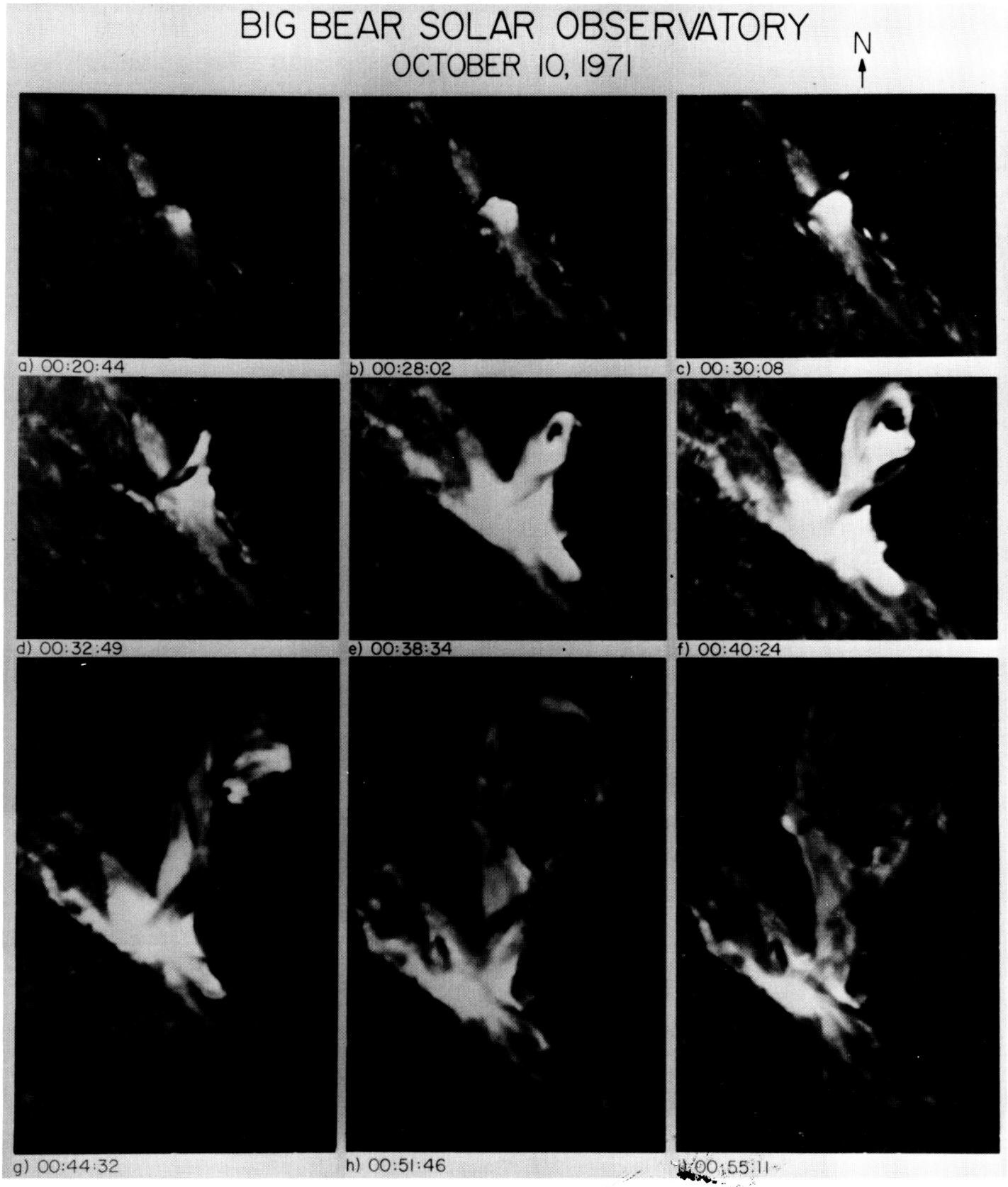

Figure 51. Example Filament-Eruption Flare

Ultraviolet Spectrometer and Polarimeter Observations of the Transition Region

Eight years after launch, the Ultraviolet Spectrometer and Polarimeter (UVSP) onboard the Solar Maximum Mission continues to furnish useful observations of the solar atmosphere. Current observations, though confined to the solar chromosphere, still reveal the microflares previously discovered in transition region observations.

Most of the recent analysis continues to concentrate on the existing large set of observations of the transition region. In particular, one set of data consists of spatial rasters obtained every 2 min at 11 partially overlapping positions in the C IV 1548 Å line. These show many ultraviolet (UV) brightenings throughout the magnetic network in the quiet Sun. Some bright sites persist through many rasters (although they fluctuate in brightness during this time), but others are shorter-lived than the 2-min repeat time of the observations. Comparison with Kitt Peak magnetograms shows that both types lie on neutral lines of small magnetic bipoles, with most of the long-lived sites corresponding to the stronger bipoles. The long-lived sites also correspond to dark points (DP) on He I 10830 Å spectroheliograms and thus are probably x-ray bright points. Plots of intensity versus time suggest that the persistent enhancements at the long-lived sites are the result of a rapid succession of impulsive events like those seen in isolation at the short-lived sites (Fig. 52). The location of the events on neutral lines together with their rapid rise times, short durations, and small spatial scales (<6 arc-sec) has led to the interpretation that they are microflares occurring in short (<4000 km) loops spanning the neutral lines.

A further analysis of the data supports the suggestion that the long-lived C IV sites (He I DP) are maintained by a series of microflares like those at the short-lived sites. If this is indeed the case, the line profiles of the long-lived sites should be like the profiles during events at short-lived sites. The average profile of the long-lived sites might be narrower if these sites are primarily heated by some less impulsive process (waves, for example) and only occasionally subject to a microflare. Since no simultaneous measurement of intensity at different wavelengths is available from the spectroheliograms, a true line profile for any given site or event cannot be obtained. However, by setting a uniform intensity cutoff (5 times raster mean) for a bright site or event at any position in the line and then fitting a Gaussian curve to the resulting set of qualifying intensity

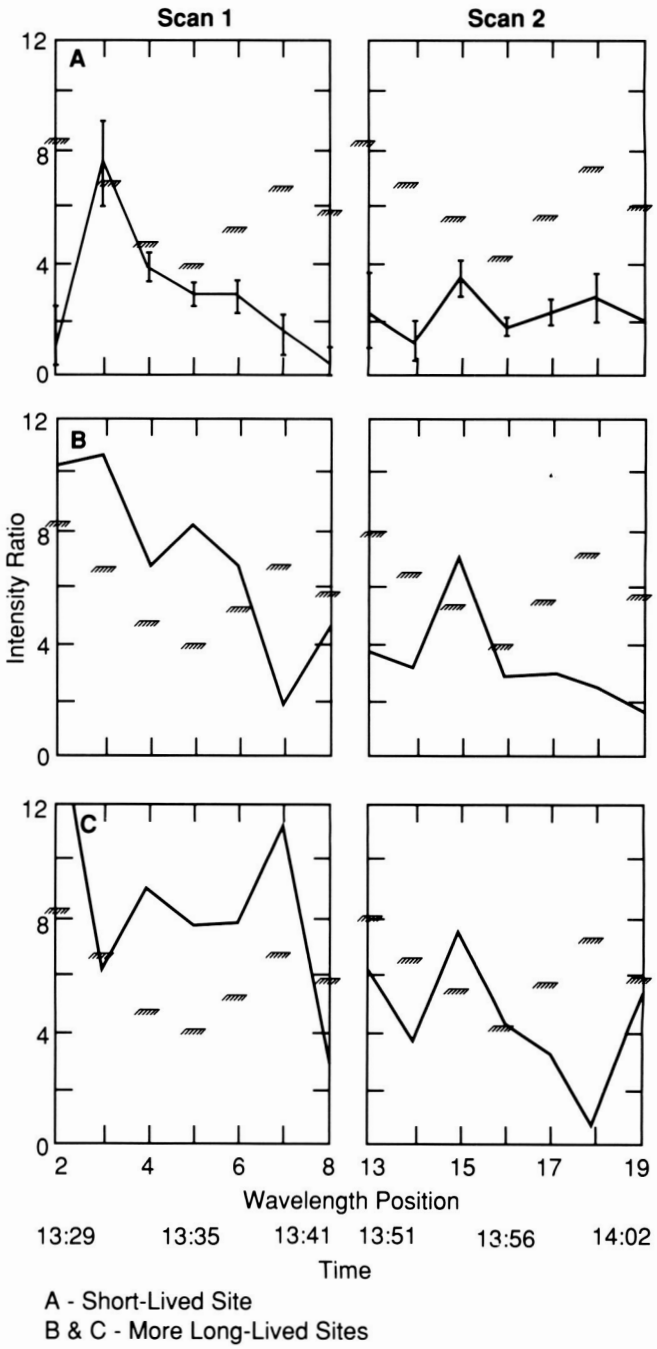

Figure 52. Spectral/Temporal Variations of C IV Intensity

measurements versus wavelength, the profile of an average short-lived event or long-lived site can be synthesized. Comparison of such profiles for long-lived sites (three or more consecutive intensities above 5 times raster mean) and short-lived sites (no more than one consecutive intensity above this cutoff) shows them to be nearly identical, with e-folding widths of 145 mÅ and 154 mÅ, respectively. These correspond to turbulent velocities of 25 to 27 km s^{-1}.

Order of magnitude estimates suggest that these microflares supply the necessary energy to heat the corona. There are about 10^4 events at or above our cutoff intensity on the Sun at any one time. Combining the microflare morphology conclusions of Porter, et al. (loops <4,000 km in length; 2,000 km is used in the estimate) with Moore's (1988) model for the release of magnetic energy in flares yields an estimate of 10^{26} erg available per microflare. This is supported by an estimate for the total thermal energy of the transition region and corona in the microflaring loops, which is based on independent observations of density derived from Si IV – O IV line ratios in similar events. The second estimate is about a factor of 2 lower than the first; the difference may go into heating adjacent structures. Other data show that the full-width-at-half-maximum lifetime of these events is 20 to 30 sec. Assuming that the energy of each event is released over a 30-sec interval, the resulting global average flux is 5 x 10^5 erg cm^{-2} s^{-1}. This is approximately equal to the heating requirement for the quiet corona, lying between the estimates for coronal holes and closed regions.

This scenario for the heating of the corona is consistent with recent work. It was found that the majority of the energy in flares is released within closed loops rather than at some interaction site between bipoles, but that considerable energy is often transferred out of the flaring loop and into adjacent structures via interaction sites. In the microflare scenario, the energy for coronal heating is the result of primary energy release in short low-lying loops, with transfer to adjacent larger structures that reach into the corona. The transfer might be driven by upward expansion of the low loops, possibly by way of secondary neutral sheets at interaction sites (Fig. 53).

Porter, J. G., Moore, R. L., Reichmann, E. J., Engvold, O., and Harvey, K. L.: Microflares in the Solar Magnetic Network. Astrophys. J., Vol. 323, p. 380, 1987.

Machado, M. E. and Moore, R. L.: Observed Form and Action of the Magnetic Energy Release in Flares. Adv. Space Res., Vol. 6 (6), p. 217, 1986.

Moore, R. L.: Evidence that Magnetic Energy Shedding in Solar Filament Eruptions is the Drive in Accompanying Flares and Coronal Mass Ejections. Astrophys. J., Vol. 324, p. 1132, 1988.

J. G. Porter/ES52
(205) 544-7607
Sponsor: Office of Space Science and Applications

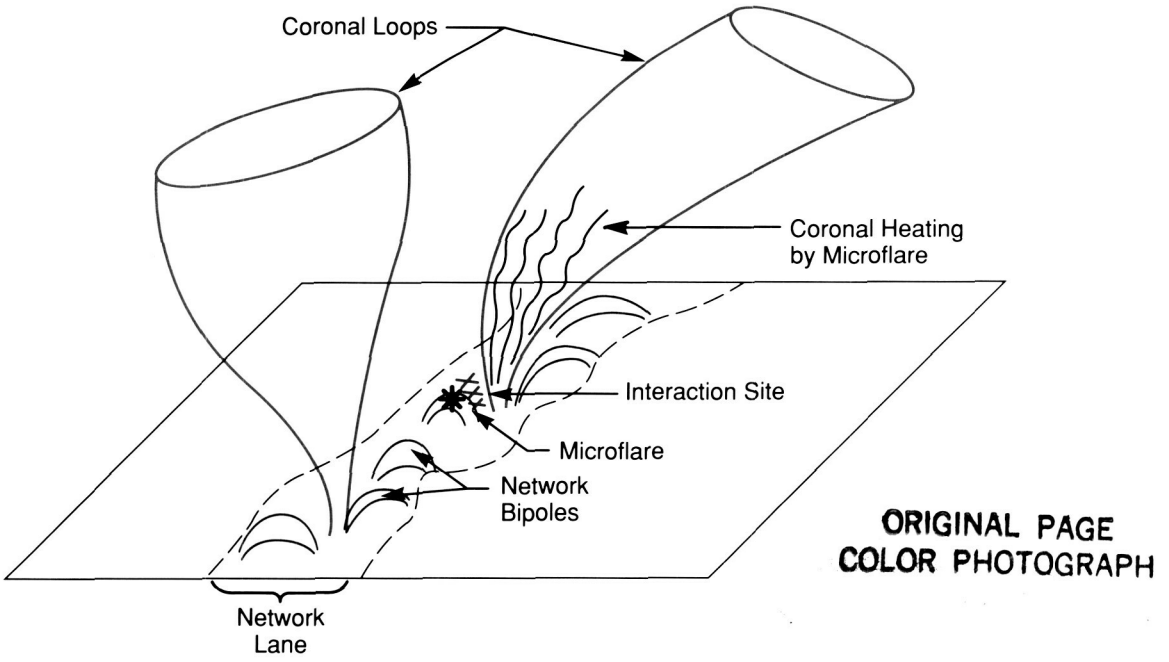

Figure 53. Scenario for the Heating of High Coronal Structures by Microflares in Short Low-Lying Loops

Coronal and Interplanetary Dynamics

The solar atmosphere, or corona, expands supersonically and becomes the solar wind. The Sun's highly structured magnetic field superimposes a complex pattern on this expansion and is also the source of a large variety of temporal variations.

Eventually, the solar wind runs into the local interstellar medium (LISM), is slowed, and deflected. The resulting structure of the heliosphere, the upper half profile of which is shown schematically in Figure 54, is reminiscent of the Earth's magnetosphere. There is a heliotail (region V in Fig. 54), down which the deflected solar wind flows, and a heliopause (interface A and the boundary layer) that deflects the gas in the LISM. There is also a heliospheric termination shock (interface B) which marks the outer limit of the supersonic solar wind.

The termination shock has recently received much attention from scientists all over the world because of the tentative remote detections that suggest it lies 40 to 60 AU (astronomical units) from the Sun. (AU is the mean distance between the Sun and the Earth, ~1.50 x 10^8 km.) If these detections are real, then the shock is being rapidly approached by Pioneer 10 and Voyagers 1 and 2. Interest has now focused on theoretical predictions of the shock position and its asymmetry in an effort to determine which spacecraft might be the first to reach the shock.

Physically, the shock is an important boundary in the solar system because the galactic cosmic ray spectrum and composition will be significantly different just beyond the shock. Galactic cosmic rays are used to determine properties of the galaxy and to verify some ideas on the evolution of the Universe. Therefore, the information that will be gained after the penetration of the shock is eagerly awaited.

Scientists at MSFC and Rice University have reconsidered the processes determining the asymmetry of the termination shock and have made an important discovery that will affect predictions of the first spacecraft to the shock, and will be used to interpret measurements made at high heliographic latitudes by the upcoming Ulysses mission to be launched in 1990. This discovery is the result of applying simple hydrodynamic concepts to the motion of the heliosphere through the galaxy.

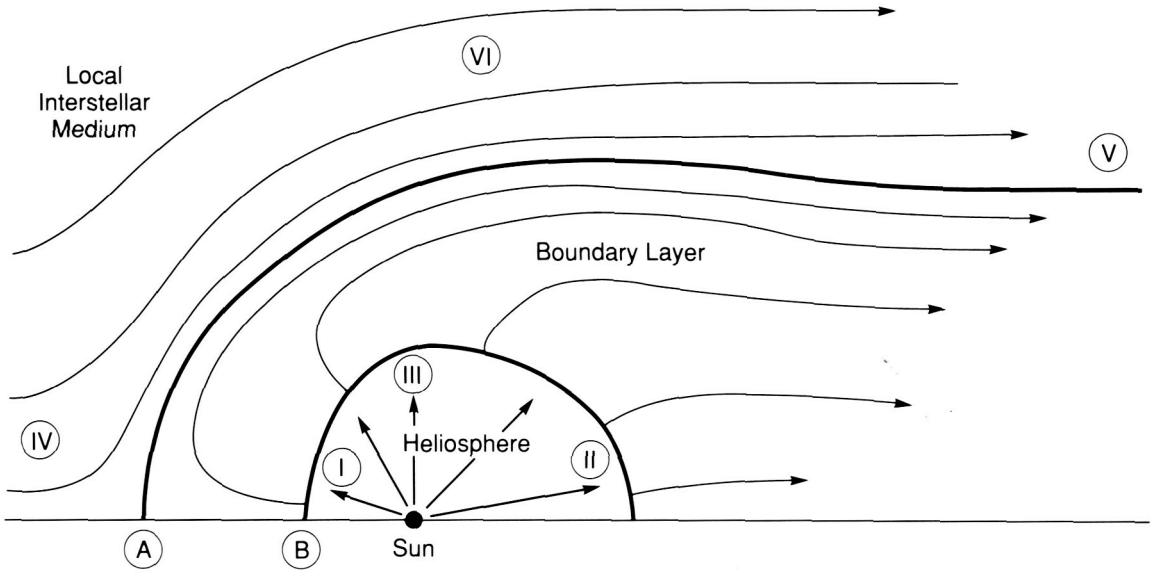

Figure 54. Upper-Half Profile of the Heliosphere

Remote measurements are used to show that the motion of the solar system through the LISM is slower than the local Alfvén speed and probably slower than the local sound speed. In this case, the external gas accelerates as it flows around the heliosphere, reducing the pressure on the flanks (regions VI and III in Fig. 54) due to the Bernoulli effect. Dynamic pressure presses in on the front of the heliosphere, reducing the distance to the shock at I. However, at III, the pressure will be much lower. The result is that the termination shock is flattened, being closer at I and II than at III. In fact the distance on the flanks may be more than twice as large as in any other direction.

An immediate consequence of this result is that Voyager 1 may not reach the shock before Voyager 2, even though it is considerably more distant from the Sun, because Voyager 1 is traveling at a larger angle with respect to the upstream direction (I) than Voyager 2. It can also be inferred that those cosmic rays which undergo acceleration at the termination shock will have radically different properties at high heliographic latitudes in comparison to what we presently measure near the heliographic equator.

Suess, S. T., Hathaway, D. H., and Dessler, A. J.: Asymmetry of the Heliosphere. Geophys. Res. Lett., Vol. 14, pp. 977-980, 1987.

S. T. Suess/ES52
(205) 544-7611
Sponsor: Office of Space Science and Applications

Solar X-Ray/XUV Images

The first high resolution soft x-ray/extreme ultraviolet (XUV) images of the Sun with normal incidence multilayer x-ray telescopes were obtained on October 23, 1987, by the Stanford/MSFC Rocket X-Ray Spectroheliograph. Professor A. B. C. Walker, Jr., of Stanford University is the principal investigator. R. B. Hoover of MSFC, J. Lindblom of Stanford, and T. W. Barbee, Jr., of Lawrence Livermore National Laboratory serve as co-investigators. The instrument was launched on a Nike-boosted Black Brant (flight 27.092) at 18:05 UT (Universal Time) from the White Sands Missile Range, New Mexico. The images produced on this flight conclusively demonstrated the value of multilayer x-ray optics for solar x-ray/XUV research.

For the past two decades, grazing incidence optics based on the designs of H. Wolter have comprised the primary imaging systems for the soft x-ray/XUV regime. Mirrors capable of reflecting soft x rays at normal incidence rather than at grazing incidence represent a new approach to x-ray imaging systems. These multilayer mirrors are made by precisely depositing (on extremely smooth substrates) multiple layers of a high-Z diffractor material separated by low-Z x-ray spacer material. The coatings behave like synthetic Bragg crystals and have been called layered synthetic microstructures (LSMs). Now they are more commonly called multilayers. Multilayer coatings can be deposited on flat, concave, or convex substrates. Although only a very small reflectivity by Bragg diffraction occurs at each high-Z/low-Z interface, excellent reflectivities (> 40 percent) can be achieved when many layer pairs are used. The modern multilayer mirror technology was pioneered less than a decade ago by Eberhard Spiller of the IBM Watson Research Laboratory and by Troy W. Barbee, Jr., while at Stanford University. Although laboratory tests had previously established that multilayer optics could produce images at soft x-ray/XUV wavelengths, prior efforts to demonstrate that they could yield images of astronomical objects comparable to those obtainable with grazing incidence telescopes had not been successful.

The Stanford/MSFC Rocket X-Ray Spectroheliograph employed several normal incidence multilayer soft x-ray/XUV telescopes in addition to a grazing incidence Wolter-Schwarzschild x-ray mirror (Fig. 55). In order to maximize the scientific data that could be obtained in the very short time (~5 min) available during the sounding rocket flight, several optical systems simultaneously recorded solar x-ray/XUV images on different cameras. This multiplicity of independent imaging systems guarded against total data loss by a single point (filter, camera, etc.) failure. Specifically, the payload employed nine independent 35 mm Canon T-70 cameras, each equipped with a soft x-ray/XUV filter. One camera was in the prime focus of the Wolter/Schwarzschild telescope to record images in the 8 Å to 20 Å waveband.

Convex normal incidence multilayer optics were used to reimage beams from segments of the Wolter-Schwarzschild primary and produce magnified images at 44 Å, 173 Å, and 256 Å. This is a version of the Spectral Slicing X-Ray Telescope configuration developed at MSFC under the auspices of the Center Director's Discretionary Fund (CDDF). Magnified solar x-ray images were successfully produced by these systems. The Wolter-Schwarzschild primary was a diamond turned metal optic which flew in 1983 for stellar spectroscopy. It had excessively high x-ray scatter, possibly due to microstructure memory problems known to affect diamond turned mirrors after vibration. Indeed, x-ray scattering is one of the most serious problems with grazing incidence optics. One exciting result is that calibration test and flight images produced by convex multilayer mirrors refocussing the beam from the grazing incidence primary appear to have significantly lower x-ray scatter than those produced by the primary mirror alone. It had been previously established during the CDDF program that normal incidence optics can improve the optical performance of a grazing incidence telescope by reducing the overall system offense against the Abbé sine condition. Furthermore, multilayer optics allow the telescope plate scale to be increased without increasing the overall system length, thereby improving the spatial resolution. The possibility that normal incidence multilayer optics may also reduce x-ray scatter in selected narrow spectral bands is potentially valuable to a wide variety of planned future solar and cosmic x-ray/

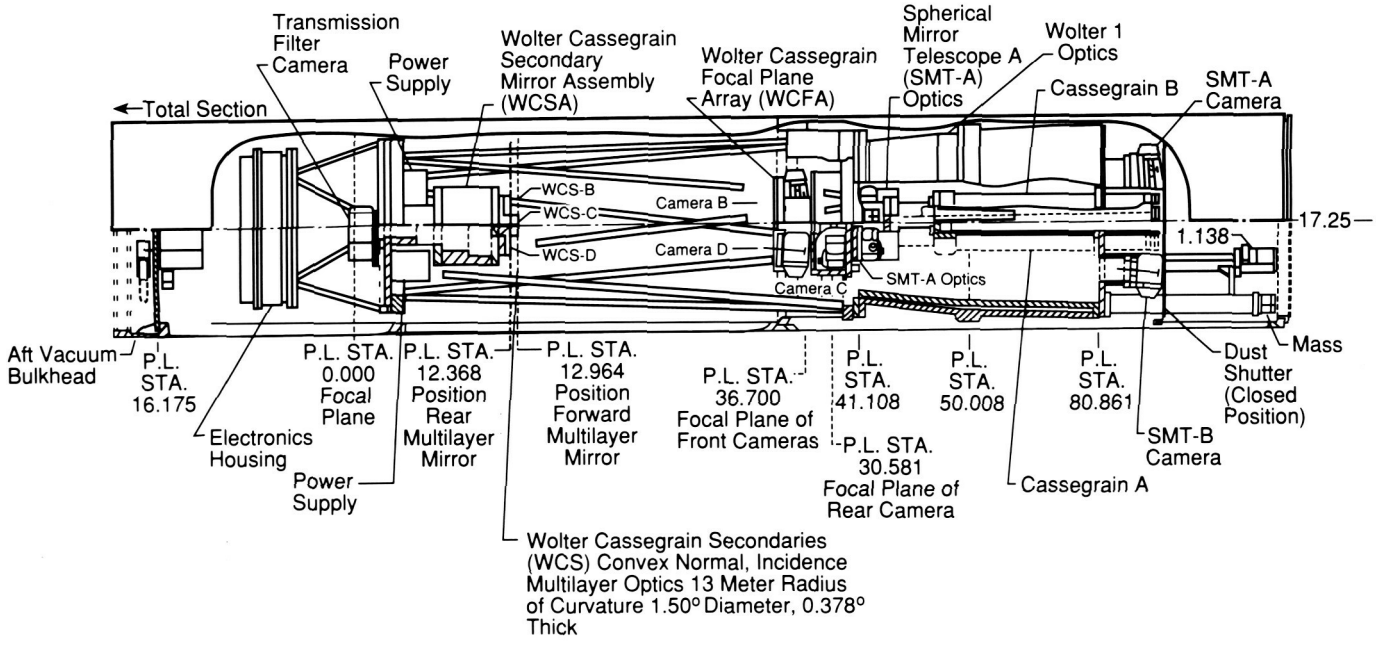

Figure 55. Schematic Layout of the Stanford/MSFC Rocket X-Ray Spectroheliograph

XUV programs. These preliminary results will be verified by conducting experiments using the full beam (rather than segments of the primary) with low scatter, highly polished fused-silica grazing incidence mirrors.

The Stanford/MSFC Rocket X-Ray Spectroheliograph also used small concave multilayers as spherical mirror telescopes with bandpasses centered at 44 Å and 256 Å. Excellent images were obtained with the 256 Å spherical mirror telescope in exposures as short as 1 sec. The 64-sec and 200-sec images with this system exhibited extremely high densities even though the film was processed for minimum grain. These results clearly demonstrate that very high reflectivity (~40 percent) was obtained with this normal incidence XUV multilayer optic.

Approximately 100 solar x-ray/XUV images were produced by the diverse optical systems on this flight. In addition to demonstrating the value of normal incidence multilayer optics, these images also established that the new experimental T-grain emulsion, provided by the Eastman Kodak Company, is extremely sensitive over the entire 8 Å to 256 Å wavelength regime covered by this payload. This special film is similar to the Kodak T-MAX 100 emulsion. It was provided to us without a gelatin overcoat (for maximum sensitivity in the soft x-ray/XUV regimes) and with a Rem-Jet backing (for protection against static discharges after exposure to vacuum). The payload had to be evacuated prior to launch to prevent acoustic vibrations from destroying the extremely thin filters (1720 Å aluminum on nickel mesh). These highly fragile filters are necessary to allow the soft x-ray/XUV radiation to be efficiently transmitted. They also must reduce the intense levels of visible light from the Sun to sufficiently low levels so that the sensitive film will not be exposed by visible light in a 200-sec exposure time. This flight marked the first successful astronomical use of this important new emulsion. The T-grain emulsions may soon replace the Schumann emulsion technology which has dominated XUV astronomical research for the past several decades.

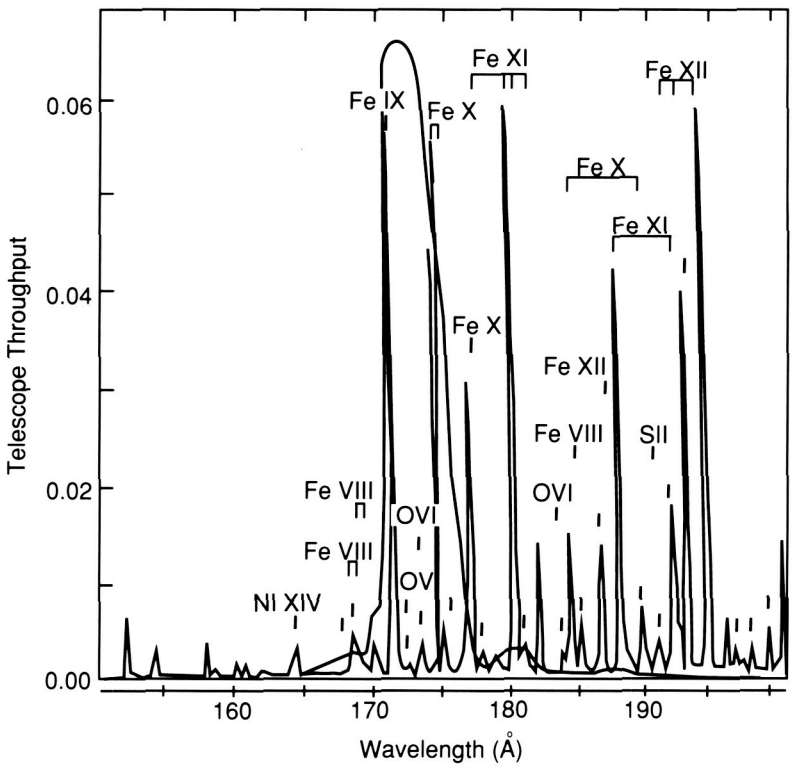

Figure 56. Spectral Response of the Cassegrain Telescope Superimposed on the Solar Spectrum

The most dramatic solar x-ray/XUV images were obtained with the doubly reflecting Cassegrain telescopes operating at 173 Å and 256 Å. These small telescopes employed a concave spherical primary of 6.4 cm diameter and 1.2 m radius of curvature. The convex secondary was also spherical of 2.5 cm diameter and 0.5 m radius of curvature. The effective focal length of the system was 2 meters, yielding an f/34 system. Theoretical ray trace studies showed the optics to be capable of spatial resolution of 0.5 arc-sec. However, the resultant resolution was limited by film grain characteristics to the 1.0 to 1.5 arc-sec range. The multilayer optics for the the 173 Å instrument were made by coating extremely smooth (< 3 Å rms) substrates with Molybdenum/Silicon layers of 36.8 Å and 55.2 Å thickness, respectively. The telescope structures were fabricated at MSFC, where the optical alignments, visible light, and x-ray tests were conducted.

The normal incidence multilayer Cassegrain telescopes produced full disk solar soft x-ray/XUV images with virtually no x-ray scattering in 173 Å and 256 Å regions. The images in the 171 Å to 175 Å bandpass are extremely exciting. In this bandpass, the solar emission is dominated by Fe IX and Fe X lines produced by coronal plasma at 0.95 to 1.3 million degrees K (Fig. 56). These images show many features of coronal structure, such at magnetically confined loops of hot plasma, prominences and filaments, polar coronal holes, and numerous small discrete structures on the size scale of supergranulation and smaller. The long exposures show large, faint coronal structures, such as the polar coronal plumes.

The payload was successfully recovered from a cliff near the summit of North Oscura Peak and the flight film processed immediately thereafter. The payload is now being configured for a reflight, currently planned for February 1989. During the reflight, soft x-ray/XUV and VUV images of the Sun will be obtained with spatial resolution approaching 0.3 arc-sec at numerous wavelengths. The optical systems being developed for the reflight should yield very high spatial resolution images of chromospheric, transition region, and coronal plasma in several very narrow spectral bands simultaneously. Such observations should provide important new information relevant to the solution of a number of current solar physics problems.

Walker, A. B. C., Jr., Lindblom, J. F., Hoover, R. B., and Barbee, T. W., Jr.: Monochromatic X-Ray and XUV Imaging with Multilayer Optics. Proc. of International Astronomical Union Colloq. No. 102 Beaulieu-Sur-Mer, France, in Journal de Physique-Colloque, in press, 1988.

Hoover, R. B., Barbee, T. W., Jr., Lindblom, J. F., and Walker, A. B. C., Jr.: Solar Soft X-Ray/XUV Imagery with an Experimental Kodak T-Max Film. Kodak Tech Bits, June 1988.

Walker, A. B. C., Jr., Barbee, T. W., Jr., Hoover, R. B., and Lindblom, J. F.: Soft X-Ray Images of the Solar Corona with a Normal Incidence Cassegrain Multilayer Telescope. Science, in press, 1988.

R. B. Hoover/ES52
(205) 544-7617
Sponsor: Office of Space Science and Applications

Magnetospheric Physics

The Earth's otherwise dipolar magnetic field is distorted by the outflow of ionized gas or plasma from the Sun, which is called the solar wind. It is compressed upstream or dayside and stretched out into a long tail on the downstream or nightside, forming a structure referred to as the magnetosphere. Magnetospheric physics is the application of continuum mechanics and plasma physics to obtain an understanding of the flow of matter, momentum, and energy near and within the magnetosphere. With such an understanding, MSFC can comprehend and anticipate interactions between solar events, interplanetary conditions, and terrestrial responses. The solar-terrestrial environment also serves as the laboratory of opportunity for in situ observations of processes which are of importance in other astrophysical plasma situations such as planetary and cometary magnetospheres and stellar atmospheres. Having studied such processes both remotely and in situ, MSFC will be able to interpret electromagnetic radiations received from distant astrophysical plasmas.

Magnetospheric plasma was initially thought to have originated in the solar wind, but measurements have shown that the Earth's atmosphere and ionosphere evaporate continuously into space, providing a dominant source of plasma within the magnetosphere. Dissipation of solar wind energy into the ionospheric plasma enhances this outflow and influences its composition. The importance of this terrestrial plasma source and the processes by which ionospheric plasma is energized and transported within the magnetosphere have motivated MSFC research in magnetospheric physics, influencing the design of instrumentation, analysis of data from multiple spacecraft, laboratory study of flowing plasmas, development of ionospheric and magnetospheric models, and development of advanced data networking systems.

Plasma Interactions Monitoring System

The Plasma Interactions Monitoring System (PIMS) (Fig. 57) is intended to provide comprehensive measurements of the Space Station Freedom environment. These measurements will be used to develop an environmental model around the S. S. Freedom. A study is now underway to define plasma and fields measurements required for the ambient S. S. Freedom environment. The measurements will also define the effects on this environment by natural (e.g., solar flares and geomagnetic storms) and induced (e.g., Shuttle dockings, reboost operations, vacuum venting, extravehicular activity, and airlock operations) perturbations. The study is also addressing required placement of the instrument units. The resulting model developed from these measurements will be useful to S. S. Freedom users as well as engineers working on station evolution and upgrades.

There will be approximately 10 PIMS units developed and placed at strategic locations around S. S. Freedom, such as the vicinity of payload attach points, near reboost modules, airlocks, and vacuum vent ports. The initial PIMS units will be preintegrated and will be part of the first element launch. Subsequent units may be preintegrated or may be integrated on-orbit as a part of the S. S. Freedom buildup sequence.

It has been proposed that the PIMS program be a joint venture between the Office of Space Science and Applications and the Office of Space Station.

W. T. Roberts/PS02
(205) 544-0621
Sponsors: Office of Space Science and Applications
Office of Space Station

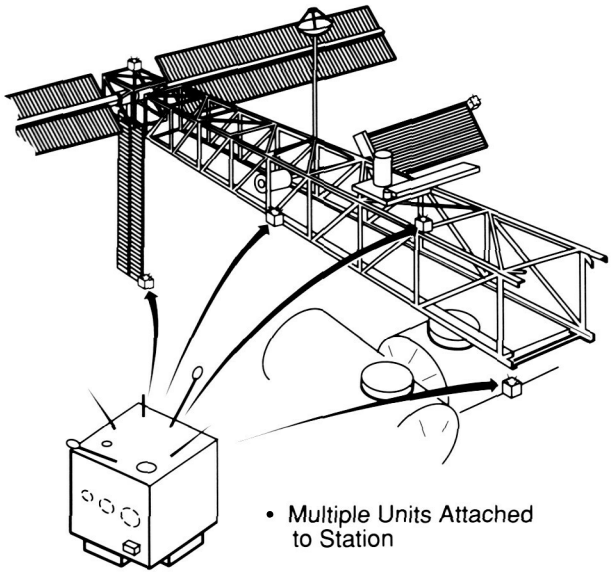

Requirements Summary	
Dimensions (m)	.8 x .8 x .8
Volume (m^3)	.5
Weight (kg)	100/Unit
Power (kW)	.1/Unit
Data (kbps)	100/Unit
Thermal	N/R (Passive)
SIA	N/R
Operation (Time)	Continuous
Pointing (Deg)	5

Figure 57. The Plasma Interactions Monitoring System

Ion Outflows at High Latitudes

The upward flow of ionospheric ions at high magnetic latitudes continues to be a subject of detailed study at MSFC because of the important roles these ions play in plasma processes within the magnetosphere. The Dynamics Explorer (DE) 1 satellite with its instrument complement has been sampling the magnetosphere of Earth for 6 years. Among the many accomplishments of this mission is the long-term observation of the outflow of low-energy ions from the polar region. This outflow is comprised of the classical polar wind flow of H^+ and He^+ as well as significant outflows of heavier ions such as O^+ and O^{++}. Using data from the first 2 years of the DE mission, statistical databases of ion density, composition, and velocity have been accumulated from observations of these outflows. The results from studies of these databases are beginning to allow quantitative characterization of these outflows under different conditions in the polar regions.

The observed average upward flux from the polar cap region is in the range predicted by theoretical models (6×10^7 and 5×10^6 cm^{-2} s^{-1} for H^+ and He^+, respectively). The magnitude of the light ion outflows is variable and, while the major sources of the variations are known, the relative magnitudes of their influence are yet to be determined. A complex interplay of factors such as the output of solar ultraviolet radiation, geomagnetic activity, and the season, ultimately determines the rate of outflow. An understanding of this interplay will come from further statistical analysis of the database already accumulated.

The flux of ions from the polar cap is carried by high ion velocities (up to 20 km s^{-1} for H^+) which increase in magnitude from the topside ionosphere (about 1,000 km) up to around 2,500 km. The resultant profiles of ion velocity versus altitude provide a wealth of new information regarding the acceleration and upward transport of these ions. For example there exists a well-defined correlation between the

H^+ and He^+ velocity (Fig. 58). Such a correlation is a result of the similarity in the forces which drive both ions upward from the ionosphere.

The major upward force on the light ions is due to a polarization electric field established by the separation in charge between the highly mobile and negatively charged electrons and the less mobile and heavier ions. The strength and variation with altitude of this electric field is largely determined by the dominant ion present. Over the altitude range of the observations included in the database (500 to 4,000 km), O^+ dominates H^+ in density by a ratio of 10 to 1 with the He^+ density being approximately 10 percent of the H^+ density (Fig. 59). For such a case, theoretical models predict that the minor ions (H^+ and He^+) should decrease in density with altitude at the same rate as the major ion (O^+) (Fig. 59). From this information, and some knowledge of the temperature of the ions and electrons, a quantitative determination of the electric field can be made providing further information on the nature of high-latitude ion outflows.

M. O. Chandler/ES53
(205) 544-7645
Sponsor: Office of Space Science and Applications

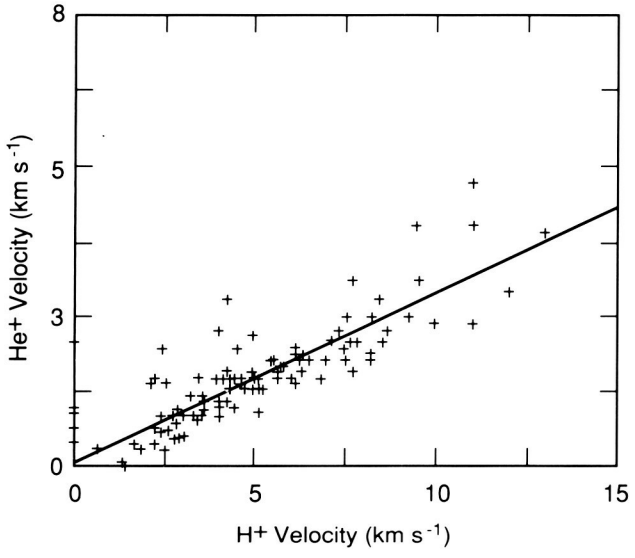

Figure 58. Correlation Between H^+ and He^+ Velocities in the Polar Cap

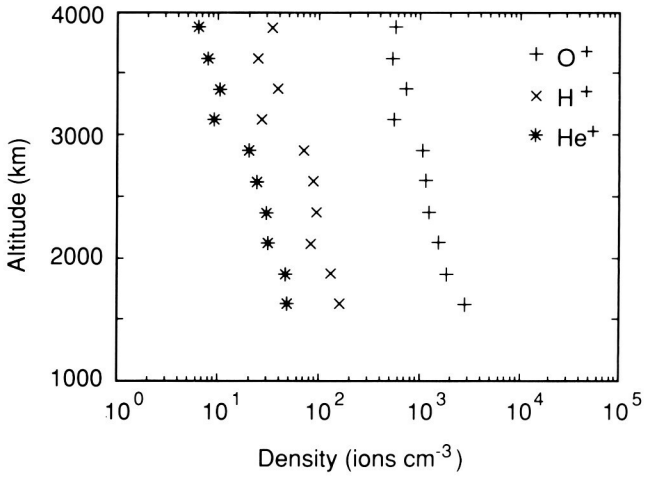

Figure 59. Ion Densities as a Function of Altitude in the Polar Cap

Outer Planet Investigations

Research on the atmospheres and ionospheres of the outer planets has centered on the effects of water on the atmosphere-ionosphere ring system of Saturn and the study of the production of auroral emissions by heavy ion precipitation into the Jovian high-latitude atmosphere.

An influx of water from the rings of Saturn into the atmosphere has been suggested as an explanation for the observations by Pioneer 11 of unexpectedly low peak electron densities in the Saturnian ionosphere. Further support for this hypothesis came from observations of Saturn electrostatic discharges that suggest peak electron densities had a strong diurnal variation and latitudinal structure that was tied by way of magnetic field lines to features in the ring plane. Recent steady state ionospheric calculations have shown that the measured Saturn ionospheric profile can be explained reasonably well using a water influx from the rings on the order of 10^8 cm^{-2} s^{-1}.

The research on the Jovian aurora used a combination of aeronomical modeling and International Ultraviolet Explorer (IUE) images to assess the role of heavy ion precipitation in Jovian aurora. Earlier observations of Jovian x-ray aurora and in situ measurements of energetic oxygen and sulfur ions indicated that these ions were precipitating into the high-latitude Jovian ionosphere. Building on earlier work concerning Jovian electron aurora, a quantitative model was formulated for the interaction of energetic oxygen ions and atoms with an atmosphere consisting of H_2 and hydrogen. The model indicated that sulfur and oxygen emissions in the ultraviolet (UV) at 1256 Å and 1304 Å should be detectable with the IUE UV telescope. However, observations showed no detectable emission at 1304 Å and an uncertain detection of sulfur at 1256 Å suggesting that the bulk of the observable UV auroral emissions was probably due to electrons or possibly protons rather than heavy ions. If heavy ions do precipitate into the atmosphere they are quite energetic (greater than 300 keV/nucleon) and they therefore deposit the bulk of their energy well below the methane homopause.

Waite, J. H., Jr. and Cravens, T. E.: A Current Review of the Jupiter, Saturn, and Uranus Ionospheres. Adv. Space Res., Vol. 7, p. 119, 1987.

Horanyi, M., Cravens, T. E., and Waite, J. H., Jr.: The Precipitation of Energetic Heavy Ions Into the Upper Atmosphere of Jupiter. J. Geophys. Res., in press, 1988.

M. O. Chandler/ES53
(205) 544-7645
Sponsor: Office of Space Science and Applications

Development of Ion Analysis Systems for Space Flight Applications

The thermal and suprathermal plasma analysis research efforts at MSFC continue to be a central point of focus for the Magnetospheric Physics Branch. MSFC scientists have been involved in numerous space missions in the past, and future missions include the International Solar-Terrestrial Program, the Comet Rendezvous and Asteroid Flyby (CRAF) mission, the Combined Release and Radiation Effects Satellite (CRRES) Program, and the TOPAZ series of sounding rockets. For these missions, the Magnetospheric Physics Branch in cooperation with the University of Texas at Dallas, The University of Alabama in Huntsville, and the Southwest Research Institute is developing new concepts and instruments for the analysis of low-energy ions in space plasmas.

The development and application of the Low-Energy Ion Calibration Facility (LEIF) continues to be essential to our instrument development and calibration tasks. In the past year a series of improvements have been made, and the facility has been used extensively for instrument development and calibration. Additional cryogenic pumping capability has been added and software and hardware upgraded to enhance the capabilities for automated data collection and instrument positioning. At present, electron beam and ultraviolet beam generators are being added to the system to allow the capability of testing instrument response to these radiation, as well as for the future development of thermal electron instruments. An X-Y positioning table and spot-beam generator are being fabricated to allow detailed mapping of the response of ion instruments with large aperture. Also, a particle imaging system has been acquired that can be placed at the output of an instrument or at any intermediate stage, and that will allow a detailed mapping of the particle trajectories through the ion optics.

Extensive testing has been done on two different types of ion analysis systems. The first was the instrument Superthermal Ion Composition Spectrometer (STICS). The STICS is differential in all three parameters (mass, energy, and arrival angle); i.e., by appropriate selection of bias potentials, the instrument is sensitive to ions of a single mass (type) with a selected energy and arrival direction. This capability is very important as it allows study of the complex, nonthermal plasma ion distributions commonly found in space. Figure 60 is an example of the angle differentiation capability where the vertical axis is relative response, the horizontal axis is the ion beam arrival angle (varied by the tilt table in the LEIF), and the parameter on the curves is the value of the angle deflection bias potential. An energy analyzer follows the angle analyzer and, finally, a magnetic mass analyzer and detector complete the detailed mapping of the ion distribution function. A prototype of this STICS instrument has been flown on the TOPAZ -2 sounding rocket and the STICS will be further developed for a Scout-class satellite which will be a component of the CRRES chemical release active perturbation science program.

The demands of thermal plasma research have required development of instruments with large collecting areas to provide adequate sensitivity for measurements of very low-density plasmas, while at the same time retaining the capability of making

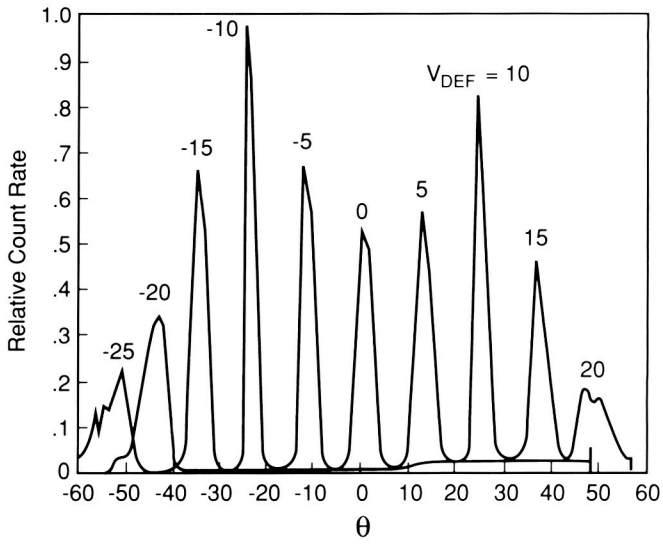

Figure 60. Angular Response at Various Angle Deflection Potentials

measurements that are differential in mass, energy, and angle. Significant progress has been made in the development of an ion optics system that uses a parabolic-shaped electrostatic mirror to focus a large-area ion beam onto the relatively small entrance slit of an ion mass spectrometer. Selection of the potential on the mirror effectively selects ions with an upper energy limit, since higher-energy ions are not reflected and do not reach the focus. A retarding grid placed near the focus point selects a minimum energy for ions to be passed, and the combination of the two (mirror potential plus retarding grid potential) effectively allows measurement of ions in a certain differential energy window. The focusing properties of the mirror in combination with the mass spectrometer entrance slit result in differential angular sensitivity. As an added refinement, a system has been developed to mechanically rotate the mirror system while keeping the retarding grid and ion mass spectrometer fixed in order that a range of arrival angles may be scanned. The angle in the other plane is scanned electronically, similar to that which is done in the STICS instrument. Overall, the focusing mirror concept allows a large acceptance area, while at the same time allows an ion mass spectrometer with a small entrance slit, so that the ability to separate ions of differing masses is retained. This focusing mirror instrument will be developed into the Cometary Retarding Ion Mass Spectrometer for flight on the CRAF mission. Its primary purpose will be to investigate the thermal and suprathermal plasma resulting from the interaction of a comet with solar radiation and solar wind.

Biddle, A. P., Reynolds, J. M., Chisholm, W. L., Jr., and Hunt, R. D.: The Marshall Space Flight Center Low-Energy Ion Facility – A Preliminary Report. NASA TM-82559, October 1983.

Biddle, A. P. and Reynolds, J. M.: Integrated Development Facility for the Calibration of Low-Energy Charged Particle Flight Instrumentation. Rev. Sci. Instrum., Vol. 57, p. 572, 1986.

D. L. Reasoner/ES53
(205) 544-7636
Sponsor: Office of Space Science and Applications

Ionospheric Mass Spectrometry and Outflow Studies

A sound understanding of the response of the ionosphere to the localized and time variable energy inputs it receives from the magnetosphere must be based upon detailed observations of plasma behavior. Increasingly sophisticated measurements are needed which are sensitive to the mass, energy, and direction of motion of the individual ionospheric plasma particles. Particle flux must be measured over a very wide range of these parameters, in particular for all possible directions relative to the measurement platform. These observations must be interpreted by means of comparison with theoretical models of expected behavior.

A very promising instrument concept has been developed for the type of observations described above. No new data sets have been acquired from passive observation rocket payloads, but preparation of an instrument for an active experiment payload, based on operation of an ion beam source, has been initiated. Two modeling studies have also been completed: a study of the low-altitude collisional constraints on ionospheric outflows, and a study of the consequences at high altitude of the distinct effects of selective ion or electron heating. This work has been done in collaboration with the University of Texas at Dallas, The University of Alabama in Huntsville, the University of New Hampshire, Cornell University, and Utah State University.

The Superthermal Ion Composition Spectrometer (STICS) responds differentially in energy and angle, with each electrostatically selectable over the range of the instrument (0 to 100 eV, +60° to -60°). The instrument is designed for mounting in a spinning payload so that the zero angle look direction is radially outward — perpendicular to the spin axis. Laboratory response data for energy and angle parameters are shown in the section on development of thermal electron instrumentation.

Figure 61 shows flight summary data from the flight of this instrument onboard the Cornell University of

New Hampshire, TOPAZ-2 rocket flight. This payload, launched January 19, 1988, passed over active auroral forms poleward of Poker Flat Research Range, at altitudes up to 1,000 km. Figure 61 consists of two panels, for H^+ and O^+ data, respectively, presented as count rates plotted as a logarithmically contoured surface in the energy-polar angle plane. The thermal population of each species appears as a ridge centered on an energy of 1 to 2 eV, and extending across the full range of polar angles due to the changing motion of the payload relative to the plasma during flight. The variation of the ridge count rate with polar angles provides a qualitative indication of the altitude profile of the thermal ion density, H^+ increasing in density with altitude (peak at small polar angles, near apogee), and O^+ decreasing in density with altitude (minimum at small polar angles).

Also of interest is the presence of heating of the ion populations, appearing in both H^+ and O^+, but with somewhat different character in each. In the H^+, the ion heating appears as a broadening of the thermal distribution, but peaking at upward polar angles near 25 deg; hence an apparent conic distribution of the distribution core. In O^+, the heating appears as a hot tail appearing on an otherwise unheated thermal core with a very broad angular distribution. Further analysis of these data will be conducted in correlation with other measurements from the payload instrument complement.

Modeling activities have included both hydrodynamic descriptions of the topside F region and kinetic models of the higher altitude outflow regions of the magnetosphere. Very briefly, hydrodynamic results have shown that ion outflow flux composition responds readily to increases in the total ion flux demanded by the energetic processes at higher altitudes, changes in the neutral atmosphere structure in response to solar extreme ultraviolet output, and effective altitude of the energetic processes imposing the ion demand. Kinetic model results have addressed the relative roles of electron and ion heating in producing ion outflow, using a semi-kinetic code which computes the self-consistent ambipolar electric field and thereby the outflow of multiple ion species to altitudes of several R_E.

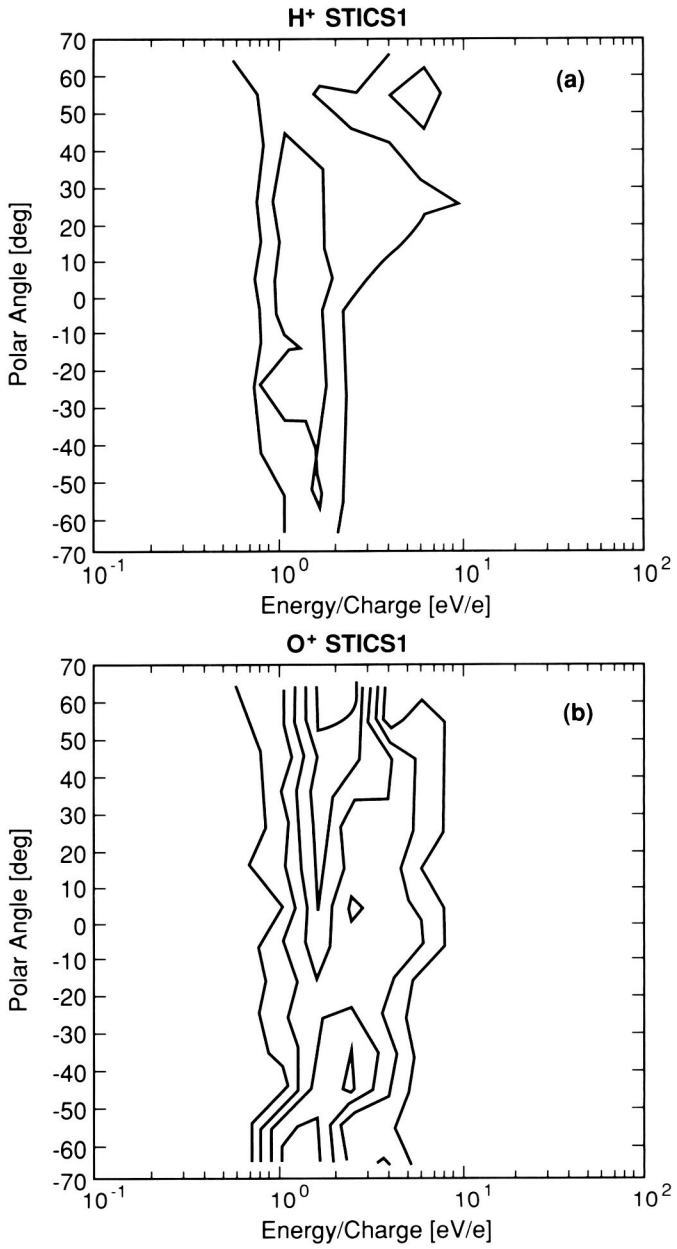

Figure 61. Flight Summary Count Rates for H^+ (a) and O^+ (b)

Barakat, A., Schunk, R. W., Moore, T. E., and Waite, J. H., Jr.: Ion Escape Fluxes from the Terrestrial High Latitude Ionosphere. J. Geophys. Res., Vol. 92, p. 12255, 1987.

Moore, T. E., Pollock, C. J., Arnoldy, R. L., and Kintner, P. M.: Observations of Preferential O^+ Heating. Geophys. Res. Lett., Vol. 13, p. 901, 1986.

Li, P., Wilson, G. R., Horwitz, J. L., and Moore, T. E.: Effect of Mid-Altitude Ion Heating on Ion Outflow at Polar Latitudes. J. Geophys. Res., Vol. 93, in press, 1988.

T. E. Moore/ES53
(205) 544-7633
Sponsor: Office of Space Science and Applications

Relationship Between Spacecraft Potential and Ambient Particle Density

This research continues the development of an empirical model of the Earth's plasmasphere, describing the temperature and density of thermal H^+, He^+, and O^+ as functions of latitude, longitude, and geomagnetic activity. Analytical expressions fit to observations are being developed to permit computer generation of densities for arbitrary locations in the plasmasphere.

In the initial development of this model, the impact of spacecraft charging on plasma measurement had to be investigated. Spacecraft potential strongly affects the measurement of core plasma density in that a positive potential on the spacecraft has a retarding effect on the ambient ions. A potential of a few volts is sufficient to exclude the bulk of the lowest energy ambient plasmasphere ions from entering instruments mounted on the spacecraft. Geodetic Earth-Orbiting Satellite 2 (GEOS 2) measurements of spacecraft potential as a function of ambient particle density*† cover the range in potential from about 1.5 to 9 volts and the range in density from about 2 to 70 ions cm^{-3} (these data are shown as multi-sized stars in Figure 62). By combining observations from the Retarding Ion Mass Spectrometer (RIMS) on the Dynamics Explorer (DE) 1 satellite with those from GEOS 2, these ranges have been extended down to about -1.5 V in potential and up to about 7,000 ions cm^{-3} in density (about 2 orders of magnitude above the GEOS 2 data). The RIMS results are shown as the +'s in Figure 62. The combination of the results from these two satellites suggests that a systematic relationship exists over large variation of these parameters (Fig. 62).

An analytical expression that is strictly empirical (of the form: $f = A + B/N^c$) has been fit to these data and is shown as the solid line in the figure. In this expression, A, B, and C are constants, N is the total ion number density, and f is the potential on the spacecraft. This empirical relationship will be used in the analysis of core plasma measurements to remove variations in the total particle density due to spacecraft potential effects. Limits on the use of this relationship have yet to be determined. The determination of these limits is part of a continuing research effort. It is significant that results from two separate and different spacecraft appear to, on average, show the same systematic response of spacecraft potential to changes in ambient total density.

* Knott, K., Korth, A., Decreau, P., Pedersen, A., and Wrenn, G.: Observation of the GEOS Equilibrium Potential and its Relation to the Ambient Electron Energy Distribution. In Proc. of the 17th ESLAB Symposium, ESA SP-198, pp. 19-24, 1984.

† Schmidt, R. and Pedersen, A: Long-Term Behavior of Photo-Electron Emission from the Electric Field Double Probe Sensors on GEOS 2. Planet. Space Sci., Vol. 35, pp. 61-70, 1987.

P. D. Craven/ES53
(205) 544-7639
Sponsor: Office of Space Science and Applications

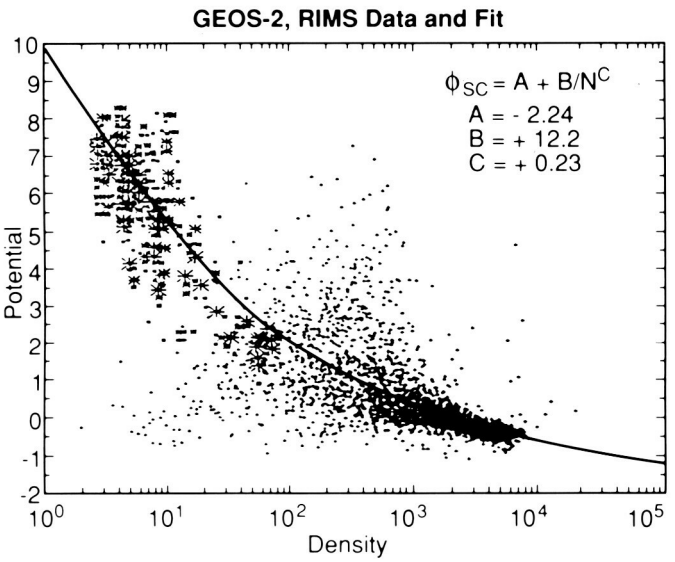

Figure 62. Potential vs. Density From GEOS 2 and RIMS (DE 1)

Atomic Physics and Aeronomy

The interaction of solar electromagnetic radiation and energetic charged particles with the mixture of gases comprising the upper atmosphere results in a wide variety of processes. Aeronomy is the study of the physics and chemistry of this range of processes characterizing the upper atmosphere. Solar radiation (photons) in the x-ray, ultraviolet, visible, and the infrared part of the spectrum is absorbed, emitted, and scattered by atmospheric gases at various levels. Solar photons with sufficiently high energies ionize and dissociate atmospheric molecules producing reactive species or free radicals which interact with other molecules in a complex set of reactions. Composition and thermal structure of the atmosphere and its response to natural or man-made perturbation is determined by photochemical and dynamic processes. A quantitative knowledge of the interaction of both solar radiation and energetic particles with atmospheric constituents, and the rich array of photochemical and dynamical processes that result, is crucial to an understanding of the nature and balance of this part of the Earth's environment.

Atmospheric gases absorb or emit radiation in discrete quanta involving rotational, vibrational, and electronic transitions. An observed spectrum of the atmosphere therefore exhibits lines which are characteristic of the gases and energy transitions involved. A great deal of knowledge about the physical state of the atmosphere and complex photochemical and dynamical processes can be obtained by combining information obtained from observed spectra with data from laboratory experiments and the results from theoretical studies and comprehensive predictive numerical models.

Studies of the Upper Atmosphere Using Imaging Spectroscopy

The emission spectrum of the sunlit thermosphere measured from Spacelab 1 contained a number of surprises that were inconsistent with current scientific knowledge of the physics and chemistry of that region. In order to obtain additional data on upper atmospheric emissions for comparison with the Shuttle data, the Imaging Spectrometric Observatory, an array of spectrometers that flew on Spacelab 1, and which will fly again on the ATLAS-1 Shuttle mission, was taken to a ground-based observing site in southwest Texas. A clean-room-quality mobile observatory was established on the top of a mountain on the property of the McDonald Observatory. By operating from an altitude of nearly 7,000 ft above sea level, and at a site remote from city lights, it is possible to glimpse some of what can be seen from an orbiting observatory. While on the ground, the instrument can only operate at visible wavelengths, rather than its full extreme ultraviolet to near infrared range. While scattered sunlight on the lower atmosphere prevents observations of the fully sunlit thermosphere, it is possible to observe in the short intervals of time just before sunrise or shortly after sunset, when the lower atmosphere is in darkness and the Sun is illuminating the upper atmosphere.

Observations have been attempted at the McDonald Observatory site (weather conditions permitting) for a 1-week period around new moon each month since July 1987. A most valuable data base has been obtained, from which a series of studies has commenced that will greatly enhance our ability to interpret data acquired from the Shuttle. For example, the emission spectrum of the N_2^+ molecule as measured from the Shuttle was quite unanticipated and indicated the need for a new and energetic source of N_2^+ not previously included in the theoretical models. Because the Spacelab 1 observations provided the

first spectral imagery of the first negative system of N_2^+, we had no way to distinguish between two possible options: is there a previously unidentified and significant source mechanism for N_2^+ operative in the thermosphere, or were the Shuttle data perturbed by the passage of the vehicle through the ionosphere? The evidence was leaning toward the latter possibility prior to the McDonald program. However, in the past several months, the observing and data extraction techniques have been steadily refined, allowing observing capabilities to be pushed closer and closer to the daytime. In the January 1988 data, there were indications of unusual spectral distributions in the data acquired from the ground. This indicates that the processes in the 150 to 250 km region are not as well understood as had been thought. The database will be expanded in order to confirm the findings.

In addition, a number of other atmospheric features have been studied. By observing the $O^+(^2P)$ feature at 7320 Å, and using these data with a comprehensive model of the upper atmosphere, it is possible to infer the altitude profile of atomic oxygen in the thermosphere.

Figure 63 shows an example of observations made between December 19 and December 22, 1987. This time period coincided with a major meteor shower, and bright Ca^+ emissions are seen in the spectrum. The Ca is deposited near 90 km as a result of the meteorite ablation in that region. The Ca atoms become Ca^+ through charge exchange, and then have a lifetime of days. The data show that the Ca^+ layer at the start of the shower (December 19) was near 96 km. By the morning of December 22 (Fig. 64), ionospheric processes have moved the Ca^+ layers to very high altitudes. Some 12 hours later, the Ca^+ layer had descended to near 150 km. These data provide a valuable tracer for such effects.

The program at McDonald will be reduced in October 1988 when the Imaging Spectrometric Observatory is returned to MSFC for refurbishment for the

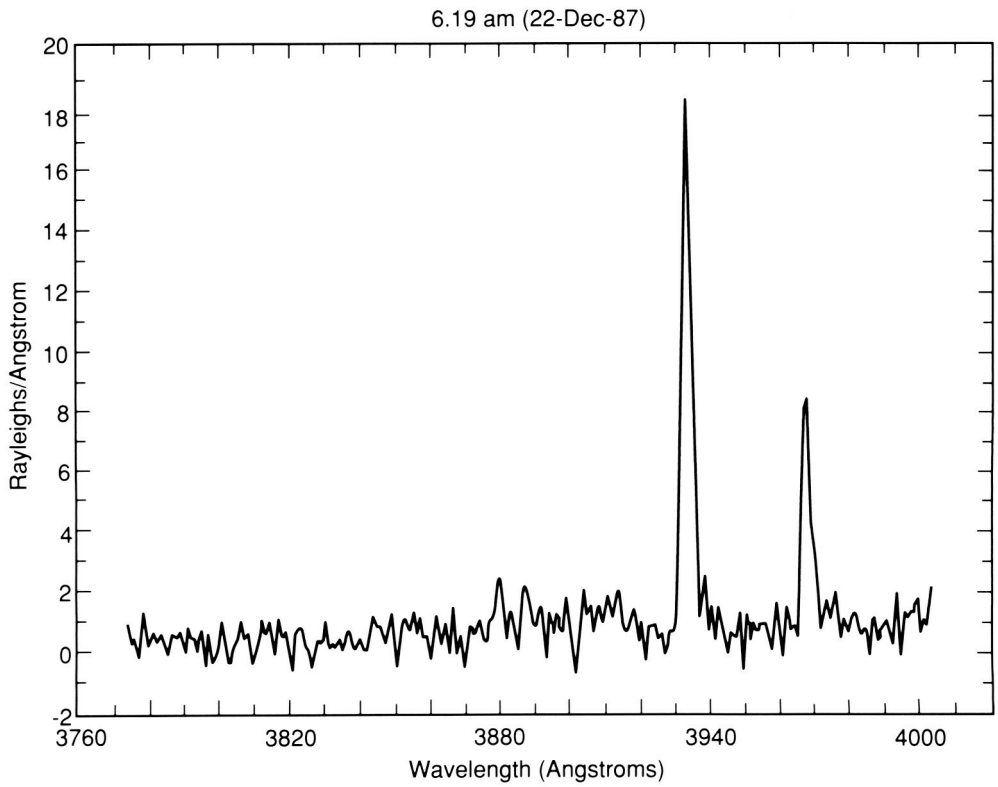

Figure 63. Measurement of Ca^+ Emissions in the Twilight Spectrum of the Upper Atmosphere

ATLAS-1 mission. A smaller program will continue using engineering models of MSFC's imaging spectrometers.

Fennelly, J., Torr, D. G., Torr, M. R., Dougani, H., Hamilton, C., and Swift, W.: Atomic Oxygen Composition Extraction from Twilight Airglow Measurements Taken at McDonald Observatory. EOS, Vol. 69, p. 420, 1988.

Torr, M. R., Torr, D. G., Eun, J. W., Swift, W., Dougani, H., and Harrison, D.: Observations of the N_2^+ First Negative Emission System in the Dayglow. EOS, Vol. 69, p. 420, 1988.

Torr, M. R., Torr, D. G., Bhatt, P., Wills, F., and Dougani, H.: Ca^+ Emission in the Sunlit Ionosphere. J. Geosphys. Res., submitted, 1988.

M. R. Torr/ES51
(205) 544-7591
Sponsor: Office of Space Science and Applications

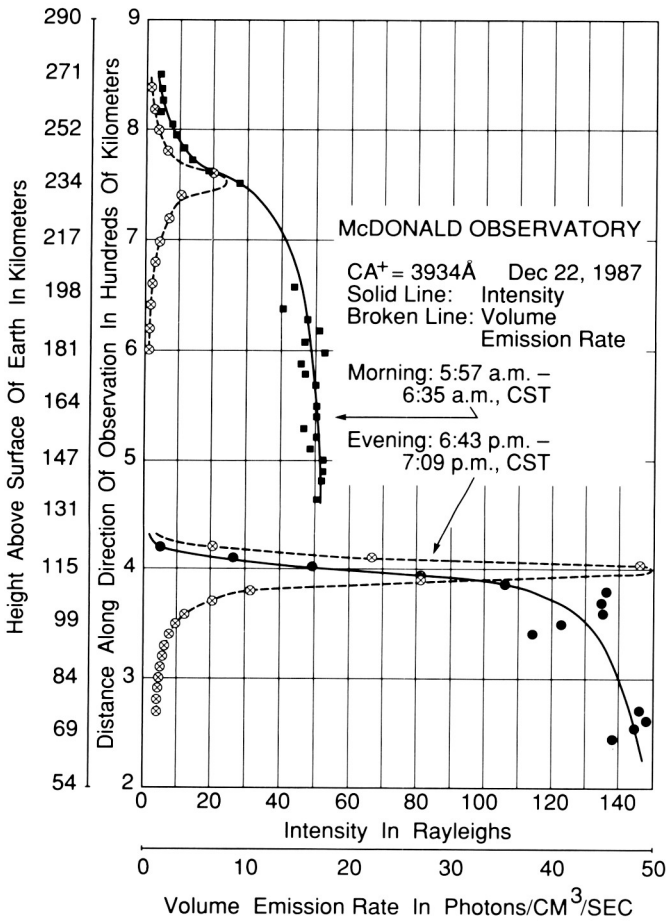

Figure 64. Measured Altitude Distributions of Ca^+ in Upper Atmosphere on Morning and Evening of December 22, 1987

Infrared Spectroscopy of the Stratosphere

The infrared spectrum of the Earth's stratosphere contains a wealth of information about its thermal structure and composition. A research program based on observations of balloon-borne thermal emission spectra of the Earth's stratosphere and development of analytical techniques is in progress in collaboration with the Goddard Space Flight Center. A liquid nitrogen cooled Michelson interferometer spectrometer (SIRIS) has been developed for high resolution thermal emission measurements of the Earth's stratospheric limb in the 600 to 2,000 cm^{-1} region. The instrument records spectra simultaneously in four preselected narrow band channels (175 cm^{-1}) with an unapodized spectral resolution of 0.025 cm^{-1}. An analysis of the observed spectra provides simultaneously determined profiles of temperature and concentrations of a large number of trace gases in the $C1_x$, HO_x, and NO_x families over a complete 24-hour cycle.

Infrared limb thermal emission spectra have been obtained with this instrument in two balloon flights made in 1984 and 1986, exhibiting spectral features of a large number of trace gases. The second successful balloon flight was made at night on September 15-16, 1986, from Palestine, Texas, and large numbers of complete limb sequences of stratospheric spectra were obtained for a period of about 10 hours. The data obtained in the second flight are currently being analyzed. The stratospheric constituents identified in the observed spectra (Fig. 65) in the two flights so far include: CO_2, O_3, H_2O, CH_4, HNO_3, N_2O, NO_2, NO, N_20_5, $C\ell ONO_2$, CF_4, $CC\ell_4$, $CFC\ell_3$, $CHF_2\ell$, and $CF_2C\ell_2$.

A portion of the data obtained on November 6, 1984, was analyzed for retrieval of trace constituent profiles. The analysis is based on a radiative transfer model and inversion techniques developed for high resolution limb thermal emission spectra. The model employs line-by-line and layer-by-layer calculations and includes curvature and refraction effects as well as aerosol extinctions. The pointing angles are

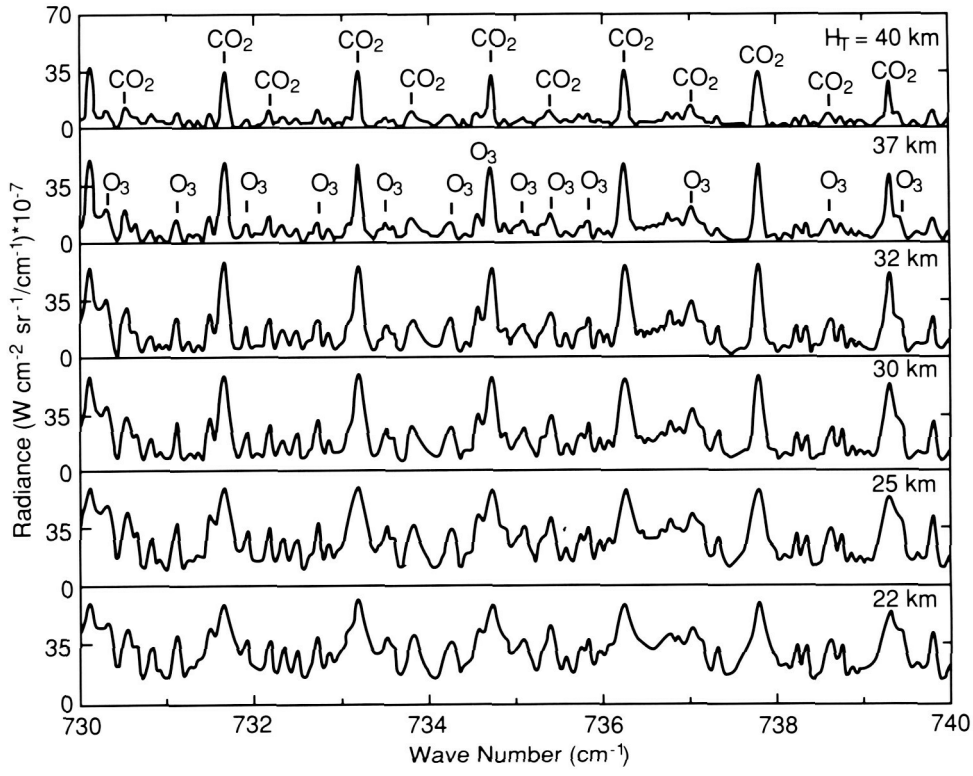

Figure 65. Complete Limb Sequence of the Observed Thermal Emission Spectra in the 730 to 740 cm^{-1} Region

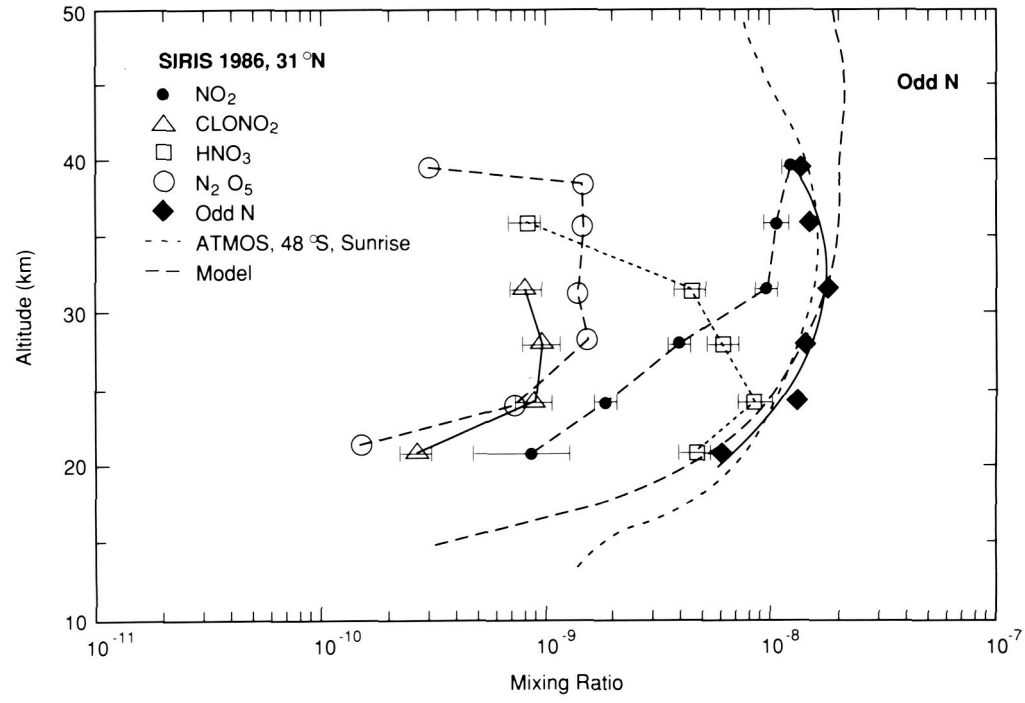

Figure 66. The Average Volume Mixing Ratio Profiles of HNO_3, NO_2, N_2O_5, $ClONO_2$ and Total Odd N. Also Shown for Comparison are: the ATMOS Profile Measured at 48° at Sunrise, and a Model Profile Obtained by Using a One-Dimensional Photochemical Model

retrieved from an inversion of the CO_2 features in the observed spectra. Simultaneously measured vertical mixing ratio profiles of O_3, H_2O, CH_4, N_2O, and $C\ell ONO_2$ were obtained and compared with measurements made with a variety of techniques by other groups. The comparison showed good agreement with the published data for all retrieved gases, indicating the unique potential of high resolution limb thermal emission measurements for remote sensing of trace gas profiles over a full 24-hour cycle.

A portion of the data set obtained in the 1986 balloon flight is being analyzed at the present time. Additional data are expected to become available from the ongoing balloon-based observational program. The diurnal variations of the simultaneously measured distributions of a number of trace gases, in particular the main elements of the NO_x (N_2O, NO_2, NO, HNO_3, N_2O_5, $C\ell ONO_2$) family, are being retrieved and compared with predictions of one-dimensional photochemical models (Fig. 66). The observational program is focusing on obtaining the diurnal variations and the nighttime measurements of the main elements of the NO_x family, and the total odd nitrogen budget. This capability is provided only by thermal emission measurements and is ideal for the instrument employed in this program.

Abbas, M. M., Shapiro, G. L., Conrath, B. J., Knude, V. G., and Maguire, W. C.: Thermal Emission Spectroscopy of the Stratosphere from Balloon Platforms. Advances in Remote Sensing Retrieval Methods, pp. 133–148, A. Deepak Publishing, Hampton, VA, 1985.

Abbas, M. M., Guo, J., Conrath, B. J., Kunde, V. G., and Maguire, W. C.: Finite Field of View Effects on Inversion of Limb Thermal Emission Observation. J. Geophys. Res., Vol. 90, pp. 3903–3909, 1985.

Abbas, M. M., Glenn, M. J., Kunde, V. G., Brasunas, J., Conrath, B. J., Maguire, W. C., and Herman, J. R.: Simultaneous Measurement of Stratospheric O_3, H_2O, CH_4 and N_2O From Limb Thermal Emissions. J. Geophys. Res., Vol. 92, pp. 8343–8353, 1987.

M. M. Abbas/ES55
(205) 544-7680
Sponsor: Office of Space Science and Applications

Atomic Oxygen Simulator

Studies have indicated that the impingement of all materials by the atomic oxygen in low-Earth orbit results in degradation, some severely. Because of the difficulty in obtaining space data it is necessary to simulate the atomic oxygen exposure conditions on the ground. This is difficult to do since oxygen is normally in the molecular form and to simulate space the oxygen atoms must be accelerated to an energy of approximately 5 eV.

An atomic oxygen simulator has been built under contract to MSFC. The approach to providing the atomic oxygen beam is to extract an ion beam from an oxygen plasma, focus the high energy beam into a magnetic sector (so that only the desired beam constituent is selected), and then into a decelerator. The result is an ion beam of pure atomic oxygen ions. Presently the system can provide a flux of 10^{14} ions $cm^{-2}\ s^{-1}$ at an energy of 5 eV over a 1 cm diameter beam. A satisfactory means of neutralizing these ions to produce a neutral beam has not been identified although work in this area will continue. Meanwhile, the source as presently configured will be useful in evaluating atomic oxygen ion effects on materials.

A contract is underway at Vanderbilt University to address some key questions. These are: what is the difference in interactions with materials due to ion beams or atom beams of atomic oxygen, and how do these interactions vary with beam energy and beam flux?

If the difference between ion beams and neutral beams is important, then a neutral beam with the desired characteristics will be needed. In case neutralization techniques are not successful with the present system, another approach being investigated by Princeton University for MSFC may fill the need.

M. R. Carruth/EH12
(205) 544-7647
Sponsor: Space Station Projects Office

Earth Science and Applications

The goal of the MSFC Earth Science and Applications program is to develop and utilize space technology to observe the Earth's atmosphere, land, and ocean from space in order to gain an improved understanding of the geophysical processes and their role in the interactions between various components of the Earth system (atmosphere, hydrosphere, cryosphere, biosphere, and solid Earth), consistent with the emerging concept of Earth-System Science.

Research and development activities are conducted in support of NASA's planned Earth Observing System. The program involves theoretical/analytical model development, remote sensor development, flight payload analyses, laboratory and field experiments required in these activities, and appropriate information system development. A major area of focus is the hydrologic cycle. Ground and space-based measurements of Earth parameters are used to develop and verify analytical and theoretical models of global and mesoscale processes to establish remote sensor requirements. Field experiments provide data required to verify the operation of air- and space-borne remote-sensing instrumentation. Data derived from observations are used as input to model computer codes. Extensive use is also made of interactive data display and access systems to study time-dependent development of Earth system processes on all scales.

Coherent Doppler Lidar Research and Development

Efforts in the area of research and development of coherent Doppler lidars (laser radars) encompassed a broad spectrum during FY88. General engineering support was provided to the in-house study on the accommodation of the Laser Atmospheric Wind Sounder (LAWS) as an attached payload for Space Station Freedom. This included determining the initial system configuration, establishing pointing requirements, and performing overall system performance analyses. In addition several investigations were undertaken to improve coherent lidar system performance and to gain a better understanding of system losses. These investigations included the setup and performance of heterodyne quantum efficiency measurements on mercury cadmium telluride detectors, and detailed analyses of lidar calibration targets.

Work continued on the analysis of backscatter data collected in the Australian flights of the 10.6-μm backscatter (Beta) measurement system which occurred in 1986. The 10.6-μm Beta system was disassembled and refurbished and work on the 9.1-micron system continues. These two instruments will be flown in a Global Backscatter Experiment in 1989. The purpose of this experiment is to measure backscatter values in the upper troposphere to obtain design information for the LAWS system.

A considerable effort was expended in the continued upgrading of the ground based operation of the pulsed lidar. The system, installed in the laboratory, is shown in Figure 67. Refinements to the software for data collection and pointing control have been accomplished and two new signal processing systems have been installed. One of these systems is a new poly-pulse-pair processor which has more flexibility

than the old system. The other involves collecting raw data by directly recording the in-phase and quadrature components of the Doppler return signal. The latter system will allow for detailed investigations concerning signal processing as well as enable more in-depth studies of atmospheric effects on single pulse transmission. In addition, laboratory measurements were performed using simulated signals to better characterize the poly-pulse-pair signal processing technique.

Analysis was completed on the data collected during 1984 flight tests to determine the accuracy of the inertial platform system which provided information to the lidar system for pointing correction and position determination. This analysis was performed by the National Severe Storms Laboratory in conjunction with the University of Oklahoma. The results of the analysis indicate that the system is sufficiently accurate to meet the needs of the future flight programs. Such a flight program has been tentatively planned for 1991 and investigations to assess system modification requirements are in progress. Current plans call for the incorporation of one of the lasers under investigation in the Office of Aeronautics and Space Technology funded CO_2 laser research and development program. The feasibility of accomplishing this is yet to be determined.

Breaux, Paul N.: Heterodyne Quantum Efficiency Measurements. Internal Note, November 1987.

Johnson, Steve: Laboratory Measurements of the Performance of a Poly-Pulse-Pair Signal Processor. Presented at the 4th Coherent Laser Radar Conference, sponsored by the Optical Society of America, Aspen, Colorado, July 27-31, 1987.

Anderson, Richard and Jones, William: Classical Radiometry and Lidar Calibration. Applied Optics, Submitted, February 1988.

J. W. Bilbro/EB23
(205) 544-3467
Sponsor: Office of Space Science and Applications

Figure 67. The Ground-based Pulsed Doppler Lidar Laboratory

CO_2 Laser Research and Development

A new effort has been undertaken to investigate candidate lasers for use in the space-based coherent Doppler lidar known as the Laser Atmospheric Wind Sounder (LAWS). Although LAWS is a facility instrument under the Office of Space Science and Application's Earth Observing System, this effort is funded under the Office of Aeronautics and Space Technology's Civil Space Technology Initiative. This effort performs laboratory investigations of candidate lasers and laser subsystems to determine the optimum technology for LAWS.

Work during FY88 has consisted of in-house laboratory measurements, modeling, and setting in place out-of-house studies and laboratory investigations which will be carried out during the remainder of FY88 and in the coming year. Out-of-house investigations have been instigated at the National Oceanic and Atmospheric Administration's Wave Propagation Laboratory to characterize the two-Joule injection locked transversely excited atmospheric (TEA) laser which was built for them by Spectra Technologies Inc., including detailed measurements of frequency stability, efficiency, pulse shape, and overall lidar system efficiency. Investigations at the Jet Propulsion Laboratory to injection lock the laser developed for MSFC by Pulse Systems, Inc., involve feasibility assessment, design, development, and testing. Catalyst studies at the Langley Research Center will tailor studies in CO_2 laser catalysts to the needs of LAWS. Specifically, the effort is directed toward use with the isotope $^{12}C^{18}O_2$. A catalyst is required to prolong laser life by aiding recombination of CO and O_2. The dissociation occurs as a result of the electrical discharge through the gas, and if recombination is not affected, high concentrations of O_2 result in arcing.

Investigations into the characteristics of operation of the isotope $^{12}C^{18}O_2$ are being jointly funded by the Air Force Geophysical Laboratory as a follow-on to a similar study for the isotope $^{13}C^{16}O_2$. These isotopes of CO_2 are required for space-based operation since they eliminate atmospheric absorption by the naturally occurring CO_2 in the atmosphere. This absorption greatly reduces the signal-to-noise ratio for round trip propagation to the Earth's surface and back. The oxygen 18 isotope is more desirable than the carbon 13 since it has additional benefits due to reduced water vapor absorption and enhanced scattering properties for the 9.11 micron laser line.

In-house investigations have involved the initial setup and characterization of two laser configurations. The first, a Master Oscillator Power Amplifier (MOPA) system, built by CLS, Inc., consists of a 70-mJ hybrid TEA used as the master oscillator and a commercial Lumonics TEA used in a two-pass configuration as the amplifier. This system produced 500 mJ pulses of approximately 3 μsec duration. The second is a modification of a commercial system produced by Pulse Systems, Inc. This laser produced pulses of from 1 to 2 J. The primary pulse was 3 μsec in duration, but was often accompanied by a tail as long as 20 μsec. Pulse to pulse variation in frequency of ±30 MHz were observed with 2 to 3 MHz variations internal to the pulse. Work will continue to refine measurements of these two systems during the remainder of the year. An additional experiment was performed using the MSFC 10-mJ MOPA system developed by the Raytheon Co. In this experiment, a Pulse Systems, Inc., amplifier was inserted prior to the detector to provide amplification of the backscattered signal. A factor of two improvement was noted against a hard target. This is the first time an experiment of this type has been performed using a coherent lidar. Continued investigations of this technique are planned for the coming year.

Computer modeling studies were continued to examine the mode-medium interaction in pulse CO_2 lasers. Two codes have been developed, one a general purpose two-dimensional diffractive optics code and the other a general purpose three-dimensional diffractive optics code. Analyses were performed for frequency chirp due to the laser-induced media perturbation effect for various types of unstable resonators. Analyses were also performed for various types of unstable resonators with the Lumonics 820 laser and the Pulse Systems, Inc., LP-140 laser. Figure 68 shows the results of modeling the near-field output of the LP-140 using a scraper mirror compared to

using a mirror whose reflectivity can be characterized by a Gaussian profile. As can be seen by these two plots, the scraper mirror abruptly blocks the beam in the near-field creating edge effects due to diffraction, while the tapering effects of the Gaussian reflectivity produce a smoother transition to the central blocked region.

Smithers, Martin E.: Mode-Medium Interaction in Pulse CO_2 Lasers. Presented at the 4th Coherent Laser Radar Conference, sponsored by the Optical Society of America, Aspen, Colorado, July 27-31, 1987.

J. W. Bilbro/EB23
(205) 544-3467
Sponsor: Office of Aeronautics and Space Technology

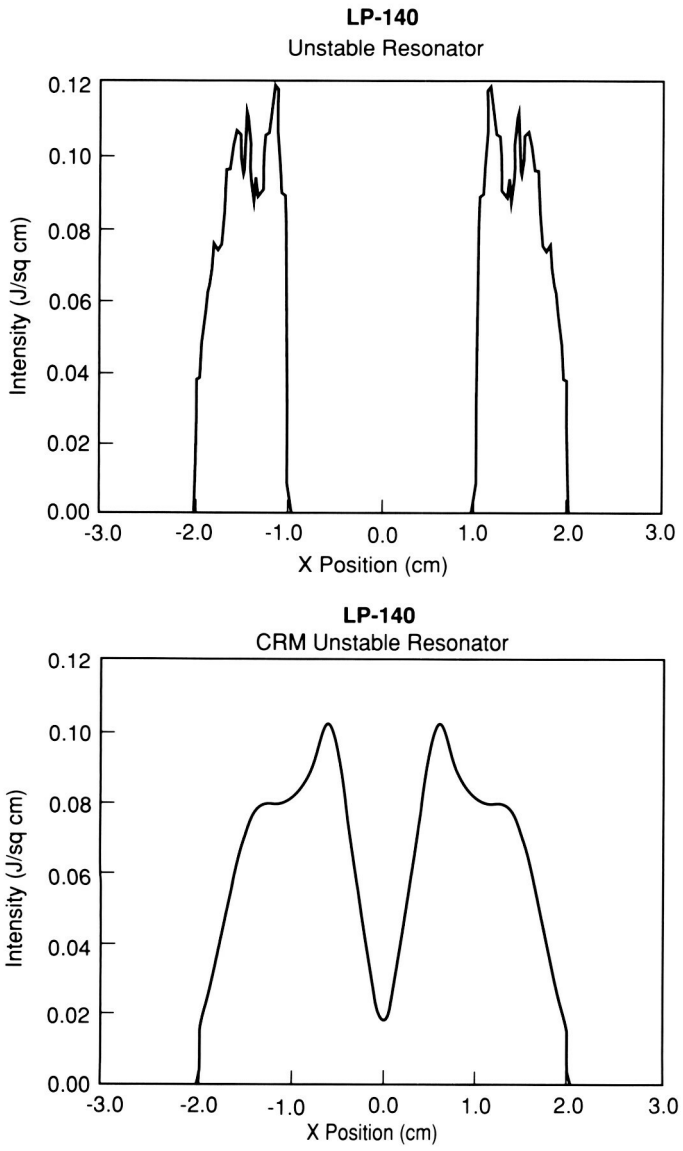

Figure 68. Modeling of Near-Field Output of the LP-140 Laser in an Unstable Resonator Configuration

Thermally-Driven Circulations in Tropical Baroclinic Zones

Tropical atmospheric motion fields are forced largely by diabatic processes such as surface boundary heating, longwave radiative flux convergence, and release of latent heat associated with deep moist convection. The latter heat source is especially important because it provides the major pathway for the Sun's energy to the atmosphere. Longitudinal and meridional overturning of the tropical atmosphere (the Walker and Hadley circulations) are driven by latent heat release.

Recent diagnostic studies at MSFC have examined the role of latent heat release in driving thermally-direct circulations in the vicinity of the subtropical jet stream over the south-central Pacific. This study was made possible by the dense atmospheric wind, temperature, and moisture data collected during the Global Weather Experiment conducted in 1979. Improved data sets from that experiment have recently become available.

Figure 69 shows the precipitation rate in mm/h that occurred over a 9-day period of study. Vertically-integrated atmospheric heating is directly proportional to the rain rate. Figure 70 depicts contours of the mean absolute horizontal temperature gradient in the upper troposphere that was measured at that time. Heavy arrows denote the axis of the subtropical jet. Note that the strongest temperature gradient lies slightly poleward (south) of the heaviest precipitation. This scenario suggests that differential heating associated with the condensation and rainfall is important in maintaining the horizontal thermal contrast supporting the jet stream. Using the frontogenetical equation to diagnose the processes which force this thermal gradient, this has been verified. It has also been found that thermally-direct vertical circulations which accompany the heating (in the plane normal to the subtropical jet) have a counteracting effect to inhibit a runaway growth of the temperature gradient.

Experiments have begun to study the response of the atmosphere to convective forcing by means of numerical simulations with an atmospheric general circulation model. A critical need also exists for better moisture data in the tropics. Studies are currently underway to use passive microwave measurements from the Special Sensor Microwave Imager sensor to develop a better understanding of tropical moisture and convection.

Robertson, F. R., Vincent, D. G., and Kann, D. M.: The Role of Diabatic Heating in Maintaining the Upper-Tropospheric Baroclinic Zone in the South Pacific. Quart. J. Roy. Meteor. Soc., submitted, 1988.

F. R. Robertson/ED42
(205) 544-1655
Sponsor: Office of Space Science and Applications

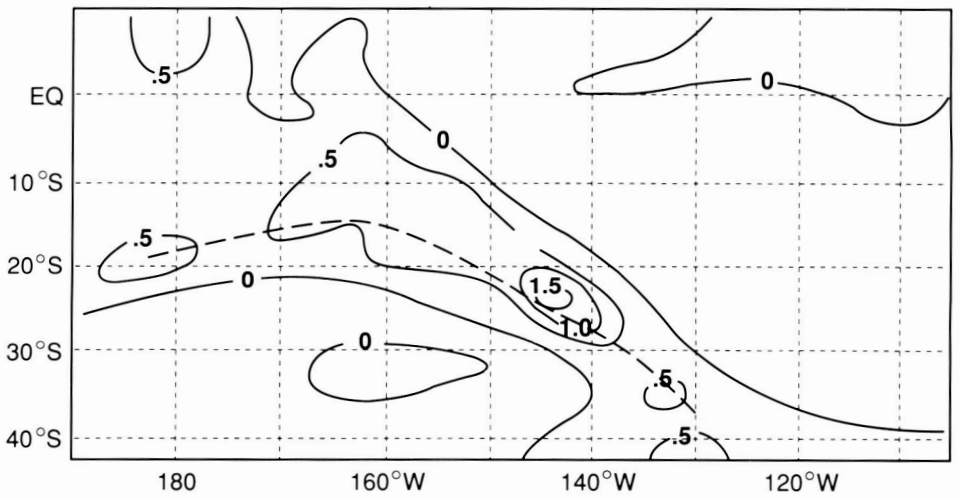

Figure 69. Average Precipitation Rate (mm/h) for January 10-18, 1979

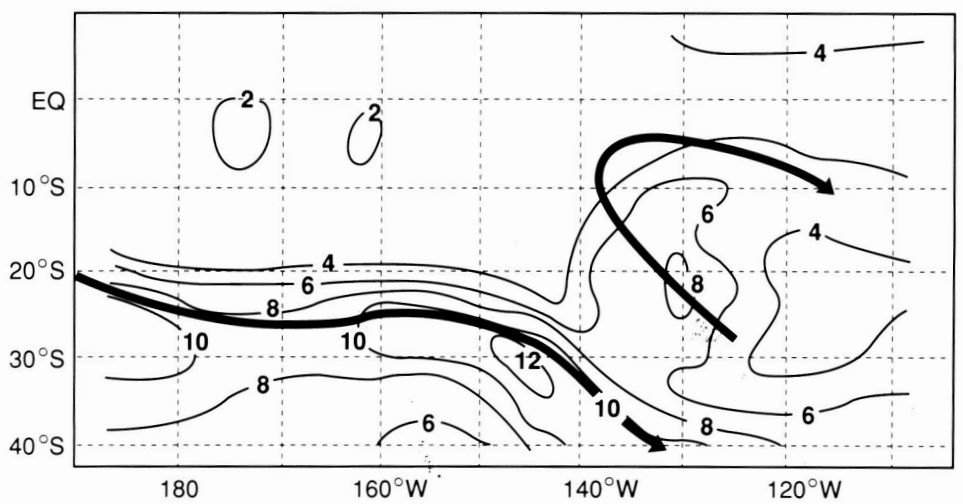

Figure 70. Upper-Tropospheric Mean Absolute Horizontal Temperature Gradient 10^{-3} K/km

Geophysical Fluid Flow Cell Experiment

The equations which govern the motion of nonlinear, thermally driven, rotating fluids have the same form as those which govern the large scale motion of the Earth's atmosphere. By maintaining dynamic and geometric similarity, laboratory models can be used to study atmospheric dynamics, much as wind tunnel models provide flow information about prototype airfoils. From early rotating dishpan experiments, laboratory models have examined the fundamental forces at work which account for the observed circulation of planetary and solar atmospheres. While analytical techniques are particularly suited to a simplified physical understanding of the problem and numerical methods attempt to describe the details of the flows, laboratory experiments offer a natural analog solution when restrictive assumptions or limited time/space resolution eliminate the other approaches.

The Geophysical Fluid Flow Cell (GFFC) experiment simulates a wide variety of thermal convection phenomena in spherical geometry. By applying an electric field across a spherical capacitor filled with a dielectric liquid, a body force analogous to gravity is generated around the fluid. The force acts as a buoyant force in that its magnitude is proportional to the local temperature of the fluid and in the radial direction perpendicular to the spherical surface. In this manner, cooler fluid sinks toward the surface of the inner sphere while warmer fluid rises toward the outer sphere. The value of this artificial gravity is proportional to the square of the voltage applied across the sphere and can thus be imposed as desired. With practical voltages, its magnitude is only a fraction of Earth's and so requires a microgravity environment to be significant.

Meteorologists and astrophysicists interested in large-scale planetary and solar circulations have come to recognize the importance of rotation and stratification in determining the character of these flows. The effect of latitude-dependent Coriolis force on nonlinear convection contributes to differences between tropical and mid-latitude circulations and is also thought to play a crucial role in such phenomena as the differential rotation of the Sun, the cloud band orientation on Jupiter, and the generation of magnetic fields in thermally driven dynamos. Most theoretical and all experimental work on these problems has in the past treated only local curvature effects. The continuous low gravity environment of the orbiting Space Shuttle offers a unique opportunity to make laboratory studies of large-scale thermally driven flows under the constraint imposed by rotation and sphericity.

Experiments performed on Spacelab 3 produced a variety of spherical convective flow regimes depending on the relative magnitudes of the rotation rate, temperature distribution, and spherical gravity. Several experiments were performed in which the inner sphere temperature was uniform and higher than on the bounding outer sphere. Believed to be analogous to the deep convection layers of the Sun, these experiments produced "banana cells" aligned with the rotation axis for fast rotation rates. Some cases showed a prograde motion of the cells at mid-latitude while equatorial cells were retrograde. These results may help to explain the differential rotation of the Sun's equator. As the relative importance of the heating increases, the flow becomes more concentrated. Numerical modeling of this phenomenon using a three-dimensional computer model showed good agreement with the observed wave number and phase speed.

Another series of experiments imposed a pole to equator temperature gradient in addition to the radial one; i.e., the pole was hot relative to the equator. In these cases, the rotation was not as fast as in the above cases and the instability became more spiral in nature. With relatively weak heating, the spiral waves are confined to mid-latitude. With an increase in heating, the pattern branches out toward the equator, but retains a tilt toward the direction of rotation.

Without the meridional temperature gradient to drive a north-south circulation, heating is weak and convective motion is organized into polygons reminiscent of Benard convection cells. In this case the

motion is slow with upward motion confined to the narrow region between polygons while descending motion occurs over the broad interior of the cell. The addition of a north-south temperature gradient along with an increase in both the heating and rotation shows the development of triangular waves. These motions were unexpected and much effort is being placed on their analysis. The pattern persists even when the heating and rotation are further increased.

More recent investigations have been carried out to understand the planforms observed in slowly rotating spherical convection. The results of mode competition indicate that slight non-Boussinesq effects or spherical gravity gradient effects may account for the observation of tilting patterns with narrow updrafts. Three-dimensional (3-D) computations of the spiral wave case (modest rotation, imposed heating with meridional, and radially unstable temperature gradients) indicate the action of the zonal flow on the instability, and suggest that the formation of isolated convective columns choke the zonal flow. The fluid in the GFFC often has a thermally unstable layer near the inner sphere underlying a stable layer generated by a meridional circulation. Such situations are of major interest in solar physics. Numerical studies of these cases have shown how the stable layer leads to gravity wave generation and convective mode selection.

A numerical code developed to simulate fluid flows in the GFFC has recently been installed on MSFC's supercomputer. The code is a 3-D numerical model of the GFFC experiment. The model is used in part to analyze Spacelab 3 data. In addition, the code will be used to examine the possibility of using the GFFC to examine baroclinically unstable flows. The model has simulated a number of features observed in the GFFC including the number and phase speed of the columnar convection and the asymmetries associated with spiral waves. Numerical simulations of low rotation rate cases revealed multiple equilibria as well as long-time evolution in computed flows. Further studies will be undertaken to verify this unexpected result, with the goal of defining further experiments for the next flight. Validating the code with experiments allows its detailed calculations to be used to diagnose the individual forces at work.

The GFFC is being refurbished and modified for another flight aboard Spacelab. Tests with video camera systems have been completed and work has commenced to incorporate such a system into the GFFC. This will allow Spacelab crewmembers and investigators on the ground to observe flow patterns in real time and interact with experiment parameters. Numerical, theoretical, and ground laboratory studies have been performed to define the next series of experiments. The next series of experiments will explore in detail the nature of the transition to turbulence in convection subject to various degrees of rotation (of particular interest is the number of modes participating in the transition, and the role of secondary instability); examine stably-stratified flows which are driven by north-south temperature gradients (these flows are analogous to the Earth's circulations which are important in distributing heat and momentum); investigate the reality of long-time (climatic scale) evolution between different states, as was suggested recently by one of our numerical models; and conduct experiments with boundary heating distributions not studied on Spacelab. Of special importance is the case of constant temperature on the outer sphere and latitudinally increasing temperature on the inner sphere. This topology roughly mimics what is thought to be the appropriate heating distribution of Jupiter.

The GFFC experiments provide a testing ground for new ideas on planetary scale dynamics. The parameter range available in the laboratory extends well beyond that accessible by computational modeling, making the space experiment the only means of getting information about this phenomena. Thus new discoveries are possible that have and will continue to motivate theoretical analyses on problems that are of fundamental importance in atmospheric science. The GFFC experiments also relate to fundamental studies of the origin of chaos in fluids. The dimensionality, or number of fundamental de-

grees of freedom active in chaotic flow, can be observed in a system that has a higher degree of similarity with geophysical flows than was previously possible in Earth-bound experiments which cannot model sphericity in a consistent and general way.

Hart, J. E., Toomre, J., Deane, A. E., Hurlburt, N. E., Glatzmaier, G. A., Fichtl, G. H., Leslie, F., Fowlis, W. W., and Gilman, P. A.: A Laboratory Model of Planetary and Stellar Convection. Science, Vol. 234, pp. 61–64, 1986.

Toomre, J., Hart, J. E., and Glatzmaier, G. A.: Spacelab Experiments on Convection in a Rotating Spherical Shell with Radial Gravity. On the Internal Solar Angular Velocity: Theory and Observation, Eds. B. R. Durney and S. Sofia: Reidel, Dordrecht, 1987.

F. W. Leslie/ED42
(205) 544-1633
Sponsor: Office of Space Science and Applications

Global Backscatter Experiment

During FY88, the Global Backscatter Experiment (GLOBE) continued determining the spatial and temporal variation of atmospheric backscatter. These data are needed to support the development of the Laser Atmospheric Wind Sounder (LAWS), under development by MSFC for the Earth Observing System of the mid-1990's.

Three science working group meetings were held to discuss the results available from GLOBE experiments in Australia, England, and the United States. As more data become available to make backscatter estimates, it is becoming apparent that there is a global background value that can be used as a design value for LAWS. The value thus far estimated from the new data indicates that the background backscatter value is very near the threshold estimated for the LAWS instrument. This means that there is every reason to go forward with the LAWS instrument development, and that the GLOBE program should also proceed to refine and chart statistics on the backscatter values.

Collaboration with a large number of researchers from various institutions and various countries continues. The majority of the data analyzed were from aircraft belonging to the Royal Signals and Radar Establishment of Great Britain, and from the Commonwealth Scientific and Industrial Research Organization of Australia. Contact was also made with researchers in Germany, France, and Japan regarding their participation in further GLOBE field activities. Papers were reviewed for an entire issue of the Journal of Geophysical Research dedicated to completed GLOBE research that will be published in the coming year.

Instrument development and organizational activities continued with the goal of fielding a major flight program in FY89 using the NASA DC-8 research aircraft. A large laser radar for onboard backscatter measurement is being developed, along with a number

of smaller instruments designed to make definitive measurements of the aerosol physics and chemistry that affect laser backscatter. This is a collaboration with scientists from MSFC, the Jet Propulsion Laboratory, Ames Research Center, the University of Hawaii, Georgia Institute of Technology, the University of Miami, and the National Oceanic and Atmospheric Administration.

This year a major new effort that was initiated was the design and planning for a GLOBE database to collect information being generated by the program into an archive for researchers and others associated with the LAWS program. The GLOBE database will be used by scientists as the basis of models of backscatter for LAWS evaluation and performance calculations.

D. E. Fitzjarrald/ED43
(205) 544-1651
Sponsor: Office of Space Science and Applications

Atmospheric Dynamics and Modeling

One of NASA's missions is to develop a better understanding of the planet Earth. An important aspect of the behavior of the Earth system is the atmosphere-ocean fluid system, which transports heat from tropical to middle and upper latitudes and which determines the Earth's weather and climate. This fluid system is a complex, nonlinear, dynamical system which results in highly unpredictable weather and climate fluctuations. Due to the complex nature of this system and the difficulty in obtaining sufficient observational data on it, predicting its behavior in the near future remains an elusive goal. Many questions about the future of the environment have been identified but remain unanswered, including those relating to the influence of human activity. Obtaining the level of understanding required to be able to predict future behavior of the system requires a three-pronged approach which includes observations, idealized theoretical and conceptual modeling, and detailed numerical (computer) modeling.

The first modeling effort in this research is a fully nonlinear model of a global (spherical) fluid system which is driven by thermal gradients and influenced by rotation (the current model lacks such detail as continents and oceans, detailed radiative transfer calculations, and moisture physics). This system will permit the advancement of theoretical study of the atmosphere by studying the nonlinear behavior of the basic fluid system in full spherical coordinates. It will be used to study the flows in the Geophysical Fluid Flow Cell (GFFC), a Spacelab experiment. The numerical code is flexible enough that it can also be operated in cylindrical geometry to simulate terrestrial laboratory experiments. Current work is developing nonlinear feedbacks between the azimuthal mean flow and waves, and feedbacks among the waves. Detailed comparisons of the results of the present code and previous work in cylindrical geometry done at Florida State University is presently underway.

Experiments in cylindrical geometry continue using a rotating, thermally-driven fluid flow cell which is similar in some respects to the spherical GFFC. These terrestrial laboratory experiments will give a large amount of data which can be compared in detail with the results from the numerical modeling of the first area. This will allow detailed verification of the numerical model, help guide the selection of experiments to perform using the Spacelab apparatus, and is an interesting fluid system in its own right.

The Limited Area Mesoscale Prediction System is an atmospheric model which includes calculations of water substance (vapor, cloud water, rain water) transport, condensation, evaporation, etc., both explicitly, through grid-resolved processes, and parameterized cloud-scale processes. This model for predicting regional moist atmospheric processes was developed at the National Center for Atmospheric Research and Drexel University and is used in some of the MSFC research described in other articles as well. In this case, the goal is to study the mesoscale (about 100 to 500 km, or of order 100 miles) processes which occur due to the presence of a great deal of potential energy due to low-level moisture and horizontal temperature gradients. The objective of the work is to better understand the processes involved and modeling techniques for intense weather situations in mid-latitude winter storms.

A channel model of large-scale baroclinic flows with topographic forcing is employed here to study the influence of topography on baroclinic waves, i.e., its influence on exciting disturbances of the same scale, and its ability to modulate growing disturbances of another scale. It is suggested that the external forcing could contribute to the occurrence of atmospheric blocking and may, in part, be responsible for the chaotic nature of atmospheric flows. The study shows that topography induces an amplitude vacillation which has a shorter period than that produced by the baroclinic instability alone. The topography tends to phase-lock the disturbance, especially the topographic scale wave, while the baroclinicity leads to the propagation of the disturbance, especially the most unstable wave.

A modeling study of combined troposphere/stratosphere dynamics has been proposed. The dynamics of the troposphere are influenced by the stratosphere through the confinement of small scale baroclinic waves to the troposphere, while large scale waves often propagate into the stratosphere. On the other hand, the stratosphere is a reservoir of potential vorticity which can influence the development of cyclones in the troposphere. A feature of the modeling studies is the inclusion of ozone in the stratosphere, to learn more about the applicability of satellite-derived total ozone data in studies of tropopause dynamics.

Chou, S. H. and Loesch, A. Z.: Effect of Topography on Supercritical Baroclinic Disturbances. Palmen Memorial Symposium on Extratropical Cyclones, Helsinki, Finland, August 1988.

Miller, T. L.: On the Design of Baroclinic Space Laboratory Experiments in Spherical Geometry. Sixth Conference on Atmospheric and Oceanic Waves and Stability, Seattle, Washington, August 1987.

Miller, T. L.: Numerical Experiments of Mesoscale Instabilities Within The Presence of Large Scale Topography. Sixth Conference on Atmospheric and Oceanic Waves and Stability, Seattle, Washington, August 1987.

T. L. Miller/ED42
(205) 544-1641
Sponsor: Office of Space Science and Applications

Infrared Detection of Atmospheric Water Vapor and Surface Variables

The use of NASA's Multispectral Atmospheric Mapping Sensor (MAMS) has been expanded in FY88 to include several new research topics. MAMS data has been used to determine atmospheric moisture variability and its importance for cloud formation and storm development at scales not available from satellites. Current applications investigate interactions between the Earth's atmosphere and its surface (both land and water) to show how space-based measurements can best be used to study the Earth and atmosphere as a system. Additional flight activities with the MAMS on NASA's ER-2 aircraft are planned for upcoming years for further investigations. These investigations support the design and development of future space-based instrumentation to study similar phenomena on a global basis.

On-going MAMS investigations are concentrated in several research areas. The Split Window Variance Ratio technique has been refined to provide a more accurate estimation of low-level moisture at fine horizontal scales. The technique uses differential absorption at two infrared wavelengths to estimate the precipitable water in the lowest 4 km of the atmosphere. Values are retrieved at a spatial resolution of several kilometers and combined in an image form to produce a pictorial display of the atmospheric moisture concentration. Refinements to the technique allow for a more unambiguous estimation of this moisture variability in partly cloudy regions.

The MAMS was also modified to measure infrared radiation in a third-window channel at 3.7 μm. This new channel is being used with the 11 and 12 μm channels to estimate land surface temperature and the thermal emissivity of naturally occurring soil and vegetation regimes. A day/night sequence of MAMS images over a prairie region of Kansas was collected in June 1987 to support this investigation.

MAMS high spatial resolution data are being used to estimate sea-surface temperature variations along coastline areas. Variations in water surface temperature along coastlines and inlets are correlated to water depth and sea state. When combined with sediment content mapped by the MAMS visible channel imagery, these data will provide a way to diagnose geomorphic changes in shallow bay areas and delta regions. A preliminary set of data was collected last January over the Mississippi river delta region of Louisiana, and additional data will be collected in FY89.

Jedlovec, G. J., Batson, K. B., Atkinson, R. J., Menzel, W. P., Moeller, C. C., and James, M. W.: Improved Capabilities of the Multispectral Atmospheric Mapping Sensor. NASA Technical Memorandum, in press, 1988

Jedlovec, G. J., : Determination of Atmospheric Moisture Structure from High Resolution MAMS Radiance Data. Ph. D. dissertation, University Microfilms International, Ann Arbor, Michigan, 1987.

G. J. Jedlovec/ED43
(205) 544-5695
Sponsor: Office of Space Science and Applications

Experimental Precipitation Measurements

Microwave radiometric data were collected by instrumentation aboard the NASA ER-2 high-altitude aircraft during the Cooperative Huntsville Meteorological Experiment (COHMEX) conducted in the northern Alabama/central Tennessee region in FY86. During COHMEX, which was sponsored by MSFC, two microwave radiometers were mounted aboard the ER-2 and flown in cooperation with Goddard Space Flight Center. These instruments were the Microwave Precipitation Radiometer, which collected data at 18 and 37 GHz, and the Advanced Microwave Moisture Sounder, which sampled at 92 and 183 GHz. Additionally, the National Center for Atmospheric Research CP-2 radar was operating during the ER-2 flights to provide storm structure information for later comparison.

Analysis of the microwave data collected during COHMEX has revealed the superior ability of the 92 GHz frequency to detect regions of light rain in contrast to the 18 and 37 GHz frequencies. A comparison of the aircraft radiometric measurements to corresponding radar-derived rain rates has suggested a preliminary threshold of brightness temperature which delineates regions of rain/no rain in microwave imagery. Although the threshold value will undoubtedly be refined during future studies, the current value correlates very well with the ongoing MSFC analysis of 85 GHz data collected by the Defense Meteorological Satellite Program's Special Sensor Microwave/Imager. This ability to delineate regions of rain/no rain in satellite microwave imagery will be of great assistance to the study of global precipitation climatology.

R. E. Hood/ED43
(205) 544-5407
Sponsor: Office of Space Science and Applications

Global Precipitation Measurements with Satellite Microwave Observations

Global precipitation measurements are important for monitoring and understanding the earth's climate irregularities and improving long-range weather forecasting. Precipitation retrieval algorithm development work has recently benefitted by the 1987 launch of a sun-synchronous polar orbiting Defense Meteorological Satellite Program (DMSP) satellite carrying the first Special Sensor Microwave/Imager (SSM/I). This instrument is providing up to twice daily measurements of the earth's thermal emission at frequencies of 19.35, 22.235, 37, and 85.5 GHz with spatial resolutions as fine as 15 km. It is the 85-GHz (H and V polarization) channels that are new to the heritage of spaceborne microwave remote sensors.

Data from the SSM/I have validated the concept that precipitation size ice within rain systems causes a cold radiometric signal that intensifies as the precipitation becomes heavier (Fig. 71). The cooling is caused by backscattering of upwelling earth radiation from below the ice, and virtually no ice-emitted radiation takes its place. This allows quantitative rainfall precipitation estimates to be made over land and over ocean. Any possible contamination by cirrus cloud ice particles, which are smaller than precipitation size, has been ruled out. Over the ocean, the H and V polarization data must be used together to avoid ambiguities between light rain and dry oceanic air. Although more detailed work needs to be done, both land and ocean algorithms have been tested, on a preliminary basis, through comparisons with ground based radar measurements of the same warm season rain systems that the satellite probed.

These new satellite measurements are allowing further refinements in a new NASA research sensor design being proposed to provide Earth observations in the microwave portion of the spectrum starting in the middle 1990's.

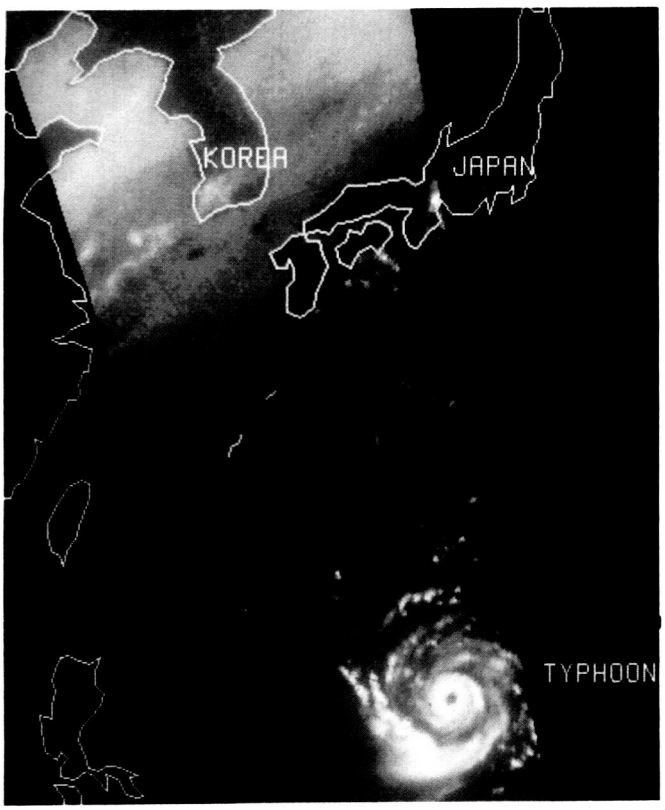

Figure 71. SSM/I 85 GHz Image of Precipitation within a Typhoon

R. W. Spencer/ED43
(205) 544-1686
Sponsor: Office of Space Science and Applications

ORIGINAL PAGE
COLOR PHOTOGRAPH

Synthetic Radiance Fields from Numerically Simulated Atmospheres

Passive sounding and imaging of the atmosphere from polar and geostationary orbits provides crucial information for measuring the global physical environment and for initializing numerical weather prediction models. MSFC, Universities Space Research Association, and Drexel University are developing software and image display techniques for examining atmospheric mesoscale model output by simulating radiance fields that a given sensor would see if viewing the evolving of the model atmosphere. The primary tools in this study are the Limited Area Mesoscale Prediction System (LAMPS) which is a mesoscale dynamical model developed at Drexel University, and a radiative transfer code that was originally developed at the University of Wisconsin and modified recently at MSFC. Simulation of atmospheric flows by the LAMPS model provide known atmospheric thermodynamic states which are then passed to the radiative transfer code to derive corresponding microwave and infrared (IR) radiances. By comparing the radiance patterns in the simulated imagery to diagnostic quantities (e.g., vertical velocity, water vapor, cloud fields, surface skin temperature) derived from model archives, a more complete dynamical interpretation of the patterns in the actual observed imagery is obtained.

Activities last year focused on the study of moist baroclinic waves which developed along the east coast of the United States during the Genesis of Atlantic Lows Experiment field program. The two events chosen for study were notable because of the mesoscale structure in the cloud fields which developed. A particularly revealing example of the utility of comparing simulated imagery with observations is given in Figure 72. The 6.7-μm IR channel shown in both panels is sensitive primarily to upper-tropospheric water vapor. Darker regions extending from the Gulf of Mexico across Florida in the observed imagery are indicative of dry air which has had a history of sinking. This pattern is well simulated by the

LAMPS imagery (a 12-hour forecast). The white streak just offshore of the Carolinas in the observed imagery is associated with convective moistening and is also present in the simulation, although it is perhaps too intense.

The consistency of the simulations and the observations encourages us to use the model history files as a data set on which more quantitative diagnostic studies can be based (i.e., air parcel trajectory analysis, moisture budgets, etc.). This approach allows use of the model simulation capability to extend interpretation of the observed satellite imagery; actual in situ measurements of atmospheric states are too sparse in most locations to yield reliable quantitative insight as to the dynamic processes responsible for producing the radiance patterns.

Current simulation capabilities include all channels for the Microwave Sounding Unit and High Resolution Infrared Sounder. The Advanced Microwave Sounding Unit, which will be the primary source of atmospheric temperature and moisture profiles in the 1990's, will be simulated next.

F. R. Robertson/ED42
(205) 544-1655
Sponsor: Office of Space Science and Applications

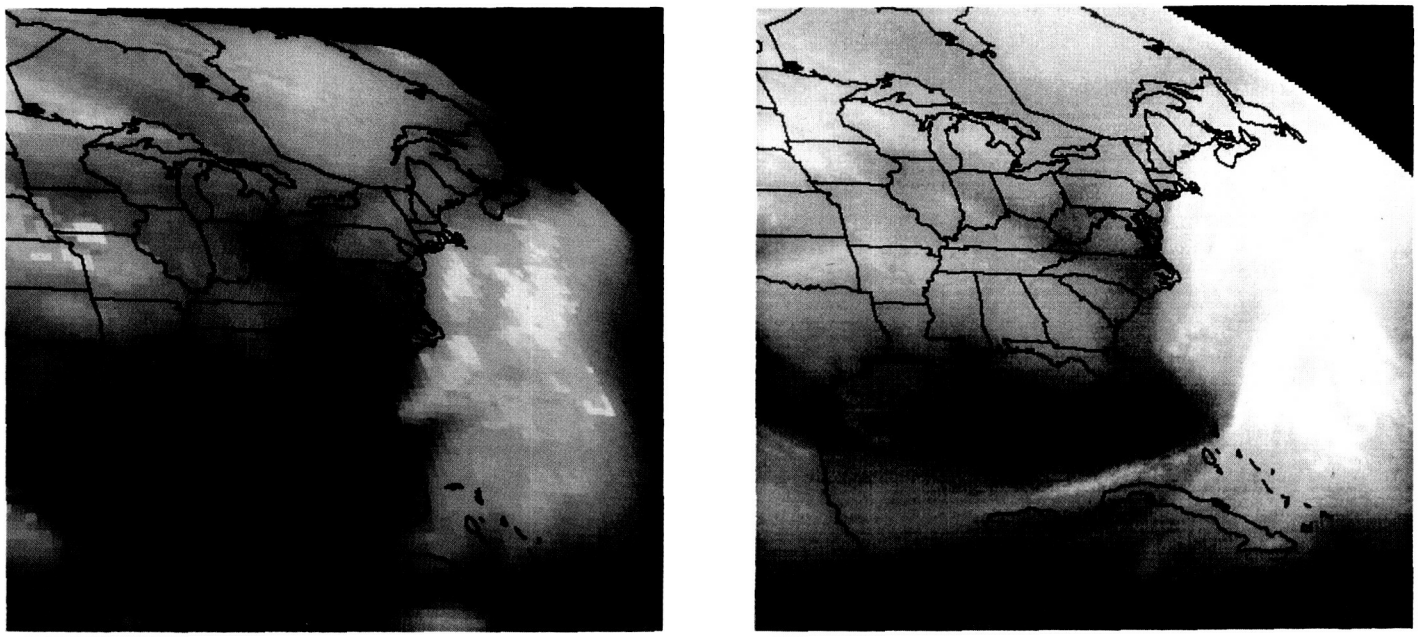

Figure 72. At Left, Simulated and at Right, Observed 6.7 Micrometer Imagery

Mosaic Array Imaging Technology

With the increasing importance of Earth system science and the deployment of polar orbiting platforms and geostationary research platforms, a new generation of remote sensing instrumentation will be needed to satisfy requirements for increased spatial, spectral, and temporal sensing of the Earth's atmosphere, oceans, and land. To obtain these enhancements a more sophisticated system and technologically advanced instrument is required. Detector technology improvements in mosaic arrays have started to replace single element detectors in mechanical scanning instruments resulting in increased detection efficiency. Increased data rates will require signal processing algorithms to provide the real-time data processing and data compression needs of these future instruments and sensors.

To develop this new generation of sensors, an image technology laboratory and a remote sensing laboratory have been established at MSFC. These facilities will focus on the development, calibration, and evaluation of visible sensors and instrumentation. Scene simulators will also be developed in order to provide realistic end-to-end testing. This sensor development effort will emphasize mosaic-array focal planes and Charged-Coupled Devices with both closely coupled, off-focal-plane, real-time data processing and on-focal-plane processing using HYMOSS stacked silicon Z-Technology. Also development efforts utilizing infrared sensors and arrays will be investigated for possible airborne scanning applications. Instrumentation developed will be utilized for Earth system science experimentation on airborne platforms and provide a test bed for space applications.

M. W. James/ED43
(205) 544-5020
Sponsor: Office of Space Science and Applications

Atmospheric Electricity Research

Measurements of the optical and electrical emissions of lightning and the electrical environment above thunderstorms have been obtained over active thunderstorms from a NASA high-altitude U-2 aircraft. This research has tried to determine the baseline design requirements for a satellite-borne optical lightning mapper sensor (LMS); study the overall optical and electrical characteristics of lightning as viewed from above cloudtop; and investigate the relationships between the storm electrical development and the structure, dynamics, and evolution of thunderstorms and thunderstorm systems. Since the need to acquire a quantitative database for design of LMS has largely been satisfied, the primary research goals now focus on basic research rather than the characterization of optical signals produced by lightning.

Present research objectives include establishing lightning-precipitation and lightning-storm relationships, determining electrical current output and the energy balance of thunderstorms from topside optical measurements, and investigating the detailed physical properties of lightning discharges and cloud microphysics. Other areas of interest involve using spectral observations to study both the concentration and production of NOx above cloudtop, and optical pulse data to study the radiative transfer properties of thunderclouds.

The need to obtain correlated ground-based, airborne, and satellite data has driven many of the planning and mission objectives of the U-2 lightning program. During 1986, many of the flights were coordinated with a large meteorological field program, the Cooperative Huntsville Meteorological Experiment (COHMEX) which was conducted in the central Tennessee, northern Alabama, and northeastern Mississippi area to study the initiation, development, and structure of summertime airmass thunderstorms. Data sets acquired during COHMEX in conjunction with the U-2 lightning measurements

include Doppler and conventional radar, ground-based and in situ electricity and microphysical observations, detailed precipitation measurements, ground strike lightning mapping, and visible and infrared Geosynchronous Operational Environmental Satellite images. Recent results suggest strong relationships between precipitation and lightning flash rates. In fact, there seems to be almost a direct proportionality between total rain volume and the number of lightning flashes.

Electric currents generated by thunderstorms are generally thought to maintain the air-Earth global electric circuit. Since measurements of the electric field and conductivity can provide an estimate of the charging current flowing from a thunderstorm to the ionosphere, electric field mills and conductivity probes were added to the U-2 instrument package to investigate this problem. The electric field mills provide a measurement of the vertical component of the electric field at the aircraft, and they also show abrupt field changes associated with lightning. The conductivity probes measure the air conductivity at the aircraft's altitude (approximately 20 km). From these measurements, a relationship may be established between a storm's electrical current output and cloudtop optical emissions. Analysis of conductivity measurements shows that air conductivity tends to remain steady over active thunderstorms (Fig. 73). Further, estimates of the storm currents derived from the conductivity and electric field measurements reveal a linear relationship, shown in Figure 74, between the total lightning flash rate and the Maxwell current generated by the thunderstorm. If this relationship holds, the LMS will be able to provide unique information on the global distribution of current flowing in the Earth's electrosphere.

R. J. Blakeslee/ED43
(205) 544-1652
Sponsor: Office of Space Science and Applications

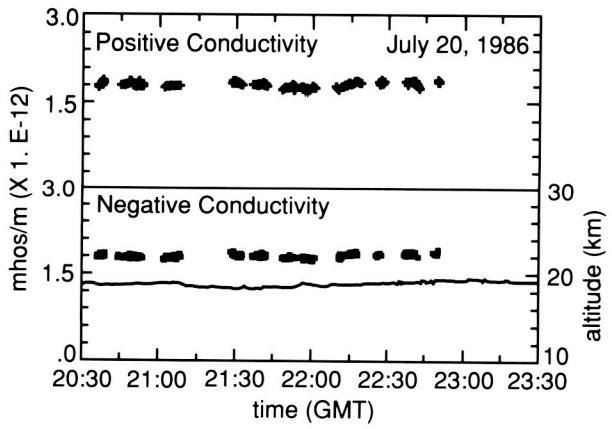

Figure 73. Positive and Negative Air Conductivity on July 20, 1986. The Aircraft Altitude is Indicated by Line in Lower Panel

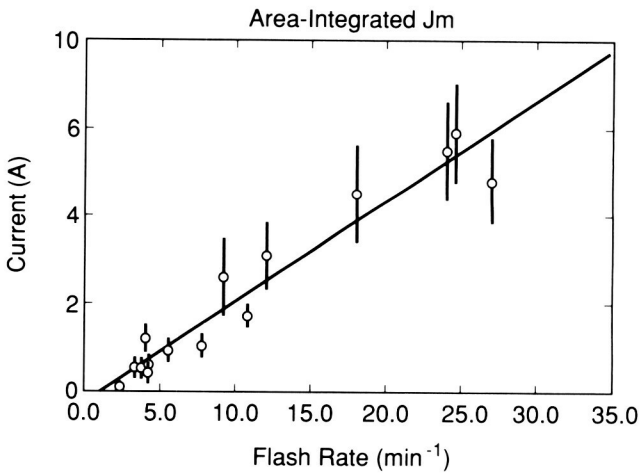

Figure 74. Area-Integrated Maxwell Current Density (J_m) as a Function of Storm Flash Rate

Analysis of Winds Measured with an Instrumented Aircraft

NASA is developing an instrumented aircraft for measuring launch wind profiles which may be used in prelaunch ascent performance wind loads assessments. Subsonic flights were completed in May 1988, at NASA Dryden Flight Research Center, at altitudes below 40,000 ft. Supersonic flights are to be completed by August 1988, for altitudes between 40,000 ft and 60,000 ft.

The requirement on the instrumentation system was that the measured wind speeds be equivalent or more accurate than those measured with the present Jimsphere system. A study was carried out to assess the required accuracy of the instruments individually and collectively and to investigate the effects of Schuler drift on the Inertial Navigation System (INS) measured inertial winds and position during climb and curved flight maneuvers. Results have been presented on the comparison of the full nonlinear equations versus the commonly used linear equations for determining wind speed from aircraft measurements. The basic vector equation is given by:

$$^{w>}\text{wind} = {}^{w>}\text{relative} - {}^{\nabla>}\text{inertia}$$

The inertial velocity of the aircraft is computed from parameters measured onboard the aircraft (e.g., pitch rate, roll angle, INS velocity, etc.). The relative airspeed is also determined from onboard measurements (e.g., airspeed, side slip angle, etc.).

An error analysis of these equations was first carried out to determine how accurately the aircraft motions and the relative air velocity must be measured in order to achieve a wind speed accuracy of 0.5 m/s. The value of 0.5 m/s is the reported RMS accuracy of Jimsphere measurements. Second, because the flight path required to measure winds along the Space Transportation System profile requires strong climb angles and possible sharp turns due to spiraling upwards or downwards, analysis of the effects of the turning motion and climbing rate on measurement accuracy was investigated. This investigation also used data gathered during the earlier NASA B-57B Gust Gradient program. The Gust Gradient program was directed primarily towards measuring turbulence at low altitudes but the data are also useful for the analysis reported in the paper.

The current program recommended specifications on the required instrument and INS accuracy including the INS output. It is also recommended that the full nonlinear system of equations be required to determine the effects of steep flight path angles and tight turns on the calculations of the inertial velocity. If this program is determined to be successful for operational use, it will be implemented at Kennedy Space Center in 1989.

D. C. Skow/ED44
(205) 544-1670
Sponsor: Office of Space Flight

Resolution and Accuracy of Balloon Wind Sounding Systems

The noise level present in Jimsphere wind measurements has been identified through spectral and cross spectral analyses of pairs of wind profiles obtained from two different radars that simultaneously tracked a Jimsphere balloon. Similar analyses were done on a data set containing pairs of profiles obtained from Jimspheres and Windsondes to provide information on the performance of the Windsonde relative to the Jimsphere. This work was performed by Steve Smith of the Universities Space Research Association under contract to MSFC.

Spectra and cross spectra of the profiles for 20 pairs of dual-tracked Jimspheres were computed and averaged. If it is postulated that the measurements are composed of the wind plus independent radar noise, averaging causes the autospectral estimates to converge to the spectra of the actual wind plus the spectra of white noise. However, the average cross spectrum will converge to the spectrum of the actual wind that is present in both of the independent radar profiles. Since the noise in the profile from one radar is not correlated with the noise in the profile measured with the other radar, the noise will average to zero in the cross spectra.

The information in the auto- and cross-spectral amplitude curves can be summarized by computing the quantity known as coherence squared. Coherence squared is the ratio of the magnitude of the cross spectra squared to the product of both of the autospectra, which can be approximated by the ratio of signal-to-signal plus noise.

The point at which signal equals noise is chosen as the effective resolution point because at shorter wavelengths the spectra consists of more noise than signal, while at longer wavelengths the spectra is composed of more signal than noise. The signal equals the noise power spectral density at a wavelength of approximately 150 m for the u component and approximately 300 m for the v component.

Seven nearly simultaneous profiles from Jimsphere and Windsonde releases were obtained during the Kennedy Space Center prototype Profiler tests in March and April, 1985. Cross spectral analyses of these data show that the coherence between Jimsphere and Windsonde profiles is not as strong as between two independent radars tracking the same Jimsphere. The coherence squared spectrum demonstrates that the effective resolution of the Windsonde is approximately 500 m.

The amplitude of the incoherent noise in the Jimsphere measurements can be estimated by assuming that the flattening of the spectra at the high wave number end is due to broadband white noise. The amplitude of Jimsphere noise is approximately 0.25 m/s while that of the Windsonde is approximately 1.2 m/s.

The amplitude of the noise fluctuations determines the effective resolution of the wind sounding systems. The inability of the Jimsphere or the Windsonde to measure wind fluctuations with vertical scales smaller than 150 m is a result of the noise amplitude induced by tracking inaccuracies concealing the smaller amplitude wind fluctuations.

In summary, the small number of profiles used in these studies show:

	rms error amplitude	effective vertical resolution
Jimsphere	0.25 m/s	150 - 300 m
Windsonde	1.2 m/s	> 500 m

C. K. Hill/ED44
(205) 544-1664
Sponsor: Office of Space Flight

Winds Aloft Statistical Analysis in Support of Day of Launch Shuttle Systems Evaluation

In connection with development of the Meteorological Interactive Data Display System for utilization by the Launch Systems Evaluation Advisory Team, requirements have been established to expand the pre-launch analysis of winds aloft for the Space Shuttle. Statistical analyses developed for the system include comparison of pre-launch wind component profiles to wind component extremes at each altitude calculated from launch site historical data; conditional probability ellipses for wind vectors at a future time, given the wind vector at an initial time; comparison of observed extreme wind shear and associated wind speed with launch site historical data utilizing the bivariate extreme value (Gumbel) distribution; estimation of extremes of wind speed or wind shear at a future time, given the extremes of either variable at an initial time, utilizing the conditional extreme value distribution; and power spectrum analysis for tracing wind perturbation energy in sequential pre-launch Jimsphere wind profiles. Examples are given in Figure 75 and 76. This work was performed by S. I. Adelfang, O. E. Smith, and G. W. Batts of the Computer Sciences Corporation, Huntsville, Alabama, under contract to MSFC.

Wind profile analysis and trajectory and loads simulations are essential to pre-flight evaluation of Shuttle system performance. Any wind profile measurement prior to launch is an approximation of the wind profile "seen" by the vehicle. Therefore, loads calculations based on a wind profile measurement hours before launch have an uncertainty attributable to the lack of complete knowledge of the vehicle wind environment. This uncertainty is overcome to some extent by reducing load limits by an amount associated with wind variability over a time period between the last wind profile used for simulation and the time of launch. It is anticipated that for future launches the time interval will be reduced to approximately 2 hr compared to 3.5 hr for past launches. Wind analyses have indicated that the 2-hr interval will reduce wind uncertainty by 20 to 35 percent. Studies have indicated that further reduction in time interval does not result in a proportionate reduction of uncertainty. There will always be significant residual wind uncertainty that contributes to uncertainty in anticipated vehicle loads.

Wind profile characteristics such as large isolated shears, quasi-sinusoidal large amplitude perturbations, and large deviations of the wind profile from the monthly mean can individually and in concert produce large vehicle loads. Because of wind profile uncertainty, identification, tracking and estimation of these characteristics at launch time are important pre-launch tasks.

For this task two Jimsphere wind profiles obtained prior to the delay of Shuttle launch (51A) on November 7, 1984, are used to illustrate the various forms of statistical analysis that can be used on the day of launch. The time interval between the profiles is approximately 5 hours (941 to 1440 Z). In addition to the day-of-launch profiles, long-term samples of Jimsphere and Rawinsonde profiles at Kennedy Space Center are used for statistical comparisons and application of statistical models.

The statistical analyses presented herein represent a variety of tools that can be utilized on the day-of-launch. In practical application, all the analyses may not be performed or presented to the mission management team; as discussed earlier, to address the requirements for relevant and concise data, emphasis must be given to analyses that describe specific wind profile characteristics that have been identified as being problematic from the viewpoint of the loads analyst.

The in-plane and out-of-plane wind components of the two Jimsphere wind profiles are illustrated in Figure 75. Since the launch azimuth is 90°, the in-plane component is equivalent to the zonal (east-west) wind in the meteorological coordinate system with the sign reversed. Similarly, the out-of-plane component is equivalent to the meridional (north-south) wind with the sign reversed. The solid lines in

Figure 75 represent the component limits of the 95 percent probability ellipse at each altitude calculated from the synthetic vector wind model Rawinsonde data base for the month of November. The dots represent the monthly mean components at 1 km intervals. The large deviation from the monthly mean and the large perturbations in the out-of-plane component are the features of the profile that lead to the 51A launch postponement.

The 50, 85, 95, and 99 percent probability ellipses for November, the monthly mean (M), and the observed wind vectors (1) and (2) at 11 km are illustrated in Figure 76. The probabilities associated with the observed wind vectors are listed in the figure caption.

It is indicated that for the most part the 5-hr wind change is in the out-of-plane component.

Conditional probability ellipses for wind vectors at a future time, given the wind vector at an initial time, are derived from the quadravariate normal statistics of the components of the initial and final vectors. It is indicated that the observed wind vector after an elapsed time of 5-hr (profile 2) is on the 99 percentile conditional ellipse.

C. K. Hill/ED44
(205) 544-1664
Sponsor: Office of Space Flight

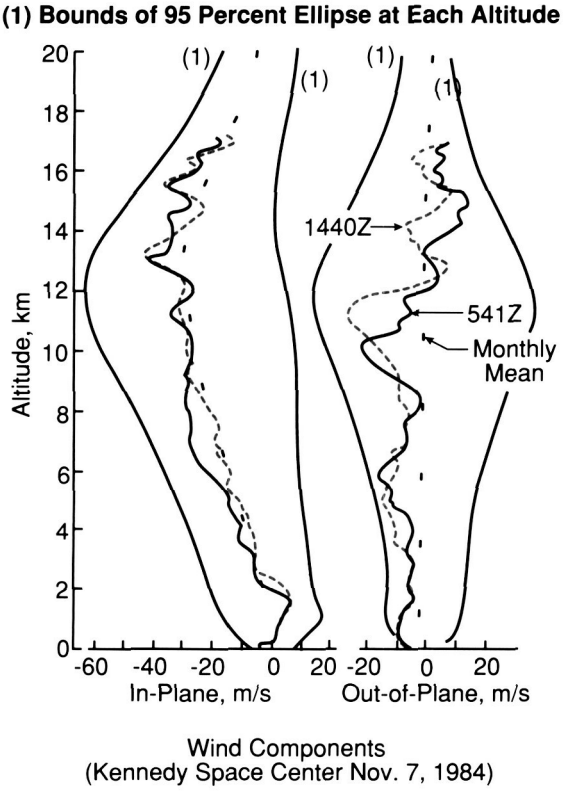

Figure 75. Pre-Launch Jimsphere Wind Profiles, Means, and 95 Percentile Bounds

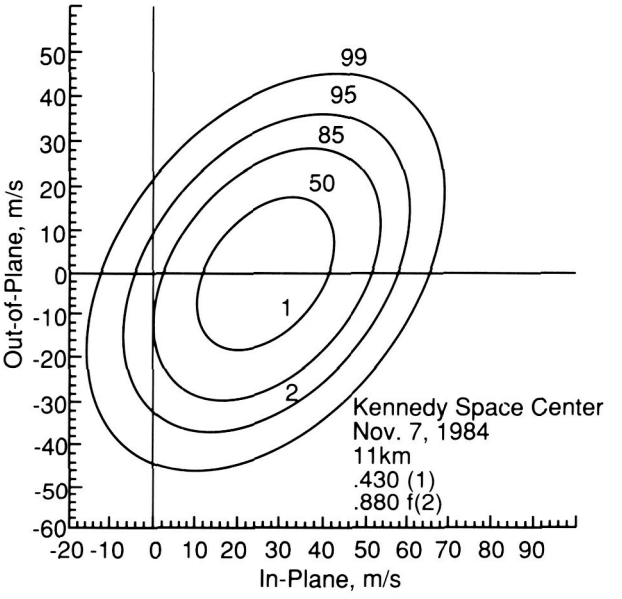

Figure 76. Pre-Launch Wind Vectors and Probability Ellipses

Microwave Radiative Transfer Studies of Convective Storms

A study of the microwave radiative transfer properties of convective storms is being conducted by the Electrical Engineering Department of Colorado State University under the supervision of Dr. V. N. Bringi. The specific focus of this research effort has been an investigation of the microphysical structure of several convective storms which took place during the Cooperative Huntsville Meterological Experiment (COHMEX), and the effect of that hydrometeor structure upon passive microwave radiometric measurements made from high-altitude aircraft flying above the storms.

COHMEX was a multi-agency atmospheric science project coordinated by MSFC and conducted in the northern Alabama/central Tennessee region during the summer of FY86. Aircraft microwave data were measured at 18, 37, 92, and 183 GHz using two radiometers sponsored by Goddard Space Flight Center. The National Center for Atmospheric Research CP-2 radar sampled the convective storms from the ground and has provided useful storm structure information. For two case studies in particular, the vertical profiles of multiparameter radar data indicate the presence of distinctly different microphysical structures which appear to account for the differing radiometric signatures of the two storms.

To gain a better quantitative understanding of the relationship of these hydrometeor structures to observed microwave radiometric properties, the radar-deduced microphysics were input to a radiative transfer model. A scaler radiative transfer model which assumed the hydrometeors were spherical has demonstrated the importance of accurately defining the properties of an ice-melting layer within a convective storm in order to realistically model the storm's radiometric characteristics. A new vector radiative transfer model which considers nonspherical ice and water particles has been developed and is currently being tested. This model should provide greater flexibility in the types and shapes of hydrometeors to be considered in the storm structure as well as added insight into the influence of various regions of the storm which have different hydrometeor compositions. The overall knowledge gained from research of this type should greatly improve the interpretation of satellite passive microwave observations of precipitation regions.

R. E. Hood/ED43
(205) 544-5407
Sponsor: Office of Space Science and Applications

Global Aerosol Backscatter Assessment

Scientific research into the Laser Atmospheric Wind Sounder (LAWS) was continued at MSFC during FY88 by Dr. Jeffery Rothermel, Universities Space Research Association, Huntsville, Alabama. Part of the NASA contribution to the Earth Observing System (EOS) and a MSFC facility instrument on EOS, LAWS will make global tropospheric wind measurements from either Space Station Freedom or a polar orbiting platform. Wind profiles will be obtained by measuring Doppler-shifted laser radiation backscattered by micrometer-size aerosol particles. The wind measurement accuracy is a function of the strength of the backscattered signal, which, in turn, is a function of the aerosol backscatter coefficient.

Knowledge of the spatial and temporal distribution of global aerosol backscatter is important to design and performance studies for LAWS. Preliminary design studies have suggested that LAWS may be required to operate in areas of marginal signal conditions, coincidentally where wind measurements are needed most. The existing backscatter data base is expanding to include recently-analyzed measurements made by the Royal Signals and Radar Establishment , United Kingdom, over the UK, and by the Wave Propagation Laboratory of the National Oceanic and Atmospheric Administration over Boulder, Colorado. Despite their large geographic separation, both data sets of vertical profiles show remarkably similar features and, particularly, a high frequency of occurrence of low backscatter over a limited range of values in the middle and upper troposphere. This narrow range is interpreted as indicating a ubiquitous "clean background" aerosol mode for global backscatter. The agreement is remarkable in view of the natural tropospheric backscatter variability (over 4 orders of magnitude), the diverse measurement conditions, and the injection of aerosols by El Chichon and other volcanoes during the measurement period. Details on the existence and magnitude of this global background mode will constitute a part of the data base to be used during industry definition and design studies, expected to begin in the near future. The data base will also include measurements that are being analyzed by the Jet Propulsion Laboratory in California. Measurements were initiated in FY88 using the MSFC Ground-Based Doppler Lidar System (GBDLS) to accumulate a data base of wind profile measurements that could be used to simulate the LAWS lidar and scanning systems. These data will be used to investigate techniques for averaging individual measurements to derive wind profiles that will be most beneficial to the atmosphere science community.

Previous aerosol backscatter studies, for which concurrent meteorological measurements existed, have suggested a direct correlation between vertical profiles of backscatter and water vapor. Consequently, studies were initiated at MSFC to attempt to quantify this relationship. In June 1988 a series of intercomparison measurements was begun using the MSFC GBDLS, locally-released rawinsonde balloons, and the Multispectral Atmospheric Mapping Sensor (MAMS). The MAMS and rawinsondes will provide vertical profile measurements of water vapor for comparison with aerosol backscatter profiles obtained with the GBDLS. A measurable correlation between water vapor and backscatter would suggest the use of water vapor as a "surrogate" for backscatter measurements in LAWS performance simulation studies and preflight global numerical weather prediction experiments.

Rothermel, J. et al., 1988: Calculation of Aerosol Backscatter From Airborne CW Focused CO_2 Doppler Lidar Measurements, Part 1, Algorithm Description, and Part 2, Algorithm Performance. Submitted, J. Geophys. Res., 1988.

Rothermel, J., Bowdle, D. A., Vaughan, J. M. and Post, M. J.: Evidence of a Tropospheric Aerosol Backscatter Background Mode. Submitted, Nature, 1988.

Rothermel, J., Bowdle, D. A., and Vaughan, J. M.: Aerosol Backscatter Variability at 10.6 μm Over Colorado High Plains during JAWS Experiment. Third Conference Satellite Meteor., and Oceanography, Feb. 1 to 5, Anaheim, California, Amer. Meteor. Soc., 1988.

D. E. Fitzjarrald/ED43
(205) 544-1651
Sponsor: Office of Space Science and Applications

Earth Science Geostationary Platform Science and Mission Requirements

The Earth viewing geosynchronous platform offers the possibility of observing broad regions of the Earth with high time and space intervals and spatial resolution. The only resolution limitation is the capability of the instrumentation involved. Such resolution is of extensive scientific value in observing processes on the Earth's surface or atmosphere which change significantly each hour. Events having this characteristic time scale are primarily atmospheric processes and other highly transient geophysical phenomena such as:

- Precipitation and lightning
- Mesoscale atmospheric/oceanic circulations
- Coastal processes including tides
- Environmental pollution
- Volcanoes and earthquakes
- Oceanic phytoplankton blooms
- Water vapor sources/sinks and structure
- Solar flux and constant
- Atmospheric trace gases
- Diurnal terrestrial ecosystem processes
- Cloud evolution and severe storms
- Earth system radiation balance

For the past 10 years, the Geosynchronous Operational Environmental Satellite (GOES) has been used to monitor such phenomena as tropical depressions and hurricanes, atmospheric fronts, and severe squalls and storms. These observations have been used to predict the most probable future positions of these phenomena. Although the instruments placed on GOES were used to make quantitative predictions, the imagery has traditionally been used in a more qualitative picture mode. The most recent GOES is capable of quantitative temperature and moisture sounding of the Earth's atmosphere and has identified the scientific usefulness of sounding the Earth system with high temporal frequency and reasonable horizontal spatial resolution.

The goal for the next generation of geosynchronous observations of the Earth from the Earth Science Geostationary Platform would be to improve the quantitative measurement capabilities already demonstrated in low-Earth orbit, as well as to provide new observations of lightning and atmospheric, oceanic, and land phenomena that are best observed from geosynchronous altitudes. Observations would be used to better understand all physical processes in the Earth's System. This understanding would subsequently be applied to develop techniques useful in operational monitoring, and form a key element of NASA's Earth Observing System capability and "Mission to Planet Earth" initiative.

During FY88, an Earth Science Geostationary Platform Science Steering Committee was supported to establish the science and mission requirements for Earth science at geostationary orbit as shown schematically in Figure 77. Figure 78 shows a mission concept including sensors for the atmosphere, land, ocean, solid Earth, and space environment from numerous instruments contained on the mission.

G. S. Wilson/ED41
(205) 544-1628
Sponsor: Office of Space Science and Applications

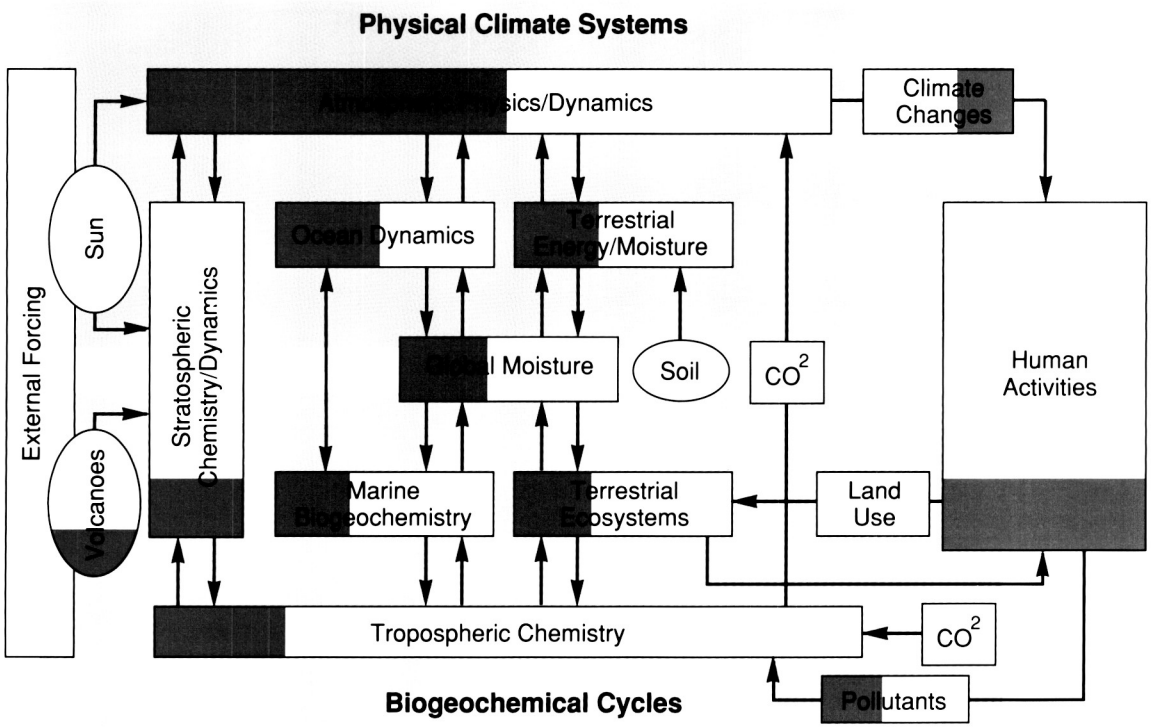

Figure 77. Simplified Earth System Wiring Diagram. Yellow Areas Show Processes Uniquely Measured from the Earth Science Geostationary Platform

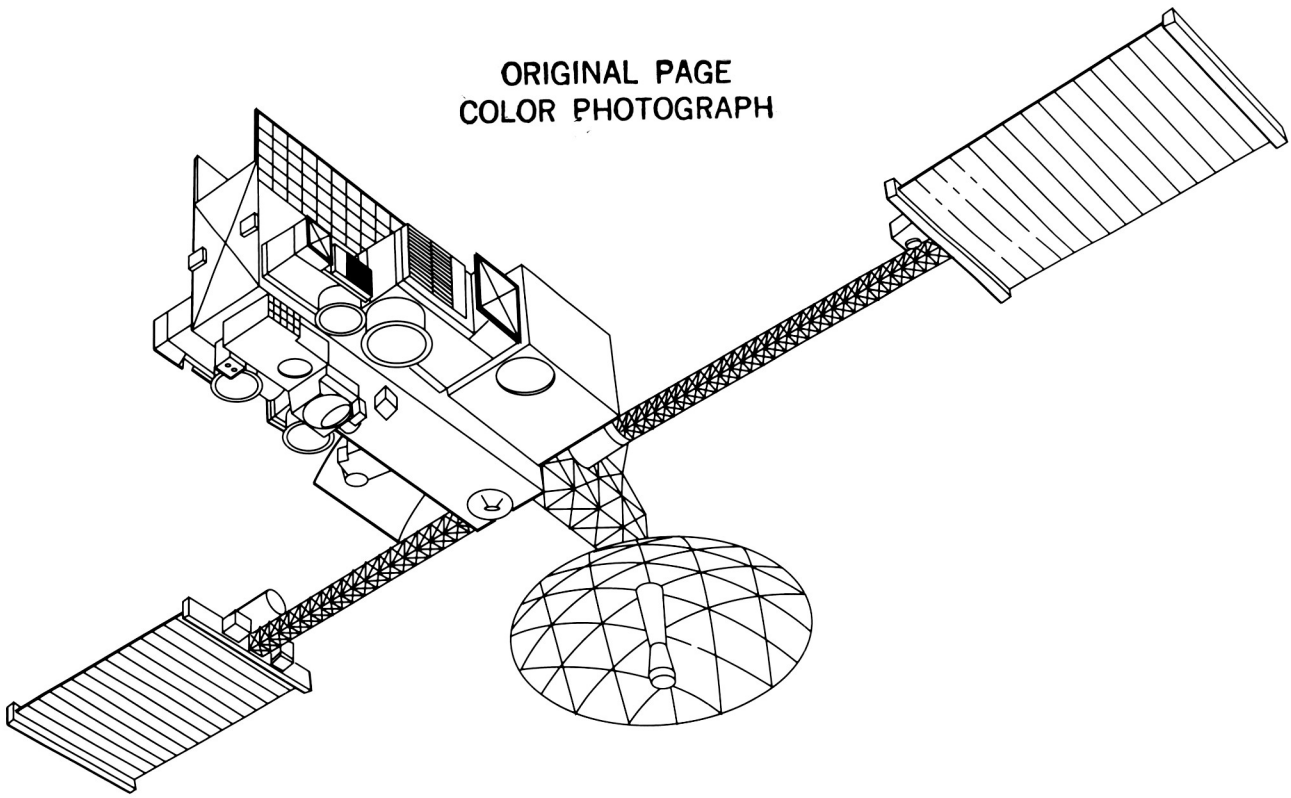

Figure 78. One Possible Earth Science Geostationary Platform Configuration

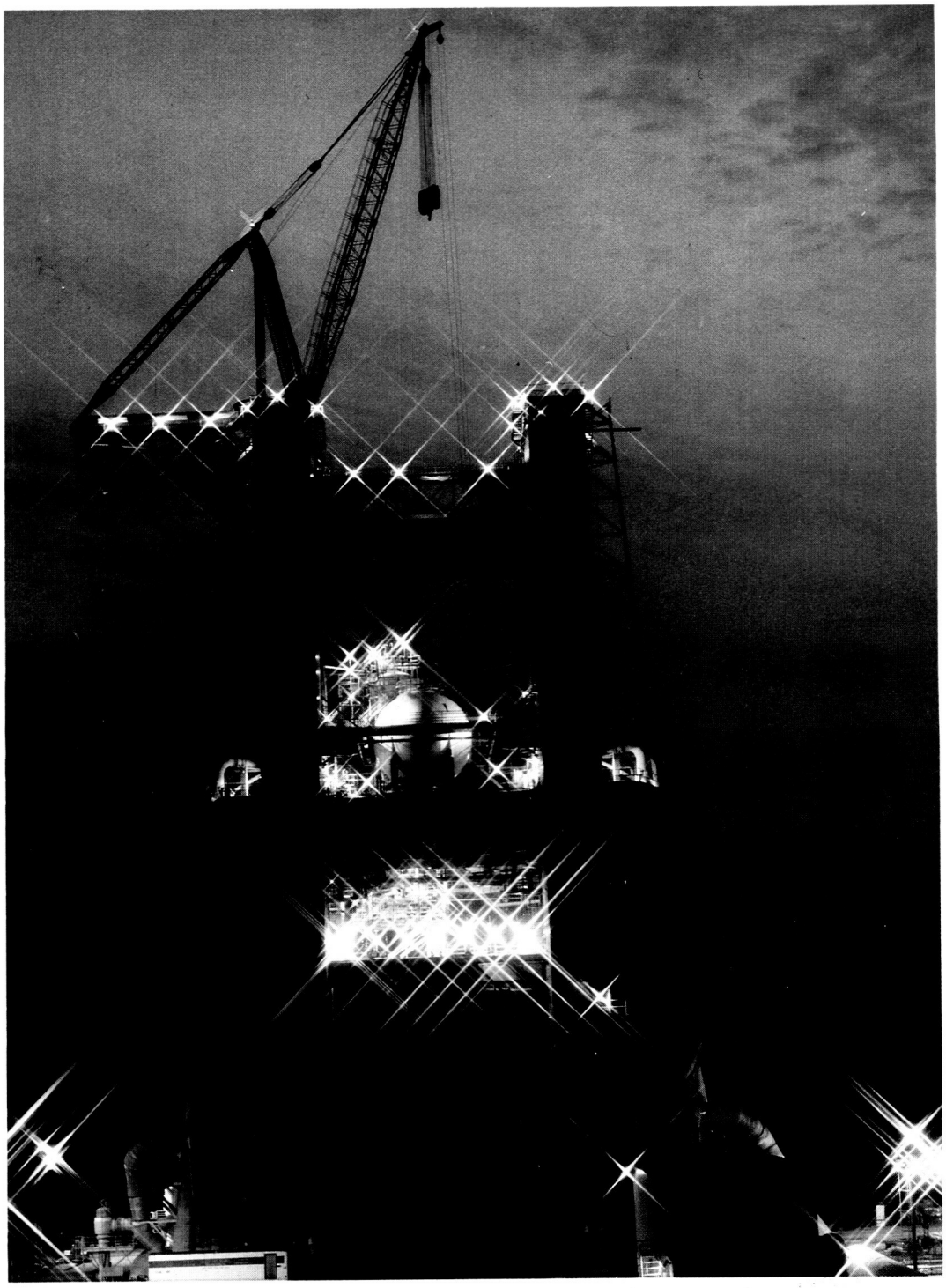

Technology Programs

Technology is seen as the principal catalyst in humankind's evolutionary process of change. Technology not only enables change, it often forces it. We are, therefore, compelled and committed to invest in technology advances that will provide innovative engineering solutions to design and development problems that are the mainstream of this Center's interest and responsibility.

The technology programs at MSFC are focused on enhancing and enabling the Center's goal of leadership in the development and utilization of space transportation systems, and other key space systems/facilities that will advance the frontiers of human knowledge and exploration.

The technology programs outlined herein have been categorically grouped under one of the following discipline headings; Propulsion, Materials and Processes, Structures and Dynamics, Automated Systems, and Space Systems. Propulsion is by far the larger category and is further subdivided into focused technology efforts in the areas of analyses – tools and techniques, instrumentation, and propulsion-unique materials and processes.

The programs outlined on the subsequent pages of this report define the technology effort by MSFC in FY88.

Propulsion

Advanced Launch System Propulsion Focused Technology

Focused technology and advanced development activities have been initiated and are divided into the following task areas: LOX/Hydrogen Engine, LOX/Hydrocarbon Engine, Booster/Core Propulsion Subsystems, and Solid Propulsion. The primary emphasis of these activities is to develop and demonstrate design concepts, manufacturing processes, and techniques that provide a significant cost reduction over conventional propulsion systems in each of the respective areas.

Activities in LOX/H_2 development include conducting detailed trade studies, investigating low cost manufacturing processes, developing design concepts that are compatible with a low cost philosophy utilizing advanced manufacturing techniques, and demonstrating low cost fabrication processes. Emphasis will be placed on the evaluation of materials and processing/manufacturing techniques to minimize costs. The total effort will include the design, fabrication, and test of a LH_2 turbopump, LH_2/LOX thrust chamber assembly, LH_2/LOX gas generator assembly, the electromechanical propellant valve flow control system, and a brass board controller/sequencer.

LOX/Hydrocarbon development activities include conducting detailed trade studies, and developing design concepts that are compatible with a low-cost philosophy utilizing advanced manufacturing/techniques. Emphasis will be placed on evaluation materials and processing/manufacturing techniques to minimize costs. The total effort will include th design, fabrication, and test of a methane turbopum a LOX/hydrocarbon thrust chamber assembly, and LOX/hydrocarbon gas generator assembly. In add tion, studies and hardware demonstrations to verif LOX/hydrocarbon injector stability, tripropella thrust chamber stability and efficiency, and critic thrust chamber technologies (i.e., material compat bility, fuel cooling limits, gas side heat flux an advanced cooling concepts) will be accomplished

Booster/core propulsion subsystems technolog activities include the definition of system archite ture for low cost auxiliary propulsion systems, def nition of advanced development Advanced Launc System design requirements and design criteria, th design and validation of a prototype LOX tan pressurization system remote from the engine, an demonstration of control authority and stability.

Solid propulsion technology that provides the den onstration of high rate, low cost processing of hydr chloric acid-free propellants that enhance reliabili and reduce costs is underway. Total efforts inclu the building of a pilot-scale propellant plant, demo stration of continuous processing, and characteriz tion of clean propellant. The evaluation and tes verification of design concepts and materials, an fabrication of low cost, high reliability cases, nozzle and castable nozzles have also been initiated.

J. C. Monk/HA31
(205) 544-7110
Sponsors: Office of Space Flight
USAF/Space Division

Solid Rocket Motor Roundness Measurement

The Solid Rocket Motor (SRM) measurement tool has been built at MSFC and used at Morton Thiokol in Utah. An updated model has been built and tested at MSFC. Figure 79 shows the new version in position to make a measurement.

The first version has now measured many cases for upcoming flights. It is used primarily to measure absolute diameters of several surfaces on the case. Cases are selected based on these measurements to give the desired interference fit at the joints of the assembled SRM.

The least squares method used to determine diameters has been replaced by a simple summation of chords method. Suspended cases had much more out-of-round than expected and the least squares diameter decreases as a result. Least squares is still used to find the tool center offset and may be used later for diameters when the out-of-round is not more than 6 mm (0.25 in) from circular.

Improvements in the newer tool include bigger ball-slides on the end of the radial arm and four temperature sensors that attach to the case. The ball-slides will last longer and have less flex. The temperature sensors are read by the computer and eliminate manual measurement. The calibration method was improved to use one laser instead of two, making calibration not only more accurate but much faster as well. Tool support brackets now use a better design so mounting is easier and more rigid.

Absolute accuracy of the tools is expected to be less than 0.1 mm (0.004 in) on the diameter with repeatability of better than 0.025 mm (0.001 in). Periodic calibration assures continued accuracy.

R. R. Kissel/EB24
(205) 544-3510
Sponsor: Office of Space Flight

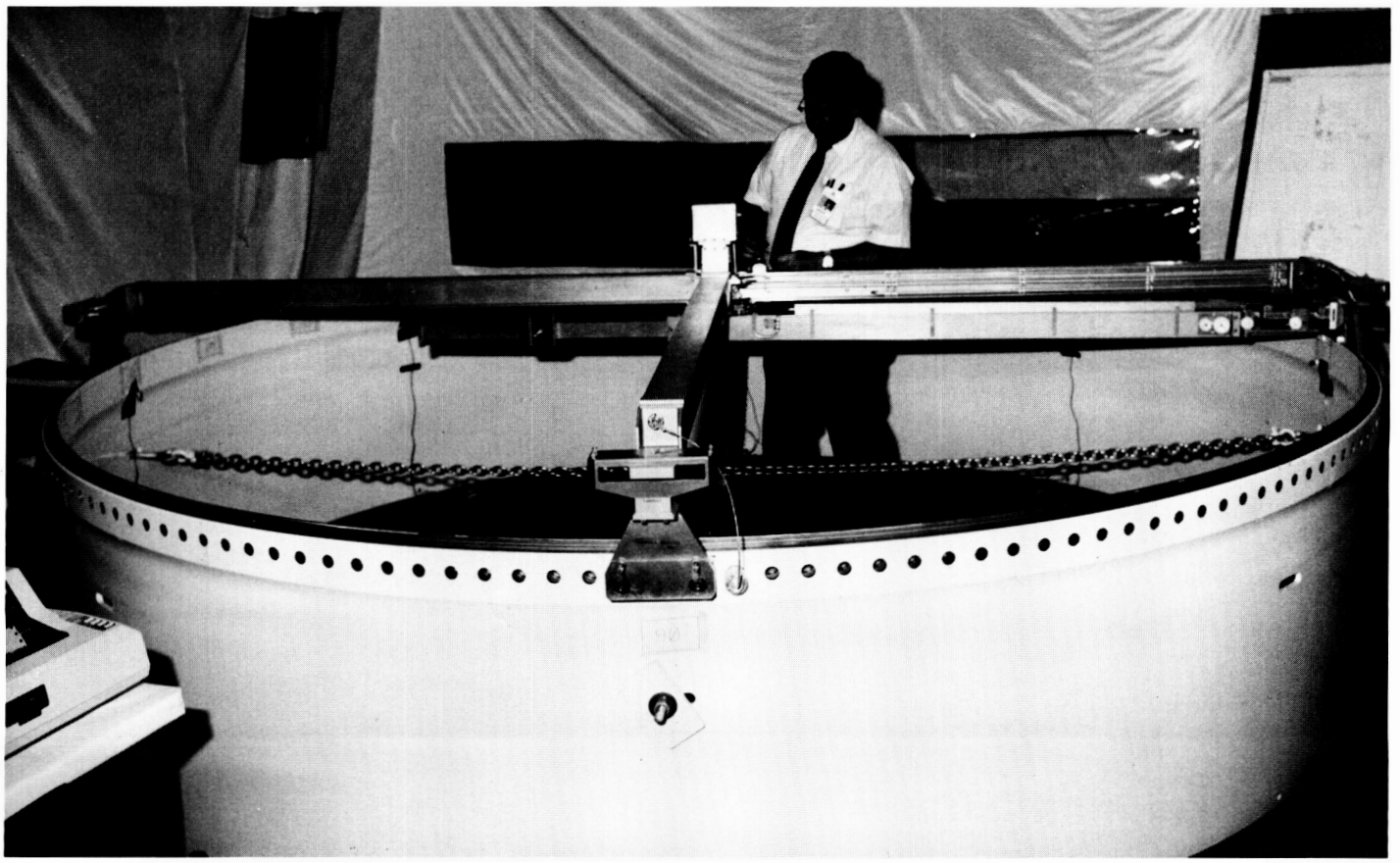

Figure 79. The Solid Rocket Motor Measurement Tool

Alternate Seal Material Characterization for Solid Rocket Motor Joint Redesign

One of the primary issues of the Solid Rocket Motor (SRM) redesign effort was the selection of an O-ring material to be used in motor case joints. A critical requirement for candidate joint seal materials was to demonstrate sufficient resiliency to accommodate very rapid joint gap opening without losing contact with the sealing surface. Resiliency performance was established as the initial screening gate in the overall seal material evaluation which included numerous material characteristics and performance factors. Two types of resiliency tests were conducted, free and programmed release. The free resiliency testing is distinguished by removing the sealing surface rapidly enough so that the material is permitted to dimensionally recover freely. This approach was utilized primarily to screen materials and provide a preliminary ranking. In the programmed release tests, the sealing surface was moved according to a precise simulation of the worst-case predicted gap opening and the residual sealing load applied by the O-ring material to the sealing surfaces was continuously monitored. This report addresses the free resiliency test series.

The original list of candidate seal materials is presented in Table 6. Complete free resiliency data were not collected on all materials, since other critical screening tests produced negative results early in the study and influenced the selection for the more extensive resiliency testing.

The test fixture for this study was designed to enable the measurement of recovery from a face seal compression load. The fixture consists of five basic components: the base plate containing the O-ring specimen, coupling plate, top plate, extensometer, and cooling/heating coils for temperature control. These elements can be seen in the assembled fixture shown in Figure 80. Although not visible, the O-ring specimen is centered beneath the aluminum coupling plate directly below the extensometer arm contact point. The nominal O-ring test specimen was 0.280 inch in cross-sectional diameter and 3.625 inch in circumferential inner diameter. Test fixture temperature was monitored using thermocouples in the upper and lower plates in close proximity to the O-ring. Temperature was controlled to within ±2 °F of specified test temperature.

The basic test matrix for the evaluation of seal materials consisted of recovery-versus-time experiments in which temperature and compression level

Table 6. Candidate Seal Material Summary

Material Designation	Type	Supplier
V747 (Baseline)	Flourocarbon	Parker
V835	Flourocarbon	Parker
N304	Nitrile	Parker
N602	Nitrile	Parker
N1084	Nitrile	Parker
Arctic Nitrile	Nitrile	Cameron
S604	Silicone	Parker
S383	Silicone	Parker
S650	Silicone	Parker
L677	Fluorosilicone	Parker
Eypel-F	Polyphosphazene	Ethyl
E692	Ethylene/Propylene	Parker
E592	Ethylene/Propylene	Parker
E515	Ethylene/Propylene	Parker
Composite Seal	Flourocarbon/Silicone	Hunger

were the primary variables. Two series of tests were performed. The first was a series designed to evaluate the performance of the candidate materials at a standard initial compression level (.040 in) for ambient and selected subambient temperatures. The preliminary resiliency rankings were evaluated with the results of other critical screening tests to select the most promising materials for further investigation. The materials selected were baseline fluorocarbon (V-747), modified fluorocarbon (V-835), silicone (S-650), fluorosilicone (L-677), nitrile (N-602), and arctic nitrile. The Parker product designation is shown in parentheses, as applicable.

The second series of tests involved more extensive characterization of the candidate materials. Various compression levels (0.040, 0.052, and 0.065 inch) were imposed on the test samples at temperatures ranging from 10 °F to 120 °F. The effects of Conoco HD-2 grease on the recovery capability of the O-ring materials were also investigated.

The generic response characteristic of the above materials consists of a rapid transient recovery which generally occurs within the first 5 msec after release, followed by a steady state creep recovery. The initial response is strongly influenced by both temperature and compression level. The steady state recovery is not a strong function of either of these two variables.

Silicone and arctic nitrile materials exhibited the most rapid and greatest recovery; however, these materials were also strongly affected by Conoco HD-2 grease. A grease preconditioning cycle was subsequently implemented for both materials.

The complete results of this test program and the programmed release test scores will be published.

Clinton, R. G.: Alternate Seal Material Characterization for SRM Joint Redesign. NASA Technical Paper, in preparation.

R. G. Clinton/EH34
(205) 544-2682
Sponsor: Office of Space Flight

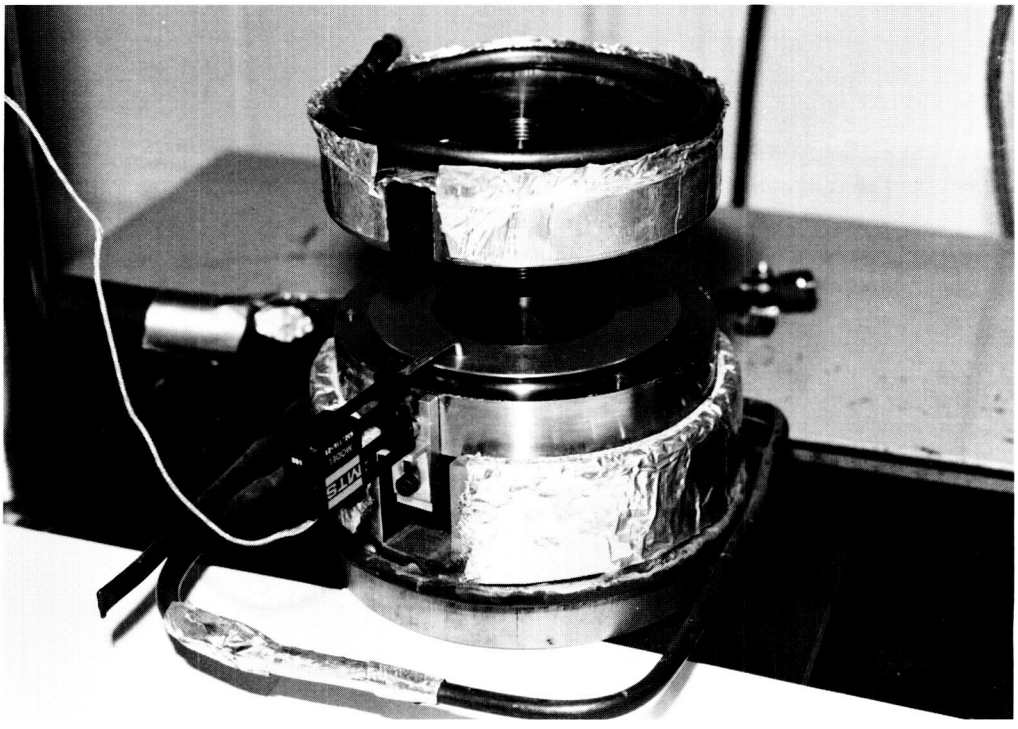

Figure 80. Assembled Free Resiliency Test Fixture

Trowelable/Moldable Ablator Development for Booster Structures

Ablative materials, part of the Thermal Protective System (TPS) for the Solid Rocket Boosters (SRB's), are used as heat shields to protect vehicles as they are subjected to high velocity and high temperatures during launch and reentry to the Earth's atmosphere. A new thermal protection ablator, designated the Booster Trowelable Ablator (BTA), has been developed in the MSFC Productivity Enhancement Facility to replace two current TPS materials, MTA-2 and K5NA. MTA-2 was earmarked for replacement after the identification of a suspected environmental hazard in the Shell Z catalyst, the curing agent for the MTA-2 epoxy system. Replacement of K5NA was prompted by economic considerations: K5NA is costly and has a relatively short pot life.

Selected through screening studies of seven candidates, BTA is formulated from epoxy resins filled with glass eccospheres and ground cork, is easily applied, and cures at room temperature. Mechanical tests this year characterize BTA as a very durable insulator with good substrate adhesion characteristics that prevent delamination throughout the flight-cycle. Its ablative properties were improved by mixing ingredients in a vacuum chamber to minimize air/moisture entrapment; extensive evaluations at the Large Radiant Lamp Facility have shown improved thermal integrity from the vacuum mix process. Low density, light weight, and reduced costs further enhance viability.

Qualification of this new material and process for full scale hardware application at Kennedy Space Center is nearing completion. 1988 tests have qualified troweled application to SRB acreage areas and closeouts; engineering documentation is being converted into specifications for the production activity. The formulation has also been verified as a moldable ablator for selected SRB protuberances, the molding process controlling the amount and thickness of material that surrounds a given hardware part. Innovative techniques will enable expeditious and economical in-house fabrication of molds for actuator stiffeners, hold-down posts, the lower attach strut, the aft skirt lip, etc. Molded BTA models representing 16 types of components are awaiting MSFC radiant and hot gas testing for flight qualification.

W. E. Hill/EH41
(205) 544-2725
Sponsor: Shuttle Projects Office

Sheet Metal Net Forming for Space Shuttle Main Engine

Sheet metal parts on the Space Shuttle Main Engine (SSME) are presently cold formed to near net shape and then hand fitted for welding. In the case of the high pressure fuel turbopump (HTFTP) volute, this imprecise approach can cause fitup, alignment, and clearance problems later in the manufacturing cycle. Welding of the volute is made more difficult and time-consuming because of poor fitup of parts.

A development program at MSFC to hot form the eight Inconel 718 parts that comprise the HPFTP volute promises to provide finished pumps with more uniform fuel flow, less fitup and alignment problems, and the cost savings due to automatic welding.

The hot forming process involves pressing sheet metal between two halves of a die that conforms to the exact contour of the finished part. This assembly is then heated in a furnace to a temperature that removes the residual stresses in the metal that cause springback to a shape other than the exact one required. The result of this process is a complex contour for the sheet metal that exactly fits the pump housing and other sheet metal parts that comprise the whole volute assembly. Removing stresses also reduces the propensity of the part to distort when heat from the welding process is applied.

The program has developed the necessary heating cycle to produce the requisite metal properties. A new method of describing the complex shape of the part was developed on the MSFC institutional computer-aided design/computer-aided manufacturing (CAD/CAM) system. Computer numerically controlled machine tools that cut dies from raw metal were automatically programmed by the CAD/CAM system. One part of the volute has been formed by the new process and its improved fitup and welding properties verified on test SSME hardware.

C. S. Jones/EH42
(205) 544-2701
Sponsor: Office of Space Flight

Redesigned Solid Rocket Motor Composite Material Testing

Routine acceptance testing such as that utilized on the Redesigned Solid Rocket Motor Nozzle carbon-phenolic components is an integral part of flight qualification. Tape wrapped carbon-phenolic rings are typically made oversized to provide for tape wrap angles, contour machining, and acceptance test specimens. The acceptance test specimens (tag-end samples) are extracted from excess material, and are tested for strength and process variances. The data obtained from the testing of these samples are used not only to verify component compliance to established limits, but also add to the statistical data base of the process and materials in question.

Tag-end test specimens (across ply tensile) are machined from material samples that cannot exceed 0.75 inch length in the across ply direction (Fig. 81). This limitation introduces a geometry that creates

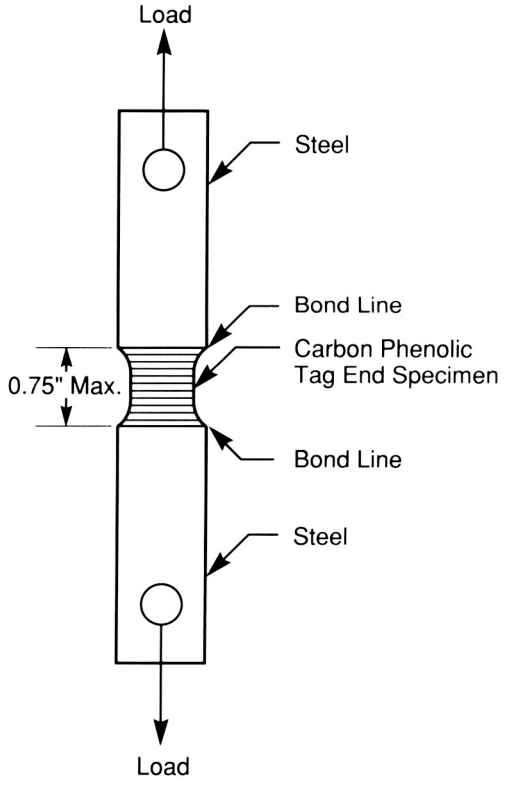

Figure 81. Tag-End Test Specimen Set

stress concentration in the radius that results from the bond and sample tensile strength capabilities. Design iterations using the finite element method (ANSYS) have aided in the design of an optimal configuration that will minimize this concentration. The three-dimensional finite element model is used to evaluate stress concentrations due to geometry as well as the orthotropic nature of the sample materials.

Future efforts will include verification of analytical techniques employed (material properties, analysis techniques, etc.) by direct comparison with test data. This relatively simple test configuration can also aid significantly in the development of verified failure criteria, crack propagation studies, and fatigue evaluations.

Tag-end tests are also utilized to evaluate shear strength and varied ply angle orientations. As with the tensile tests described above, the correlation of analysis predictions to test data and the optimization of design by analysis will serve well in the ongoing effort of composite material characterization.

W. R. Colberg/EH43
(205) 544-2725
Sponsor: Office of Space Flight

High Speed Cryogenic Turbopump Bearings

Internal heat generation is being studied at MSFC as the prime life and performance limiter for Space Shuttle Main Engine high pressure oxidizer turbopump (SSME HPOTP) bearings. These angular contact duplex pair bearings (45 mm pump-end, 57 mm turbine-end) support a 29,000 hp shaft that rotates up to speeds of 30,000 rpm when the engines operate at 104 percent of their rated power level. Originally conceived for 55 flights and 7.5 hours of total operation, these bearings currently fall far short of this goal. Post flight and ground test inspection has revealed excessive heating, wear, and degradation of the bearings after about 2,000 to 3,000 seconds of total operation, sometimes sooner. MSFC research is focusing on substantiating excessive bearing internal heat generation, identifying the causes, and testing potential solutions.

Examination of flight and test bearings has exhibited characteristics of excessive heating: discoloration and wear of the 440c balls and races, decreased wear track contact angle, and excessive ball pocket wear of the cage (ball retainer). When more heat is generated by the bearing than can be transferred to the liquid oxygen coolant the thermal growth of the balls and races reduces internal clearance which decreases the contact angle between the balls and races. This increases the effective loads and contact area between the balls and races and in turn the force between the cage and balls. These force increases mean additional friction, which is the source of internal heat, and the degenerative process repeats itself, similar to an undamped feedback loop.

Excessive heat generation is further substantiated by computer analyses sponsored by MSFC. These analyses include such codes as SHABERTH, SINDA, and ADORE to model the configuration of the bearings and various operating conditions used to predict thermal and mechanical interaction and their effects on the bearing's heat transfer and loading. Results from MSFC's Bearing and Seal Materials Tester

(BSMT) have correlated with computer predictions. Computer results have also shown that an operational bearing temperature limit exists beyond which a thermal excursion will occur and a computer solution is no longer feasible. Such a temperature limit has since been demonstrated in the BSMT.

The BSMT, a full scale two-pair bearing tester simulating the operating conditions of the HPOTP bearings (i.e., loads, speeds, and coolant flow), is being used to verify the excessive internal heating, establish thermal operating limits for the current bearing configuration, and test candidate solutions to improve bearing performance.

Currently, the cage material, a polytetrafluorethylene (PTFE) impregnated fiber glass cloth, is being considered a significant contributer to internal heat generation. The glass fibers in the cage, while imparting necessary tensile strength, are abrasive to the 440c steel balls. The relative rubbing velocity between the balls and the cage can exceed 2,400 ips at a shaft speed of 30,000 rpm with the normal force varying between 40 and 60 pounds. The coefficient of friction between the ball and the cage can exceed 0.3, which leads to high frictional heating. Alternate cage materials and designs are being considered that would have a lower coefficient of friction and thereby reduce heating. However, many candidate lubricating composites lack the structural strength necessary due to the centrifugal loads, side loads from the coolant and tensile or compressive loads from differing ball velocities. The material must also be compatible with liquid oxygen.

A worthy candidate cage design is a composite of bronze and PTFE that would be shrouded with a nickel alloy for strength. This approach has been used before in rocket turbopumps, but not at these loads, speeds, and life requirements.

Another aid in reducing internal friction is coating the balls and races with a fatigue resistant and low friction metal such as titanium nitride or with a quasi-lubricating film such as gold. This approach is limited, however, by the current high temperature coating processes that would alter the final 350 °F temper of the 440c. As a result of this, alternate bearing steels with higher tempering temperatures are being considered, as well as development of a lower temperature coating process.

Emphasis has also been placed on improving the cooling of bearings by increasing coolant flow rate and the subcooling of the LOX. BSMT tests have shown improved results from this approach. Similar tests with normal flow rates and subcooling have shown higher bearing temperatures and evidence of two-phase (liquid and gaseous) coolant flow. This approach has correlated well between computer predicted results and actual testing. While not solving the source of heat generation, this does help prevent the thermal excursion process by removing more heat.

The next few years promise heightened activity in reducing the heat generation within these bearings which would ultimately yield longer life and increased performance of the SSME's.

L. E. Moore/EH14
(205) 544-2516
Sponsor: Office of Aeronautics and Space Technology

Space Shuttle Main Engine Exit Diagnostics

With continued improvements and upgrades planned for the Space Shuttle Main Engine (SSME), it would be beneficial to have a diagnostic system capable of measuring pertinent flow variables, such as temperature, species concentration, and velocity in the exhaust plume. A map of these variables measured in a plane at the nozzle exit would be invaluable for anchoring engine performance codes or for monitoring the performance of individual engines. Physical probes would cause perturbations in the flow stream, and combined with the need to correct data makes desirable a nonintrusive measurement technique.

A number of possible approaches were considered during the study phase of this project. The requirement that the technique used not require seeding the flow eliminated many of the better known methods of measuring flow. An approach was selected that does not require seeding of particles of trace molecules – enhanced oxygen hydrogen (OH) flow tagging by ultraviolet-laser photodisassociation of H_2O (Fig. 82). A system using a narrowband injection locked excimer laser (KrF at 248 nm) focused into a sample area produces a small photodisassociation of H_2O, which results in a large local enhancement of the OH radical concentration. In order to measure velocity, a time-delayed, pulsed dye laser beam at 308 nm excites fluorescence from OH, and the location of the supersonic, convected enhanced-OH zone is measured above the background with an optical multichannel detector set. The Raman radiation from the initial excimer pulse yields the information needed to determine the temperature and specie OH concentration. Laboratory feasibility experiments are underway, using diluted H_2/air flames to simulate SSME exit plane conditions.

This system would be coupled into a two-dimensional scanning telescope assembly which would allow full mapping of the exit area. Several samples can be shot in one second, thus rapid data accumulation is possible. With a proper timing circuit for firing, laser accuracies on the order of 2 percent (full-scale) are possible.

Boedecker, L. R. and Shirley, J. A.: United Technologies Research Center; Nozzle Exit Plane Measurement Instrumentation. Presented at 1988 Conference on Advanced Earth-to-Orbit Propulsion Technology, MSFC, May 12, 1988.

W. T. Powers/EB22
(205) 544-3452
Sponsors: Office of Aeronautics and Space Technology
Office of Space Flight

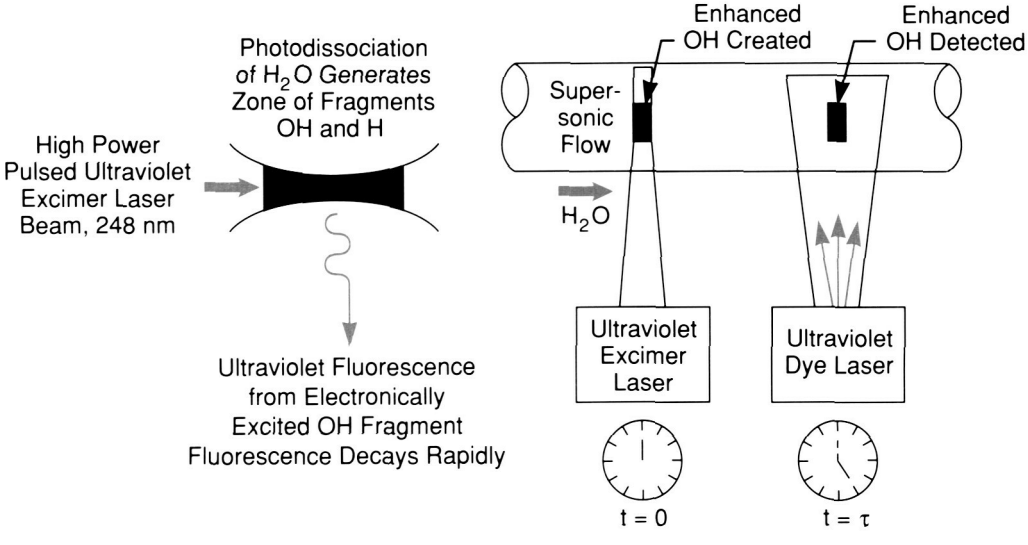

Figure 82. Flow Tagging For Velocity Determination

ORIGINAL PAGE
COLOR PHOTOGRAPH

Vortex Shedding Flowmeter for Space Shuttle Main Engine Use

The vortex-shedding flowmeter was examined as an alternative meter for the Space Shuttle Main Engine (SSME) ducts. It offers advantages over the turbine meter in that it has no moving parts. Because its output is linear with flow, it has the potential of being more accurate at low flows than the venturi, as well as being physically shorter. Its geometry is such that fewer modifications are required for installation.

Several meter designs were built and flow-tested with water at velocities encountered in the SSME ducts. Most testing was done in ducts of 1.6 inch and 2.3 inch. Meters have also been tested in two of the actual SSME ducts.

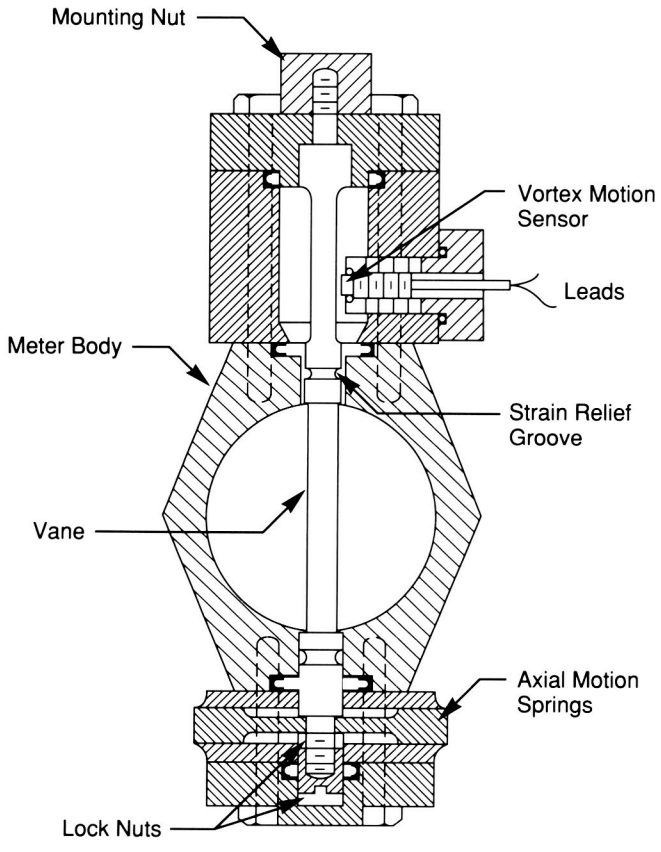

Figure 83. The 87-9-2 Meter Design with Axial Relief Springs

One design criterion is to prevent tieing the sides of a duct directly together with a solid structure such as a shedder vane in order to prevent introducing mechanical stresses due to thermal factors. An early design to circumvent that problem employed dual cantilevered beams, but it was found to be overly sensitive to the gap between the beams. The current design (Fig. 83) uses a beam fastened to the duct at one end and to a "spring" beam (or "washer" assembly) at the other. These latter designs work well, yielding a very clean output, making it easier to interface detecting electronics to the system. The method of sensing the vibration is still under study but methods tried include PZT (lead zirconate titanate) pickups, flexing strain gage sensors, optical sensors, eddy current sensors, and inductively coupled pick-ups. Except for the sensing method, the meters for use in liquid oxygen are designed. The LH_2 meters are being tested in high velocity air flows to prove the design used for gas.

Siegwarth, J. D.: Vortex Shedding Flow-meter Performance at High Flow Velocities. NBS Tech Note 1302, October 1986.

Siegwarth, J. D.: Vortex Shedding Flow-meters for Space Shuttle Main Engines. Presented to 1988 Conference on Advanced Earth-to-Orbit Propulsion Technology, MSFC, May 12, 1988.

W. T. Powers/EB22
(205) 544-3452
Sponsor: Office of Aeronautics and Space Technology

Optical Plume Anomaly Detector

During review of minor and major failures of the Space Shuttle Main Engine (SSME) during tests, there were frequent visual events which appeared to be precursors to the incidents. Thus a program was undertaken to acquire spectral data by way of an optical monitor of the plume. Such data might provide a warning of impending component failure and make it possible to save an engine before a catastrophic incident occurred. The approach was an attempt to monitor certain metallic emission lines and to establish a normal background level of those chosen species. A significant increase above background levels would indicate impending failure.

The spectral region from about 200 nm to about 16 μm was studied with ultraviolet, visible, and infrared radiometers, spectrometers, cameras, and optical multichannel analyzers (OMA's). The radiometers and cameras provided continuous coverage; the OMA's provided higher-resolution data during certain sample periods. Instruments available in the laboratory were mounted on a test stand approximately 7.6 m (25 ft) from the plume center line.

The resulting studies showed the need for a high resolution instrument capable of resolving metallic lines above the high background noise. Some molecular species also were seen to be important, for example, CAOH proved to be important as a tracer for pump bearing cage wear. Ni and Cr are indicators of combustion chamber problems. Even with relatively low spectral resolution (as obtained with good filters) the above species can be detected if the problem is sufficiently severe. Detection of these would permit shutdown decisions. The highest resolution system might permit more critical choices to be evaluated.

The first instruments designed, (Fig. 84) based on the above, will go on line this year. It is a 16-channel, grating spectrometer based system, with fully filled entry aperture and separately adjustable field-of-view, having integral data archiving capability and capacity for making decisions on the order of 3 to 5 msec. Covering the spectral range 0.25 to 1 μm, with resolution of 2 to 3A, it should detect all the species necessary. A continuous spectrometer, employing a similar front-end but having a linear diode array detector set, will be added later. These units will be first calibrated at Stennis Space Center and then later moved to the test bed engine at MSFC.

Powers, W. T. and Sherrell, F. C.: Plume Spectrometry for Liquid Rocket Engine Health Monitoring. Presented at the Symposium on Engine Health Monitoring, Quebec City, Quebec, Canada, June 3, 1988.

W. T. Powers/EB22
(205) 544-3452

Sponsor: Office of Aeronautics and Space Technology

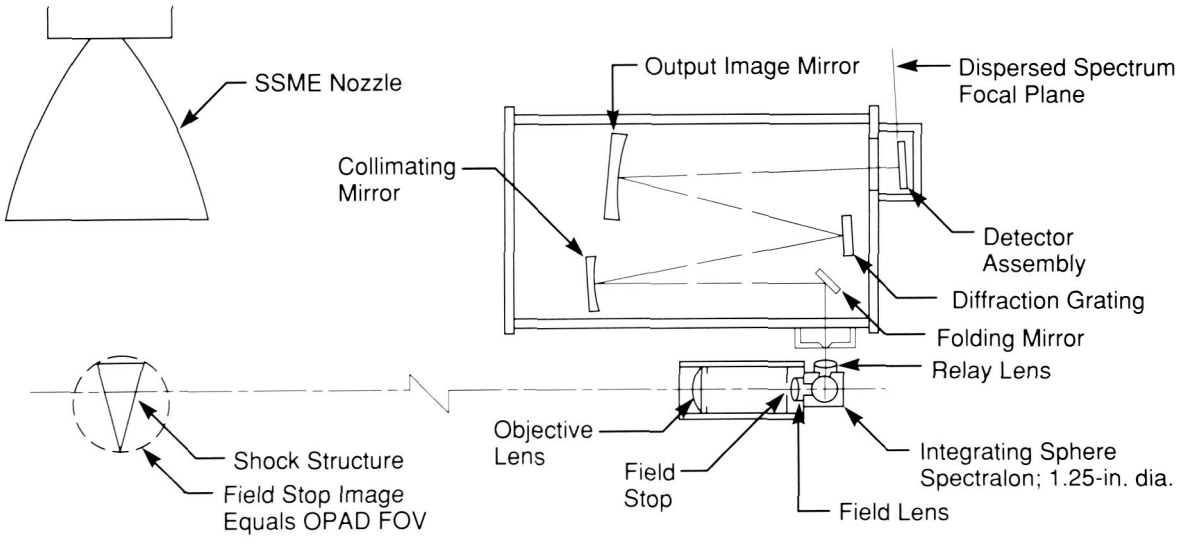

Figure 84. Optical Plume Anomaly Detector With Discrete Detector Array

An Advanced Solid State Pressure Transducer

An advanced pressure transducer is being developed for Space Shuttle Main Engine (SSME) application using silicon microcircuit technology to improve operational reliability and temperature compensation over the operating temperature range. The selected design approach is to ion-implant piezoresistive elements into a silicon chip which acts as a pressure sensitive diaphragm. All zero, span, and temperature compensating elements would also be processed into this chip. The implant resistors can be laser trimmed to exact values while pressure is applied to the diaphragm, resulting in the best possible interchangeability and temperature compensation.

Development efforts during the past year have concentrated on the design of the deliverable units. Design reviews were held to determine if any materials or processes planned for use would preclude application of the transducer on an SSME. Approval was granted for the transducer mechanical design and also for the layout of the silicon wafer which includes redundant sensing and compensation elements.

Piece parts procurement and fabricating has progressed in parallel with the wafer processing. All parts required for the assembly and test of the deliverable sensors should be available by August 1988.

J. E. Zimmerman/EB22
(205) 544-3458
Sponsor: Office of Aeronautics and Space Technology

Nonintrusive Hot Gas Temperature Sensor

A method of measuring the temperature of hot gas flowing within the Space Shuttle Main Engine (SSME) is desired which does not use an intrusive sensor. A probe disturbs flow, presents mechanical/aerodynamic difficulties, and is slow in response. An instrument yielding the gas temperatures from sensing thermal radiation is being developed. Detection of narrow-band, filtered radiation emitted from combustion unique molecules presents the best opportunity to accomplish the needed measurement. This program will provide an optimized detector and electronics, a window assembly fitting a standard SSME instrumentation port, and the interface required to mate the device with the SSME. Several locations on the turbopumps and hot gas manifolds are being considered.

It is intended to provide a system having a pressure sealing window capable of withstanding temperature and thermal flux environments and a fiber-optic cable assembly, with appropriate fore-optics, coupled to the window assembly. Detectors, and other electronics, are to be mounted in a benign environment.

Laboratory testing is underway to allow for known error sources such as backwall radiation, cooler near-wall flow layer radiation and absorption, window reflection, refraction, and absorption, optic cable coupling effects, detector response (spectrally and temporally), and electronically related effects. This program will produce a sensor which is responsive to the flowing gas temperature with good frequency response (time response in msec or less) such that monitoring dynamic reactions is possible as well as providing for closed loop control. This will require a highly reliable, stable, and rugged system.

W. T. Powers/EB22
(205) 544-3452
Sponsor: Office of Aeronautics and Space Technology

Space Shuttle Main Engine Preburner Temperature Profiler

A diagnostic system for nonintrusive temperature profiling in the fuel preburner of the Space Shuttle Main Engine (SSME) has been developed. The approach is based on the measurement of laser-excited, Raman-shifted, backscattered radiation and employs optical fibers for use in the hostile SSME environment. A breadboard system has been completed in a heated cell containing high pressure hydrogen.

The light energy from an argon-ion laser is transmitted through a multimode optical fiber (at lengths of up to about 50 m) to an optical transceiver head, mounted on the engine, which focuses the radiation into the measurement volume and collects the returned radiation, which is transmitted through a second fiber to remotely located instrumentation for spectral analysis (Fig. 85). The hydrogen gas temperature is determined from the distribution of radiation scattered from hydrogen Q-branch nonvibrational transitions. Measurements in the pressure cell indicate that accuracies in the order of 20 to 25 K can be expected, with the probe volume less than 1 cm long and 0.5 mm in diameter, having a time response of 10 msec. Response time and accuracy can be traded off against each other. The system will be mounted in the hard core of the SSME Technology Test Bed stand with the fiber-optic cable routed to the engine. The transceiver head will be mounted to the fuel preburner body by way of an existing port with an appropriate window added; evaluation of candidate materials for the window and design of the window assembly is underway (Fig. 86). The transceiver head may also need to provide backup pressure containment should the window fail. Operationally, the system is ready; integration with the engine is now being performed.

Shirley, J. A.: United Technologies Research Center; Fiber Optic Raman Thermometer. Presented at 1988 Conference on Advanced Earth-to-Orbit Propulsion Technology, MSFC, AL, May 12, 1988.

W. T. Powers/EB22
(205) 544-3452
Sponsor: Office of Aeronautics and Space Technology

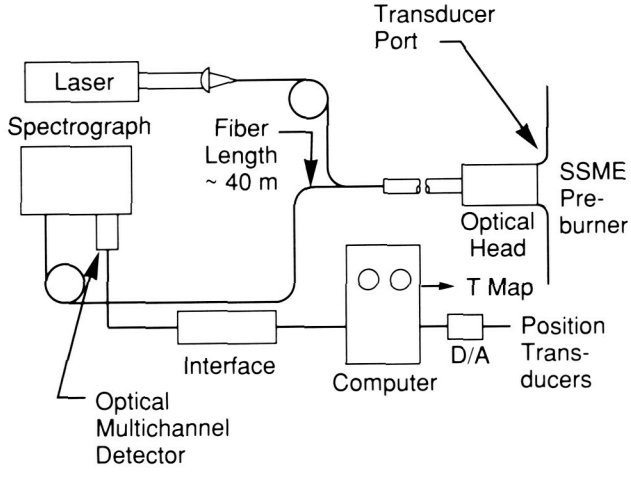

Figure 85. Raman Diagnostic System

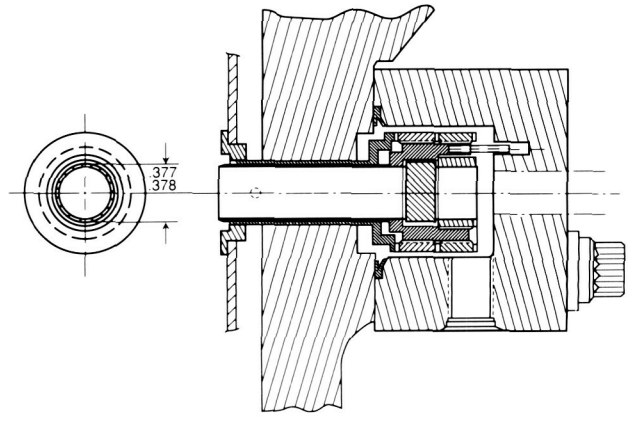

Figure 86. Preliminary Access Port Design

Plume Temperature Measurements

Research is being conducted to measure the exit plane properties of the Space Shuttle Main Engine (SSME) systems for determination of performance code accuracy and to provide data to guide development of future codes. Nonintrusive techniques are being developed which are based on measurements of the emission and absorption of infrared and ultraviolet (UV) radiation from the plume gases. The two techniques which are being utilized are infrared emission/absorption spectroscopy and hydroxal radical (OH) resonance line absorption spectroscopy.

The Infrared Emission/Absorption technique is being used to determine the temperature profile and species concentration in the exit plane of the SSME, using available infrared transitions of the H_2O molecule at 2.7 μm. A band model for radiative transport* in the plume is utilized to compute the distribution and temperature of emitting molecules in each assumed axially-symmetric zone of the plume gases (Fig. 87). The solution is obtained from a best fit of the emission/absorption data and from experimentally determined band model parameters for the H_2O molecule. Subscale experiments conducted using a hydrogen-air hot-gas generator demonstrated the accuracy of the technique by comparison with thermocouple measurements. A test stand system for full-scale demonstration of the measurement technique on the SSME has been designed and will be utilized to characterize the SSME exit plane on the MSFC Technology Test Bed.

The OH radical resonance line absorption technique is based on the use of a microwave-pumped discharge to produce characteristic OH radical radiation which is transmitted through the plume to determine rotational temperature and species concentration of OH. The OH concentration is of particular interest due to its impact on the kinetics of the rocket

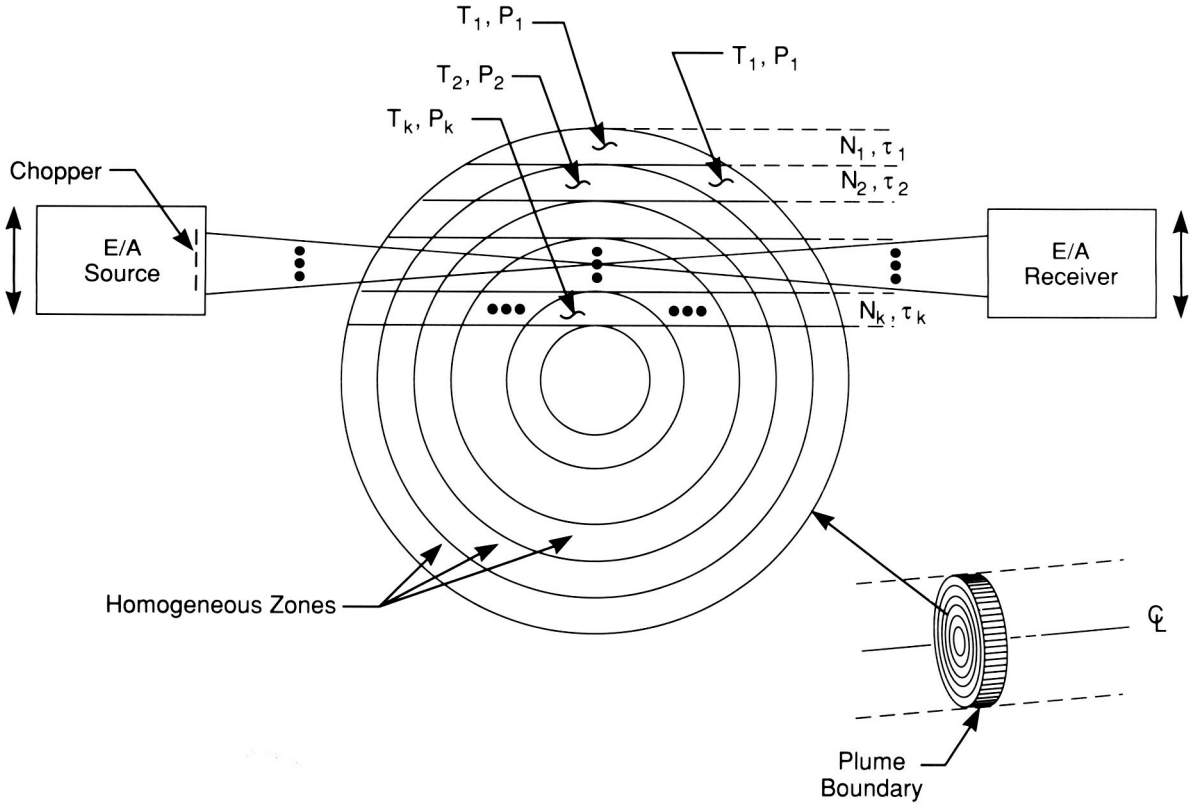

Figure 87. Inhomogeneous Cylindrically Symmetric Source

engine combustion and expansion process. Such data will provide an excellent check for chemical kinetic models which are currently being used. The OH absorption data will be acquired with an optical multichannel analyzer and a 1/2 meter UV spectrograph which captures the (0 to 0) band OH radiation from 306 to 320 nm. The OH data reduction technique is based on early work by Neer† and more recent advances at Langley Research Center.‡

*Brewer. I.E.: A Non-Interference Method for Determining Temperature and Water Vapor Concentration Profiles in Cylindrically Symmetric Combustion Systems. AEDC-TR-71-80, July 1971.

†Neer, M. E. and D. H. Burde: The Advanced Development of a High Frequency Response Spectroscopic Probe for Analysis of Supersonic Combustor Flowfields. NASA CR 145363, July 1978.

‡McCullough, R. W.: Improvements to the NASA OH Temperature Measurement System. ARAP report no. 548, Contract NASI-14853, April 1985.

R. H. Eskridge/EP55
(205) 544-7119
Sponsor: Office of Aeronautics and Space Technology

Brushless Torquemeter

Direct measurement of rocket engine turbopump shaft power (torque and speed) is a difficult task. The standard method of measuring torque is to strain gauge the shaft and use a slipring to remove the strain gauge output from the shaft. Rocketdyne's instrumentation group has conceived a method of measuring torque without using a slipring, i.e., a brushless torquemeter.

The brushless torquemeter (Fig. 88) uses a magnetostrictive material deposited on the shaft and a pickup consisting of a coil mounted between two permanent magnets of opposite polarities. The pickup coil is placed adjacent to the deposit on the shaft. As the shaft rotates and the deposit transitions between the two magnets, the polarity of the deposit magnetization reverses. This switching of the magnetization induces voltage in the pickup coil. Since the magnetic properties of the deposit vary with shaft strain, and strain is a function of shaft torque, the magnitude of the pickup coil output can be correlated to torque.

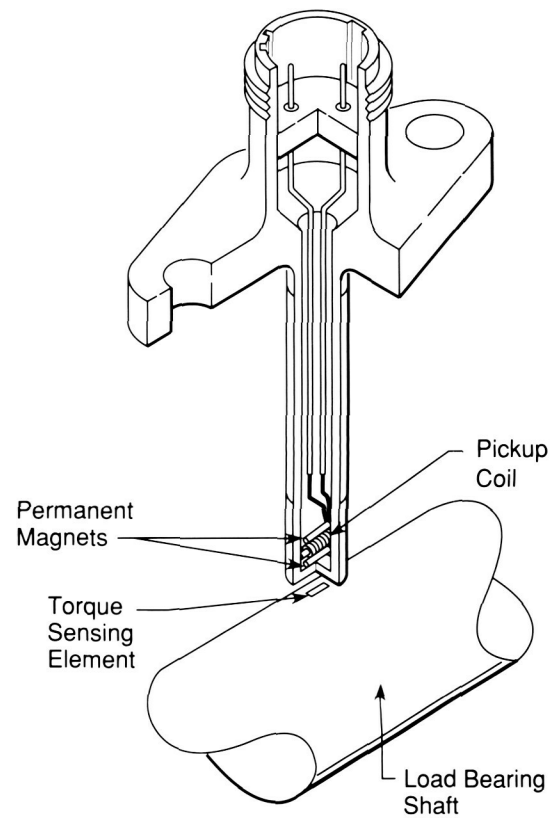

Figure 88. The Brushless Torquemeter

Rocketdyne used a low speed test apparatus to demonstrate concept feasibility. Based on this, the technology test bed program funded an effort to investigate the feasibility of using this device in the Space Shuttle Main Engine (SSME) turbopumps. The program consisted of two phases. The first phase investigated deposit integrity and production of a usable output at cryogenic temperatures and shaft speeds typical of the SSME turbopump operating speeds (approximately 40,000 rpm). The second phase consisted of selecting one of the SSME turbopumps for installation of the brushless torquemeter and performing initial design analyses for the selected turbopump.

Both phases of this program have been successfully completed. Phase I demonstrated deposit integrity when exposed to cryogenic thermal cycling. Also, a functional relationship was shown to exist between shaft strain, speed, temperature, and torquemeter output. In Phase II, the SSME low pressure fuel turbopump (LPFTP) was selected for installation of the brushless torquemeter. This selection was based primarily on easy access and minimum modifications required for installation. Preliminary design analyses of the hardware modifications and torquemeter pickup have been completed.

The major concern associated with the torquemeter is achieving an accurate calibration. As shown in Phase II, the pickup output is a function of the variables (strain, speed, and temperature) and shaft strain will not be only torsional. Although precise calibration of the torquemeter in the LPFTP may not be practical, a program to complete the design and fabricate the hardware necessary to test the torquemeter in a LPFTP on the SSME technology test bed is being considered. This will demonstrate the instrument's integrity at the engine level and define its usefulness as a diagnostic tool for identification of within test and test-to-test torque changes. If this engine level demonstration is successful, the calibration problem can likely be overcome when use of the device is considered in the design of a new turbopump.

H. P. Stinson/EP62
(205) 544-7077
Sponsor: Technology Test Bed

Advanced Turbulence Models For Space Shuttle Main Engine

Liquid fueled rocket engines like the Space Shuttle Main Engine (SSME) have gaseous reactants and combustion products flowing at high velocities through internal paths in the engines. This flow is turbulent and the flow paths may involve bends through large angles at a small radius of curvature. The flow is normally used to drive turbines during part of its transit through the system. This implies flows with significant rotation. In order to deal with these rotating-flows and flows with large streamline curvature in computational models, turbulence models which are consistent with the physical processes in these systems must be developed and implemented in operational codes. Computational techniques using these turbulence models must be able to accurately calculate mixing processes in the flows as well as flow structures such as recirculation zones. Configurations which represent these conditions (rotation and curvature) and for which some experimental data are available were subjected to three-dimensional computational analyses using both the standard k-ε and a multiple scale turbulence model. First, the case of a rotating duct was considered and comparisons with data were made. Then, the case of flow in a highly curved duct was considered and compared with experimental data. The next logical problem to examine is the case of flow through a curved duct with rotation. No data are available for this however. Results for computations using both models were compared with the available experimental data. It was found that the multiple scale model was better able to predict overall flow features. As they are developed, the verified models are available for incorporation into engineering models for calculations of flows in the SSME system.

Chen, C. P. and Schafer, C. F.: Development and Assessment of Turbulence Models for SSME Internal Flow Fields. Office of Aeronautics and Space Technology–Advanced Earth-to-Orbit Propulsion Conference, May 1988.

C. F. Schafer/ED42
(205) 544-1642
Sponsor: Office of Aeronautics and Space Technology

Boundary Layer Simulation Improvement

Development of propulsion systems for orbit transfer vehicles permit nozzle designs with very large area ratios (ε >1,000). The energy to drive the propellant feed system shall be extracted from the main thrust chamber regeneratively to operate the engine in an expander cycle mode. It is evident that the chamber pressure depends on the transferred heat energy which in turn dictates the expansion process and its related specific impulse.

Since the current boundary layer programs are formulated with the assumption that the viscous layer is small and the pressure remains locally constant, steps have been taken to advance the calculation method for conditions to be encountered under large area-ratio/high-expansion situations.

Methods which affect the heat transfer process are surface roughness, turbulent flow conditions with relaminarization behavior, and the condensation phenomena (liquid/solid phases) under sufficiently low pressures during the expansion process.

The Boundary Layer Integral Matrix Procedure, the recommended Joint Army, Navy, NASA, and Air Force reference program, is being modified to account for the effects mentioned. In addition, the maximum possible specific impulse state shall be predicted when the growth in friction loss cannot be overcome by the impulse gain due to nozzle area ratio increase.

All conditions affecting the heat transfer are being introduced into the turbulence model since its behavior controls the viscous or friction loss calculation as well. Surface roughness enhances fluctuating motion when the hydraulically smooth wall condition is exceeded. High acceleration, especially when coupled with a large temperature gradient across the boundary layer, stretches the oscillating motion such that a more laminar behavior seems to exist. The presence of particles in the viscous domain acts as a damping component reducing the turbulence corresponding to the particle size.

The boundary layer growth, exceeding the constant pressure assumption criterion, requires an improved coupling with the core flow to arrive at more accurate edge conditions during an iteration process. Figure 89 indicates how far the boundary layer penetrates into the superimposed stream-line domain, calculated with the inviscid core Two-Dimensional Kinetics (TDK) flow model. The associated pressure profiles from the TDK solution disclose the significant difference when data along the potential wall contour or from locations along the boundary layer edge are used as boundary conditions to account for the viscous effects. The impact is evident in Figure 90 where the total thrust deficit is presented for the

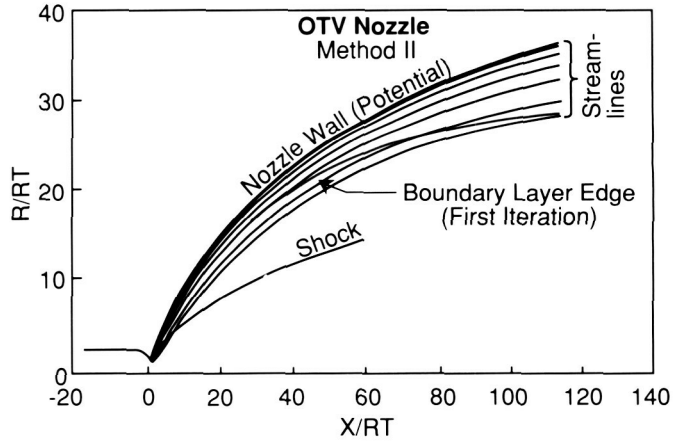

Figure 89. Two-Dimensional Kinetics Derived Streamlines Near the Nozzle Wall and Boundary Layer Thickness

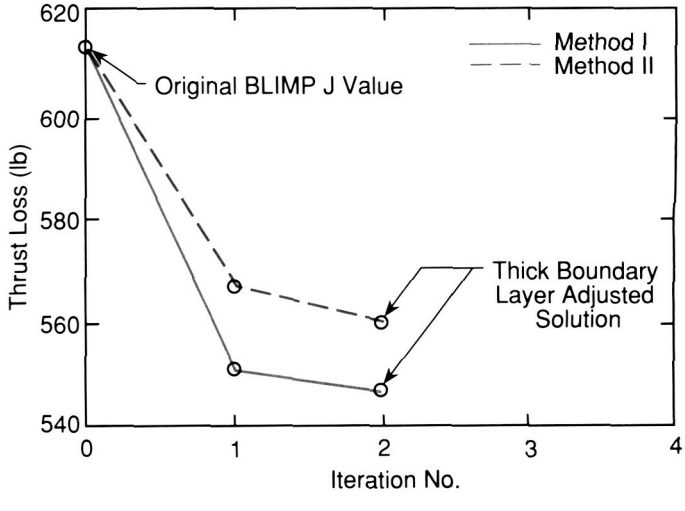

Figure 90. Thrust Loss Iteration

potential wall condition and a thick boundary layer. Method I used properties in radial direction of the nozzle, whereas method II is based on properties normal to the wall.

The boundary layer modification effort, conducted by Remtech, Inc., of Huntsville, Alabama, has already provided significant results. The Cebeci turbulence model has been extended to account for wall-roughness which can be varied as a function of wall-length as required. Further modification includes the temperature effect due to wall cooling for studying relaminarization conditions. A new module has been programmed which couples the TDK inviscid flow parameters with the boundary layer edge quantities to predict the thrust loss. Boundary layer thickness and pressure profiles normal to the wall can be calculated as well. These features are also considered for inclusion into other boundary layer codes which are directly coupled with the TDK program.

K. W. Gross/EP55
(205) 544-2262
Sponsor: Office of Aeronautics and Space Technology

Thrust Chamber Performance Using Navier-Stokes Equations

The advent of high speed computers with large core capacities permits the simulation and analysis of complex physical processes which occur in rocket engine thrust chambers. Today the performance of such an engine is still determined by a methodology which starts with the maximum possible specific impulse of a chemically reacting rocket motor which is then adjusted by particular losses to arrive at a predicted value. During this analytical approach the injector flow is characterized by empirical relationships or pure scaling information. For the boundary layer simulation, significant assumptions and constraints for the boundary conditions must be accepted. However, no other prediction tools exist which have undergone such extensive checkout and application by many users to affirm consistent results quickly and conveniently. This history has built a strong confidence in the existing programs and their solutions.

In addition to the specific impulse, flow conditions downstream of the injector and along the thrust chamber wall can soon be predicted accurately. To obtain an optimum atomization, evaporation, mixing, and chemical reaction process in the combustion chamber, and to provide benign conditions near the wall to protect the material or control the heat flux for long engine life demands, all empiricism must be replaced in the flow simulation by a correct physical process description. The Computational Fluid Dynamics (CFD) codes contain these basic postulates, and with knowledge of the physical mechanism, the proper simulation can be achieved.

Work continues on advancing CFD programs aimed towards the comparison of solutions with the existing approach on an equal basis. Two computer programs are being extended to calculate the Space Shuttle Main Engine's (SSME's) entire internal flowfield including equilibrium chemistry and viscous behavior. One is the Progressive Assembly of Interpolated Differences (PAID) code, developed by the Lockheed Missile and Space Co., in Huntsville,

Alabama; the second code is the Parabolic Hyperbolic Or Elliptic Numerical Integration Code Series (PHOENICS) program by CHAM of North America, also in Huntsville, Alabama. These two codes use different numerical solution schemes. The PAID program is a finite element/finite difference combination, whereas PHOENICS uses a finite volume concept. Both models have the capability to solve the elliptical flow field. However, the viscous effects are modelled differently. The k-ε turbulence model and the Baldwin-Lomax formulation are involved. The current method uses a one-dimensional equilibrium approach in the chamber, patched with a one-dimensional finite rate chemistry solution and a perturbation scheme in the transonic region, which allows inviscid Method of Characteristics calculations governing the supersonic flowfield down to the nozzle exit plane. In contrast, the CFD solution is two-dimensional throughout the subsonic, transonic, and supersonic regimes and includes boundary layer characteristics through the use of the pertaining turbulence model. To assess the state of program maturity, the SSME performance simulation has been selected as the sample case.

Since the calculation mesh is of utmost importance for the solution accuracy, a Grid Generation Package has been developed and will be available to the propulsion community. The subject program has already been applied to assist flow analysis of a dual-bell-contour nozzle where an intended flow separation at the wall discontinuity will be examined. Another application serves in the analysis of TRW's Variable Thrust Engine (VTE) where the single pintel injection element must yield optimum performance while providing a sufficient low mixture ratio near wall-zone to hold the wall temperature down for life time reasons. Figure 91 shows a first approach to investigate the recirculation behavior in the VTE chamber. A third task addresses the flow condition at the wall-lip in the SSME exit plane to study the flow separation phenomenon and the flow recirculation behavior for vacuum operation. For either problem the flow domain must be extended to cover areas outside of the nozzle flow with boundaries far enough away to represent boundary conditions with confidence. The extended grid and first results are exhibited in Figure 92.

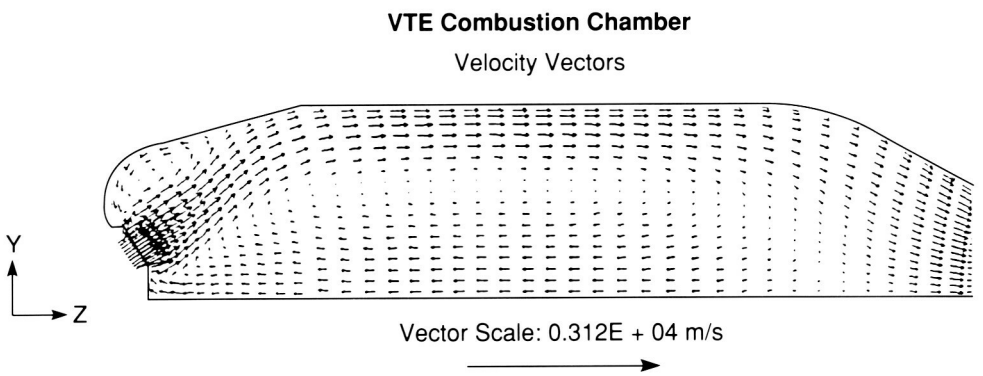

Figure 91. Variable Thrust Engine, Combustion Chamber Flow-Field

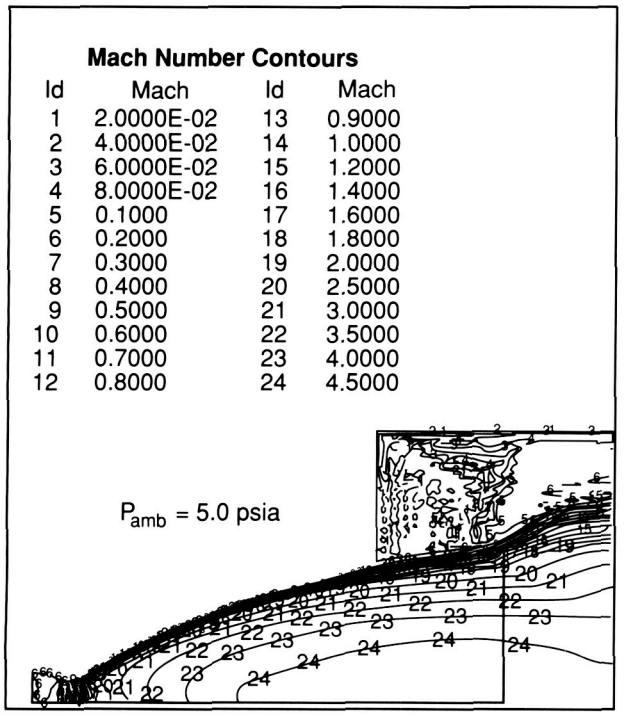

Figure 92. Space Shuttle Main Engine Thrust Chamber Results

The code development process increases the solution capability of many problems, but new ones appear which were not realized before. The continuous strive to advance the flow simulation technology will improve the design of optimum performing thrust chambers with a long operation lifetime.

K. W. Gross/EP55
(205) 544-2262
Sponsor: Office of Aeronautics and Space Technology

Finite Area Combustor Theoretical Rocket Performance

The Joint Army, Navy, NASA, Air Force reference computer program, calculating the thrust chamber performance for one-dimensional chemical equilibrium conditions, has been amended with an option to account for the nonisentropic combustion process occurring in the cylindrical section of the combustion chamber. This option required the inclusion of the momentum equation for the domain of interest. Subject concept assumes that the chemical reaction is complete before the flow starts accelerating due to the expansion process in the convergent section upstream of the nozzle throat.

During the required iteration process the nonisentropic flow behavior is represented by a total pressure loss in the cylindrical chamber segment. Reducing the injector face pressure by subject pressure loss, the irreversible combustion region can be represented with an adjusted infinite area constant entropy process. From the start of contraction (Fig. 93) the flow expands isentropically for either case.

Two options are available with the new concept. Option one requires the combustion chamber contraction ratio (cross-section of the chamber divided by the throat area) while option two calls for the combustion product mass flowrate per unit chamber cross-sectional area as an input.

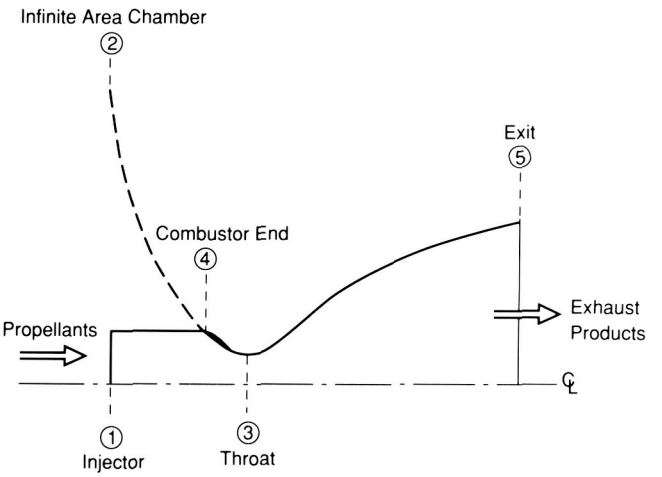

Figure 93. Reduction of Injector Face Pressure by Subject Pressure Loss

Changes were made to the internationally recognized program, CET86 by S. Gordon (Sanford Gordon and Associates) and B. McBride (NASA/Lewis Research Center). All new analytical formulations, the conceptual approach, and sample cases with slightly modified print-out format (Table 7) are contained in the NASA Technical Memorandum 100785. In Table 7 the finite area combustion process of the cylindrical chamber section is represented by values in the Injector and CN Ratio columns. The entropy S

Table 7. Constant Entropy Process Sample Case Print-Out Format

PINJ = 773.3 PSIA
AC/AT = 1.5800
Case No. 2

	Chemical Formula	Wt Fraction (See Note)	Energy KJ/KG-MOL	State	Temp. Deg K
Fuel	H 2.00000	1.000000	-9012.332	L	20.17
Oxidant	O 2.00000	1.000000	-12978.762	L	90.18

O/F = 5.5516 Percent Fuel = 15.2635 Equivalence Ratio = 1.4297 PHI = 1.4297

	Injector	Inf Cham	Throat	CN Ratio	Exit	Exit	Exit	Exit	Exit	Exit
PINJ/P	1.0000	1.0848	1.8868	1.1955	10.000	100.000	1000.00	283.87	714.18	1225.05
PINF/P	0.92182	1.0000	1.7393	1.1020	9.2182	92.182	921.82	261.68	658.35	1129.28
P,MPA	5.3317	4.9149	2.8258	4.4600	0.53317	0.05332	0.00533	0.01878	0.00747	0.00435
T,DEG K	3395.7	3387.6	3190.3	3352.6	2601.0	1784.2	1132.3	1463.1	1214.9	1084.4
RHO,KG/CU M	2.3995 0	2.2155 0	1.3666 0	2.0353 0	3.2325-1	4.7461-2	7.4796-3	2.0391-2	9.7609-3	6.3749-3
H,KJ/KG	-1026.10	-1026.10	-2211.87	-1240.26	-5306.21	-8483.37	-10572.3	-9547.52	-10323.7	-10713.9
U,KJ/KG	-3248.13	-3244.56	-4279.62	-3431.63	-6955.64	-9606.76	-11285.1	-10468.6	-11088.5	-11396.6
G,KJ/KG	-64354.4	-64383.5	-61880.1	-63943.6	-53952.3	-41852.2	-31748.9	-36911.2	-33045.2	-30995.8
S,KJ/(KG) (K)	18.6496	18.7029	18.7029	18.7029	18.7029	18.7029	18.7029	18.7029	18.7029	18.7029
M,MOL WT	12.706	12.696	12.828	12.720	13.111	13.205	13.207	13.207	13.207	13.207
(DLV/DLP) T	-1.02061	-1.02105	-1.01545	-1.02003	-1.00372	-1.00007	-1.00000	-1.00000	-1.00000	-1.00000
(DLV/DLT) P	1.3750	1.3837	1.2982	1.3687	1.0860	1.0021	1.0000	1.0001	1.0000	1.0000
CP, KJ/(KG) (K)	8.3873	8.5031	7.6085	8.3518	4.9770	3.4295	2.9787	3.2107	3.0406	2.9415
GAMMA (S)	1.1453	1.1447	1.1469	1.1449	1.1717	1.2260	1.2680	1.2440	1.2611	1.2723
SON VEL, M/SEC	1595.3	1593.6	1540.0	1584.0	1390.2	1173.6	950.7	1070.4	982.1	932.0
Mach Number	0.000	0.000	1.000	0.413	2.105	3.291	4.596	3.857	4.391	4.723
Performance Parameters										
AE/AT			1.0000	1.5800	2.2253	11.482	64.394	25.000	50.000	75.000
CSTAR, M/SEC			2335	2335	2335	2335	2335	2335	2335	2335
CF			0.659	0.280	1.253	1.654	1.871	1.768	1.846	1.885
IVAC, M/SEC			2882.7	4002.8	3489.5	4152.8	4532.6	4351.4	4489.6	4556.9
ISP, M/SEC			1540.0	654.5	2925.8	3861.9	4369.5	4128.3	4312.2	4401.8
Mole Fractions										
H	0.03442	0.03515	0.02793	0.03387	0.00910	0.00024	0.00000	0.00001	0.00000	0.00000
HO_2	0.00002	0.00002	0.00001	0.00002	0.00000	0.00000	0.00000	0.00000	0.00000	0.00000
H_2	0.29457	0.29444	0.29387	0.29428	0.29661	0.30041	0.30055	0.30054	0.30055	0.30055
H_2O	0.63378	0.63254	0.65140	0.63603	0.68910	0.69932	0.69945	0.69945	0.69945	0.69945
H_2O_2	0.00001	0.00001	0.00000	0.00000	0.00000	0.00000	0.00000	0.00000	0.00000	0.00000
O	0.00225	0.00233	0.00136	0.00214	0.00010	0.00000	0.00000	0.00000	0.00000	0.00000
OH	0.03306	0.03354	0.02423	0.03183	0.00501	0.00004	0.00000	0.00000	0.00000	0.00000
O_2	0.00190	0.00197	0.00120	0.00182	0.00009	0.00000	0.00000	0.00000	0.00000	0.00000

Additional Products Which Were Considered but Whose Mole Fractions Were Less Than 0.50000E-05 for all Assigned Conditions

03 $H_2O(S)$ $H_2O(L)$

Note: Weight Fraction of Fuel in Total Fuels and of Oxidant in Total Oxidants

increase here is evident. The pertaining total pressure loss, required to simulate the finite area combustion with a constant entropy infinite injector area process, is represented by the pressure difference or pressure ratio terms in the Injector and Inf Cham columns, and the entropy remains constant throughout the entire thrust chamber combustion-expansion process.

Inclusion of the finite area combustion algorithm in the reference program provides a well documented standard procedure which shall be used by the propulsion community. Solutions obtained with this program can be used with confidence, and the current confusion of results by way of various schemes will be avoided.

The computer program can be obtained from the authors or from COSMIC, University of Georgia, Athens, GA 30602.

K. W. Gross/EP55
(205) 544-2262
Sponsor: Office of Aeronautics and Space Technology

Interphase Stresses in Two-Phase Flows

Two-phase flow environments are characterized by strong mechanical, thermal, and reactive interactions within and between the phases of the flow. In the formulation of theoretical models of mixture flows, the mechanical process is described by a set of intra- and interphase interaction terms. Axiomatically, these are also the terms which mathematically couple the systems of flow-modeling field equations.

In the modeling of two-phase flows two distinct analytical approaches are used: the Lagrangian or trajectory model and the Eulerian, two-fluid, or continuum model. The principle difference between the trajectory and continuum models is whether the equations of motion for the dispersed phase are cast on a material reference frame and the motion of a collection of discrete particles, or droplets are flowed or tracked through the flow domain or whether the equations of motion are cast on a spatial frame, when the average motion of the discrete phase at a point in space is the dependent variable. Rational arguments for the applicability of both models have been made. Modifications and subsequent applications have been made with these early models for fluid/solid jet flows, solid rocket motor analysis, and geophysical flows, including the effects of a turbulent regime.* For these models, the interaction between the phases is restricted to fluid/solid drag in the Stokesian regime.

In many two-phase flows the particulate phase may become nonhomogeneously distributed, the net result being concentration maxima and minima in what otherwise should be a homogeneous mixture. These demixing phenomena are the result of forces, transverse to mean flow, imposed on the discrete phase due to interaction with the shearing motion of the fluid phase. The consequences of and the need to predict the occurrence and location of particle or droplet concentration extrema is vital in design flows such as jets, nozzles, and combustors.

During FY88, analytical efforts and the attendant computation problems associated with transverse or lift forces on the discrete phase in shearing two-phase shear flows was undertaken. The result has been an improved but still incomplete understanding of the mechanics of two-phase shear flow. As a consequence, and given the importance of two-phase shear flows in aerospace technologies, a conference on this specific subject was held at MSFC in February 1988. The manuscripts and narratives from this conference are now available as a NASA Conference Publication. †

*Adeniji-Fashola, A., and Chen, C. P.: Turbulent Reacting Gas-Particle Flows in Practical Combustor Geometries. AIAA Paper #88-3226, 1988.

†Decker, R. and Schafer, C. F.: Mixing and Demixing Processes in Multiphase Flows with Application to Propulsion Systems. NASA Conference Publication, NASA CP 3006, 1988.

C. F. Schafer/ED42
(205) 544-1642
Sponsor: Office of Aeronautics and Space Technology

Turbulent Reacting Two-Phase Flows

The flow passages encountered in the Space Shuttle Main Engine (SSME) are typically complex. In addition, the flows are usually turbulent. This combination results in complex and difficult to predict phenomena such as flow separation and reattachment. The problem is further heightened by the co-flowing of two different phases or species of significantly different densities. In order to obtain solutions to the highly non-linear sets of differential equations describing these flows, the numerical modeling approach is invariably called for.

Two modeling approaches that are commonly adopted for two-phase flows are the Eulerian or two-fluid approach and the Lagrangian or trajectory approach. The two-fluid approach, which is a derivative of the mixture theories formulation, has received the greater attention among investigators. In particular, important phenomena of turbulent dispersion of the particulate-phase and turbulence modulation by the particulate-phase which are manifestations of the coupling between the phases have been incorporated into two-fluid models. However, while the turbulent dispersion effect has been included in existing Lagragian formulations, the turbulence modulation effect has, until very recently, been ignored.

One problem associated with the two-fluid modeling approach is its inability to efficiently model a dispersed-phase having a polydisperse size distribution. This is due to the requirement of a complete set of governing differential equations for each size group. Indeed, the approach becomes a "multi-fluid" modeling scheme.

The multiple-realization particle trajectory scheme has been developed and applied to the numerical prediction of confined, turbulent fluid-particle flows. The results obtained from the numerical scheme agree well with the available experimental data lending confidence to the modeling approach. The multiple-realization particle trajectory turbulent-flow modeling scheme is believed to be a more elegant

and accurate approach to the extension of single-particle hydrodynamics to dilute multi-particle systems than the more commonly employed two-fluid modeling approach. It is also better able to incorporate additional terms such as lift, virtual mass, and Bassett history terms directly into the particle equation of motion as appropriate. This makes it a suitable candidate for particle-migration studies and the extension to liquid particulate-phase for such propulsion related studies as spray combustion follows naturally. The particle streamwise velocity for the turbulent particle-laden coaxial jet flow in a recirculation chamber predicted using the particle trajectory scheme is shown in Figure 94.

The very important phenomena of particle dispersion by fluid turbulence and modulation of the turbulence by particles have been included in the present effort. The effect on particle motion of the transverse force, due to interaction between velocity-shear existing in the fluid and velocity-slip between the particle and the fluid, has been incorporated. It is found that incorporation of all these effects in the description of confined turbulent fluid-particle flows in certain ranges of particle size and particle-to-fluid density ratio is necessary for a more realistic modeling of this class of multiphase flows.

The work in Figure 94 involving a solid dispersed phase is not directly applicable to the situation in the SSME in which only fluid phases are present. The extension to a fluid dispersed phase is not trivial. This is due to the extra degrees of freedom associated with growth as well as breakup and coalescence of bubbles and droplets. Also, a different set of degrees of freedom is associated with introduction of chemical reaction into the turbulent flows being studied. In particular, interaction between the chemical reaction and turbulence introduces additional complexities into the flow. Work on this extension is in progress.

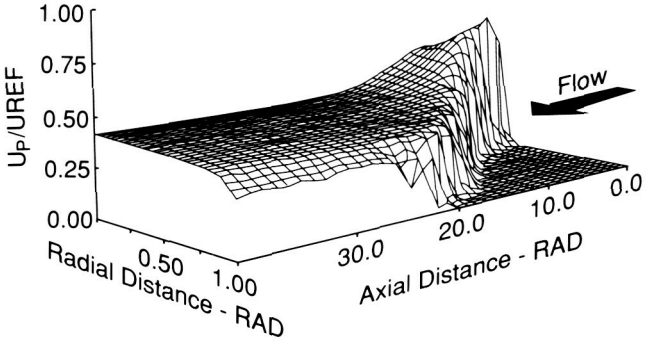

Figure 94. Particle Streamwise Velocity in Confined Turbulent Particle-Laden Coaxial Jet Flow

Adeniji-Fashola, A.: Confined Turbulent Fluid-Particle Flow Modeling Using Multiple-Realization Particle Trajectory Schemes. NASA Technical Publication, Eds. Schafer, C. and Decker, R., in press, 1988.

Adeniji-Fashola, A., and Chen, C. P.: Turbulent Reacting Gas-Particle Flows in Practical Combustor Geometries. AIAA Paper 88-3226, 1988.

Adeniji-Fashola, A., Schafer, C., and Chen, C. P.: Numerical Modeling of Complex Two-Phase Flows. SSME Computational Fluid Dynamics Sixth Working Group Meeting, NASA-MSFC, April 26-28, 1988.

C. F. Schafer/ED42
(205) 544-1642
Sponsor: Office of Aeronautics and Space Technology

Ball Bearing Coolant Flow

Analysis of the three-dimensional (3-D) turbulent two-phase flow inside a tandem ballbearing assembly of the Space Shuttle Main Engine (SSME) high pressure oxygen turbopump (HPOTP), U/N 2217 ball bearing continued during FY88. A three-dimensional finite difference Navier-Stokes flow solver is being used. A homogeneous two-phase model has been employed to simulate the boiling/evaporation process in the liquid oxygen (LOX) inside the flow passage (on the basis of LOX thermodynamic properties, in conjunction with the fluid flow characteristics and the conjugate heat transfer in the ball bearings). An extended two-equation turbulence model has been used for the turbulent flow computations.

To obtain proper inflow boundary conditions, a 3-D inlet jet plenum study was also performed to determine the time-averaged inlet jet angle and velocity profiles. The calculated jet angle agrees with what has been experimentally observed.

For the simulations of coolant flow inside the ball bearing assembly, a complex 3-D mesh system including inner-race, outer-race, solid ball, and cage was generated using an algebraic grid generation technique. Frictional heat generation rates inside the contact areas are provided by the analysis of Rocketdyne.

Computational results of the present analysis (e.g., Fig. 95) were presented at the Sixth SSME Computational Fluid Dynamics (CFD) Working Group Meeting. High-temperature regions with evaporated LOX were predicted in this analysis. Results showed that the pick temperature on the solid ball surface can reach 1,600 to 1,800 degrees Rankine.

Chen, Y. S.: Homogeneous Two-Phase Flow Calculation Inside the HPOTP Ball Bearing Assembly. Sixth SSME CFD Working Group Meeting, NASA-MSFC, April 1988.

N. C. Costes/ED42
(205) 544-1637
Sponsor: Office of Space Flight

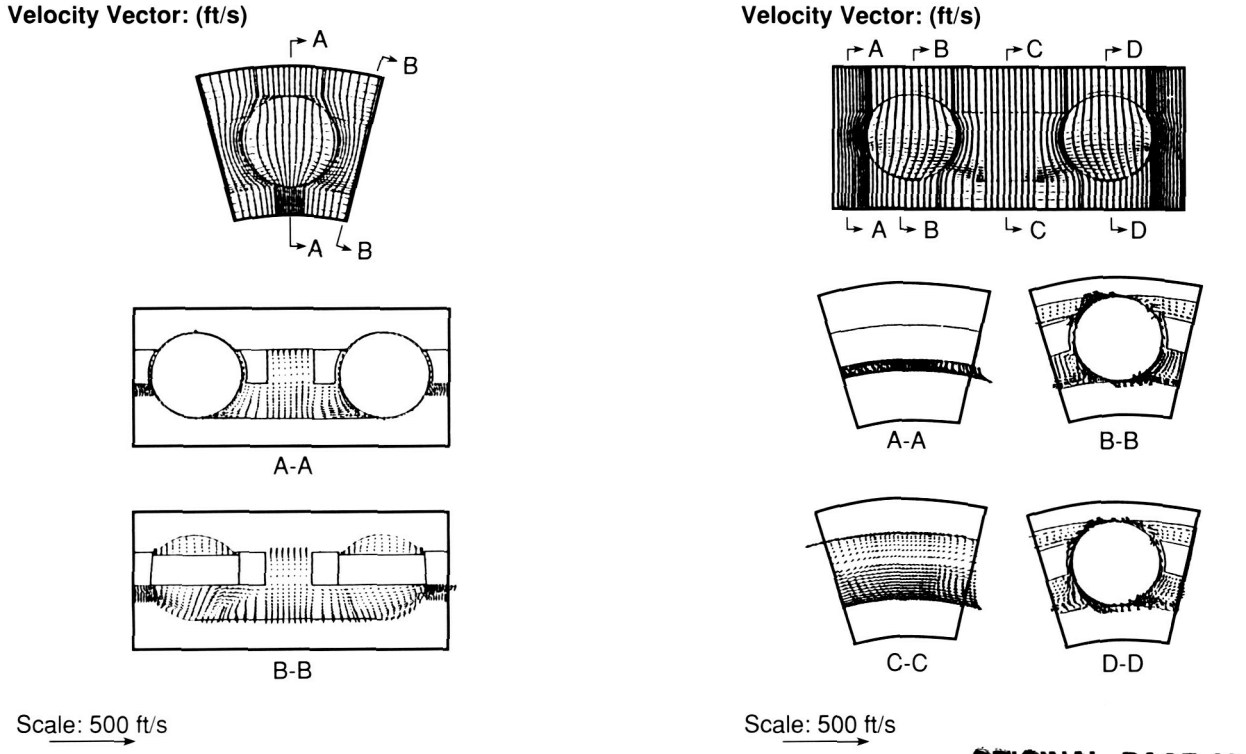

Figure 95. Computational Results of Two-Phase Flow Analysis

Computational Fluid Dynamics Methodology

During FY 1988 the development of a general purpose Navier-Stokes flow solver (CNS3D) was continued. The main effort of this work has been concentrated in the area of numerical accuracy and efficiency for the simulations of unsteady flow problems. A multiple-corrector solution algorithm with a time-centered (Crank-Nicholson) time-marching scheme has been implemented for efficient transient calculations. For spatial discretizations, a second-order central plus a fourth-order damping scheme is employed for good numerical accuracy.

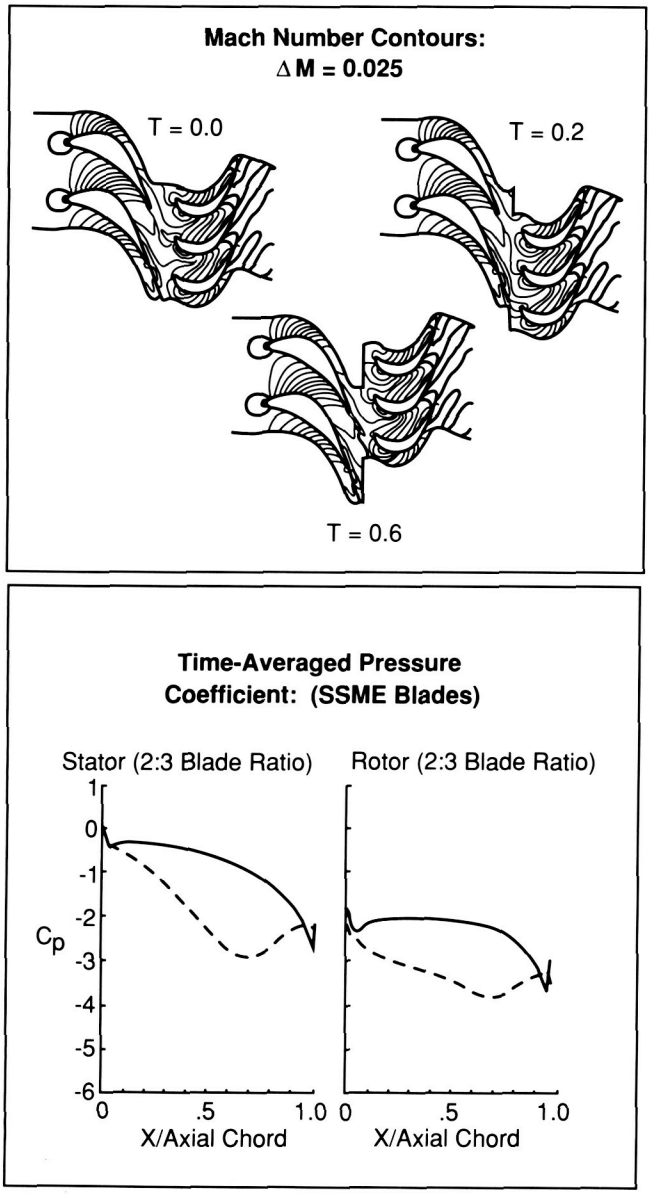

Figure 96. Mach Number Contours (at Top), and Time-Averaged Pressure Coefficient for SSME Blades (Below)

For compressible flow problems, an adaptive artificial dissipation scheme has been developed for accurate shock capturing capability. This adaptive scheme is similar to the Jameson's scheme, which was originated from the idea of Harten's Total Variation Diminishing scheme. Applications of the present method to various flow problems, ranging from incompressible flows to Mach-8.0 compressible flows, have demonstrated good accuracy and robustness of the present numerical method.

In order to provide good predictions for simple and complex turbulent flow computations, an extended k-ε turbulence model has also been developed and tested. This turbulence model employs an extra time scale in the turbulent kinetic energy dissipation equation. It has been shown that this model is superior to the standard k-ε model for many complex turbulent flows.

To demonstrate the time accurate feature of the present flow-solver, computational results from a benchmark stator-rotor interactions test case, as well as from stator-rotor interactions in the Space Shuttle Main Engine, were presented in the 1988 Advanced Earth-to-Orbit Propulsion Technology Conference (Fig. 96). For this analysis a multizone solution method with sliding grid arrangements was incorporated in the present flow-solver. Linear interpolation was used to allow the signals to propagate through the zonal interface. The results of this analysis show good agreements with measured data in terms of time-averaged and time-dependent pressure distributions on the surfaces of the turbine blades.

Chen, Y.-S.: Viscous Flow Computations Using a Second-Order Upwind Differencing Scheme. AIAA 88-0417, Jan. 1988.

Chen, Y.- S. and Kim, S. W.: Computations of Turbulent Flows Using an Extended k-ε Turbulence Closure Model. NASA CR-179204, 1987.

Kim, S.-W. and Chen, Y.-S.: A Finite Element Computation of Turbulent Boundary Layer Flows with an Algebraic Stress Turbulence Model. Computer Methods in Applied Mechanics and Engineering, Vol. 66, No. 1, pp. 45-63, Jan. 1988.

N. C. Costes/ED42
(205) 544-1637
Sponsor: Office of Space Flight

Applications of the Fluid Dynamics Analysis Package

The finite-element Fluid Dynamics Analysis Package (FIDAP) has been applied to laminar and turbulent benchmark flows and Space Shuttle Main Engine (SSME) Computational Fluid Dynamics (CFD) problems. A consistent integration penalty finite-element method with biquadratic interpolations (9-nodes) for velocities and linear discontinuous interpolations (3 degree of freedom) for pressure, which is known as one of the optimum choices to handle incompressible flow problems, has been used as a basic algorithm. The streamline upwinding-scheme was necessarily required for the computations of turbulent flows to improve numerical stability of turbulent transport (k-ε) equations.

For benchmark cases, the following problems have been considered: two-dimensional (2-D) incompressible laminar flow inside a wall-driven cavity (Reynolds No., Re = 100 to 10,000); 2-D incompressible laminar flow over a backward-facing step (Re = 100 to 800); and 2-D incompressible turbulent flow over a backward-facing step (Re = 69,610). Computational results have been compared with other finite difference solutions and/or experimental measurements. For SSME-CFD problems, turbulent flows through 2-D and axisymmetric 180-degree turnaround-ducts have been solved and also compared with experimental data (Fig. 97).

Some of these results were presented to the sixth SSME-CFD Working Group Meeting at MSFC.

Sohn, J. L.: Evaluation of FIDAP on Some Classical Laminar and Turbulent Benchmarks. International Journal for Numerical Methods in Fluids, in press, 1988.

Sohn, J. L.: Applications of the Finite Element Method to Some Laminar and Turbulent Incompressible Flow Problems. Sixth SSME CFD Working Group Meeting, NASA/MSFC, April 26-28, 1988.

Sohn, J. L.: Numerical Analysis of Laminar and Turbulent Incompressible Flows Using the Finite Element Method. AIAA Paper 88-3699, 1988.

N. C. Costes/ED42
(205) 544-1637
Sponsor: Office of Space Flight

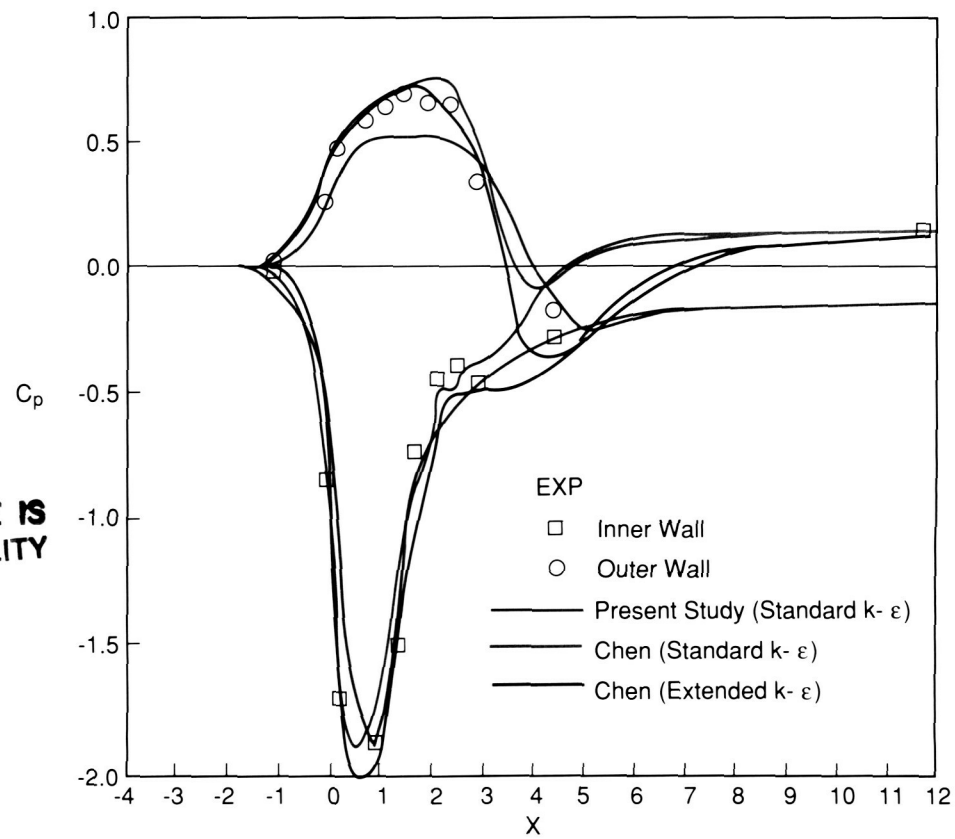

Fig. 97. Comparison of Predicted and Measured Pressure Coefficient of 2-D Turbulent Flow

Impeller Blade/Diffuser Vane Interaction

Unsteady impeller blade and diffuser vane pressures resulting from blade vane interaction have historically been estimated as a percentage of the impeller discharge pressure. The uncertainty of the resulting dynamic loads is large and diffuser vane cracking has occurred during the turbopump development process. The Rotor Force Test Facility at the California Institute of Technology has been utilized to measure unsteady diffuser vane pressures for the Space Shuttle Main Engine (SSME) high pressure oxidizer turbopump (HPOTP) impeller/diffuser and impeller blade unsteady pressures measured on a two-dimensional impeller tested with the SSME HPOTP diffuser.

A diffuser vane showing the location of the pressure taps at midvane height and the geometry of the vane and blade pressure taps is presented in Figures 98 and 99. Unsteady pressure measurements were made at three locations on the blades of the two-dimensional impeller. These pressure taps were located at the blade pressure side (tap radius to impeller discharge radius, $r/R_2 = 0.987$) at the blade suction side ($r/R_2 = 0.937$), and at the blade trailing edge ($r/R_2 = 1.00$).

As expected, the unsteady pressure fluctuations are periodic at the impeller blade passing frequency. On the diffuser vane the largest pressure fluctuations occur on the suction side near the vane leading edge. The magnitude of these pressure fluctuations is on the order of magnitude of the pressure rise across the pump. Pressure fluctuations on the pressure side of the blade are of significantly less magnitude. The magnitude of the largest pressure fluctuations was also found to change substantially as a function of impeller to diffuser radial gap. When the gap width was increased from 1.5 percent to 4.5 percent of the impeller discharge radius, the magnitude of the largest pressure fluctuations decreased approximately 50 percent.

On the impeller vane the largest pressure fluctuations occurred at the impeller trailing edge and were on the same order of magnitude as the pressure rise across the pump. The blade suction side pressure fluctuations were an order of magnitude less than the pump pressure rise, and the pressure side fluctuations were two to three times the suction side. Trailing edge pressure fluctuations increased with decreasing flow coefficient, whereas the pressure and suction side fluctuations were almost independent of flow coefficient.

These experiments have shown, for certain operating conditions, pressure fluctuations on impeller blades and diffuser vanes to be substantially higher than previously estimated. Based on these results, improved predictions of the dynamic loads on these parts can be made for new turbopump designs.

H. P. Stinson/EP62
(205) 544-7077
Sponsor: Office of Aeronautics and Space Technology

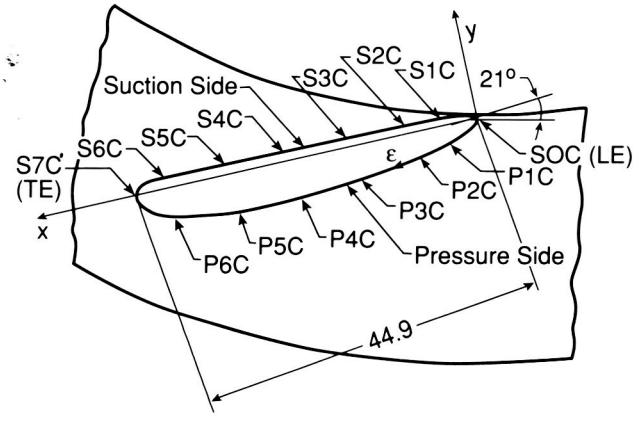

Figure 98. Diffuser Vane Showing Location of Pressure Taps at Midvane Height

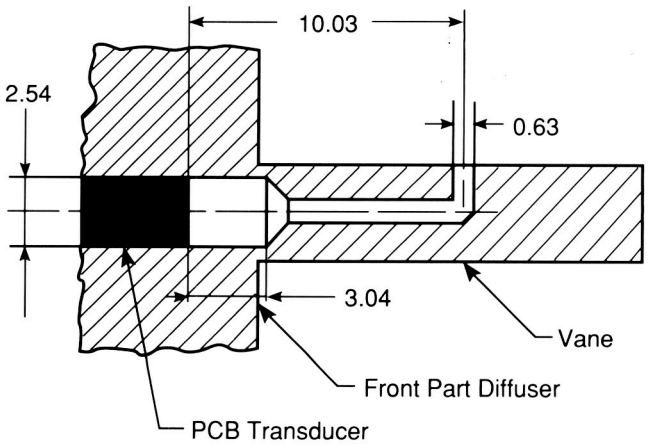

Figure 99. Geometry of Vane and Pressure Taps

Comparison of Finite Element Methods for High Reynolds Number Fluid Flows

A comparative study of velocity pressure integrated and consistent penalty finite element computations of high Reynolds number laminar flows has been made. In both methods, the pressure was interpolated using linear shape functions for a triangular element. The triangular element is contained inside the biquadratic isoparametric element. The pressure interpolation method, when used in the velocity-pressure integrated method, yields accurate computational results for high Reynolds number flows. Use of the same pressure interpolation method in the consistent penalty finite element methods yields, in general, accurate velocity and pressure fields which are comparable to those obtained by using the velocity-pressure integrated methods. However, it was also found that pressure interpolation polynomials of the form (1, x, y) yielded severely distorted pressure contours for the example flow cases (Fig. 100). The accuracy of the two finite element methods has been demonstrated by comparing the computational results with available experimental data and/or fine-grid finite difference computational results. Advantages and disadvantages of the two finite element methods are discussed on the basis of accuracy and convergence nature. Example problems considered include a lid-driven cavity flow for Reynolds number of 10,000, a laminar backward-facing step flow, a laminar flow through a nest of cylinders and a channel flow with an internal blockage. A finite element computer program, NSFLOW/P for the two-dimensional, incompressible Navier-Stokes equations was also developed as a result of this effort. This program employs the consistent penalty finite element method with linear shape functions for pressure interpolation.

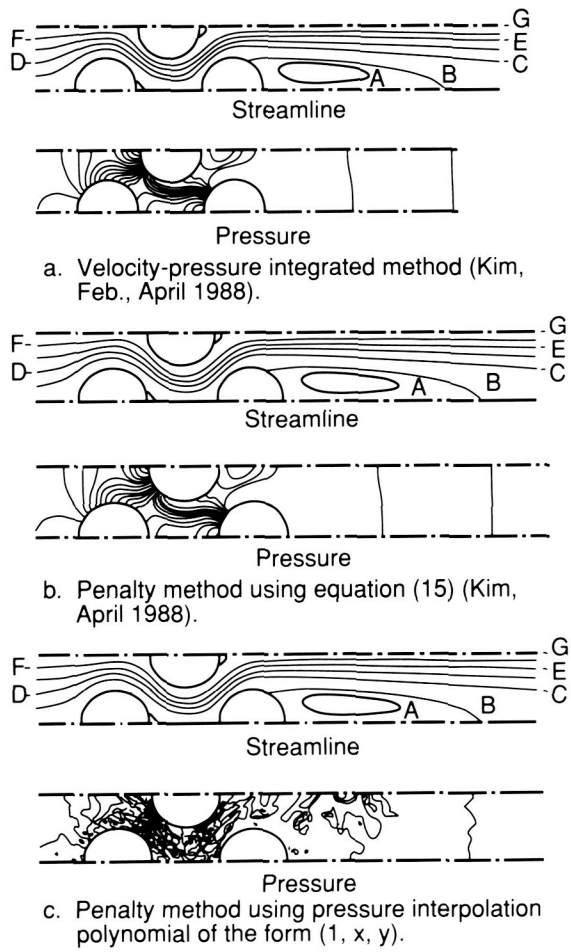

Figure 100. Flow Through a Nest of Cylinders

Kim, S. -W.: Velocity-Pressure Integrated Versus Penalty Finite Element Methods for High Reynolds Number Flows. NASA CR in press, April 1988.

Kim, S. -W.: A Velocity-Pressure Integrated, Mixed Interpolation, Galerkin Finite Element Method for High Reynolds Number Laminar Flows. NASA CR-179264, February 1988.

Kim, S. -W.: A Fine Grid Finite Computation of Two-Dimensional High Reynolds Number Flows. To appear in Computers and Fluids, 1987. Also available as: A Finite Element Computational Method for High Reynolds Number Flows, NASA CR-179135, 1987.

N. C. Costes/ED42
(205) 544-1637
Sponsor: Office of Space Flight

Extended Eddy Viscosity Turbulence Model

In FY88 an extended two-equation eddy viscosity turbulence model was developed and tested. This turbulence model takes into account the effect of an extra time scale (i.e. production range time scale) on the turbulence dissipation rate equation. An additional source term is introduced. A new set of turbulence modeling constants are then identified by matching data of some homogeneous turbulence. Testing of this model against many benchmark boundary-layer type turbulent flows, including fully developed channel and pipe flows, plane jet (Fig. 101), round jet, flat plate turbulent boundary layer flow, etc., has demonstrated the applicability and accuracy of the present model. For complex turbulent internal recirculating flows, including turbulent flows over a backward-facing step, a turbulent confined swirling flow (Fig. 102), turbulent flows inside turnaround ducts, etc., the present model also gives much better results than that of the standard model. In this study, a second-order accurate finite difference Navier-Stokes flow solver has been used.

Chen, Y.-S.: Development of a High Accuracy Finite Difference Upwind Differencing Scheme for Viscous Flow Computations. Fifth Space Shuttle Main Engine Computational Fluid Dynamics CFD Working Group Meeting, MSFC, April 1987.

Chen, Y.-S. and Kim, S.-W.: Computations of Turbulent Flows Using an Extended k-ε Turbulence Closure Model. NASA CR-179204, 1987.

N. C. Costes/ED42
(205) 544-1637
Sponsor: Office of Space Flight

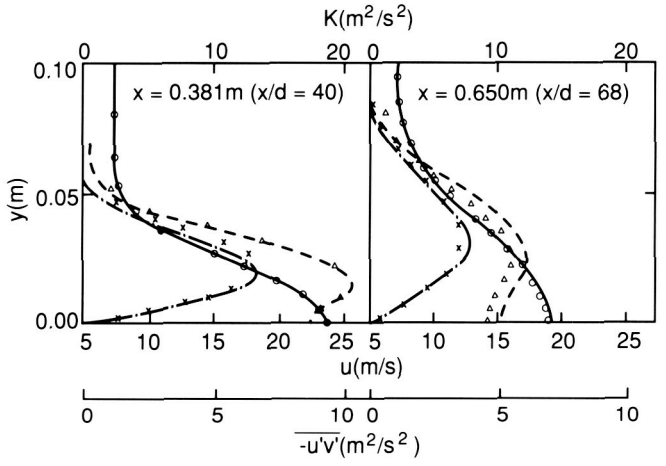

Figure 101. Plane Turbulent Jet Exhausting Into a Moving Stream

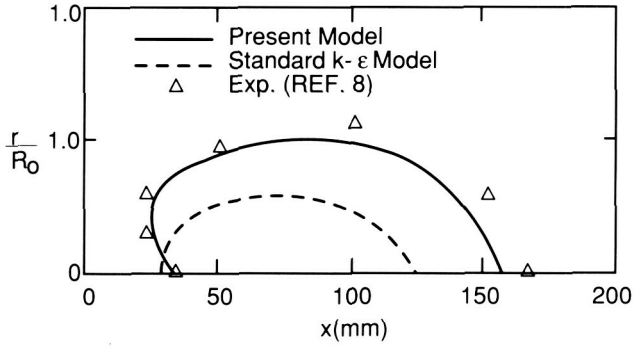

Figure 102. Envelope of Central Recirculation Zone of a Confined Swirling Turbulent Flow

Development of Multiple-Time-Scale Turbulence Models

To simulate complex three-dimensional flow fields in the Space Shuttle Main Engine (SSME), advanced turbulence models which account for nonequilibrium spectral energy transfer mechanism, rotation effects, curvature effects, etc., have to be used. A multiple-time-scale turbulence model of a single point closure and a simplified split-spectrum method have been developed. In this model, the effect of the ratio of the production rate to the dissipation rate on eddy viscosity is modeled by use of the multiple-time-scale and a variable partitioning of the turbulent kinetic energy spectrum. The concept of a variable partitioning of the turbulent kinetic energy spectrum is based on the algebraic stress model. Detailed wall region models including wall-functions, two-layer approaches and low-Reynolds number approaches have also been considered.

Several benchmark cases have been tested: a fully developed channel flow, a plane jet, a wall jet, a wake-boundary layer interaction flow (Fig. 103), two-dimensional backward-facing step, confined swirl (Fig. 104), and non-swirl co-axial jet flows. For SSME-related problems, three-dimensional rotating flows, 180-deg turn-around-duct and 90-deg elbow flows have been tested. The present model has been shown to give much better overall flow predictions compared to conventional single-scale models.

Kim, S.-W. and Chen, C. P.: A Multiple-Time-Scale Turbulence Model Based on Variable Partitioning of Turbulent Kinetic Energy Spectrum. NASA CR-179222, also AIAA paper-88-0221, AIAA J., submitted, 1988.

Kim, S.-W. and Chen, C. P.: A Two Layer Multiple-Time-Scale Turbulence Model and Grid Independence Study. Int. J. Numerical Method in Fluids, submitted, 1988.

N. C. Costes/ED42
(205) 544-1637
Sponsor: Office of Space Flight

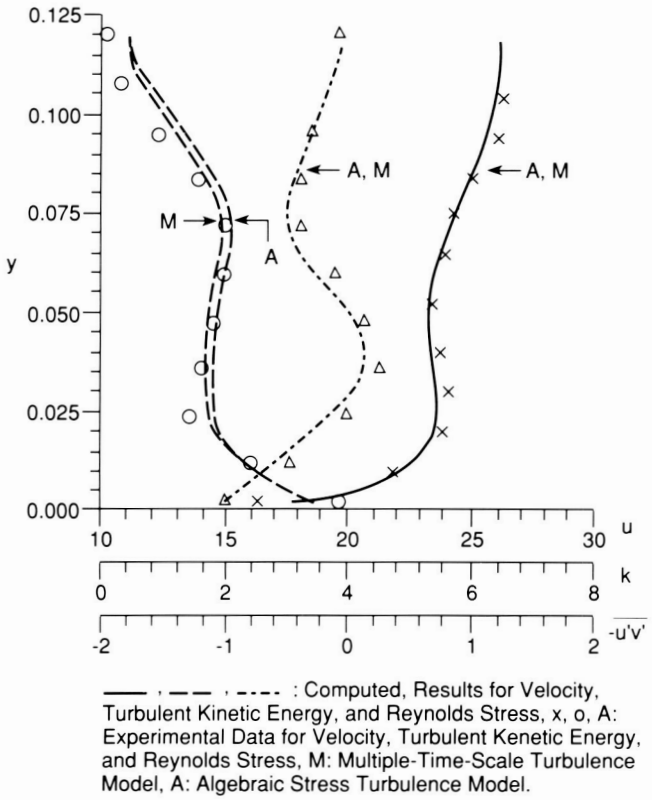

Figure 103. Wake-Boundary Layer Interaction Flow

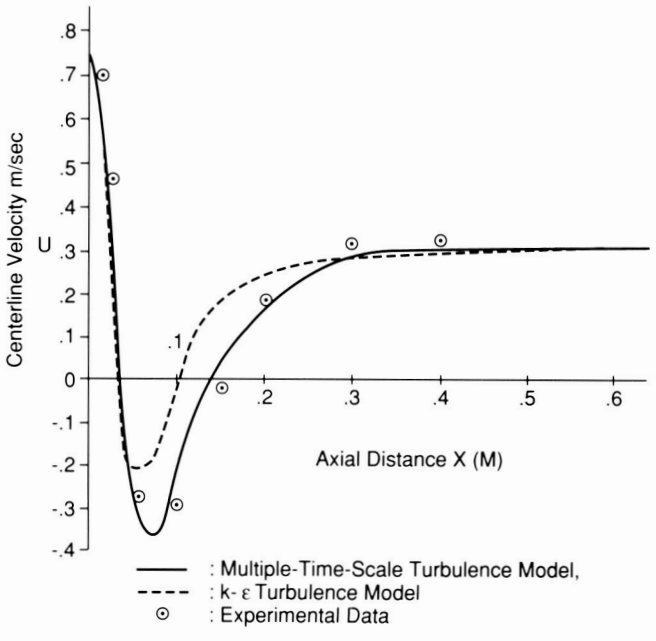

Figure 104. Confined Coaxial Swirling Jet Showing Development of Mean Axial Velocity Along Center Line

Mixed-Interpolation, Finite-Element Method for High Reynolds Number Laminar Flows

A velocity-pressure integrated, mixed-interpolation, Galerkin finite element method for solving incompressible fluid-flow problems using the Navier-Stokes equations has been developed. In this method, the velocity variables are interpolated using complete quadratic shape functions and the pressure is interpolated using linear shape functions. For the two-dimensional case, the pressure is defined on a triangular element which is contained inside the complete biquadratic element for velocity variables; and for the three-dimensional case, the pressure is defined on a tetrahedral element which is again contained inside the complete triquadratic element. Thus the pressure is discontinuous across the element boundaries. Example problems considered included: a cavity flow for Reynolds numbers of 400 through 10,000; a laminar backward-facing step flow; and a laminar flow in a square duct of strong curvature (Fig. 105). The computational results compare favorably with

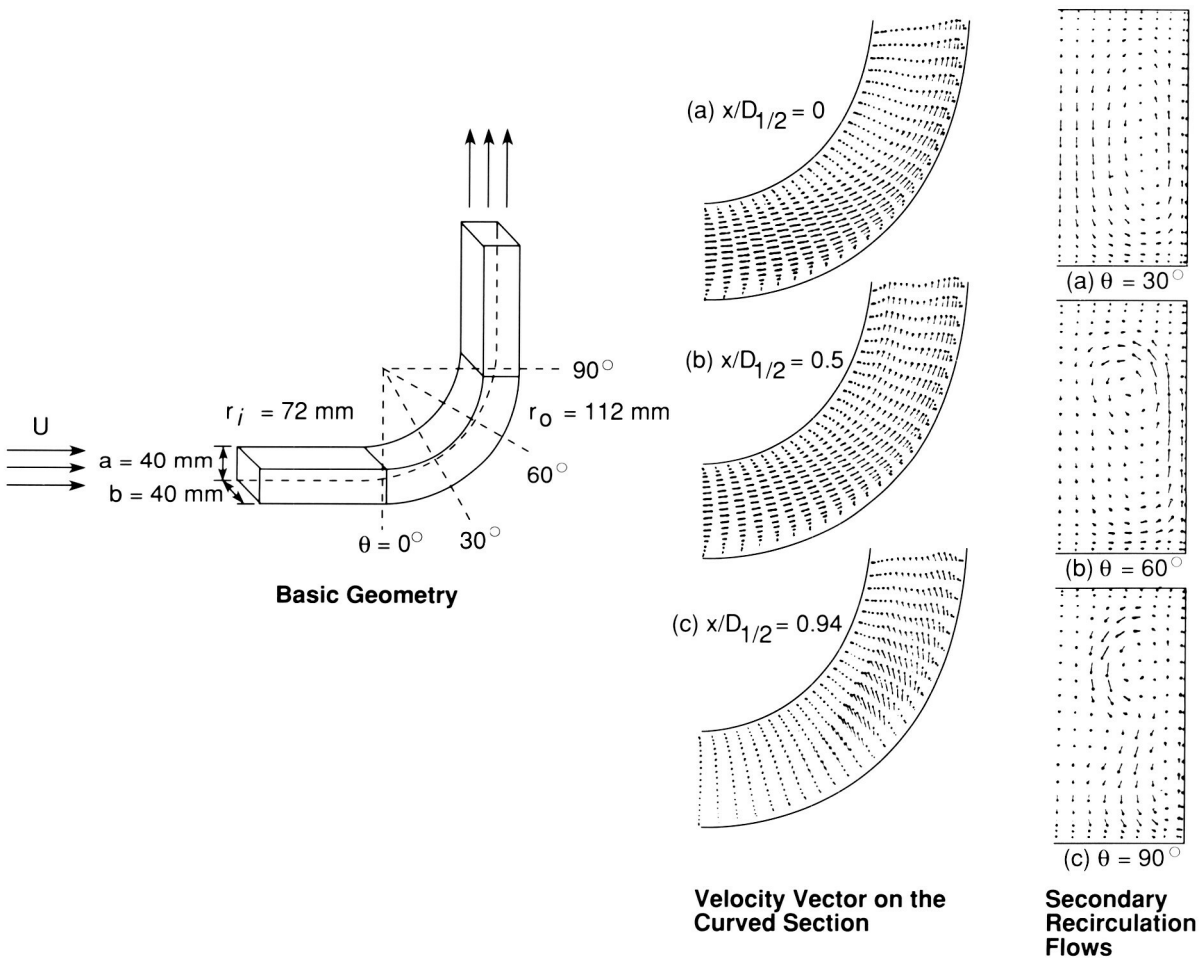

Figure 105. Laminar Flow in a Duct of Strong Curvature

those of finite difference methods as well as experimental data available. In addition, it was found that the present method can capture the delicate pressure driven recirculation zones, yields accurate velocity and pressure distributions for the problems considered, and requires many fewer grid points than the finite difference methods to obtain comparable computational results. A finite element computer program (NSFLOW/L) has also been developed and is available for incompressible, laminar flows of the class considered in this effort.

Kim, S.-W.: A Velocity-Pressure Integrated, Mixed Interpolation, Galerkin Finite Element Method for High Reynolds Number Laminar Flows. NASA CR-179264, February 1988.

Taylor, C. and Hughes, T. G.: Finite Element Programming of the Navier-Stokes Equation. Pineridge Press, Swansea, U.K., 1980.

Kim, S.-W.: A Fine Grid Finite Element Computation of Two-Dimensional High Reynolds Number Flows. Computers and Fluids, in press, 1988.

N. C. Costes/ED42
(205) 544-1637
Sponsor: Office of Space Flight

Algebraic Stress Turbulence Model

A finite element computational procedure for turbulent boundary layer flows and an algebraic stress turbulence model have been developed. The finite element method is based on the semidiscrete Galerkin finite element method, the convergence nature of which has been reported previously (Kim and Payne, 1985). The algebraic stress turbulence model used in the present study can be characterized by the following three aspects: firstly, the eddy viscosity expression has been derived from the Reynolds stress turbulence model; secondly, the turbulent kinetic energy dissipation rate equation has been improved by including a production range time scale; and lastly, the diffusion coefficients for turbulence equations have been adjusted so that the kinetic energy profile extends further into the free stream region which can be found in most experimental data. Example problems considered include: a fully developed channel flow, a fully developed pipe flow, a flat plate boundary layer flow, a plane jet exhausting into a moving stream, a circular jet exhausting

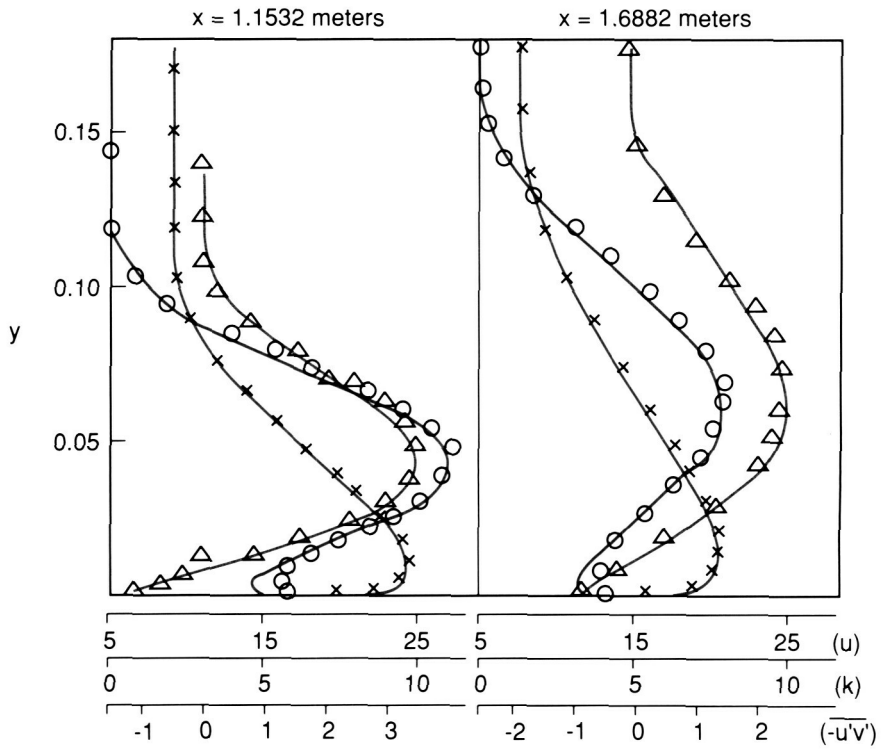

Figure 106. Wall Jet Flow

into a moving stream, and a wall jet flow. Computational results compared favorably with experimental data for most of the example problems considered. Comparison of the same computational results with the results obtained using finite difference methods and the standard k-ε turbulence model indicates that significant improvements have been accomplished by the method reported herein for the jet flow and the wall jet flow (Fig. 106). The rest of the cases show that the computational results from all methods are comparable.

Kim, S.-W. and Chen, Y.-S.: A Finite Element Computation of Turbulent Boundary Layer Flows With an Algebraic Stress Turbulence Model. Computer Methods in Applied Mechanics and Engineering, Vol. 66, No. 1, pp. 45-63, J. L.

Kim, S. -W. and Payne, F. R.: Finite Element Analysis of Incompressible Laminar Boundary Layer Flows. Internat. J. Numer. Meths. Fluid, Vol. 5, pp. 545-560, 1985.

Chen, Y. -S. and Kim, S. -W.: Computation of Pathological Turbulent Flows Using an Extended k-ε Turbulence Closure Model. J. AIAA, in press, 1988.

N. C. Costes/ED42
(205) 544-1637
Sponsor: Office of Space Flight

Turbine Blade/Tip Seal Force Interaction — "Alford" Forces

The only known published test results on turbine blade tip clearance forces, sometimes referred to as "Alford" forces or clearance excitation forces, are those obtained from the test program conducted at the Technical University of Munich (TU of M). The test results indicate the measured forces are significantly larger than the predicted values. Direct correlation of the test results with the predicted destabilizing forces in the Space Shuttle Main Engine (SSME) turbines, however, are difficult to ascertain because of the difference in operating conditions and geometry of the test and the SSME hardware. The SSME turbopumps appear to be more stable than predicted by the TU of M test results. This may be due to the presence of direct damping which theoretical and experimental results do not substantiate. It is, therefore, imperative that a comprehensive investigation be initiated to better define the forces generated at the turbine blade tip seal interface.

The overall objective of this effort is to generate the necessary database from which a reasonably accurate model for predicting the turbine blade tip seal clearance excitation forces in the SSME turbopumps may be obtained. The first step taken to initiate this investigation was the work required under the original contract, NAS8-35018. Included in this effort was a thorough review of literature on turbine blade tip seal clearance excitation forces, the development of an analytical model for predicting these forces for both shrouded and unshrouded turbine blades, and the definition of a test program for measuring stiffness and damping coefficients. The next step was to design, fabricate, and checkout a test article and facility to measure the turbine blade tip seal force interactions. This was accomplished by an extension to the original contract. The third and final phase is the actual empirical investigation of "Alford" forces.

The first phase of this effort has been completed and completion of Phase II, namely, the design, fabrication, and checkout of the test article and facility is nearing completion. The Massachusetts Institute of

Technology has responded to the procurement request for the third and final phase with a proposal. It is anticipated that the actual empirical investigation will begin in FY88.

The test facility (Figs. 107 and 108) and test article, now nearing completion, will be used to investigate the level of "Alford" forces within the SSME high pressure turbomachinery. The empirical results will be used to adjust the analytical model to provide a more accurate tool to be used to predict these destabilizing forces within the SSME turbopumps and other similar machines.

G. E. Wilmer, Jr./EP62
(205) 544-7115
Sponsor: Office of Aeronautics and Space Technology

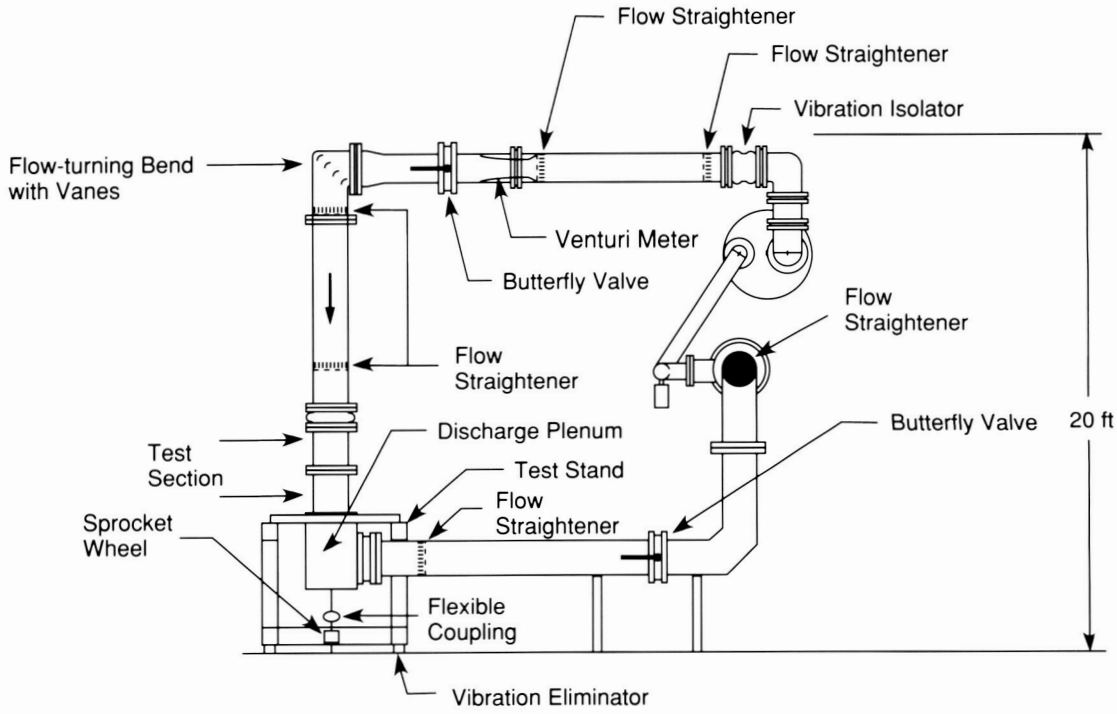

Figure 107. Front View of the Test Facility

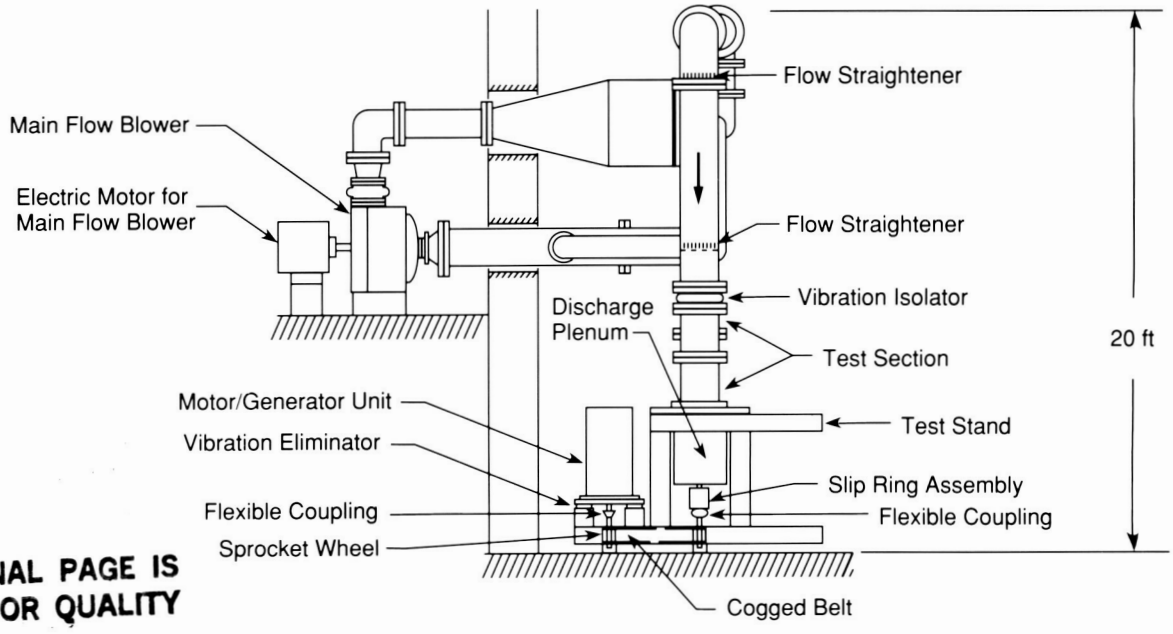

Figure 108. Side View of the Test Facility

Nickel-Based Superalloy Microstructure Enhancement

Microstructure tailoring was investigated as a means of optimizing the properties of a nickel-based superalloy, MAR-M246 (Hf). This alloy was chosen for study because the Space Shuttle Main Engine (SSME) turbine blades are comprised of this material. Various microstructures were created in the laboratory with the use of a directional solidification furnace constructed of three separate cores, each controlled independently. Both temperature gradient and solidification growth rate were varied for each set of specimens directionally solidified. These specimens were then machined and high-cycle fatigue tested (HCF).

Comparisons of HCF test results and the microstructure suggest a correlation between the microstructure and HCF performance. One microstructure in particular had significantly longer life than any of the other three microstructures tested. This superior microstructure was characterized by small and well dispersed faceted (blocky-type) carbides, small primary dendrite arm spacings, and no gamma-gamma prime eutectic islands. Another similar microstructure created in the laboratory also had small, well dispersed block-type carbides, and small dendrite arm spacings. However, this microstructure did contain gamma-gamma prime eutectic islands. These results would suggest that the eutectic phase can be instrumental in HCF performance.

Results also indicated that the microstructure with small block-type carbides and small dendrite arm spacing had approximately twice the HCF life of a microstructure containing large script type carbides and large dendrite arm spacing. Both these microstructures contained eutectic.

Further research is planned with the use of a highly sophisticated computer-controlled directional solidification furnace with roughly 24 zones, each controlled independently. This additional research should aid in the transferral of laboratory research technology to private industry.

Efforts are now underway to secure a Joint Endeavor Agreement between NASA and a commercial casting house. This endeavor will attempt to control the resulting SSME turbine blade microstructure through the solidification process. The end result should be a turbine blade with prolonged life.

Comparisons were also made between HCF data supplied from specimens processed with a cluster of SSME blades and the superior laboratory microstructure. The laboratory microstructure's fatigue life was 10 to 100 times greater. Because the clustered specimens were cast with the blades, it was not surprising to find that the microstructure was very similar to that found in the fir-tree area of the SSME turbine blades. Both had microstructures containing large, script-type carbides and numerous large gamma-gamma prime eutectic islands.

Schmidt, D. D., Alter, W. S., Hamilton, W. D., and Parr, R. A.: The Effects of Temperature Gradient and Growth Rate on the Morphology and Fatigue Properties of MAR-M246(Hf). To be published as a NASA Technical Memorandum.

D. D. Schmidt/EH22
(205) 544-4943
Sponsor: Center Director's Discretionary Fund

Computer Controlled Scanning/ Optically Stimulated Electron Emission Surface Contamination Measurements

Computer controlled contamination scanning (CONSCAN) is a system developed by MSFC utilizing the optically stimulated electron emission (OSEE) technique for scanning solid rocket motor (SRM) cases for surface contamination prior to critical bonding operations.

The CONSCAN system has the principal advantages of providing the sensitivity and spacial resolution necessary when scanning large areas, to ensure that surfaces are sufficiently free of contaminants that reduce bond strength.

Scanning the surface with the CONSCAN provides a map of surface contamination levels, which clearly identifies those areas that require further cleaning; rescanning after the additional cleaning operation provides results of that recleaning. This data provides a permanent record of surface cleanliness levels. This record may be used at a later date to help identify the specific process during which contamination occurred and to correlate surface cleanliness levels with subsequent debond locations.

Principle of operation of the OSEE may be briefly described as follows. When a surface is exposed to ultraviolet (UV) light of sufficient energy, photoelectrons will be released from the surface. Contaminants on the surface will normally reduce the number of these photoelectrons which are emitted. The OSEE sensor has two major components: the electron UV light source and the electron collector. The photoelectron current emitted from the irradiated surface is measured by the electron detector. This current can be calibrated to the contaminant level on the surface.

The technique as applied to measuring contaminants on surfaces was developed and reported by Tennyson Smith in April 1975. He demonstrated both the sensitivity of the technique to contaminant level and bond strength variation due to contamination.

The technique with MSFC support was utilized on the External Tank foam debond study in 1979. This technique was instrumental in identifying the surface contaminant causing debonds as silicone which originated from simultaneous processing of other hardware in the same building.

Since the original instrument configuration in 1979, significant OSEE instrument improvements have been implemented, including increased signal amplification, noise filtering, higher output UV light sources, compact sensor configurations, and computer data analysis.

MSFC initiated a study of the SRM debonds associated with propellant liner insulation to case, and the carbon and glass phenolics used in the nozzle. Research studies determined that the corrosion protective HD-2 grease used on the SRM case has a significant effect on bond strength. Quantitative levels that affect bond strength and associated OSEE signal levels were determined by extensive laboratory testing. This calibration data was incorporated in the design, development, and implementation of the CONSCAN system.

J. M. Zwiener/EH12
(205) 544-2528
Sponsor: Space Shuttle Solid Rocket Booster Office

Weld-Bead Profile Control and Inspection

When welding the Space Shuttle External Tank, defects that occur are generally easily detected by observing the shape of the solidified weld bead. Similarly while welding, the operator keeps a close watch on the weld-bead to be sure that the process is under control. Since a large proportion of the labor involved in the welding and inspection of welds on the tank is related to measuring the joint and weld-bead geometry, automating this process has the potential of large cost savings.

Due to recent advances in the technology of computer vision, a television camera in conjunction with a structured laser light source has been developed to measure the joint geometry automatically. Use of a system as described will allow the joint to be measured more quickly and at closer intervals than are presently possible by any manual method. The measurement device (Fig. 109) is attached to the same motive system as the welding torch. It performs the inspection as the weld is being made, saving the time required to set up a manual inspection process, or time taken between weld passes to arrange for an appointment with inspection personnel. The system, equipped with a print-out device, would not require manual entry of inspection data which is the present practice. This system will be able to assist in the alignment of panels to be welded, help verify preweld joint fitup, and allow inspection of interpass bead geometry and post-weld joint geometry.

A prototype measurement system has been set up at MSFC and has demonstrated that it can measure the bead geometry. Computer software has been developed that analyzes the solidified bead and enacts controls on the welding equipment to maintain the proper bead shape.

Sensor control of the welding process promises to reduce welding defects and the cost of inspection.

C. S. Jones/EH42
(205) 544-2701
Sponsor: Office of Space Flight

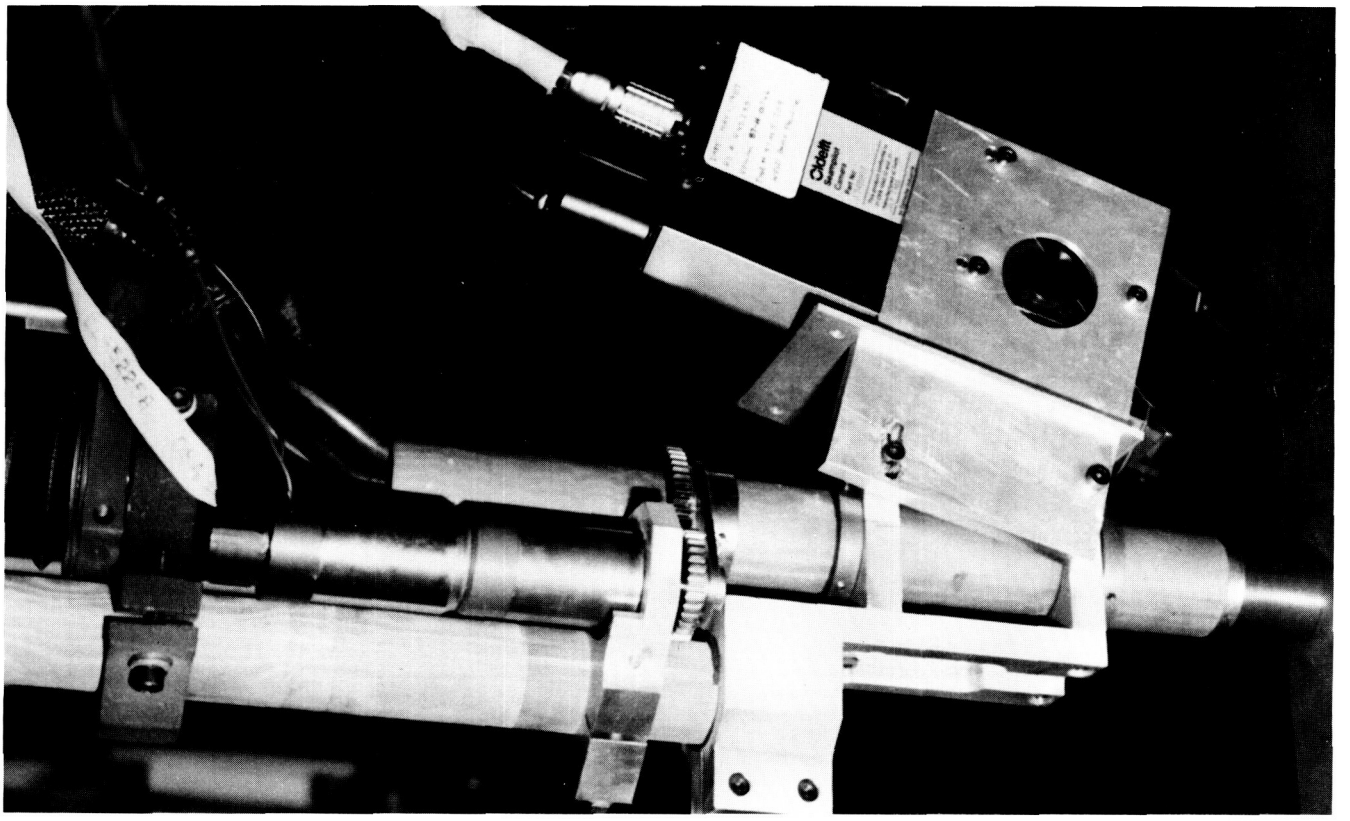

Figure 109. Weld Bead Inspection Device

ORIGINAL PAGE
BLACK AND WHITE PHOTOGRAPH

Gas Tungsten Arc Welding Torch with Integral Vision System

An automatic means of correcting preprogrammed paths for robotic arc welding is mandatory for increasing production rates while maintaining quality. A vision-based system, originated by Ohio State University (OSU) under NASA contract, is being applied to gas tungsten arc welding of Space Shuttle Main Engine (SSME) components. The optical system provides a magnified view of the weld seam and molten puddle by way of a combination of lenses and filters built into the torch body. With the optical path coaxial to the welding electrode, maximum visual information can be obtained in the smallest possible package. The latter is extremely important for engine fabrication, because the weld joint is often tucked into a relatively inaccessible location. Several prototype versions of the custom welding torch have been developed, with the latest version providing a working envelope similar to standard machine welding torches.

A sectional view of the vision torch is shown in Figure 110. The inert gas injection ring, developed in the original OSU laboratory torch, is a unique method of providing excellent flow of argon to protect the weldment from oxidation. A further advance of this design is that the optical components are self aligning, facilitating use in a factory environment.

The charge-coupled device sense head at the top of the package relays a video image to the processing computer and to a video monitor. An electronic light valve developed by MSFC for computer control of camera exposure levels accommodates the changes in arc light intensity resulting from pulsing the weld current. Thus the system can be used for both automatic path correction and remote monitoring by humans.

One version of the vision system torch is presently being tested in the production of SSME flight hardware. Welds are being monitored and videotaped, and these stored images are processed off-line to perfect automatic seam tracking algorithms.

C. Kurgan/EH42
(205) 544-2705
Sponsor: Office of Space Flight

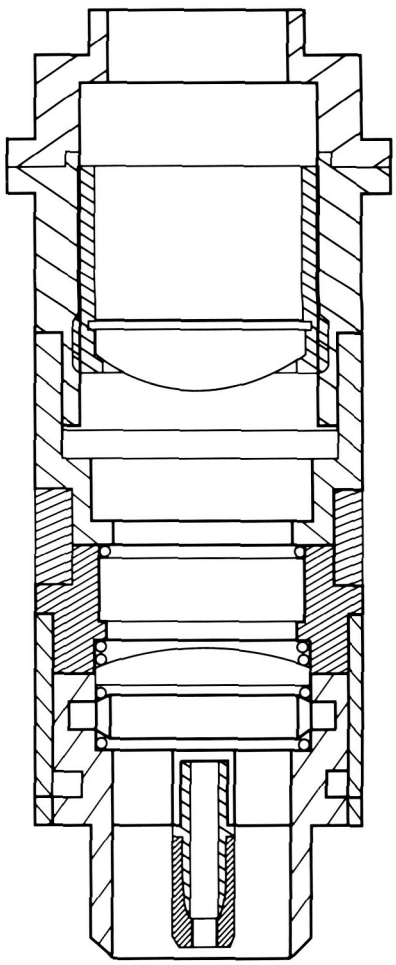

Figure 110. Sectional View of Gas Tungsten Arc Welding Torch

Quick Disconnect Torch for Robotic Welding

Robotic gas tungsten arc (GTA) welding has been implemented into the manufacturing of the Space Shuttle Main Engine at the Rocketdyne production facility. This application for robotics is unique in that strict aerospace weld quality requirements are maintained on one-at-a-time production parts. In fact, each production weld requires a unique set up for weld torch, robot path, and tooling. To enhance productivity, set up times have to be minimized. Offline programming and universal tooling concepts are being developed to address the latter two set up problems. To eliminate delays due to weld torch set up, a quick disconnect GTA torch has been designed and fabricated through a joint development effort between NASA and on-site Rocketdyne engineers.

The quick disconnect torch (Fig. 111) draws on concepts developed in the machining industry, where cutting tools are loaded and unloaded automatically. Complicating factors unique to a weld torch are the necessity of accommodating a power lead, shielding gas lines, and water cooling lines. The weld torch must be light weight and compact to achieve accessibility and maintain robot accuracy capabilities. These requirements were met using standard components where possible.

The power lead and water and gas lines utilize standard quick connectors. The welding power is transferred through the torch bracket by a copper contact. The torch bracket is light-weight aluminum with slides and set screws for last minute fine adjustments of all three axes. The torch is positioned in a tooling set point fixture to assure correct orientation of the tungsten. The robot moves to the tooling fixture and automatically grips the torch tooling. The pre-programmed weld path can then be executed.

This quick disconnect torch concept is currently undergoing acceptance and durability tests at MSFC. Modifications, if needed, will be incorporated in the next generation production quality GTA torch prior to introduction into manufacturing at Rocketdyne.

C. Kurgan/EH42
(205) 544-2705
Sponsor: Office of Space Flight

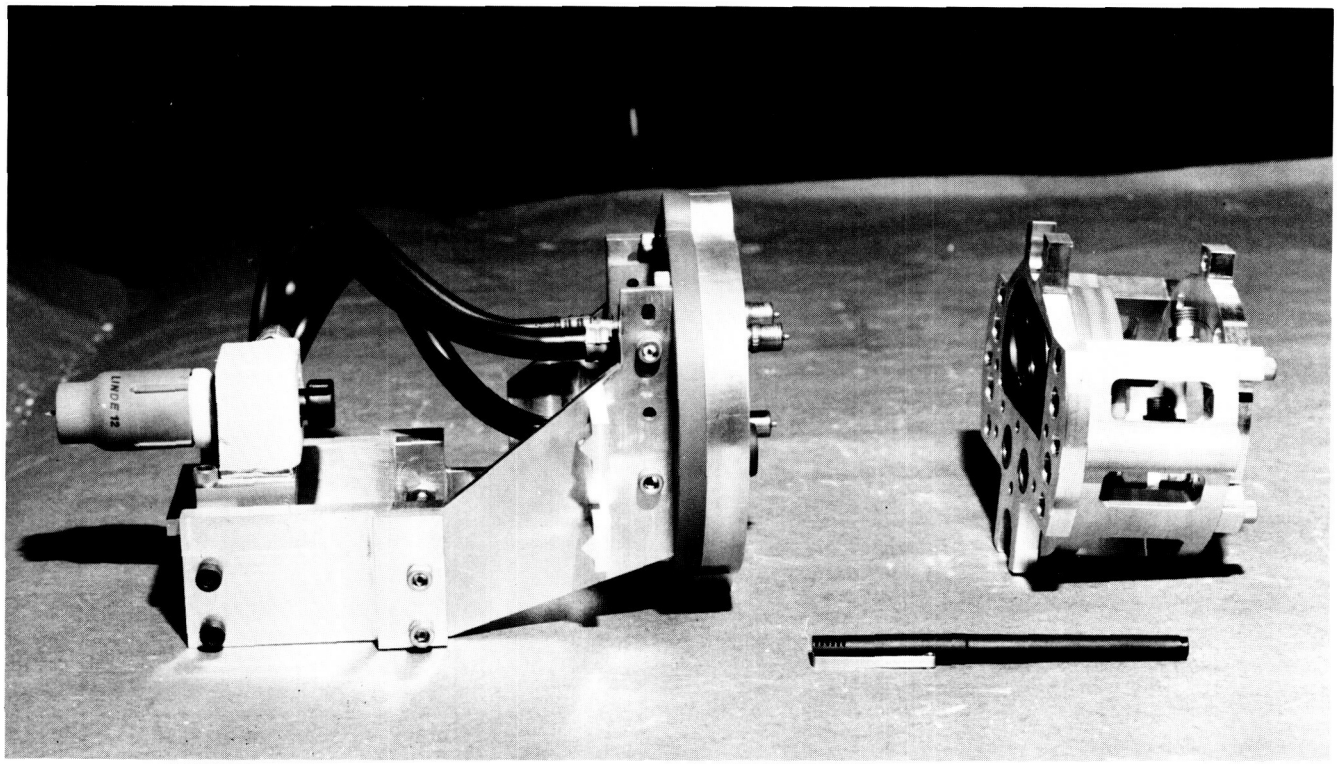

Figure 111. The Quick Disconnect Torch

Weld Process Modeling

A lumped parameter mathematical model of the Variable Polarity Plasma Arc (VPPA) welding system is being developed with two objectives in mind: to better understand the system and so pave the way for parameter optimization for improved weld quality and for possible improvements in configuration design, and to provide the means for an automatic control system to operate the VPPA system in a mode that requires optimal control of multiple system parameters.

The model is to relate VPPA system control parameters to weld-bead geometry and weld-bead geometry plus additional parameters (such as weld speed) to an estimated weld strength.

The system is characterized by 16 temperatures, 6 of which are determined by the design or parameter settings (for example, gas influx temperatures) and others requiring computation (for example, electrode tip and orifice inner wall temperatures), 7 fluxes (gas, current, and coolant flows as well as torch travel speed) all fixed by the control system, and 18 dimensions, 10 of which are fixed by the design and 8 of which are weld-bead dimensions which are to be computed.

At present a skeleton model with heat flows proportional to temperature drops has been written, and work is proceeding to fill in actual computations.

A. C. Nunes/EH42
(205) 544-2699
Sponsor: Office of Space Flight

Radiographic Straight-Line Indications in 2219 Aluminum Weldments

X-rays of welds in the Space Shuttle External Tank (ET) sometimes show fine, sharp, black lines, somewhat broader white lines, and combinations of black/white lines at the edge of the weld fusion zone. Ultrasonic evaluation of these welds reveals no ultrasonic echo, and, until recently, these indications were not associated with any known weld structural feature. Straight-line indications (SLI's) strongly resemble radiographic indications from a lack of fusion or lack of penetration defect.

MSFC has undertaken an investigation of the SLI with the objective of explanation of the origin and metallurgical characterization, duplication in the laboratory, and assessment of any possible detrimental effects and recommendations for prevention.

After several years of study the SLI was duplicated. The SLI is a filament of copper segregation with associated microporosity and/or copper depleted material adjacent to the segregation (copper produces a light line, while associated microporosity or copper depleted material produces a dark line). Figure 112 shows the cross section of an artificially produced pair of SLI's in a completed weld. SLI's are produced by laying a cover-bead over surface segregation in a trough (Fig. 113) such that the surface segregation in the trough is remelted but not dispersed. A thin layer (.001 in) of surface segregation appears to be common on the surface of weld-melted 2219 aluminum.

Troughs can be produced using several techniques. Depending upon material thickness, two techniques were used to produce the troughs for our SLI's. For .375 inch material, we welded vertically up, with excessive torch-to-work distance (as the sample in Fig. 112). For .800 inch material, we used a slight torch offset from the weld centerline within a surface preparation groove. A cooler than normal cover pass completed the operation in both material thicknesses.

These procedural variations are common enough in welding so that the origin of SLI's in production is not mysterious.

The effects of SLI's upon weld properties are still under investigation. To date, only minor property reductions (believed already included in mechanical property development statistics) have been attributed to SLI's.

A. C. Nunes/EH42
(205) 544-2699
Sponsor: Office of Space Flight

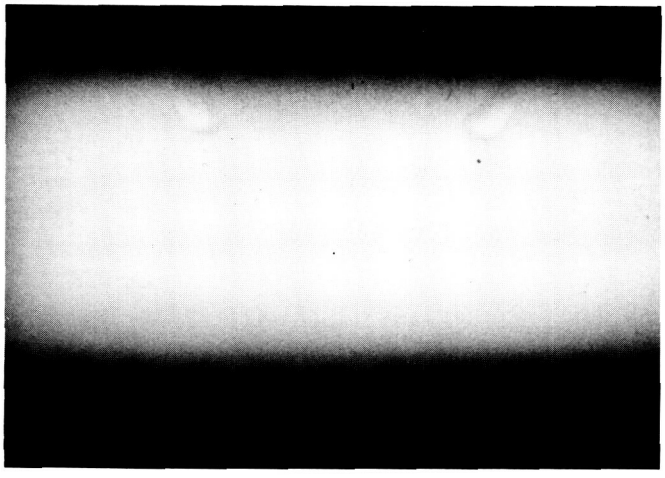

Figure 112. Cross Section of .375 Inch Thick 2291 Aluminum Weldment Showing Weld Structure Responsible for SLI

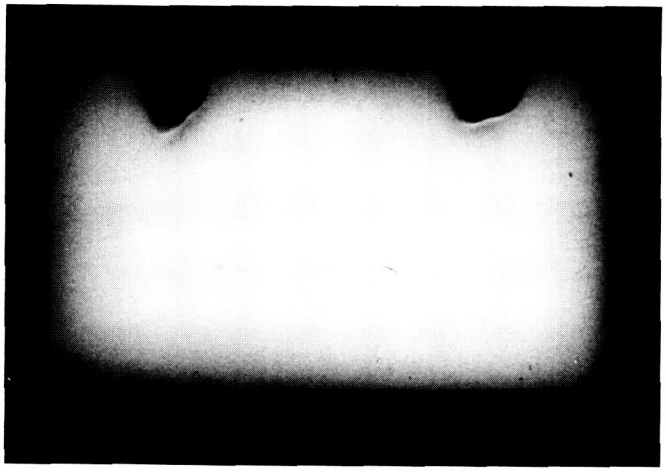

Figure 113. Weld Cross Section Showing Troughs with Thin Layer Segregate

Carbon/Glass-Phenolic Processing Cure Model

A computer math model is being developed by MSFC and Morton Thiokol, Wasatch Division, to describe the physical and chemical phenomena of curing carbon/glass-phenolic laminates for processing rings on the solid rocket motor nozzle.

As can be seen from Figure 114, the computer math model will be able to make *a-priori* determinations regarding changes in material properties due to process and material variations with any part configuration. Thus, optimum material and process parameters can be determined for any nozzle part.

The model is based upon the SINDA heat transfer program, with considerable effort involved in modeling other physical phenomena within the available user subroutines. In these subroutines separate submodels are used to describe the exothermic chemical reactions, viscosity, resin flow, diffusion, and flow compaction. The model also includes the capability of generating color contour plots showing the change of properties throughout the part during cure (Fig. 115).

The computer-aided cure model incorporates numerous math models. Based upon the computer prediction of the degree of cure, viscosity, volatile concentration, resin content, and residual stresses and strains, the material properties versus position in the part can be determined. Subsequent performance characteristics of the material in a rocket motor environment can then be correlated with these predictions. The submodels will be verified using data from standard physical tests of preimpregnated and cured material.

Verification of the thermal and reaction kinetic model has been completed. Predicted temperatures at the center of the part compare very well with the measured data. A three-reaction model was needed to predict exothermic and viscous effects apparent in the experimental data. The kinetic portion of the model is also required for predicting viscosity. This model

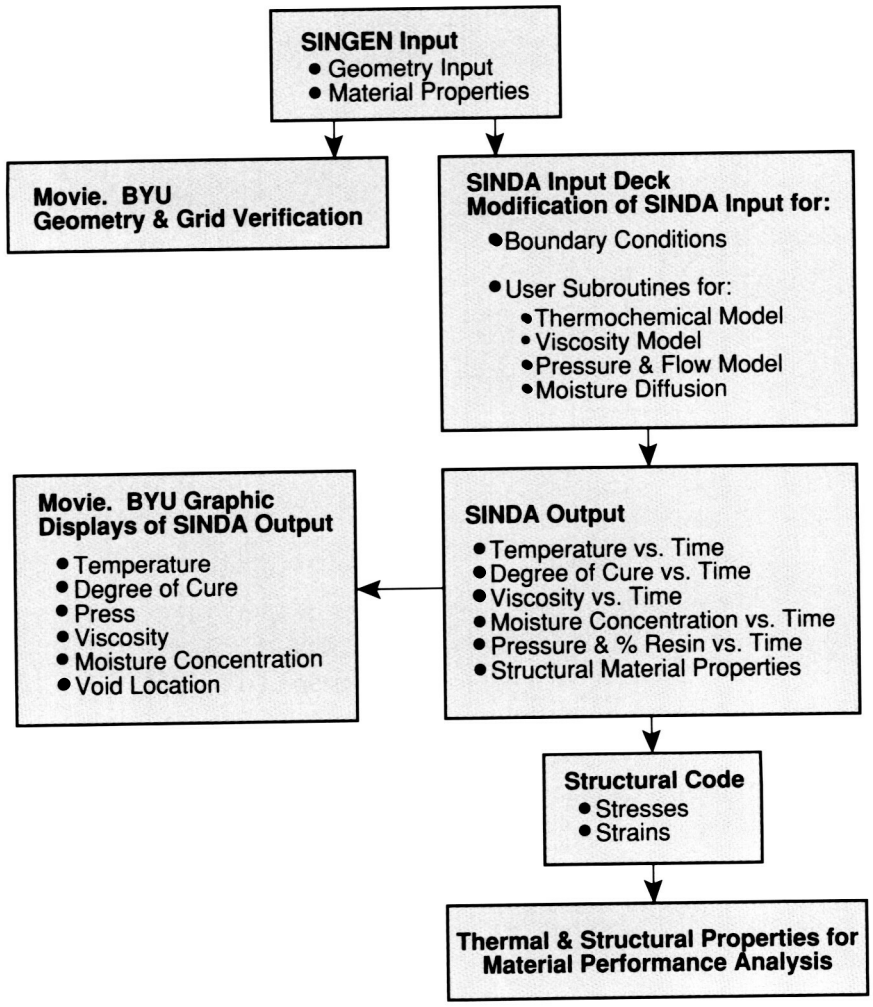

Figure 114. Computer Aided Process Model Development for Carbon Phenolic Material

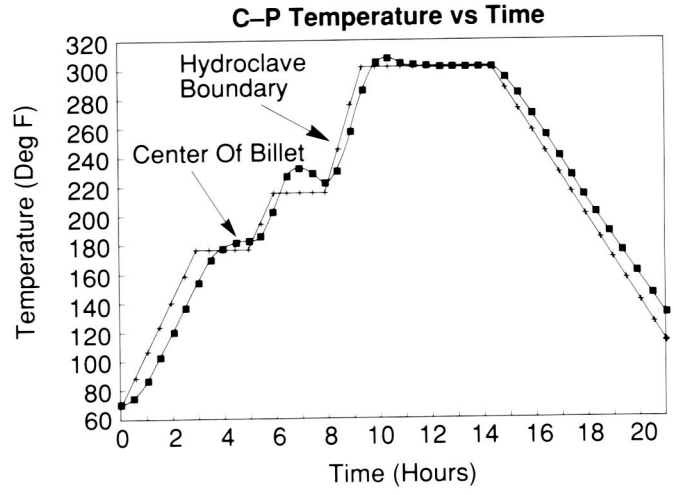

ORIGINAL PAGE
CO[illegible]

Figure 115. Nose Ring Second Wrap Grid

ORIGINAL PAGE
COLOR PHOTOGRAPH

has been achieved and is in the process of being verified for hydroclave and autoclave-processed components.

The computer model is being verified and correlated by modeling the simulated section of a 504 inlet ring in the nozzle. Many panels have been fabricated using different cure cycles, and the data have been analyzed and compared with predictions using the computer math model. Submodels for the heat transfer, thermochemical reaction kinetics, viscosity, and moisture concentration have been completed. A considerable effort will be required to complete the submodels of resin flow and stress and strain.

The model has been used to analyze several SRM nozzle rings during cure, including the SRM nose ring, throat ring, and aft exit cone. Results of these analyses are being used to determine if alternative cure cycles could be used to improve the integrity of the parts and to determine allowable deviations from the cycle.

Correlation and verification of the viscosity and moisture diffusion submodels is being made. Panels are to be cured to different points of the same cure cycle, and the panels cut and tested to determine actual values of these parameters, as well as volatile concentration, resin content and degree of cure.

W. R. Colberg/EH43
(205) 544-2725
Sponsor: Office of Space Flight

Foam Applications Development

Formulation development of polyisocyanurate (PIR) foam systems for use on the Space Shuttle External Tank (ET) was initiated at MSFC in FY87. Development of a PIR molding foam has been undertaken in-house because it is not consistently available from vendors. In-house formulations have shown definite promise, although further development will be necessary before one or more of the foams will be qualified for ET use. These foams will be formulated specifically for use in the reaction injection molding equipment being put into production use at the Michoud Assembly Facility.

A state-of-the-art formulation laboratory is being designed. It will be used for pour and spray foam formulating as well as foam processing equipment development.

An investigation is underway to develop foam processing equipment designed specifically for ET use. Development of an improved spray gun is being investigated because of the additional control needed when spraying specific areas of the ET in automated development activities. This effort is managed under a separate task designed to investigate the development of a foam spray delivery system which will have capabilities for automated control and will incorporate improvements not available on the commercial market. Due to different thickness requirements needed in different areas of the tank, variable outputs are needed to spray foams to minimum thickness requirements at close tolerances and process and material optimization requirements.

The present spray-on foam insulation (SOFI) spray booth is presently being upgraded with a state-of-the-art environmental control system, a computerized SOFI control system, and an advanced technology data acquisition system to help the research engineers develop better processing methods.

J. B. Thaxton/EH43
(205) 544-2786
Sponsor: Office of Space Flight

Tape-Laying Machine Development Software

A Cincinnati Milacron tape laying machine has been installed in the MSFC Productivity Enhancement Facility and will be fully operational this year. This state-of-the-art system is utilized to develop advanced composite tape-laid parts for the Shuttle, Space Station Freedom, and future programs. In support of this system, software has been developed to provide composite engineers with an end-to-end automated environment for creating composite parts. This unique software environment consists of several commercial packages and specially developed programs working together in a VAX 11/780 computer. The tape-laying machine software consists of four packages: University Computing Company's Automatically Programmed Tool (UCC APT), and a preprocessor (ACRAPATH), post-processor (ACRAPOST) and graphics package (ACRAGRAPH), purchased from Cincinnati Milacron. Software has been developed in-house to allow input of complex surface geometries through the use of Computer Vision and Intergraph computer-aided design systems. The composites engineer inputs the part geometry and ply parameters into the ACRAPATH preprocessor, which optimizes the placement of courses of tape on the part and produces APT source code. The APT code is compiled and the resulting cutter location file is post-processed, generating a part program containing machine instructions for the tape-laying machine. The part program is loaded into the tape-laying machine controller and the optimized part is produced. The tape-laying machine development software can be used to evaluate composite parts in an off-line mode. The ACRAGRAPH software enables detailed evaluation of parameters such as tape gap and fiber orientation. Figure 116 is an ACRAGRAPH plot of the gap between adjacent tape plies as function of course length. This software also provides the capability of looking at the overall geometry of the part surface with the tape courses indicated, as shown in Figure 117. This software provides the composites engineer with a comprehensive tool for developing composite parts without the knowledge of programming languages. The ACRAGRAPH package allows for part optimization on an off-line basis, thus minimizing material waste during part development.

E. Martinez/EH43
(205) 544-2724
Sponsor: Office of Space Flight

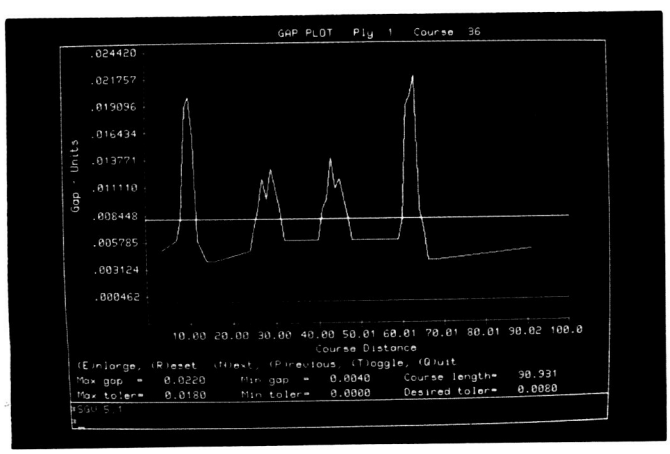

Figure 116. Tape Gap Versus Course Length

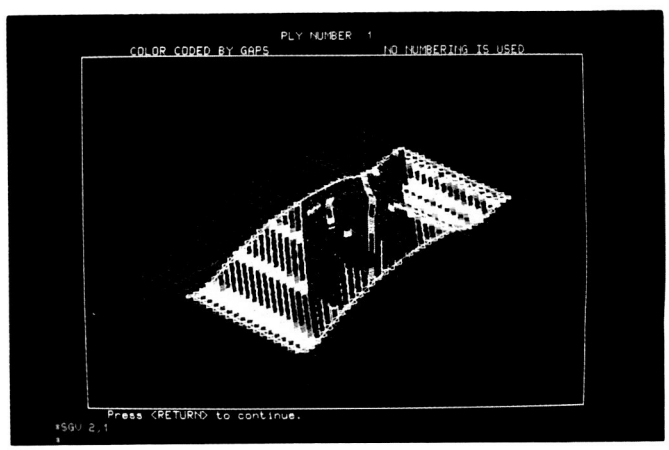

Figure 117. Overall Part Geometry

ORIGINAL PAGE
COLOR PHOTOGRAPH

Metallized Kevlar Space Tether System

The primary objective of the metallized Kevlar space tether system program is to replace a conventional conductive space tether construction (i.e., Kevlar filament for strength and copper wire for electrical conductivity) with metal-coated Kevlar, which will then serve as both the strength member and the conductive member of the tether.

To date, the optimum metal coating is a 1-μm copper coating on Kevlar 49 (1420 denier) with a light nickel overcoat to prevent oxidation of the copper. Electrical resistance of 0.3 ohm/ft has been achieved for one multifilament tow of Kevlar at this level of coating. Insulating polymeric coatings of Teflon FEP, Teflon PFA, and Tefzel have also been successfully extruded over the metal-coated Kevlar.

Past testing has shown that the metal coating does not degrade the physical properties of Kevlar and actually improves resistance to self-abrasion. Testing has also indicated that the metallized tether holds up well in vacuum and to nominal low earth orbit atomic oxygen influences. Samples with a Nomex overjacket indicated degradation of the Nomex by atomic oxygen.

Demonstration tethers of 1,000-ft length were fabricated of braided, metallized Kevlar. Some of these had only the overjacket of Nomex while some had an insulating Teflon layer over the metallized Kevlar.

M. R. Carruth/EH12
(205) 544-7647
Sponsor: Small Business Innovation Research Program

Corrosion Studies of Painted Metals Using Alternating Current Impedance

The alternating current impedance technique is a relatively new method for studying corrosion mechanisms, and has been under development for the past few years. This method has the advantage, as compared to the more widely used direct current methods, that only small alternating current signals are necessary, and the method is more sensitive and can be applied to relatively thick coats of paint or other materials on metal surfaces. A suitable equivalent circuit model has been developed for the study of primer-topcoat combinations and for a suitable means for obtaining corrosion rates of metals with the ac impedance method.

A model which was found to be suitable for these purposes is shown in Figure 118, and its physical description in Figure 119. For primer-topcoat combinations, the unit on the right side of Figure 118 becomes the metal-primer unit, and that on the left the primer-topcoat unit. Contributions from a pos-

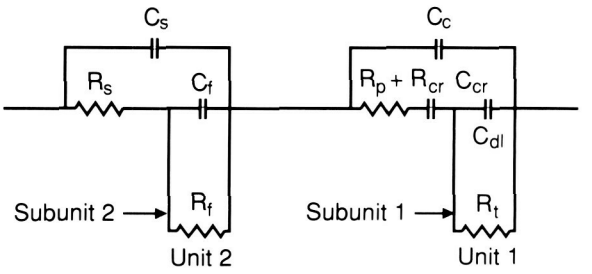

C_S	Solution Capacitance
R_S	Solution Resistance
C_f	Faradaic Capacitance (Coating/Solution)
R_f	Faradaic Resistance
C_c	Coating Capacitance
$R_p + R_{cr}$	Coating Resistance + Chemical Reaction Resistance
C_{dl}	Metal/Coating Interface Capacitance
R_t	Charge Transfer Resistance
C_{cr}	Chemical Reaction Capacitance

Figure 118. Circuit Representing Alternating Current Impedance Response for Primer Coated and Primer Top-Coated Steel

sible topcoat-solution unit are negligible in this case. The addition of the capacitor C_{CR}, shown in the metal-primer unit of Figure 118, allows the determination of corrosion rates. The corrosion rate varies linearly with value of this capacitor. When properly calibrated, the hypothesis assumes that the capacitor value should be proportional to the corrosion current, and hence the corrosion rate, in all cases.

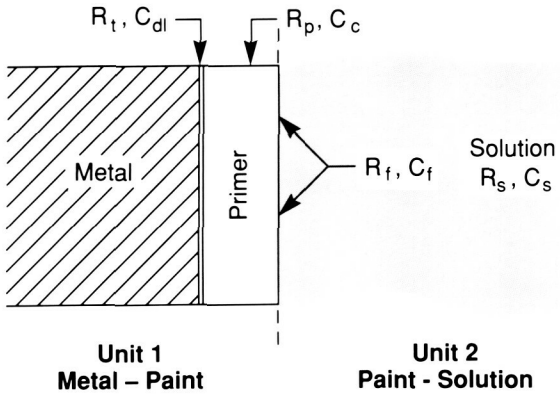

Figure 119. Physical Description of Circuit Parameters for Coated Steel

A least squares procedure which results in a fit of the theoretical Bode Magnitude data (Log |Z| versus log W, where |Z| is the absolute magnitude of the ac impedance vector and W=2π multiplied by the frequency) to the observed data has been developed, and gives the properly refined values of the various parameters shown in Figure 118. The method has been successfully applied to a study of 4130 steel coated with zinc-rich primer and epoxy-polyamide topcoat, the paint system currently used on the solid rocket boosters of the Space Shuttle transportation system, as well as to a red-lead oxide primer and epoxy-polyamide topcoat system, which was studied for comparison. It was found that there is little difference in the corrosion protection afforded by both systems and that the coating thicknesses presently being applied are adequate.

Mendrek, M. J., Higgins, R. H., and Danford, M. D.: An Electrochemical Study of Corrosion Protection by Primer-Topcoat Systems on 4130 Steel with ac Impedance and dc Methods. NASA Technical Paper, in press.

M. D. Danford/EH24
(205) 544-2612
Sponsor: Office of Space Flight

Replacement Bearing Using Alternate Self-Lubricating Retainer Materials

One of the life-limiting components of the Space Shuttle Main Engine (SSME) is the high pressure oxidizer turbopump (HPOTP) bearings. One of the major factors that limits bearing life is wear due to an apparent lack of lubrication. LOX coolant essentially provides no lubrication, so any lubrication of the present bearings is derived from the initial dry film lubricant applied to the raceways and balls prior to assembly or from the transfer of dry film from the cage to the ball and thus the raceways.

Current and past research on the present Armalon cage, which is a fiberglass reinforced polytetrafluorethylene (PTFE) material, indicates that this material provides only a very limited amount of lubrication initially. Once the initial lubricant has been removed, the glass fibers of the laminate material become exposed and act as an abrasive. Thus, the transfer of dry film, PTFE, to the balls is being removed and some lapping of the underlying metal by the abrasive action of the glass fibers is taking place. In order to improve the performance of the bearing, a new bearing cage design is needed. This new design must provide enhanced transfer film lubrication, low ball abrasion, adequate cage strength, and operate within the same size envelope to minimize retrofitting time and cost.

The main objective of this effort is to design, fabricate, and deliver to MSFC replacement bearings using a bronze filled PTFE, SALOX-M, cage material as an alternate to the current Armalon cage material. Laboratory test data suggest that a considerable improvement in lubrication can be achieved with a material such as SALOX-M provided the necessary strength requirements are met. Three candidate designs have been considered: a laminate design, a ribbed design, and an insert design. The insert design was selected as the most promising. Figures 120 and 121 depict a typical insert configuration. SALOX-M will be the insert material and the cage housing will be made of a suitable high strength

metal, such as phosphor bronze or a Monel metal. Other issues such as how to anchor the inserts and the intricate machining required for the cage-housing are currently being evaluated. When the bearings are delivered, they will be incorporated into the MSFC bearing/seal materials tester for design evaluation. Successful completion of this evaluation will lead to incorporating the design into the SSME Technology Test Bed engine program for further performance evaluation.

J. L. Cannon/EP62
(205) 544-7072
Sponsor: Technology Test Bed

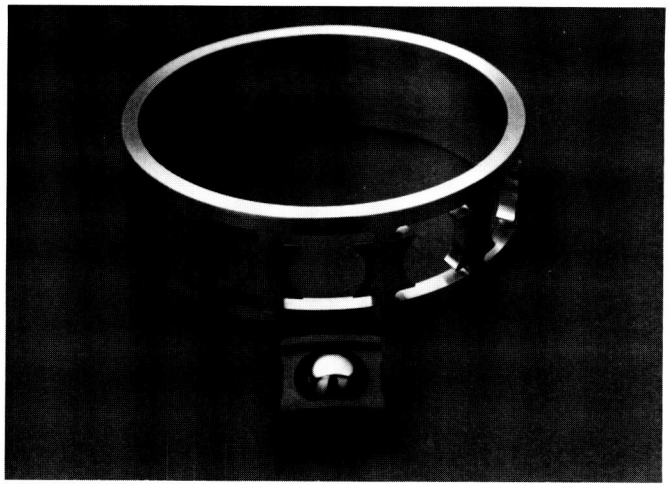

Figure 120. Metallic Retainer with SALOX-M Inserts

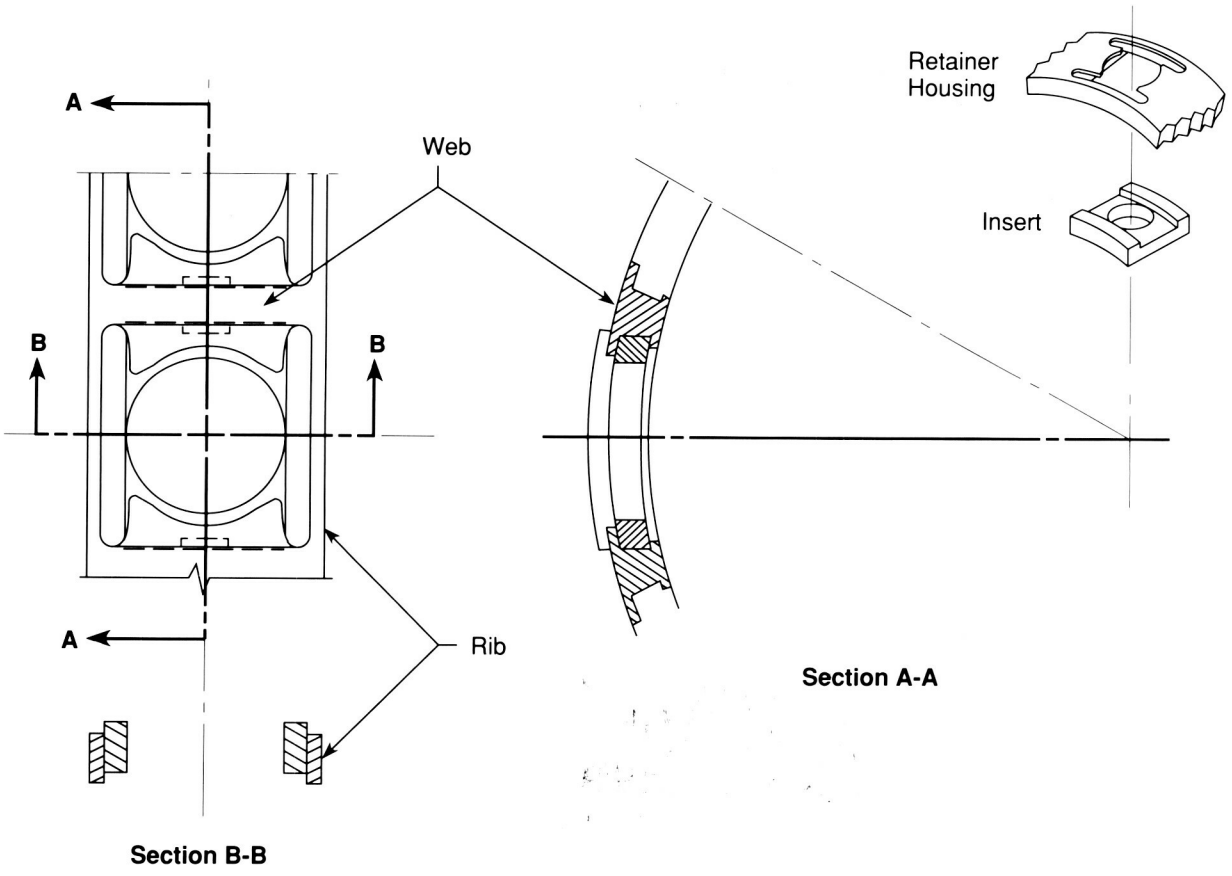

Figure 121. Cross-Section of Metallic Retainer

Quick Turnaround Bearing Tester

The Quick Turnaround Bearing Tester is a cryogenic single bearing tester that was devised to evaluate the performance of one Space Shuttle Main Engine (SSME) high pressure oxidizer turbopump (HPOTP) pump end bearing. The tester was developed because the SSME HPOTP main shaft bearings are not meeting their life requirements of 55 successive flights and 7.5 hours between engine overhauls. In order to meet the life requirements, an improved bearing configuration (i.e. an improved bearing design and/or an improved bearing material) is needed. The Quick Turnaround Bearing Tester was developed so that comparative screening tests of potentially improved bearing configurations could be performed in a timely manner using a simple, easy to manage test setup versus the baseline design.

The bearing tester was designed and built in-house at MSFC. The basic tester consists of a 304 stainless steel bearing housing mounted on a modified heavy duty Walker Turner drill press. The inner race of the bearing is press fitted on a drill press arbor adapter, and the outer race is mounted in the bearing housing. The bearing is loaded axially by way of a simple dead weight loading mechanism. The tester is designed to use either liquid nitrogen or liquid oxygen as the bearing coolant.

The test parameters of the tester include: test of one HPOTP pump end 45 millimeter bearing, with a variable coolant flow rate, (.12 lb/sec nominal), up to 500 lb axial load on inner race, rotated at 10,000 rpm, and all under variable coolant subcooled conditions.

The tester is instrumented to measure the coolant inlet temperature, the coolant outlet temperature, the coolant flow rate, the bearing outer race temperature, and the change in pressure across the bearing. A heat exchanger is used in the coolant supply line to create and control the cryogenic fluid subcooling conditions. During testing, an IBM AT computer and a Fluke Helios data acquisition system are used to control and monitor the tester.

T. R. Jett/EH14
(205) 544-2514
Sponsor: Office of Aeronautics and Space Technology

Structures and Dynamics

Unobtrusive Vibration Sensor and Effector

With the development of large space structures, a more unobtrusive means to sense and damp vibrations has become a necessity. Previous means of sensing and damping vibrations in large space structures have added significant weight and additional dynamics to the structures. Utilizing polyvinylidene fluoride (PVDF) film as a vibration sensor and as a means to damp vibrations, it is possible to achieve the goal of having an unobtrusive vibration sensor and vibration damper.

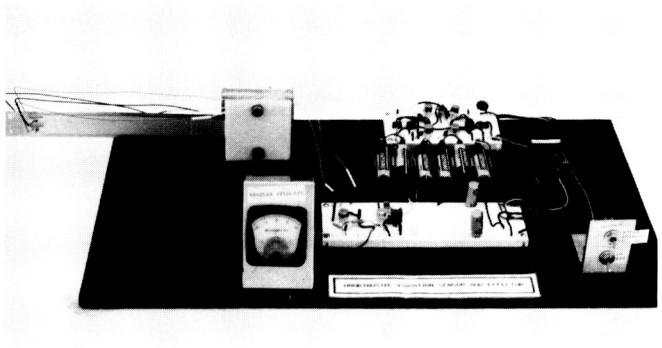

Figure 122. Unobtrusive Vibration Sensor and Effector Breadboard

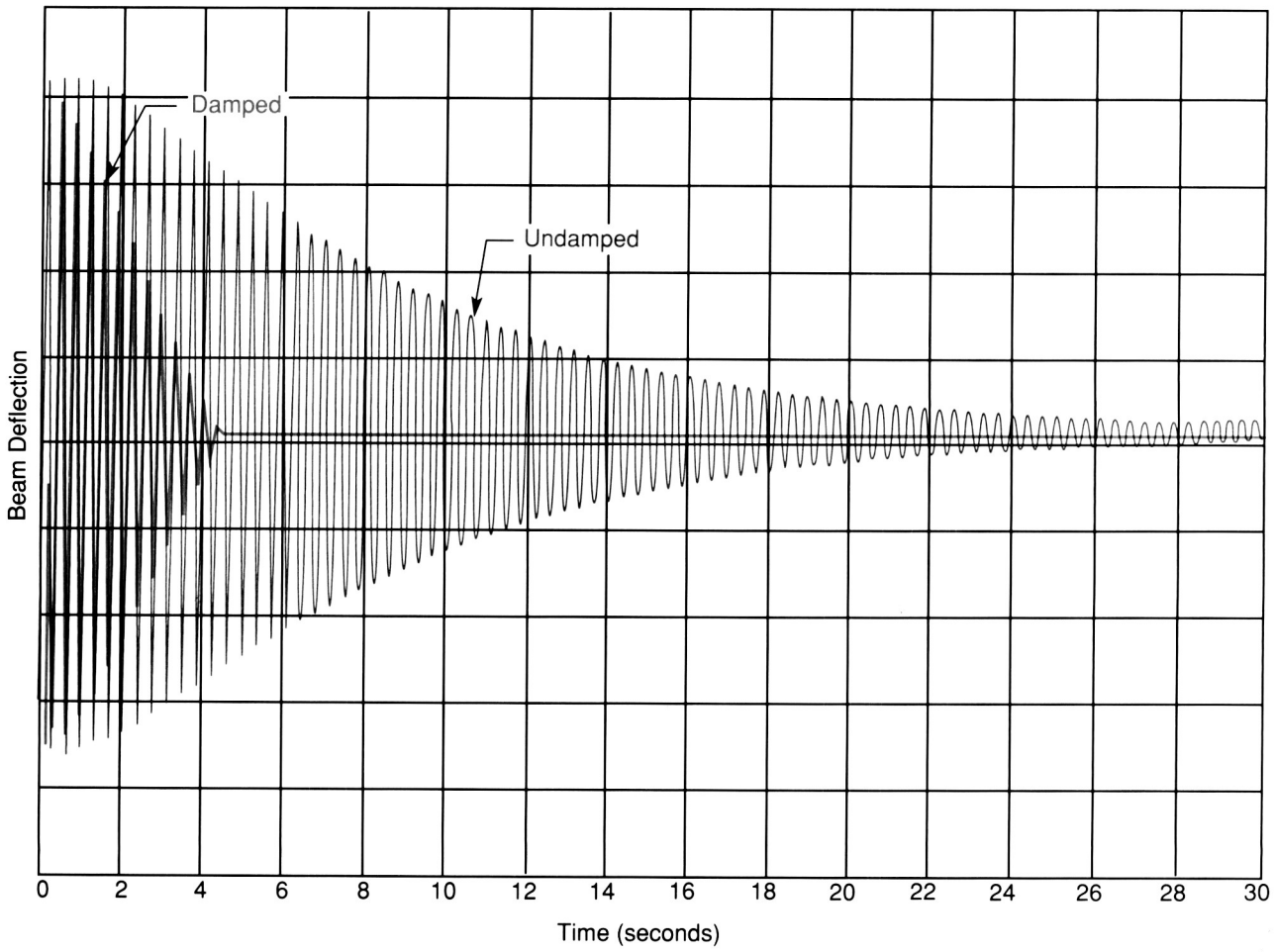

Figure 123. Breadboard Test Results

ORIGINAL PAGE
COLOR PHOTOGRAPH

A laboratory breadboard (Fig. 122) was developed at MSFC to demonstrate PVDF film effectiveness in sensing and damping vibrations in a small cantilever beam. The beam used in the breadboard was a piece of aluminum with dimensions of 0.020 inches thick by 1 inch wide by 8 inches long. A strip of PVDF film was epoxied to one side of the beam to measure angular velocity, and a second strip of PVDF film was epoxied to the other side of the beam to act as the effector. Electronics were then designed to read the angular velocity from the PVDF film sensor and apply the appropriate signal to the PVDF film effector to damp the vibrations. Tests utilizing this breadboard revealed the effectiveness of the PVDF film as an unobtrusive sensor and effector (Fig. 123).

Further development plans include upgrading this technology to larger structures, and the development of a breadboard robotic end effector which will make the required electrical connections, when grasping a payload, to sense and damp vibrations in a beam as it is moved from one location to another.

D. E. Howard/EB24
(205) 544-3517
Sponsor: Office of Aeronautics and Space Technology

External Tank — Spray On Foam Insulation Kinematic Simulation System

The External Tank (ET)–Spray On Foam Insulation (SOFI) Research Cell in the Productivity Enhancement Facility is utilized to develop and qualify SOFI materials for use as part of the Thermal Protection System on the ET and other Space Shuttle flight hardware. The foam is sprayed by a Cincinnati Milacron T3 robot on test panels mounted on a cylinder rotating on a 14-ft air bearing turntable. A kinematic simulation system is being developed to model the operations within the spray booth.

The simulation system consists of a Silicon Graphics IRIS Model 3120 workstation running UNIX, C, and a special graphics software package known as IGRIP from DENEB Robotics, Inc. This state-of-the-art graphics system provides three-dimensional solid representations of the cell and allows real-time manipulation of these objects. A model of the SOFI spray cell has been completed (Fig. 124). The robot link values and cycle time are displayed and updated real-time by simulation. This system will detect and alert the operator when the robot arm has reached its

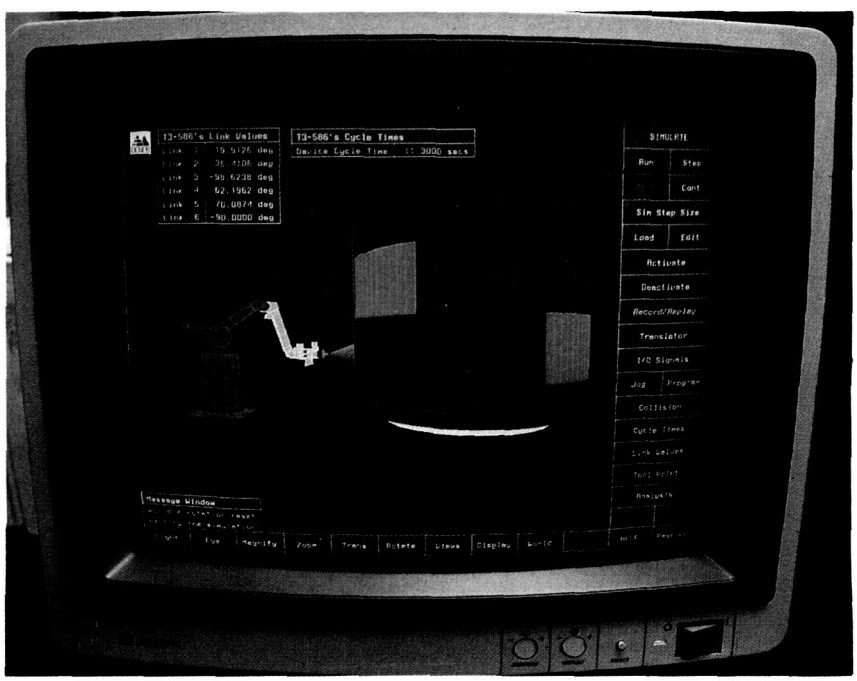

Figure 124. Model of the Spray On Foam Insulation Research Cell

travel limits or when there is an impending collision between the robot and turntable. Perspective views help to orient and enhance the observation of the process as it would appear in the work cell. Robot coordinates are optimized off-line on the workstation, translated, and converted into robot-compatible form and downloaded via a RS-232C communications link to the robot (Fig. 125).

Future work planned for this system includes the capability to spray complex parts, such as cones, requiring variable foam application rates to maintain uniform thickness. Another enhancement planned is the addition of flowrate parameters to the simulation to allow setting and controlling foam spray rates and thickness. The kinematic simulation system off-line programming capability results in cost savings to the government in two ways. First, it minimizes wasted material by optimizing spray parameters off-line. Second, spray programs can be developed on the work station without interfering with operations in the ET-SOFI Spray Cell.

E. Martinez/EH43
(205) 544-2724
Sponsor: Office of Space Flight

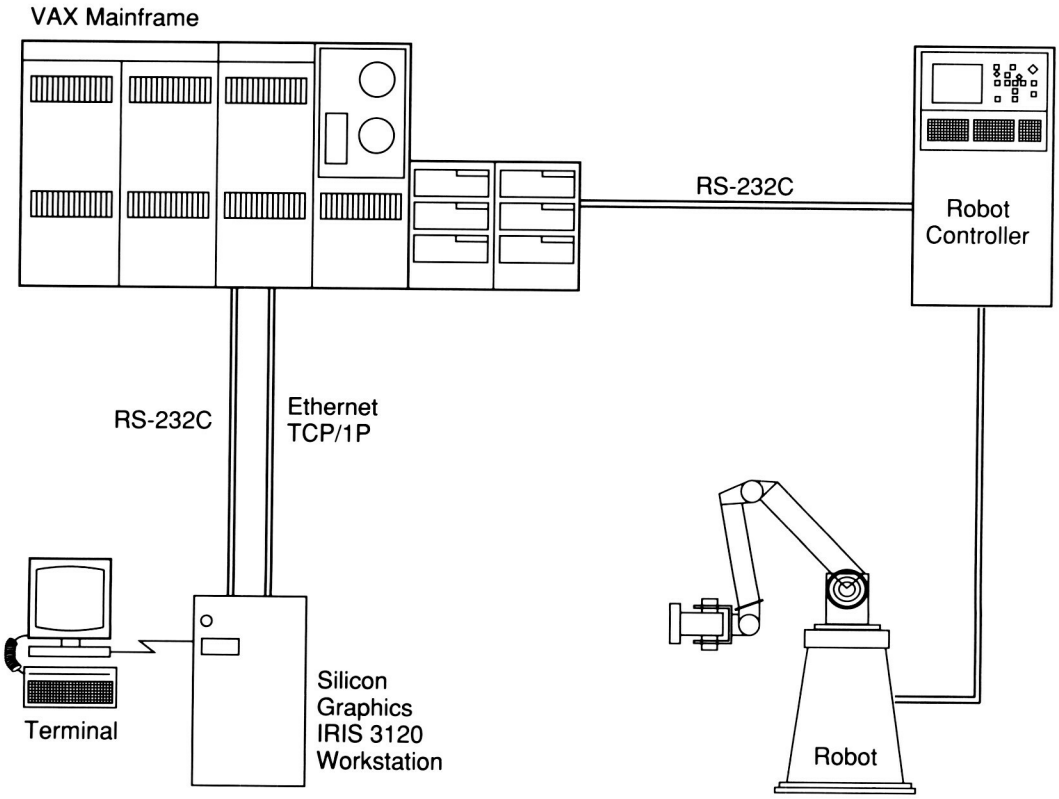

Figure 125. Kinematic Simulation Interface Diagram

Composite Structures Development

With the approval for implementation of a graphite/epoxy forward gaseous-hydrogen (GH_2) pressure line-fairing on the External Tank (ET), additional research and investigations have been conducted to determine other ET components that can be built from composite materials that provide increased component reliability/performance and reduced cost and weight. The MSFC-Martin Marietta-Michoud cooperative program has utilized a building block approach. This approach has been used to investigate structural and nonstructural ET applications.

Components being researched include cable trays and covers, liquid oxygen feedline-fairing, aft gaseous-hydrogen pressure line-fairing, forward cable tray-fairing, intertank access door, range safety system-fairing, cable tray bracket shields, nose cone-fairing, bipod and thrust struts, as well as the ET intertank.

This research has encompassed all areas of composite structures development from design and analysis to test and verification. "A" – basis allowable material databases (99 population values with 95 percent confidence level) have been developed for advanced composite materials, thermoset, and thermoplastic. Approved analysis methods are being developed and demonstrated. Automated processing equipment such as filament winders, pultruders, tape-wrappers and tape-layers are available for part fabrication. Nondestructive evaluation techniques such as ultrasound and high-energy x-ray are being optimized for composite component evaluation.

All prototype structures are built in the MSFC Productivity Enhancement Facility. Several components will be submitted for implementation approval by the end of this year.

G. H. Gordon/EH43
(205) 544-2726
Sponsor: Office of Space Flight

Nondestructive Evaluation Technology

Nondestructive Evaluation (NDE) data are often ignored or misinterpreted when dealing with solid rocket motor (SRM) components. Few outside the NDE discipline have been able to understand the complexities of the information NDE data provide, or to interpret the effect of NDE-located "defects" on SRM performance. MSFC is learning to provide NDE data in a more meaningful format to manufacturing engineers, analysts, and program managers — particularly those involved with SRM programs.

By using NDE data in a complementary manner, mapping data to a common frame of reference, and equating data to meaningful materials and performance properties, NDE becomes more contributive to overall program goals. MSFC has developed the Integrated NDE (Data) Reduction System (INDERS) to perform these functions. Digital NDE data from a variety of sources are accepted by the system and mapped to a common frame of reference. Data from different sources are then correlated and matched to materials properties. Finally, data are linked to finite element models by way of International Graphics Exchange Standard (IGES) image format to allow the incorporation of NDE data in analytical models.

INDERS provides a valuable set of statistical validation tools which can be used by engineers and analysts to develop NDE-to-materials data correlations,

performance assessments, and acceptance criteria. Tools for the quantitative development of mechanical cutting plans are included as well. The overall goal of these tools is to reduce the effects of subjectivity in dealing with NDE data.

INDERS is a generic system, capable of using NDE data from a wide range of NDE test equipment, making it useful to any organization which deals with digital NDE data. At MSFC, the system works most closely with computed tomography, advanced ultrasonics, and automated eddy current systems. Any digital data which can be obtained in American Standard Code for Information Interchange (ASCII) format can easily be used by the system. INDERS is hardware-compatible with any VAX/IBM PC-based system. No special requirements exist for graphics. Standard off-the-shelf software is used wherever possible.

The focus of the INDERS effort is to establish a standard set of tools which can be easily applied to digital NDE data from any source to decrease subjective decision-making based on NDE data.

L. H. Hediger/EH13
(205) 544-2544
Sponsor: Solid Propulsion Integrity Program

Space Debris and Micrometeoroid Testing

Spacecraft designers must anticipate many space environmental factors which affect the success and usefulness of any given mission. Two of the important factors affecting the operating conditions and the survival probability of a spacecraft are the meteoroid and space debris flux. In the last few years, studies by various organizations and individuals have identified the threat of an impact as being of a greater magnitude than previously identified. Data has been presented which concluded that some experiments flown in Earth orbit to detect meteoroids actually detected mostly aluminum oxide particulates from Solid Rocket Motors (SRM), and that the orbital debris flux in certain regions of Earth orbit was either comparable to, or greatly exceeded, the interplanetary meteoroid flux. Therefore, it is evident from the recent studies and papers presented that the orbital debris problem is a real concern for large, long term spacecraft, and collision probabilities are increasing as the orbital population increases. In fact, the rate of growth is approximately 7 percent higher than had been predicted in earlier studies.

Due to the increased threat of collision with meteoroids and principally orbital debris, a Light Gas Gun Facility was reactivated at MSFC to serve as a Meteoroid/Orbital Debris Simulation Test Facility for the Space Station Freedom Program. The facility consists of a Light Gas Gun with a 12.7-mm (0.5-in) launch tube capable of launching 2.5 to 12.7 mm (0.098 to 0.5 in) projectiles with a mass of 4 to 300 mg (14×10^{-5} to 10.5×10^{-3} oz) at velocities of 2 to 8 km/sec (6,561 to 26,246 ft/sec), and three target tanks of 0.607 m^3 (2.36 ft^3), 0.53 m^3 (16 ft^3), and 28.5 m^3 (1,000 ft^3). Projectile velocity measurements are accomplished by way of pulsed x-ray, laser diode detectors, and a Hall Photographic Station.

Orbital debris impact testing began in July 1985, and approximately 680 samples have been tested to date. Spheres and a limited number of cylinders of 6061 aluminum and 1100 aluminum ranging in diameter from 3.1275 to 9.52 mm (0.123 to 0.375 in) have been launched at velocities ranging from 2 to 7.5 km/s (6,561 to 24,606 ft/s). All cylinders consisted of a length-to-diameter ratio of 1. Test sample configurations included 6061-T6 Al 1 mm thick (0.040 and 0.063 in) and Kevlar single bumpers, and 6061-T6 Al double bumpers, triple bumpers, and 6061-T6/ Kevlar double bumpers. All multiple bumpers were configured to provide the equivalent weight of a single bumper arrangement. Various configurations and materials have been tested with and without multilayer insulation within the 10.16 to 30.48 cm (4 to 12 in) spacing between the bumper and pressure wall. Multiple bumpers were spaced 2.54 cm (1 in) apart within the overall spacing.

Predicted debris flux indicates that the majority of the orbital debris will strike the spacecraft at 45- to 60-degree incident angles; therefore, oblique testing was required. Using the same configurations as noted above, tests were performed at incident angles of 30, 45, 60, and 75 degrees from the perpendicular. Although a large number of oblique testing has been completed, more testing is required to quantify the impact damage and determine the most reliable protection system; therefore, this test program is still in progress.

R. A. Taylor/EH15
(205) 544-2554
Sponsor: Space Station Project Office

Shuttle Launch Environment Study

The airflow, temperature, and turbulence conditions on and in the vicinity of the launch pad, the Shuttle vehicle, external tank, solid rocket boosters, and service structures are being simulated using the parabolic, hyperbolic, or elliptic numerical integration code series program developed by CHAM of North America, Inc. These computations determine the influence of the natural environment on the temperature distribution around the Space Shuttle.

Various wind speeds and temperature-boundary conditions are being considered, and resulting flow velocities, temperatures, pressures, and turbulence calculated over an area of 100-m^3 encompassing the pad and structures. The mesh spacing is relatively coarse, with 33 cells in the east direction, 25 north, and 30 vertical. Several cases with varying wind speeds (2, 3, and 5 kn) at 33 °F ambient temperature have been run with pressure and temperature contours and velocity vector plots made within the launch pad area.

A larger flow domain with a finer grid will be run with another program and compared against available measurements.

Singhal, A. K.: A Critical Look at the Progress in Numerical Heat Transfer and Some Suggestions for Improvement. Numerical Heat Transfer, Vol. 8, pp. 505–517, 1985.

Mahaffey, W. A. and Keaton, L. W.: Numerical Analysis of Prelaunch Thermal Environment of the Space Shuttle Main Engine. Vol. 1 and 2, CHAM Contractor Report 4045/53 NAS8-35970, September 1986.

R. L. Holland/ED42
(205) 544-1635
Sponsor: Office of Space Science and Applications

Automated Systems

Intelligent Data Reduction

The I-DARE (Intelligent Data Reduction) is an expert system project. In most spacecraft subsystems, only a small fraction of the telemetry data are significant at any given moment. The ideal situation would be to reduce the telemetry data to its significant components on-board so that enhanced fault management, incipient failure detection, and other trends analyses can be executed in real-time. Current data reduction is a labor-intensive operation.

The objective of the I-DARE project is to autonomously capture and intelligently reduce telemetry data from a spacecraft subsystem. The approach is to develop an artificial intelligence knowledge-based system that is able to emulate the specific reasoning that subsystem test bed personnel employ in reducing such data to its significant components.

The immediate application is the Hubble Space Telescope Nickel-Cadmium Battery Test Bed located at MSFC. The principal components of this test bed are six 23-cell flight-type nickel-cadmium batteries along with associated protection and reconditioning electronics and the solar array simulators for emulation of photovoltaic power generation in low earth orbit (LEO) conditions. Test bed engineers spend great amounts of time pouring over the telemetry data to determine system responses to various conditions and to determine developing trends. In order to accomplish these tasks, the data must first be reduced to its significant components as up to 98 percent of the data are insignificant at any given time.

The telemetry data are also transmitted by way of data bus at 9,600 bps to the I-DARE workstation located in a nearby building. There, a module of the I-DARE knowledge-based system known as the data handler continuously receives and files the raw data for up to 100 LEO orbits. The data handler also performs transmission error detection and correction to ensure the system is working with good data.

The expert function of I-DARE then reduces the data in order to allow near real-time data trend analyses. Several timeframes within each orbit, such as battery end-of-discharge, battery end-of-charge, etc., are utilized to review and reduce the data. The knowledge engineer has interviewed the three principal test bed engineers and manager to determine the heuristics, facts, and other guidelines employed in reducing this data. The current prototype knowledge-based system is a rule-based approach which begins to approximate the behavior and efficiency of test bed engineers in reducing this telemetry data. This year, the knowledge base will increase to handle more context sensitivity and will improve analyzer capabilities for fault diagnosis and trends analysis including incipient failure detection.

I-DARE currently resides on a Symbolics 3620 artificial intelligence workstation in Common Lisp. The system will be ported to a color Symbolics 3650 workstation during the next several months as the current prototype is made more robust. It is hoped that the approaches and methodologies employed for intelligent reduction of the Hubble Space Telescope power system test bed telemetry data can be utilized for intelligent data reduction of other subsystem telemetry such as propulsion, thermal, environmental crew life support systems, etc., with only major changes to the man-machine interface and the knowledge base to support that particular subsystem.

The University of Alabama in Huntsville has supported this research effort under NASA grant NAG8-642. This grant is into the second year of a two year continuing award grant, originally jointly funded by the Hubble Space Telescope Program and the MSFC Center Director's Discretionary Fund.

Ford, D. R. and Weeks, D. J.: Intelligent Data Reduction: a Preliminary Investigation. To be published in the Proceedings of the 23rd Intersociety Energy Conversion Engineering Conference, 1988.

D. J. Weeks/EB12
(205) 544-3309
Sponsor: Center Director's Discretionary Fund

Telerobotics

MSFC is committed to a broadbased teleoperator and robotics program for supporting NASA missions involving rendezvous and docking missions as well as *in situ* and remote servicing of orbital platforms. The Center's unique facilities include real-time full-scale hardware simulators for investigating and testing under conditions as close as possible to those encountered in actual flight.

The Orbital Mobility Hardware Simulator Facility (Fig. 126) contains two independent simulators: a Dynamic Overhead Target Simulator (DOTS) and an Air Bearing Mobility Unit propelled by thrusters over a 4,200 ft^2 precision cast epoxy floor. The DOTS, which spans the entire floor, is an 8 degree of freedom simulator capable of positioning a 1,000 lb payload to an accuracy of 1/4 inch within the 120,000 ft^3 volume of the facility. The system incorporates force-torque sensing for simulating orbital contact dynamics to an overall bandwidth of 3.5 Hz. Simultaneous operation of both simulators support docking with stable and unstable satellites, formation flight, station keeping, etc.

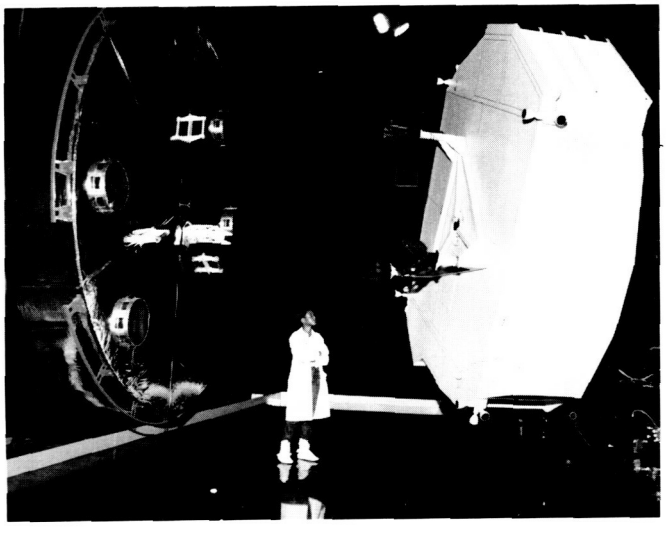

Figure 126. The Orbital Mobility Hardware Simulator Facility

MSFC's robotics laboratory has the hardware and real time capability for automated satellite servicing with the Integrated Orbital Servicer System (IOSS) and for teleoperator servicing with the Protoflight Manipulator Arm (PFMA). The IOSS is used to evaluate mating and demating mechanisms of various types of Orbital Replacement Units and for demonstrating automated modular servicing of spacecraft. The PFMA, used for supporting studies associated with Space Station Feedom and remote satellite servicing, is a 7 degree of freedom manipulator with a range of 10 to 96 in. Enhancements which were completed during FY88 include force/torque feedback displayed to operator, force/torque reflection, and a calibrated task board for quantitative evaluation of manipulators, operators, or computer control schemes. Near term enhancements include an updated real time computer system supporting task motion tracking and compensation, task primitives, automation, and interfaces for either human or artificial operators.

Both the Orbital Mobility Hardware Simulator Facility and the Teleoperator and Robotics Facility support total black-out and simulation of solar illumination for orbital lighting and camera studies. Other features include teleoperator constraints of time delay, video frame rate reduction, gray scale reduction, and resolution reduction.

T. C. Bryan/EB24
(205) 544-3550
Sponsors: Office of Space Transportation Systems
Office of Aeronautics and Space Technology
Office of Space Station

Automatic Mathematical Modeling for Real Time Simulation Systems

A methodology for automatic mathematical modeling and generating simulation models will be verified by running in a test environment using standard profiles with the results compared against known results. The major objective is to create a user-friendly environment for engineers to design, maintain, and verify their models and also to automatically convert the mathematical models into conventional code for computation.

The traditional way for simulation modeling is to define, derive, and organize the equations and then develop the program for computation manually. If any modification or correction needs to be done in the design or mathematical equations, it creates a tremendous amount of work for the rest of the process. Generally, any model will require several modifications before it matches a real system. Historically, the modifications have been time consuming and a fertile source of errors.

Some of the available Symbolics mathematics tools will help us to derive the equation symbolically and automatically produce the final equation and program code. By using LISP language, it is possible to build a user-friendly interface and generate a knowledge base for the Symbolics mathematics tool to build equations and program codes. After the equations and codes have been stored, the LISP program can combine and organize them, creating a complete compiled source code for any conventional language required.

A demonstration program was designed for modeling the Space Shuttle Main Engine (SSME) Simulation. It is written in LISP and MACSYMA and runs on a Symbolics 3670 LISP Machine. The program provides a very friendly and well organized environment for engineers to build a knowledge base for base equations and general information. It contains an initial set of component process elements for the SSME Simulation and a questionnaire that allows the engineer to answer a set of questions to specify a particular model. The system is then able to automatically generate the model and FORTRAN code. The future goal is to download the FORTRAN code to a VAX/VMS system for conventional computation. The SSME mathematical model will be verified in a test environment and the solution compared with the real data profile. Control, display, and ancillary systems will be developed which will allow the execution of a predefined profile (from a file) or interactive modification of the variables. Variables can be displayed in test format or as a plot from the control and display system. An execution control module will be available to allow time and sequence control of the model and peripheral models. A recording module will be available for execution in series with the math model and will record (or not record) interface variables transparently. This module will use packet definition variables and circular queues to determine what and when to record.

The use of artificial intelligence techniques has shown that the process of the simulation modeling can be simplified.

C. K. Wang/EB44
(205) 544-3887
Sponsor: Office of Space Flight

Automatic Gore Panel Mapping System

A research and technology program is underway at the MSFC Productivity Enhancement Facility to develop and demonstrate robotic and automation technologies for use on space structure manufacturing processes. One area is the development of an automatic system for mapping the thickness of External Tank (ET) gore panels. Gore panels are curved metal sections welded together to form four domes for use at opposite ends of the hydrogen and oxygen tanks of the ET. The panels are reduced in thickness over large areas to lower ET total weight. These panels are presently inspected for thickness manually, requiring two men three days to complete. The Automatic Gore Panel Mapping System, when fully implemented, will have the capability to accurately and quickly measure thickness, determine overall panel uniformity, and complete the process at a greatly reduced amount of time and labor.

The key part of the inspection system is a Krautkramer-Branson WDM Ultrasonic thickness measuring system. The sensor is mounted on a Cincinnati Milacron T3-776 robot which scans, measures, and stores panel thickness over a predetermined grid pattern as shown in Figure 127. Using another program, the system evaluates thickness information and identifies areas of the panel that need further reduction in thickness. This process is repeated until the desired panel thickness and uniformity are achieved. The robot sequence can be programmed and optimized off-line using a Silicon Graphics IRIS Model 3120 Workstation and a graphics package from SILMA. The optimized robot trajectories are downloaded to an IBM-PC computer via an RS-232C interface where the trajectory information is converted into robot compatible form. The robot coordinate information is then downloaded to the robot for execution using a software package known as Remote Off-line Program System (ROPS) from Cincinnati Milacron (Fig. 128).

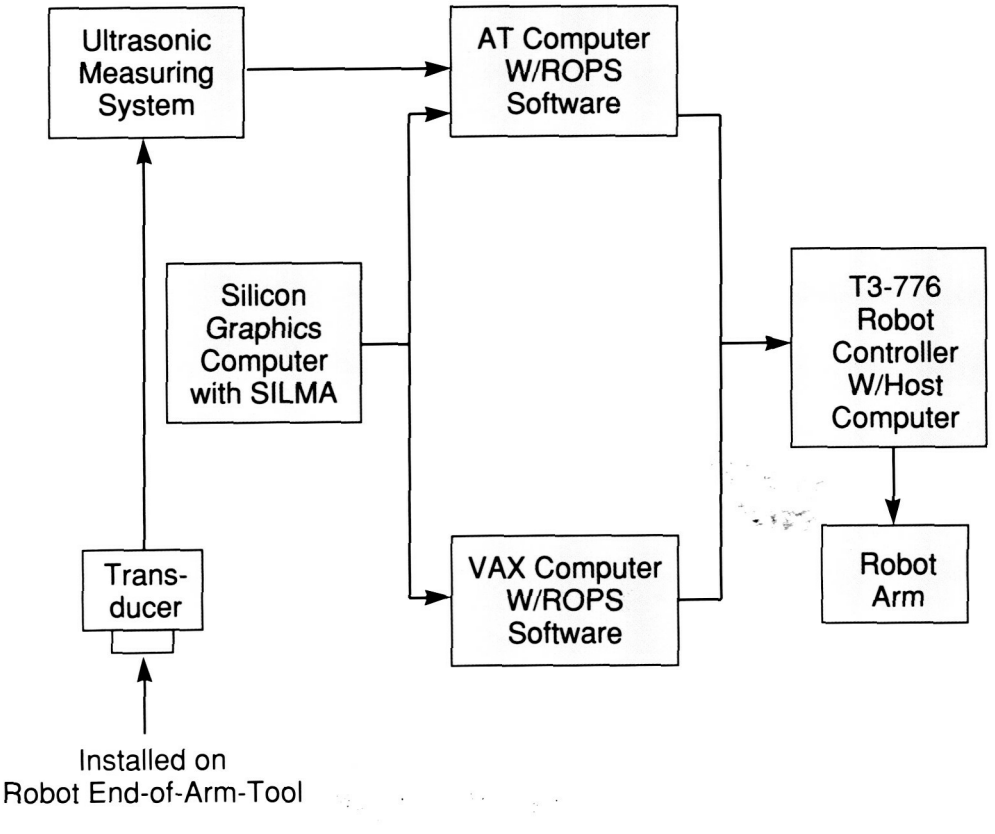

Figure 127. Gore Panel and Robot Arm

An Automatic Gore Panel Mapping System has been successfully integrated and demonstrated. When completed, this system will result in substantial cost savings on a very labor intensive manual operation. In addition, the quality and reliability of the panels will be enhanced as a result of the improved repeatability of this system. Preliminary results have shown the applicability of this advanced technology to other Space Shuttle manufacturing processes. Transfer of this technology to the production sites is feasible and under consideration.

E. Martinez/EH43
(205) 544-2724
Sponsor: Office of Space Flight

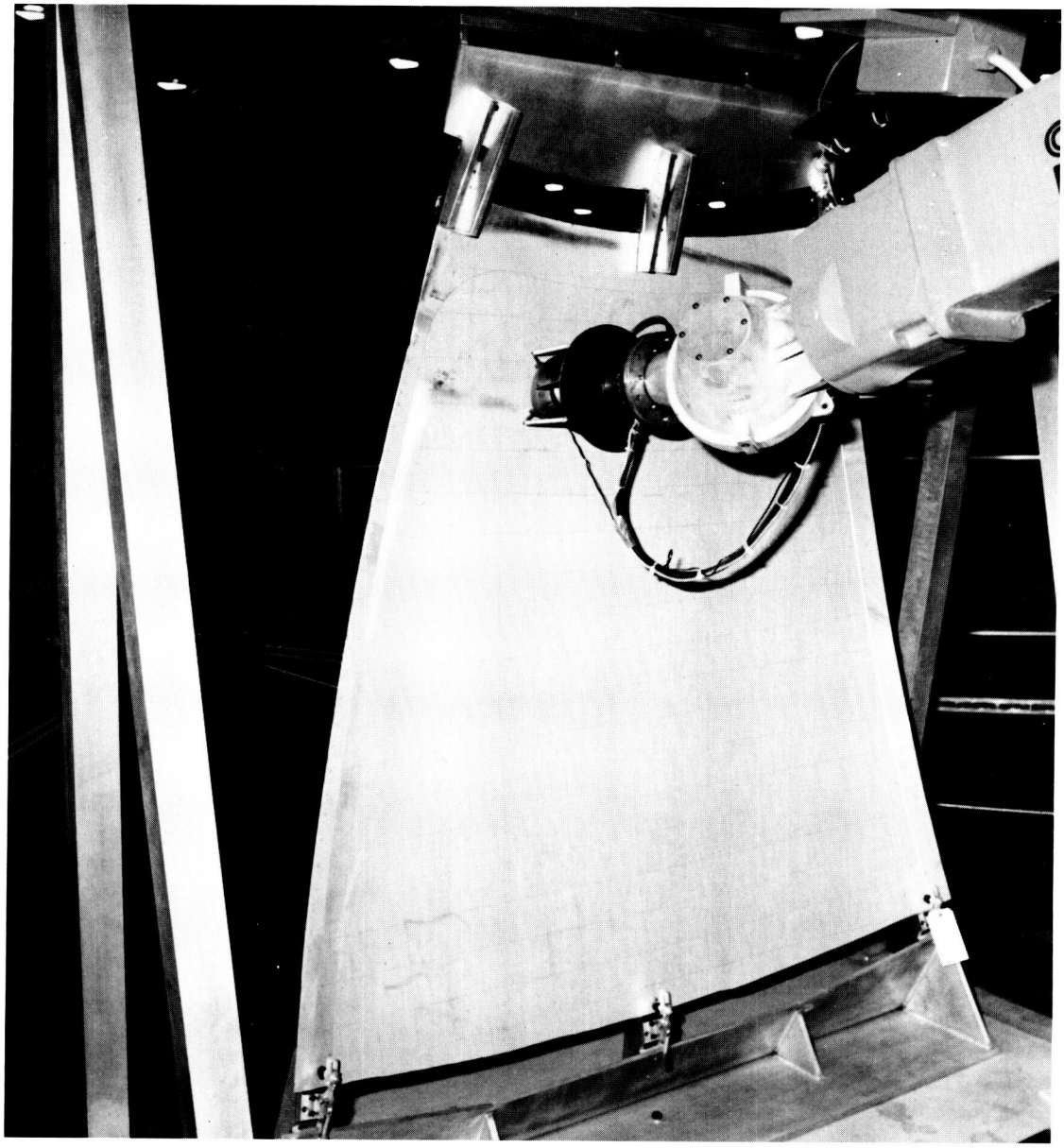

Figure 128. Automatic Gore Mapping System

Space Systems

Advanced X-Ray Astrophysics Facility's Technology Mirror Assembly

The Technology Mirror Assembly (TMA) consists of two mirrors which are approximately two-thirds the size of the innermost pair of mirrors of the Advanced X-Ray Astrophysics Facility (AXAF). The TMA program was designed to demonstrate the ability to fabricate optics to the level of precision required for the AXAF. The original program produced a set of mirrors that in x-ray testing at MSFC did not measure up to the expected performance. This performance was predicted on the basis of metrology performed at the completion of the mirror fabrication part of the program. Analysis of the data resulted in the hypothesis that an error in mirror fabrication occurred in a spatial frequency region where there was a gap in the metrology. Consequently a decision was made to disassemble the TMA and with improved metrology and polishing procedures verify and correct the mirror errors. In the initial evaluation of the disassembled mirrors it was discovered that in addition to the hypothesized error in the midspatial frequency region (4-mm period), there was a long wavelength error (200-mm period) which was polished into the glass through a mistake in the sign of a calibration file and that the microroughness (region below 1 mm-spatial period) was higher than originally thought due to incorrect bandwidth assumptions. Following the detailed assessment of the state of the mirrors, repolishing commenced. The repolishing was completed during FY88. Figure 129 shows the results of fringe scanner measurements at the beginning and at the end of the repolishing process for both the parabola and the hyperbola mirrors. The lower curve of each pair shows the long wavelength error which was inadvertently polished into the glass in the original program. The amplitude of this error can be seen to be approximately ±0.2 μm. The upper curve of each pair shows the final result after repolishing. Note that there has been a scale change, full scale now being 0.1 μm compared to 0.4 μm for the initial case. Thus the long wavelength error was reduced by an order of magnitude to something less than .01 μm. The error due to the gap in metrology is shown in Figure 130. This figure shows power spectral density plots obtained from a WYKO profilometer (a phase measuring interferometer). The left hand plot of each pair shows the initial condition of the mirror. A 4-mm ripple appears as a spike in both the parabola and hyperbola plots. A spike at 8 mm occurs in the parabola plot as well. These ripples were not observed with the original metrology set up due to the fact that the instrumentation could not cover this region of spatial frequencies. The right hand plot of each pair shows the results of the final metrology after repolishing. In both cases it can be seen that not only have the 4-mm and 8-mm ripple been removed, but the overall curve has been reduced by an order of magnitude .

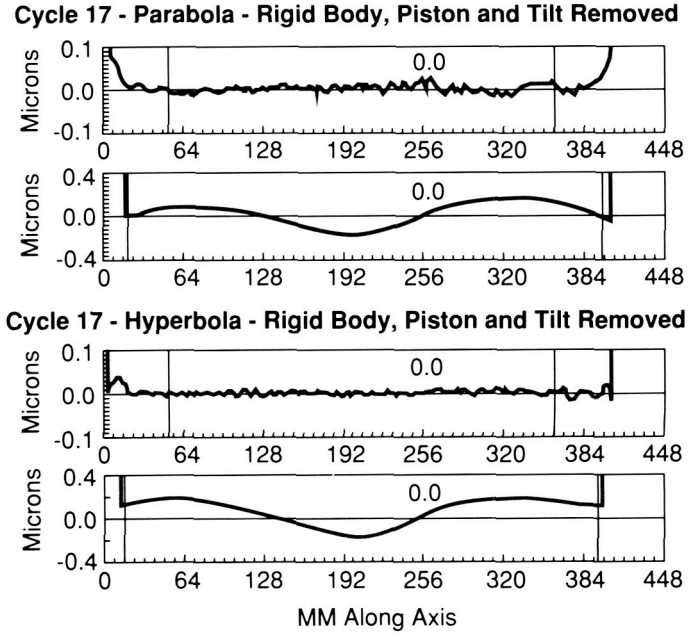

Figure 129. Fringe Scanner Measurements at the Beginning and End of the TMA Repolishing Effort

C-3

ORIGINAL PAGE
COLOR PHOTOGRAPH

One of the most significant accomplishments of the repolishing effort was the reduction of the high frequency microroughness. The original goal of the TMA program was to achieve a 15 Å rms surface roughness. At the beginning of the repolishing effort it was felt that 10 Å could be achieved and that 5 Å should be considered as a realistic goal. In fact, 3 Å was achieved. This increased smoothness greatly enhances high energy performance by reducing the amount of energy which is scattered out of the focal spot. Midspatial frequency requirements, however, were still not met. The rms amplitude in the 1-mm to 100-mm spatial band was desired to be in the range of from 20 Å to 30 Å. The polishing process was stopped for programmatic reasons before the goal in this region was met (final rms amplitude in this band was approximately 40 Å). Since the polishing process was still converging in the midspatial frequency region, it was felt that the requirements could have been met given additional time and money. The midspatial frequency region is a very challenging region which pushes both the metrology and the tooling to their limits. Particular attention will be paid to this area in follow-on work.

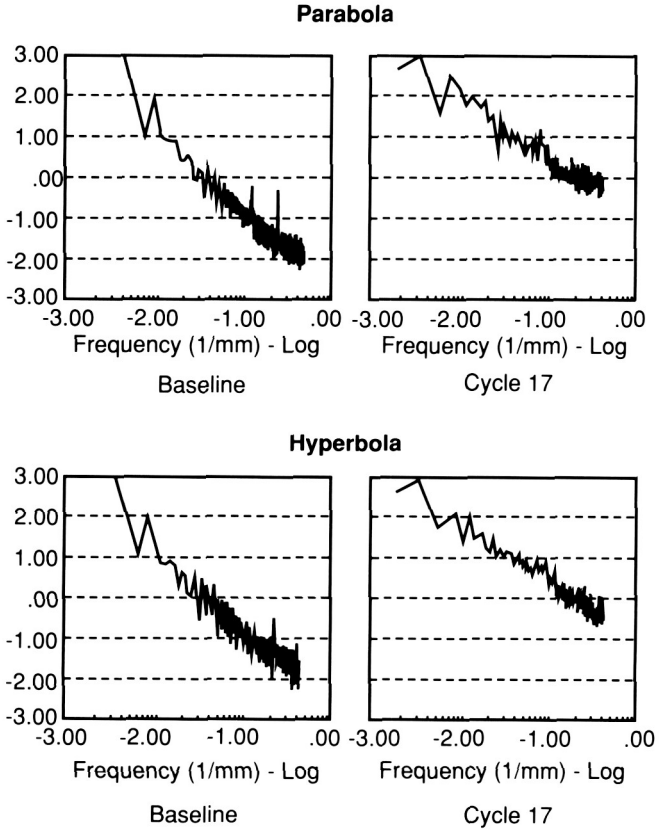

Figure 130. Power Spectral Density Plots for the Parabola and Hyperbola Mirrors

Subsequent to the cessation of polishing, the ends of the parabola mirror were cut off. This was done to eliminate unwanted x-ray scattering due to the incorrectly figured glare near the ends. Although this should have been a benign process, the parabola, in fact, warped. This could have been due to either residual stress in the glass or induced stress resulting from the cutting process. A detailed analysis is currently underway to ascertain the more probable cause prior to cutting the hyperbola.

One of the strongest lessons learned in this program has been the necessity of having metrology with overlapping coverage. This not only prevents errors of omission, but also reduces errors of commission, since it provides a check between instruments. Unfortunately, although it was felt that this had been satisfactorily accomplished, examining the parabola after the ends were cut resulted in the determination that the parabola had been supported at incorrect locations. Thus, the effect of the sag due to gravity was miscalculated. This once again resulted in a long wave-length error being polished into the glass.

In summary, although the goals were not met in their entirety, the program demonstrated that the AXAF requirements were feasible. It also pointed out the necessity of providing checks not only for metrology, but also for human error. The TMA will be tested at the MSFC X-Ray Facility in FY89. Even though there are errors in the mirrors, a complete characterization of the mirrors through metrology and subsequent successful performance prediction will provide a satisfactory conclusion to the program.

Bilbro, J. W.; Status of the AXAF Technology Mirror Assembly Program. Presented at the Huntsville Association of Technical Society's conference, Huntsville, Alabama, May, 1988.

J. W. Bilbro/EB23
(205) 544-3467
Sponsor: Office of Space Science and Applications

Analysis of Thermal Performance of the Hubble Space Telescope

The thermal vacuum test of the Hubble Space Telescope indicated the multilayer insulation (MLI) did not perform as well as expected. Interior telescope temperatures ran 5 to 7 °C colder than pre-test predictions, and heater power exceeded the prediction by more than 100 W. The principal suspect of the high MLI emittance was the poisoning effect of struts, cables, and other penetrations of the exterior shell of the telescope. When covered by planar MLI blankets, heat at the penetration tends to be conducted laterally by aluminized sublayers, increasing the quantity emitted to space.

To quantify the poisoning effects of the structural penetrations, as well as possible meteorite strikes, MSFC awarded a grant to Auburn University. The objective of the research was experimental evaluation of MLI performance and correlation of empirical data with math modeling techniques currently in use on MSFC computer systems.

Last year the university planned the test matrix and procedure, designed and built the test rig, and conducted the tests on flight MLI in a MSFC thermal vacuum chamber. The test rig included a control MLI blanket without penetrating struts and each of several test blankets with various geometric patterns of single, multiple or clustered penetrations. The testing also included the effects of thickness compression of the MLI due to differential thermal expansion.

To date the university has built finite element math models of each of the test rig configurations. NASTRAN thermal analyzer runs have been made, and the results compared to empirical data. Preliminary results indicate the degradation factors for the MLI range from approximately 1.26 to 2.95, with the effect very localized to the edge of the MLI perturbation.

R. O. Cummings/EL56
(205) 544-7264
Sponsor: Hubble Space Telescope Program Office

Space Station Freedom Contamination Modeling

In the wake of the Space Station Freedom design processes, it is vital to know the contamination data base due to natural as well as man-made contaminant environments around S. S. Freedom and on attached scientific payloads. The man-made contamination sources may come from the propulsive or the nonpropulsive systems of S. S. Freedom. Since it is difficult, if not impossible, to collect ground or flight test data, the most economical way to obtain this information is through fluid dynamics computations.

This year, development of a computer code for predicting these contamination environments has been in progress. The three-dimensional model is governed by the degenerated Boltzmann equations with known surfaces properties. The TRASYS II computer program, which was developed for the thermal analysis modeling, is used to obtain those surface-to-surface form factors of all S. S. Freedom elements. The determination of these factors is based on Lambertian surface emission properties and solid angles between surfaces and mathematical points in the volume around S. S. Freedom. Thus, the contaminant flux and deposition on surfaces and densities of gas around S. S. Freedom will be calculated. Preliminary results have shown that the ram pressure buildup on large surfaces creates gas species and densities that can exceed contamination column density requirements.

L. C. Chou/ED32
(205) 544-1591
Sponsor: Small Business Innovation Research Program

Wind Profiling Radars for Shuttle Launch Support

MSFC has been evaluating the use of wind profiling radars (popularly known as wind profilers) in launch operations since a demonstration carried out in March and April 1985. The demonstration involved a Radian Corporation radar and a NASA/National Oceanic and Atmospheric Administration radar and showed that such radars would be useful for monitoring temporal wind changes during a launch sequence and for improving wind variability climatology. Wind variability is a critical issue for Space Shuttle launches because the launch decision is partly based on winds measured by a Jimsphere two to three hours before launch. Vehicle loads are computed from a simulation of flight through the measured wind profile. The wind variability is then accounted for by including the worst expected load increase that has been determined from pairs of Jimspheres launched one to three hours apart. Wind Profiler winds cannot be directly substituted for Jimsphere winds because the vertical resolution of profilers is not as fine as the 100 to 200 m resolution of the Jimsphere.

In pursuit of the goal of monitoring wind variability over periods smaller than two hours, Tycho Technology, Inc., has been awarded a NASA contract to install a three-beam, 50-MHz wind profiling radar with an average power-aperture product of 10^8 Wm^2 next to the Shuttle Landing Facility at Kennedy Space Center. The radar will measure radial velocities along a vertical and two, orthogonal, 15° off-zenith beams sequentially every 3 minutes integrated over a radar sample volume with 150 m radial extent. The radar is scheduled to be in operation in fall 1988. An intensive comparison will be made between Jimsphere and radar winds in order to ascertain the effective temporal and spatial resolutions of both systems. Results from this comparison and examples of wind profile variability will be presented. Operational use of the radar in a launch sequence will be discussed.

C. K. Hill/ED44
(205) 544-1664
Sponsor: Office of Space Flight

Reentry Turbulence Model for the Space Shuttle

Between reentry and an altitude of approximately 10 km, attitude control jets provide stability and control for the Space Shuttle. Below 10 km, Shuttle control is by aerodynamic surfaces. Until recently, the turbulence model used by NASA for reentry simulations was the model outlined in the Shuttle design criteria. The design criteria model applied the 99.98 percent turbulent intensities all the way from reentry to 10 km. In the real atmosphere, high values of turbulence occur in patches interspersed with quiescent zones. Level turbulent intensities of 99.98 percent will never occur in the real atmosphere all the way from reentry to 10 km. The effect on the NASA simulations is an unrealistic prediction of attitude control jet fuel usage. The Shuttle has landed with as much as 280 kg of control jet fuel because of the conservative predictions of the design criteria model. The overly conservative estimate of fuel consumption caused reduced payloads and/or reduced experiment time on orbit, and necessitated a more realistic turbulence model. The present model significantly enhances the design criteria model's realism. New model options developed by MSFC include turbulent intensity class (light, moderate, or severe), and improved turbulence simulation equations. Patchiness of the turbulence is Monte Carlo simulated, i.e. the simulated Shuttle is not always in severe turbulence as was the case for the design criteria model. For example, in the severe turbulence case, the Shuttle passes through patches of severe turbulence as well as quiescent zones. The light, moderate, and severe turbulence options permit fuel consumption sensitivity analyses.

The new MSFC turbulence model will be applied to determine fuel consumption for flight through light, moderate, and severe turbulence. Secondly, the effect of turbulent model equations on fuel consumption will be investigated.

D. L. Johnson/ED44
(205) 544-1665
Sponsor: Office of Space Flight

Computed Tomography for Shuttle Components

Computed tomography (CT) has become a viable method of evaluating the internal structure of Shuttle components. CT utilizes highly collimated x-ray fan beams to reconstruct a cross-sectional image of components. The Advanced Computed Tomography Inspection System (ACTIS), developed by Bio-Imaging Research under contract to MSFC, represents a significant milestone in the development of industrial CT scanners. Other industrial scanners have been built to perform evaluation of a particular component. The MSFC approach was towards gaining maximum flexibility with the simplest man-machine interface possible. This concept is beautifully demonstrated in ACTIS.

ACTIS employs three x-ray sources to allow adjustable beam energies between 50 keV and 2 MeV. The system geometry is uniquely designed to provide variable scan field diameters and magnifications. X-ray source and geometry selection are accomplished at the touch of a button. The detector system and operating software have also been designed to allow total system optimization for any part. MSFC has received two patents as a result of ACTIS development. The system is limited to objects 1,200 mm (50 inches) in diameter and 1,000 kg (2,200 lbs) in weight.

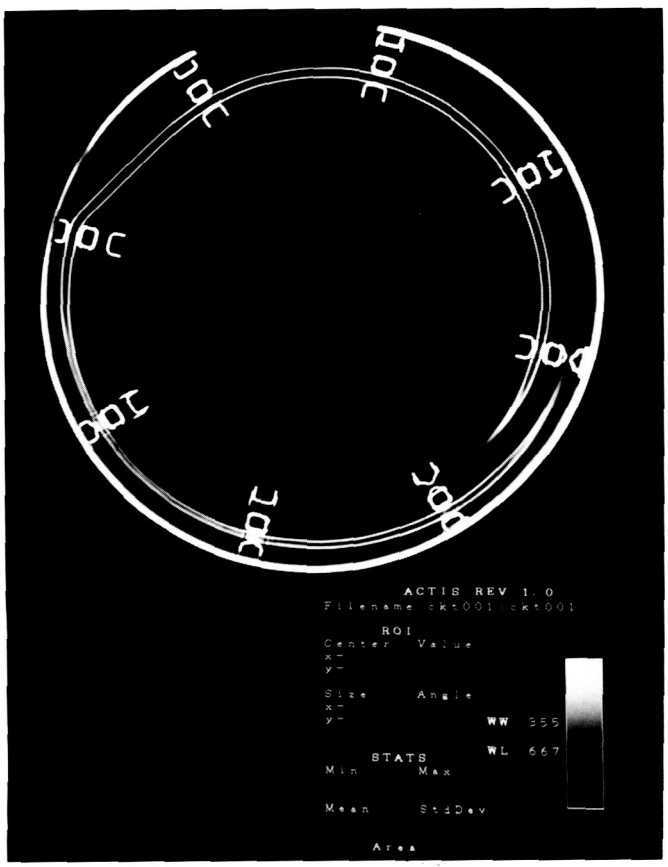

Figure 131. Computed Tomography Image of SSME Heat Exchanger

The system incorporates a number of special image processing features, including image averaging, subtraction, statistical analysis, and color imaging. The system is capable of performing multiplanar reconstruction, a feature which allows the operator to view a data set from any of three mutually perpendicular planes.

MSFC has developed links which allow ACTIS images to be downloaded to any computer-aided design and analysis station which accepts the International Graphics Exchange Standard (IGES) format. Images can then be used to build three-dimensional models of as-fabricated components.

A variety of components from the solid rocket motor, external tank, Space Shuttle Main Engines (SSME), and others have been imaged successfully. ACTIS technology will contribute greatly to the development of acceptance criteria for composite materials and the analytical modelling of as-built components.

Figure 131 shows a cross-sectional image of the SSME. This image was taken perpendicular to the heat exchanger's main axis through approximately 10 inches of steel heat exchanger. Thinning of the outside wall is visible in the upper left quadrant.

L. H. Hediger/EH13
(205) 544-2544
Sponsor: Office of Space Transportation

Space Transportation System Ground Thermal Design Criteria Revisions

Ground thermal design criteria revisions were needed to provide complete, realistic, and usable natural environments for element thermal design. There was some concern about single valued temperature limits, lack of wind specifications, whether the current data base requires updating, and the issue of the chill effect from the loaded external tank. The revision placed all essential design criteria in a complete and usable form. This was accomplished by expanding criteria definitions, checking or updating all parameters to include the latest data base, and meshing the design criteria with the launch commit criteria. Solar radiation criteria and ambient temperature criteria were included in the revision.

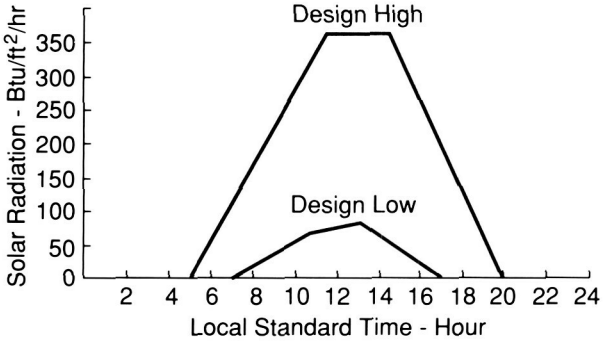

Note: Design High is Direct Incident Solar Radiation to a Horizontal Surface.
Design Low is Diffuse Incident Solar Radiation to any Surface.

Figure 132. Solar Radiation at Ground Level

Solar radiation criteria should be used to assess shuttle elements which are sensitive to radiation interchange. Figure 132 and Table 8 define high and low solar radiation design data versus time of day. The design high curve presents clear day direct incident solar radiation to a horizontal surface. The actual radiation absorbed by a surface would be a function of the surface geometry relative to the sun vector. The design low curve presents cloudy day diffuse solar radiation which would apply to all surfaces. The actual radiation absorbed by these surfaces would also be a function of surface optical properties.

The ambient temperature criteria during the prelaunch phase (prior to External Tank loading) is an extreme low value of 15 °F not to exceed 2 hours and an extreme high value of 99 °F not to exceed 2 hours.

Other parameters modified in the revision included: sky temperature criteria, propellent mean bulk temperature criteria, humidity, and precipitation specifications. All Space Transportation System thermal design requirements are provided in NSTS 07700, Volume X, Appendix 10.10.

G. L. Jasper/ED44
(205) 544-1666
Sponsor: Office of Space Flight

Table 8. Design High and Design Low Solar Radiation

Time of Day	Design High Solar Radiation		Time of Day	Design Low Solar Radiation	
Hour	Btu/ft²/hr	gm-cal/cm²/min	Hour	Btu/ft²/hr	gm-cal/cm²/min
0500	0	0.00	0655	0	0.00
1100	363	1.64	1100	70	0.32
1400	363	1.64	1300	80	0.36
2000	0	0.00	1710	0	0.00

Index of Contacts